Master's thesis

NTNU
Norwegian University of Science and Technology
Faculty of Engineering
Department of Energy and Process Engineering

Ana Erquicia De Clerck

Preliminary design of axial turbine for organic working fluids

Master's thesis in Natural Gas Technology
Supervisor: Lars O. Nord
Co-supervisor: Lasse Borg Anderson
June 2023

NTNU
Norwegian University of
Science and Technology

Ana Erquicia De Clerck

Preliminary design of axial turbine for organic working fluids

Master's thesis in Natural Gas Technology
Supervisor: Lars O. Nord
Co-supervisor: Lasse Borg Anderson
June 2023

Norwegian University of Science and Technology
Faculty of Engineering
Department of Energy and Process Engineering

NTNU
Norwegian University of
Science and Technology

NTNU

Norwegian University
of Science and Technology

Department of Energy
and Process Engineering

EPT-M-2023

MASTER'S THESIS

for

Student Ana Erquicia De Clerck

Spring 2023

English working title:

Preliminary design of axial turbine for organic working fluids

Background and objective

Large amounts of industrial surplus heat are currently unutilized around the globe. Waste heat recovery has therefore the potential of being a major factor in reaching national and international energy and environment goals. Direct use of the heat, for example in a district heating system, could be the most efficient and cost-effective alternative, but is in many cases not a feasible option. Thus, heat-to-power conversion often becomes the most attractive alternative. Electricity has very high flexibility for distribution and re-use. Organic Rankine cycles (ORC) is one of the most interesting power cycle for recovering waste heat. A critical component in an ORC is the expander since this is the device that converts the thermal energy to mechanical energy and subsequently electric energy. Because of changes in the waste heat supply, such as a temperature and mass flow rate, off-design operation of the expanders is important

The main objective of the work is to analyze mean-line (1D) turbine models for ORC cycles in waste heat recovery applications. A part of mean-line models is 1D loss models to be able to estimate entropy generation throughout the expander. The student should implement appropriate loss model and analyze off-design operation of the turbine.

The thesis builds on the specialization project.

The following tasks are to be considered:

- Literature review on preliminary design of turbines, off-design operation, and loss models
- Learning and continuing to code in Python
- Implement a loss model for improved off-design analysis in the Python mean-line code
- Validate model, perform a sensitivity analysis, and analyze results
- Recommend path moving forward in preliminary design of axial turbines that considers off-design operation

Academic supervisor:
Lars O. Nord, Professor Thermal Energy, NTNU

Co-supervisor:
Lasse Borg Anderson, PhD candidate, NTNU

Abstract

The current global energy situation calls for action to be taken to reduce fossil fuel consumption and generate clean energy. One way to reduce fossil fuel consumption is by utilizing and recovering the large amounts of waste heat generated in industrial processes. Among the different technologies available used to recover waste heat, the organic Rankine cycle is an incipient technology that has operational advantages over the conventional steam Rankine cycle when the temperature of the waste heat source does not exceed 350°C. However, the efficiency of these cycles is relatively low, as they generally employ an expander optimized exclusively for the design conditions and the conditions to which they are subjected are usually variable and far from the design point.

Of the various turbine architectures available on the market, the axial turbine fits the power ranges of an organic Rankine cycle, from a few kW_{el} up to some MW_{el}. With the idea of providing a powerful tool for the design of an axial turbine staging, previous work on this thesis has been aimed at developing a mean-line model for preliminary design under design and off-design conditions, as it provides an accurate first estimate of the turbine's key dimensions and parameters. This model has been used to evaluate the losses that occur in axial turbines, whereby entropy is generated in the expansion process and the efficiency of the turbine is reduced. Accurate determination of these losses is essential in order to obtain a precise model that can be used to increase the potential of these cycles. In order to evaluate them, various authors have proposed a series of empirical correlations to account for the different components of the internal losses of axial turbines. Among the different correlations considered, the Benner loss model has been chosen for this purpose as it takes into account the incidence losses when the turbine faces off-design conditions and has proven to predict turbine efficiency more accurately when comparing his work to other authors'.

In order to ensure the consistency of the model and to improve the optimization mode so that it can be carried out more efficiently, a sensitivity analysis has been conducted using one of the various design of experiments techniques, the face-centered central composite design. This technique is used to account not only for the main and interaction effects but also for the quadratic effects of the factors that are inputs to the model and have been selected for the study. With this aim, two sets of experiments have been carried out in Python within a wide design space and a local sensitivity analysis respectively, followed by a statistical analysis in order to determine the significance of the effects. From these experiments it has been concluded that, despite limitations found in the model which disabled studying the selected factors as a whole and despite the reliability of the results due to the regression model that has been used to obtain the coefficients, the mean-line model proposed as design tool seems to make sense, as it presents as significant those effects that had proven to have a considerable influence on the efficiency in a previous analysis, suggesting that none of them should be discarded when designing an ORC axial turbine. It was also found that reducing the design space in the optimization when using gradient-based algorithms does not necessarily lead to more efficient optimization.

Acknowledgements

I would first like to thank my supervisor, Lars, for agreeing to supervise me even before I arrived in Trondheim. From the beginning he has shown great confidence in my work and has given me a lot of freedom to carry it out in the way that best suited the circumstances. Thank you for insisting from the beginning Lars, that going out of the comfort zone is necessary to really learn, as I believe that this is only possible through humility and sharing. Thank you also for your flexibility and openness when we discovered that we were not going to be able to approach the thesis in the way we had initially planned, and for the different opportunities that you have offered me throughout the semester, which I believe have enriched my knowledge.

But it is especially my co-supervisor, Lasse, to whom I would like to dedicate a few lines of gratitude, because without his help, advice and support I would not have arrived here today, without the temptation to throw in the towel sometime. Thank you Lasse, because week after week you have made me see that no matter how insignificant the progress was, it was more than enough reason to trust in my work and to keep going forward with enthusiasm. Thank you for your availability and interest, and above all thank you for your continued patience.

Special thanks also to Edu Caro, who has shown that no matter where in the world you are, he will always be willing to help until the end. Edu, thank you very much for your advice and your sincere interest. And thanks to Andrés Sebastián for agreeing to supervise my thesis from Madrid and for his willingness to help me in any way he could.

I would also like to thank all my friends here in Trondheim and around the world for their unconditional support and friendship, Gemma, Mati, Marti, Meri, Ester, Michi, Adamo, Paolo, Arthuro and Alyssa. As well as to all the people from Spain who have made the distance inappreciable, to my great team at Recoletos, especially to Mamen, who has become an expert in axial turbines after my continuous talks, to Anita Antúnez, Mónica, Lola and Trini, who are always there, and to Toté and Pi who despite the time they don't forget me. I specially would like to thank my "Football team" and "Beganas", as well as my unconditional home town friends.

Finally, all this would not have been possible without my whole family, my grandparents, Sophie, Sol, but specially my parents. Thank you for your continuous support, advice and interest. Thank you for believing in me and for letting me live one of the best experiences of my life.

Table of Contents

List of Tables

List of Figures

Nomenclature

Symbols

$\dot{m}$	Mass flow rate	kg/s
$\dot{Q}$	Heat flow rate	W
$\dot{V}$	Volumetric flow rate	m^3/s
$\dot{W}$	Power	W
Λ	Degree of reaction	-
A	Area	m^2
a	Speed of sound	m/s
B	Blockage factor	-
c	Blade chord or Absolute flow velocity	m or m/s
c_p	Isobaric heat capacity	kJ/kg·K
c_{eq}	Vector of equality constraints	-
c_{ineq}	Vector of inequality constraints	-
D	Diameter	m
d_{spe}	Specific diameter	-
F_t	Tangential loading parameter	-
f_{AR}	Aspect Ratio correction factor	-
f_{hub}	Hub Mach number correction factor	-
f_{Ma}	Mach number correction factor	-
f_{Re}	Reynolds number correction factor	-
g	Gravitational constant	m/s^2
H/b	Blade axial aspect ratio	-
H/c	Blade aspect ratio	-
H	Blade height	m
h	Specific enthalpy	kJ/kg
i	Incidence angle	°
k	Number of factors	

K_1	First compressibility correction factor	-
K_2	Second compressibility correction factor	-
K_3	Third compressibility correction factor	-
K_p	Profile loss compressibility correction factor	-
K_s	Secondary loss compressibility correction factor	-
L	Number of levels	
l	Blade chamber length	m
le	Leading edge diameter	m
M	Molecular mass	kg/kmol
Ma	Mach number	-
N	Sample size	
o	Opening	m
p	Pressure	kPa/bar
P_i	Internal power	W
Q	Heat source	J
q	Specific heat	kJ/kg
R	Gas constant	KJ/kg K
r	Radius	m
r_{ht}	Blade hub to tip radii ratio	-
Re	Reynolds number	-
s/c	Blade pitch to chord ratio	-
s	Specific entropy	kJ/kg·K
ss	Stage spacing	m
T	Temperature	$^{\circ}CorK$
t	Blade thickness	m
t_{cl}	Tip clearance gap	m
t_{max}	Maximum blade thickness	m
t_{te}	Blade trailing edge thickness	m
u	Blade speed	m/s

u_{spe}	Specific internal energy	kJ/kg
v	Absolute flow velocity	m/s
v_{spe}	Specific volume	m^3/kg
w	Relative flow velocity	m/s
w_i	Specific work	kJ/kg
We	Wedge angle	°
Y	Pressure loss coefficient	-
Y_p	Profile loss coefficient	-
Y_s	Secondary loss coefficient	-
Y_{cl}	Tip clearance loss coefficient	-
Y_{shock}	Leading edge shock correction factor	-
Y_{te}	Trailing edge loss coefficient	-
y_{te}	Trailing edge loss multiplication factor	-
Z	Ainley loading parameter	-
z	Compressibility factor	-

Greek letters

α	Absolute flow angle	°
β	Relative flow angle	°
χ	Incidence parameter	
$\Delta\phi^2$	Kinetic energy loss coefficient	-
$\Delta\theta$	Chamber angle	°
ΔT	Temperature difference	K
δ	Deviation angle or boundary layer thickness	° or mm
δ_{fl}	Flaring angle	°
η_i	Isentropic efficiency	-
η_{ts}	Total to static efficiency	-
η_{tt}	Total to total efficiency	-
$\hat{\beta}$	Estimated coefficients	-
λ	Secondary loss geometrical parameter of the AM loss system	-

μ	Dynamic viscosity	Pa·s
Ω	Rotational speed	rad/s
Ω_{spe}	Specific speed	-
ϕ	Flow coefficient	-
ψ	Loading coefficient	-
ρ	Density	kg/m^3
τ	Torque	N·m
θ	Blade methal angle	$^\circ$
ε	Statistical error	-
ξ	Stagger angle	$^\circ$
ζ	Energy loss coefficient	-

Acronyms

AM	Ainley & Mathieson loss model
AR	Blade aspect ratio
BS	Blade solidity
CCC	Central composite circumscribed
CCD	Central composite design
CCF	Face-centered central composite
CCI	Central composite inscribed
CI	Confidence interval
CR	Convergence ratio
DC	Dunham & Came loss model
DOE	Design of experiments
KO	Kacker & Okapuu loss model
lb	Lower bound
MLR	Multiple linear regression
MSE	Mean sStandard error
ORC	Organic Rankine Cycle
PR	Pressure ratio

RSM	Response surface methodology
SA	Sensitivity analysis
SE	Standard error
SQP	Sequential Quadratic Programming
SRC	Steam Rankine Cycle
TE	Trailing edge
ub	Upper bound

Subscripts

$0, rel$	Relative stagnation state
0	Stagnation state
1	Station at the stator inlet
2	Station at stator throat
3	Station at stator outlet
4	Station at the rotor inlet
5	Station at rotor throat
6	Station at rotor outlet
θ	Tangential velocity component
Ax	Axial blade chord
c	Heat sink (cold)
cl	Clearance component
des	Design
f	Working fluid
h	Heat source (hot)
in	State at the inlet of the turbine
inc	Incidence component
$irrev$	Irreversible process
is	Isentropic process
m	Meridional velocity component
mid	Mean-line approach

n	Normal to a section
out	State at the outlet of the turbine
p	Profile component
r	Rotor row or radial direction
rev	Reversible process
s	Stator row
sec	Secondary component
spe	Specific
$stall$	Stalling component
te	Trailing edge component
x	Axial velocity component

1 Introduction

1.1 Project background

The work presented in this Master's thesis is a continuation of my specialization project *Expanders for organic working fluids*. The foundation for the thesis work was laid during the specialization project meaning that some sections of the technical background and methodology are similarly described in the project report for completeness for the thesis reader. The specialization project report is not published.

Moreover, this thesis is framed in the work of the PhD candidate Lasse B. Anderson, co-supervisor of the thesis. For its development, the mean-line model he has elaborated for preliminary design optimization and performance analysis of single-stage axial turbines has been used. This model, in turn, is based on the work of R. Agromayor during his Master's thesis and doctoral work.

1.2 Motivation

Given the urgency and need for action on climate change, it is not enough to increase the global production of energy from renewable sources at an unprecedented rate, but measures must also be taken to increase the efficiency of processes in order to reduce their energy consumption. A large amount of waste heat from industrial processes is continuously being unused. In order to recover and utilize this energy source — when a direct use of waste heat (i.e. district heating) is not possible or feasible —, various mature and developed technologies, such as the steam Rankine cycle, are employed. However, the efficiency of this technology drops when the temperature of the waste heat source is medium or low. Organic Rankine cycles are the solution to this problem, as they use organic working fluids and can operate at lower temperatures.

However, the potential of this technology is significantly low, because the conditions of the heat source are variable, and in general, the cycle expander (the element in which the conversion of heat to mechanical energy takes place) is designed for an optimum operating point. The first motivation for this is to develop a model that allows the turbine to be designed for both design and off-design conditions. Along the same lines, with this mean-line model already developed, the motivation of this thesis' work is to be able to determine the generation of entropy in the expansion process by means of the correlations of the most appropriate loss model that has been developed for this purpose. The evaluation of losses is very important in order to obtain an accurate model to assess the performance of a turbine. Furthermore, in order to test the quality of this preliminary design tool, and in order to improve its optimization mode, it is necessary to address the broad field of sensitivity analysis, as this will allow the model to be fine-tuned before it is validated.

1.3 Objectives

The objectives of this thesis are:

1. Perform a literature study and review on preliminary design of turbines, off-design operation and loss models, in order to work with a mean-line model proposed as an effective tool for preliminary design of axial turbines that considers design and off-design conditions.
2. To become familiar with the Python programming environment which has been used to develop the aforementioned mean-line model.
3. Perform a literature review on flow and losses through an axial turbine duct in order to analyze, compare and select the best loss model to assess the turbine performance in accordance with the purpose of the model (evaluating also off-design conditions).
4. Implement and validate a loss model for improved off-design analysis in the Python mean-line code.
5. Validate the mean-line model, perform a sensitivity analysis and analyze the results.
6. Perform a literature review on design of experiments and regression models in order to select the most appropriate and cost-effective technique to carry out the aforementioned sensitivity analysis, with the aim of checking whether the model makes sense and improving its optimization mode.
7. Recommend a path moving forward in preliminary design of axial turbines that considers off-design operation.

1.4 Contribution

To the author's best knowledge, there is no study similar to the one presented in this work in the open literature, in which a sensitivity analysis of a mean-line model, specifically developed for the preliminary design of an axial turbine, is carried out by means of a design of experiments technique such as the face-centered central composite design. While it is common to carry out a sensitivity analysis to check that the model under consideration makes sense, it is not often addressed by these techniques. A simpler and more commonly used practice is the one-at-a-time analysis, also known as Morris method. A paper that uses this technique with the same purpose as the one used in this thesis is that published by Meroni et al. [1]. It is not easy to find a work similar to the one that has been carried out, moreover, because there is no single way of proceeding when developing a mean-line model and none has been seen so far including the input design variables presented here.

1.5 Organization

This Master's thesis has been divided into four main chapters: technical background, methodology, results and discussions and conclusions.

The technical background consists of ten sections, of which the first two (sections 2.1 and 2.2) are intended to contextualize the reader in the current energy situation and the potential of the waste heat recovery process. The next section describes a specific type of technology for the conversion of waste heat into electricity, the organic Rankine cycle (Section 2.3). As previous studies have been carried out on the same subject, it has not been explained in too much depth. The following three sections have been devoted to give an overview of the fundamental considerations for the study of turbomachines (Section 2.4), their classification (Section 2.5) and fundamentals of one of the detailed types, the axial turbine (Section 2.6). This section will introduce the variables to be used in the model for the preliminary design of a stage of this type of turbines. To address the preliminary design of axial turbines, models often use a one-dimensional approach, being known as mean-line models, the fundamentals of which will be presented in Section 2.7.

Next, Section 2.8 presents the result of a careful and thorough literature review on the flow and different losses in axial turbines — given the importance of evaluating them to determine their performance—, as well as the different approaches to loss modelling. This is followed by a section (2.9) presenting the correlations offered by different authors for both design and off-design operation: Ainley and Mathieson, Dunham and Came, Kacker and Okapuu, Moustapha et al. and Benner. The structure of this section is based on the previous work of R. Agromayor in order to be consistent with the model used for the development of the thesis. Finally, in Section 2.10, the purpose of carrying out a sensitivity analysis is clarified and a particular approach by means of design of experiments is presented. For this, three different techniques have been briefly introduced: full factorial, fractional factorial and central composite designs.

The methods used to carry out the work of this Master's thesis have been detailed in the Methodology section (3). This section can be divided into two main parts. The first (Section 3.1), which refers to the mean-line model used and proposed as an efficient tool for preliminary design of axial turbines and the second (Section 3.2), which refers to the carried out sensitivity analysis. In the former, the mathematical model for the turbine performance analysis mode will be presented first (Section 3.1.1). Next, the selection of the loss model necessary to assess this performance with design and off-design conditions will be justified (Section 3.1.2). This will be followed by the explanation of the optimization mode of the model (Section 3.1.3). Finally, a particular case study for the final comparison of optimizations will be presented (Section 3.1.4). Regarding the sensitivity analysis, first the DOE technique selection will be exposed (Section 3.2.1), followed by a first non-rigorous factorial analysis to select the factors for the experiments (Section 3.2.2). Next, the experimental settings will be described in Section 3.2.3, to end with the regression model and statistical analysis that have been used to examine the experimental results (Section 3.2.4). A third part has been devoted to explain the methodology that has been followed to carry out the experiments, since different sensitivity analyses (wide and local) have been conducted. This is shown in Section 3.3. Finally, some comments regarding the aforementioned comparison of optimizations have been included in Section 3.4.

The results and main differences found between the two carried out analyses and the further comparison of optimizations have been presented and discussed in Section 4, trying to find a reasonable justification to explain the obtained results. Several limitations found in the model will also be introduced. The main conclusions drawn from this study can be found in Section 5, together with some future lines derived from the work carried out.

2 Technical background

2.1 Energy trends and global current situation

Energy can be considered from different points of view: scientific, technological, economic, social, environmental; but all of them converge in stating that it is one of the most valuable resources in today's society. Energy makes things happen, and in a scenario characterized by continuous population growth, tightness of resources and the prominent climate change, a worldwide increase in its demand and consumption is unavoidable.

However, energy is a scarce commodity. The limits arise not only from the aforementioned depletion of natural resources, but also from the finite capacity of the planet to receive the waste generated. Moreover, the recent COVID-19 pandemic and the crisis and war situation in Ukraine have highlighted the importance of the energy trilemma- energy security, affordability and lower carbon- while driving up energy prices to unprecedented levels.

Several studies on global energy trends are carried out every year. Their analyses show that the post-pandemic economic recovery has not only led to an increase in energy consumption, but has also resulted in a spike in the level of energy-related carbon emissions [2], making global warming an unequivocal fact due to the greenhouse effect caused by emissions of these gases.

Despite efforts to increase the amount of energy obtained from renewable sources towards the net zero scenario by 2030, one such recent study presented in Figure 2.1, from the bp Statistical Review of World Energy 2022, reveals that more than 82% of global primary energy consumption still comes from fossil fuels. Encouragingly, however, low-carbon energy is growing worldwide.

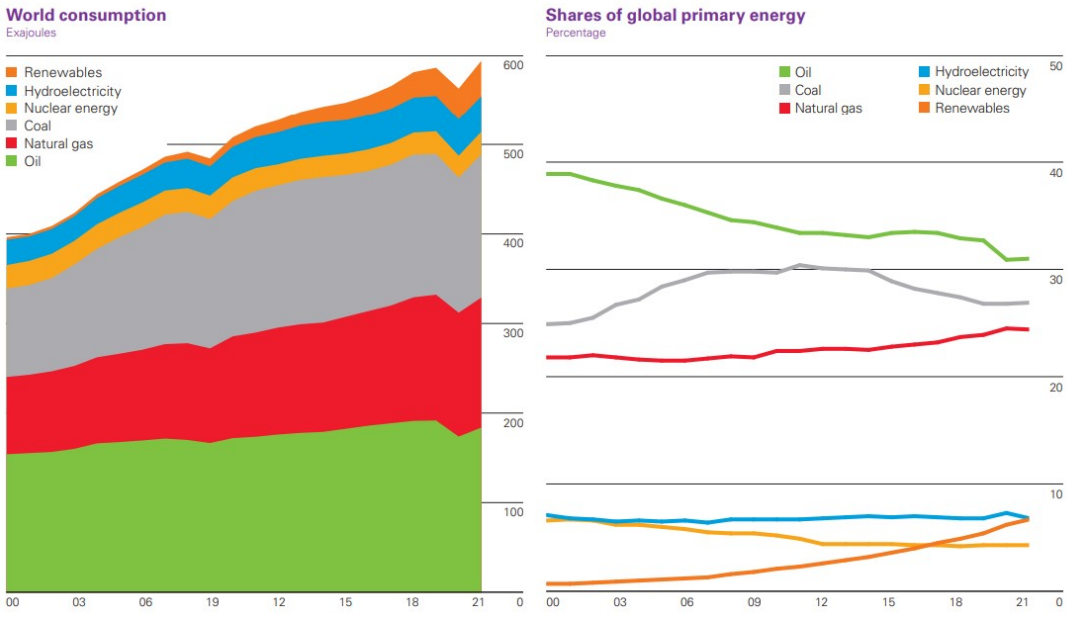

Figure 2.1: Global primary energy consumption 2021 [3].

As for the rebound in CO_2 emissions, the world remains far from the Paris Agreement targets. "The pronounced dip in carbon emissions in 2020 was only temporary", states Spencer Dale, chief economist at bp: "carbon equivalent emissions from energy increased by 5.7% last year" [3], returning to pre-pandemic trends and more than offsetting the encouraging decline. The annual change in carbon emissions is depicted in Figure 2.2.

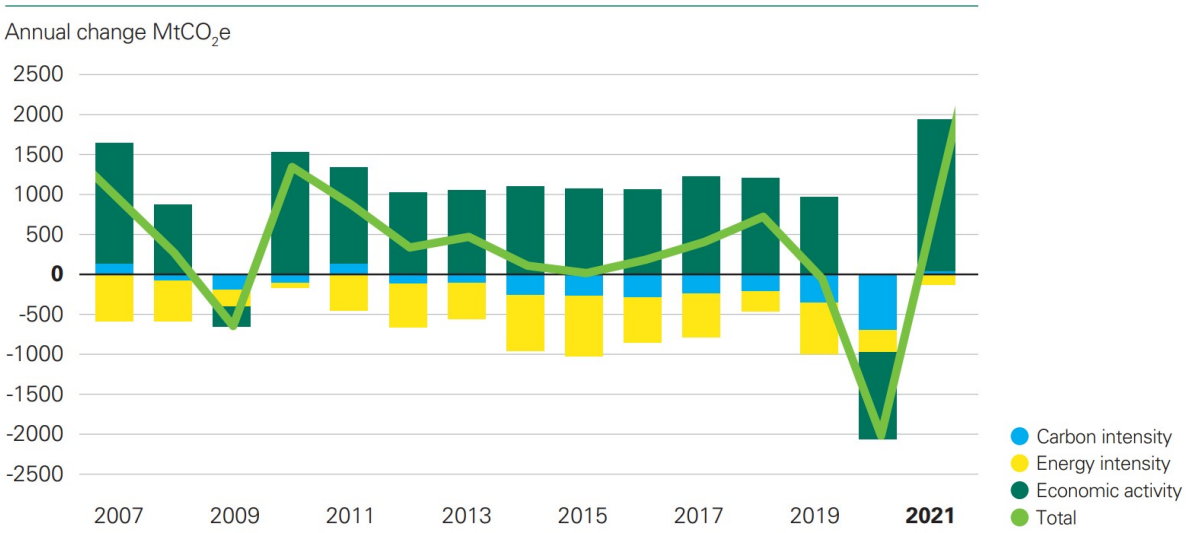

Figure 2.2: Annual CO_2 emissions in $MtCO_2e$ [3].

Renewable energy sources are indeed a solution to address societal present challenges, which could be summarized as meeting the aforementioned growing demand on available energy supplies and achieving deep and rapid decarbonization. However, as shown in the graph of Figure 2.3 obtained from Renewables 2022 Global Status Report, "the renewable power additions must triple to be on track with major net zero scenarios" [4].

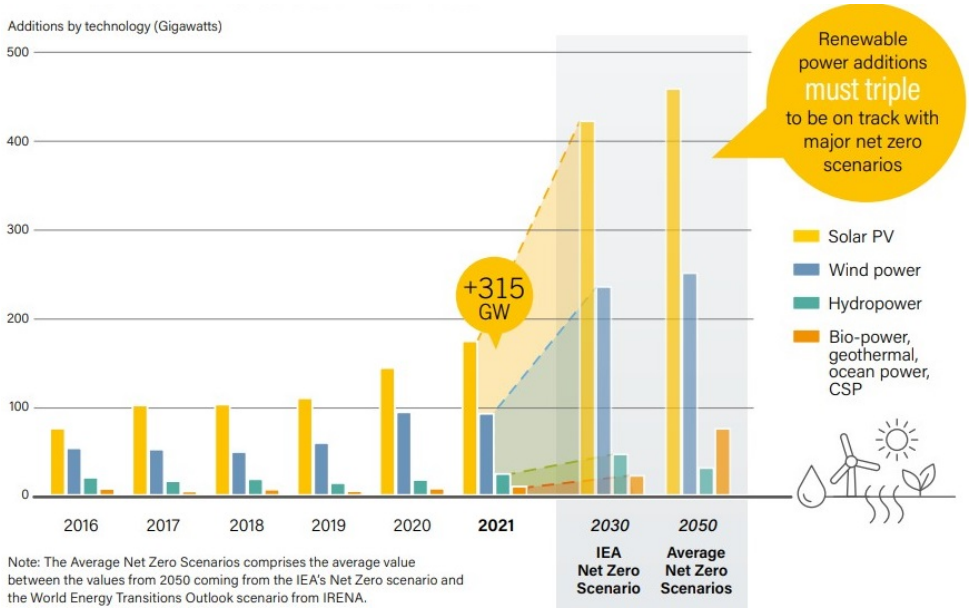

Figure 2.3: Renewables power additions in the transition towards net zero scenario [4].

In order to achieve climate change mitigation, increasing global energy production from renewable sources is not enough. Existing fossil fuels in the current energy mix must be discarded at a faster rate and scale, or displaced by other clean fuels such as biofuels or natural gas.

Industrial processes are responsible for more than a quarter of the world's final energy consumption [4], with the power sector being the largest CO_2 emitter. Therefore, it is necessary to promote the implementation of technologies that reduce CO_2, such as CO_2 capture, as well as to promote energy efficiency by improving productivity in industrial plants with lower energy consumption, as detailed in [5].

The imminence of this global problem, together with the growing energy inflation, has motivated research focused precisely on reducing the consumption of these non-renewable sources, improving efficiency in energy production and, therefore, reducing the level of emissions, as just explained.

There are different solutions that reduce the carbon footprint of industry by enabling more efficient yields. In this aforementioned line of research, the use of waste heat recovery systems in industrial processes has been key in recent decades [6], since many industrial processes generate energy waste that can be recovered and reincorporated into the process. In this way, not only are emissions and fossil fuel consumption reduced, but also more competitive processes are obtained due to a consequent reduction in cost. The following section is devoted to explaining the details of waste heat recovery.

2.2 Waste heat recovery

From what has been explained so far it can be said that waste heat recovery (WHR) is nothing more than the reuse of useless surplus energy from industrial processes that is lost due to plant inefficiencies [7], and would be released to the environment or to other cooling systems if other efficient and cost-effective direct uses, as district heating, were not feasible.

However, the process of recovering this unused thermal energy is not so easy. Therefore, many different technologies have been developed according to the classification of waste heat sources in order to obtain the optimal efficiency. These technologies will be presented in Section 2.2.4, however, only two of them will be discussed further in Section 2.3, as they are within the scope of the thesis. But first, the classification of waste heat sources will be introduced, followed by different applications in which this process can be used.

2.2.1 Classification of waste heat sources

The efficiency of the waste heat recovery process is highly dependent on the temperature of the waste heat source. Thereby, these heat loss sources can be classified into three levels: low, medium and high temperature.

Discrepancies can be found among different authors in establishing the temperature limits of these levels. For this reason, the chosen classification is: low-temperature (T < 230 ^{o}C), medium-temperature (230 ^{o}C < T < 650 ^{o}C) and high-temperature (T > 650 ^{o}C) [8]. This classification has been taken from R. Agromayor's Master's thesis, since his work is the basis on which this thesis is developed, and which is also consistent with the one selected by other authors in [9] and [10].

Table 2.1: Waste Heat source classification according to the stream temperature [11].

Level	Waste Heat source	Characteristics
Low temperature (T < 230 ^{o}C)	Boilers Steam condensate Low temperature ovens	- Energy contained in numerous small sources - Low power generation efficiencies - Recovery of combustion streams limited due to acid concentration if T < 121 ^{o}C
Medium temperature (230 ^{o}C < T < 650 ^{o}C)	Prime mover exhaust streams Heat-treating furnaces Ovens and cement kilns	- Medium power generation efficiencies - Chemical and mechanical contaminants (some streams such as cement kilns)
High temperature (T > 650 ^{o}C)	Furnaces Coke ovens Fume incinerators Hydrogen plants	- High quality heat - High heat transfer - High power generation efficiencies - Chemical and mechanical contaminants

As it can be seen, Table 2.1, developed by the Combined Heat and Power Partnership in United States Environmental Protection Agency (EPA), lists the main characteristics and sources of the waste heat streams.

2.2.2 Waste heat recovery applications

Waste heat recovery can be used in many different fields, however, its potential in industry is quite small compared to other combined heat and power processes, mainly due to some technical barriers, such as the heat recovery operation itself. Waste heat is usually disperse in industrial plants, or may contain toxic substances and contaminants that make other alternatives more cost-effective. Space limitation and the complexity of integrating waste heat recovery control systems to existing processes are other technical barriers [11]. Further on, some business and regulatory barriers also affect to the potential of this process.

Among the different applications in which WHR can be found depending on the temperature of the heat source (as the ones presented in Table 2.1), some of those discussed in [11] will be listed below along with another technology that should be mentioned for its importance in the last years.

- District heating

  District heating is a grid-based heat supply technology in which heat is generated centrally for distribution through a network of insulated pipes, generally in the form of water, to individual houses or blocks of buildings [12] to precisely meet their hot

water, heating or even cooling demand [13]. These systems can utilize several heat sources, including waste heat when designed to distribute heat at considerably low temperatures.

In this way, the heat released by various industrial processes can be used directly for this purpose, or even stored in an appropriate manner. However, this option, which a priori may seem simpler given the complexity of the heat recovery process, is not always affordable or feasible for the reasons set out below:

  - **The proximity of the heat source**: it strongly influences the feasibility, decreasing it the further the heat source is located from the area to which the heat will be distributed.
  - **The heat source capacity and availability**: when the waste heat obtained from industrial processes is not being continuously provided or it does not meet the heat requirements.
  - **The infrastructure requirements**: big areas are needed in order to set the distribution network.

- Manufacturing of primary metals (iron and steel industries)
- Manufacturing of non-metalic mineral products (glass industry)
- Petroleum refining: high-quality waste heat
- Chemical industry

2.2.3 Heat-to-Power

When waste heat recovery is used to convert the surplus heat from existing thermal processes into electricity, the process is known as heat-to-power. It could be considered as a type of combined heat and power, in which thermal energy and electricity are generated from a single fuel source [11]. However, as an asset, instead of consuming fuel for generating electricity, waste heat-to-power systems reuse the heat that would otherwise be wasted. In Figure 2.4 a diagram of the Heat to Power process is presented.

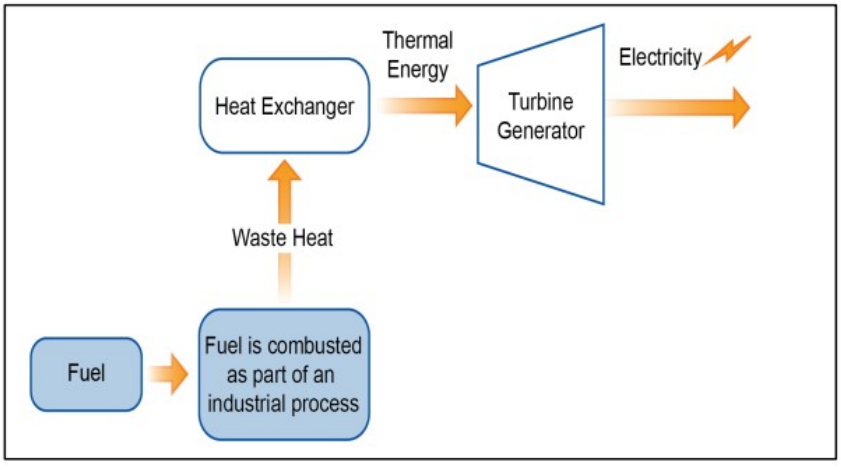

Figure 2.4: Waste Heat to Power diagram [11].

Stages in the Heat-to-power process

The heat-to-power process can be divided into the following five stages:

1. Heat recovery

   In order to obtain electricity from waste heat, firstly it has to be captured from the heat source. Depending on this heat source, thermal energy is extracted differently.

   There are heat sources such as hot water, oil or steam, which are obtained as by-products of many industrial processes and can be easily transferred and used directly for the aforementioned purpose [14].

   On the other hand, unlike this first type of heat source, heat in the form of exhaust gases — obtained from the combustion of hydrocarbons—, requires an intermediate fluid to be transferred due to the low heat capacity of these gases. This intermediate loop is quite common in waste heat recovery applications, in which a heat exchanger or heat recovery boiler is frequently used to transfer heat from one fluid to the other [15].

   In addition to the above categories of heat (liquid or thermal vapor and exhaust and gaseous heat), two other categories of available heat should be mentioned: radiative (solar thermal energy) and conductive (heat from hot surfaces).

2. Heat transfer

   As it has been said, the captured heat has to be transferred to a generator in which electricity will be produced, and this is usually done by using an intermediate loop.

   Even though direct use of heat reduces parasitic losses, the intermediate loop can cover long distances and regulate the temperature of the transferred heat [15].

3. Heat-to-power conversion

   Waste heat can be disposed of at any temperature depending on the source. As detailed in Table 2.1 and explained in Section 2.2.1, the higher the temperature (of the hot source), the higher the heat quality and the higher the power generation efficiency, in accordance to the Carnot efficiency given by:

   $$\eta_{Carnot} = 1 - \frac{T_C}{T_H} \tag{2.1}$$

   There are many different heat recovery technologies based on heat capture, recovery, exchange and production of electricity once heat has been transferred to the generator. To use them with optimum efficiency, it is necessary to know what is the maximum amount of potential heat recoverable from a process [16]. The available amount of waste heat can be calculated by using Eq. (2.2).

   $$Q = \dot{V} \cdot \rho \cdot C_p \cdot \Delta T \tag{2.2}$$

where:

$\dot{V}$ is the fluid flow rate $[m^3/s]$;
ρ is the density of the fluid $[kg/m^3]$;
C_p is the specific heat of the fluid $[J/kg \cdot K]$;
ΔT is the difference between the highest outlet temperature and initial inlet temperature of the fluid $[K]$;
and Q is the available amount of waste heat $[J]$.

The alternatives of waste heat recovery technologies are going to be listed and briefly commented in Section 2.2.4.

4. Heat rejection

   Once the heat has been expanded, a condensation stage is necessary in order to reuse the working fluid. Water and ambient air are often used for cooling. The former can be taken from nature or produced in cooling towers, while the latter usually requires a radiator [15]. The cooling temperature requirements depend on each application, being different for low temperature cycles and high temperature cycles.

5. Integration and interconnection

   This stage consists in either using or connecting the obtained power from the process to the grid. Therefore, power electronic and electrical components such as transformers, inverters, etc., may be needed.

In the following, the different technologies for recovering waste heat are going to be discussed.

2.2.4 Alternatives in waste heat recovery technologies

As said earlier in this chapter, there are different types of waste heat recovery technologies depending on the temperature of the waste heat source, in order to obtain higher efficiencies. The most spread and common technologies are briefly introduced in this section, but only the ORC will be explained in more detail in Section 2.3.

- **Rankine Cycle generators**
  - Steam Cycle:

    The steam Rankine cycle (SRC) is a thermodynamic cycle characterized by the use of water as the working fluid. Given the maturity of steam turbine technology, the SRC is the most widespread cycle for generating electricity from waste heat, which is used to generate the steam that expands in the turbine.

    The steam Rankine cycle process is as follows: water is pressurized through a pump, then heated in a boiler that uses waste heat as a heat source. Once the

working fluid leaves the boiler, it is expanded in a turbine to lower the pressure and temperature, generating mechanical energy in a shaft, energy that is converted into electricity by a generator. Before repeating the process, the working fluid is guided to a condenser where it condenses and turns back into a liquid.

Even though this cycle is suitable for large power and high temperature heat source applications, small and low temperature steam microturbines have been developed resulting efficient for some applications [15].

- Organic Rankine Cycle (ORC):

  Organic Rankine Cycles are characterized by using organic working fluids instead of water, but they follow the same principles as steam Rankine cycles. A deeper explanation will be given in Section 2.3.

  This type of Rankine cycle is suitable for low-medium heat sources and small scale power applications, and generally present lower efficiencies than SRC [15].

- Kalina Cycle:

  The Kalina Cycle is another type of Rankine cycle in which a mixture of water and ammonia is used as working fluid. Even though the complexity of this type of cycles is higher than in the ones presented above, it reaches the highest theoretical efficiencies, being suitable for both, low temperatures and large power range applications [11].

- **Other technologies**

  Not only Rankine cycles are used for heat-to-power conversion, there are many other technologies that differ in the working principle. Some of them are summarized in the table presented in Figure 2.5, which has been drawn up by Hussam Jouhara et Al. [6], while the following can be highlighted:

  - Stirling engines: which differ from Rankine cycles in the fact that the working fluid does not undergo compression.
  - Thermo-electric generators: This type of technology is characterized by producing electricity directly from waste heat.
  - Supercritical CO_2 Cycle: this cycle uses CO_2 as working fluid and operates above the fluid's critical point, leading to drastically density changes that allow extracting a large amount of energy with small size turbines at high temperatures. However, the technology is not commercially available [15].

Summary table of WHR technologies.

Technologies	Temperature Range Used	Benefits	Limitations
Regenerative Burners	High	Saving fuel by preheating the combustion air and improving the efficiency of combustion.	The system requires additional components such as a pair of heat exchange media and several control valves to function, which can be complex.
Recuperative Burners	High	Both the exhaust gas and waste heat from the body of the burner nozzle are capture and more heat from the nozzle is generated.	The burner and the nozzle needs to be inserted into the furnace body, which may require installation and modification of the furnace.
Economisers	Low – Medium	The system maximises the thermal efficiency of a system by recovering low-medium temperature heat from the waste flue gas for heating/preheating liquids entering a system.	The system may need to be made out of advanced materials to withstand the acidic condensate deposition, which can be expensive.
Waste Heat Boilers	Medium – High	The system is suitable to recover heat from medium – high temperature exhaust gases and is used to generate steam as an output.	An additional unit such as an auxiliary burner or an after burner might be needed in the system if the waste heat is not sufficient to produce the required amount of steam.
Recuperators	Low – High	The technology is used for applications with low – high temperatures and is used to decrease energy demand by preheating the inlet air into a system.	To maximise heat transfer effectiveness of the system, designs that are more complicated may need to be developed.
Regenerators	Medium – High	The technology is suitable to recover waste heat from high temperature applications such as furnaces and coke ovens and for applications with dirty exhausts.	The system can be very large in size and have very high capital costs.
Rotary Regenerators	Low – Medium	Rotary regenerators are used for low – medium temperature applications and could potentially offer a very high overall heat transfer efficiency.	The system is not suitable for high temperature applications due to the structural stresses and the possibility of deformations that can be caused by high temperature
Run around coil (RAC)	Medium – High	This unit is used when the sources of heat are too far from each other to use a direct recuperator and when cross contamination between the two flow sources needs to be prevented	This system is found to have a very low effectiveness when compared to a direct recuperator and needs a pump to operate, which requires additional energy input and maintenance
Heat Recovery Steam Generator (HRSG)	High	The system can be used to recover the waste heat from the exhaust of a power generation or manufacturing plant to significantly improve overall efficiencies by generating steam that can be used for process heating in the factory or power generation.	The system requires several components to function and may require an additional burner to improve the quality of the recovered waste heat. On the other hand, the system is very bulky and require on site construction.
Plate Heat Exchanger	Medium – High	Plate heat exchangers have high temperature and pressure operating limits and are used to transfer heat from one fluid to another when cross contamination needs to be avoided.	Parameters such as frequent variation in temperature and load must be studied and based on that suitable heat exchanger design must be chosen to avoid failure of the structure of the heat exchanger for the application
Heat Pipe Systems	Medium – High	Heat pipes have very high effective thermal conductivities, which results in a minimal temperature drop for transferring heat over long distances and long life that requires no maintenance, as they incorporate passive operation. They have lower operation costs when compared to the other types of heat exchangers.	To achieve an optimum performance from the heat exchanger, appropriate design, material, working fluid and wick type based on the application and temperature range of the waste heat must be studied and chosen.
Thermoelectric Generation	Medium – High	The system produces electricity directly from waste heat and eliminate the need for converting heat to mechanical energy to produce electrical energy.	The system has a very low efficiency of 2–5%, however, recent advances in nanotechnology have allowed electrical generation efficiencies of 15% or greater to be achieved
Piezoelectric Power Generation	Low	The system can be used for low-temperature waste heat recovery and works by converting ambient vibration such as oscillatory gas expansion directly into electricity.	The system are found to have a low efficiency, high internal impedance, need for long term durability and very high cost.
Thermionic Generator	High	The device is used for high temperature waste heat recovery and works by producing electric current through temperature difference between two media without the use of any moving objects	The functionality of this technology is shown to be limited to high temperature applications and be inefficient, however, several attempts have been made to improve their efficiency and enable their use for low temperature applications
Thermo Photo Voltaic (TPV) Generator	Low – High	These devices are used to directly convert radiant energy into electricity and offer a better efficiency when compared to other direct electrical conversion devices.	The device is found to have a limited operating temperature range and their efficiency decreases as the temperature increases. Having said that, high efficiency PV cells that can withstand high temperature ranges are also available, however, they are expensive and increase system costs.
Heat Pump	Low – Medium	Heat pumps transfers heat from a heat source to a heat sink using a small amount of energy and can be used to offer economical and efficient alternative of recovering heat from various sources to improve overall energy efficiency. Heat pumps in particular are good for low-temperature WHR, as they give the capability to upgrade waste heat to a higher temperature and quality.	In order to use this system, the method of capturing the waste heat based on its source and grade must firstly be analysed and in that respect, appropriate heat exchanger and system installation needs to be set up.
Direct Contact Condensation Recovery	Medium – High	the system uses a direct mixture heat exchanger without a separating wall and can be used to transfer heat from immiscible liquid – liquid and solid – liquid or solid-gas.	Due to absence of a separating wall in this heat exchanger, particles from the flue gas can be mixed with the water, which may require filtering before exiting the heat exchanger.
Inirect Contact Condensation Recovery	Medium – High	The system provides the advantage of eliminating cross contamination of the flue gas and water and can be designed to work as a filter of a process.	The system consists of a heat exchanger which in order to minimise corrosion from acidic condensate should be made from advanced materials and can be expensive.
Transport Membrane Condenser	Medium – High	The system works by extracting and delivering the hot water back into the system feed water directly from the exhaust gas through a capillary condensation channel. This way, the water is extracted through a membrane channel rather than directly from the flue gas and so the recovered water is not contaminated and does not require filtering.	The system employs a capillary condensation channel, which in order to minimise corrosion from acidic condensate, may need to be made from advanced materials and can be expensive.

Figure 2.5: Summary of waste heat recovery technologies [6].

2.3 Organic Rankine Cycles

As discussed in the previous section, organic Rankine cycles are characterized by using organic compounds as working fluids. These cycles arise due to the temperature limitation of the available waste heat source. When this is low or medium, the use of a steam Rankine cycle can lead to adverse effects of condensation in the expander, due to the end of the expansion in the two-phase zone of the cycle. This would have very negative effects on the performance of the turbine, due to wear and erosion of the blades by moisture, among other reasons. The use of organic working fluids is beneficial, as will be explained later.

The ORC in it simplest form is presented in Figure 2.6. In this chapter, the main components of the ORC are going to be introduced in order to explain the cycle working principle (2.3.1). One of these components will be explained in more detail due to its importance for the development of this thesis. Later, some of the characteristics of these organic working fluids will be commented (2.3.2), followed by the illustration of different ORC configurations and plant layouts (2.3.3). Finally, the main differences between SRC and ORC will be listed in Section 2.3.4.

As an extensive literature review has been developed in previous works on the Organic Rankine cycle, not much will be devoted to its explanation in this thesis. For further information, it is recommended to refer to R. Agromayor [8], Macchi and Astolfi [17] and I. Encabo [18], among others.

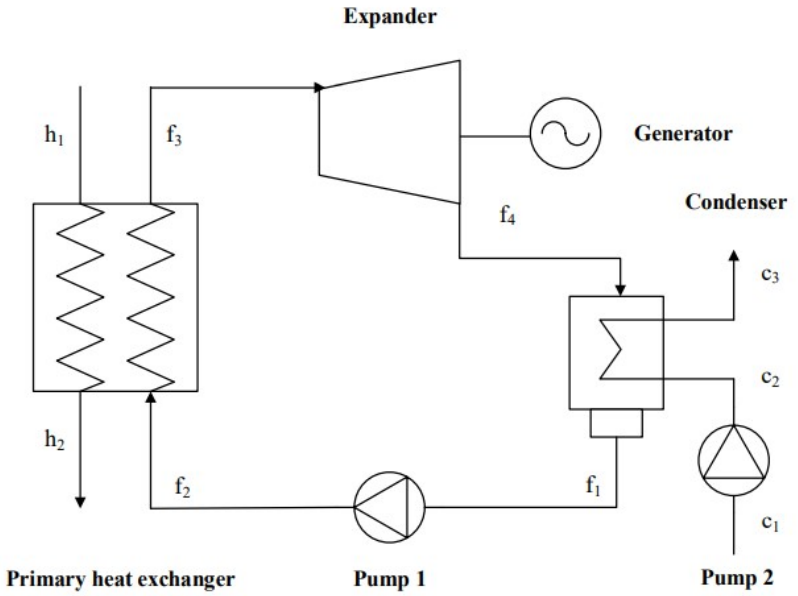

Figure 2.6: Simple Organic Rankine Cycle [8].

Four distinct processes take place in the simple Organic Rankine cycle. In view of Figure 2.6, these are: 1-2 pumping process, 2-3 constant pressure heating, 3-4 expansion process and 3-4 constant pressure heat removal process, as it was explained in Section 2.2.4 for the SRC.

2.3.1 Components

Following the same order of the processes mentioned above, the main components in which these processes take place will be presented. The main ORC components are:

- **Pumps**

  Pumps are used to drive the working fluid to the heat exchanger, and are usually centrifugal. This type of machine is characterized by consuming energy to communicate it to the fluid. This consumption will depend on the configuration of the cycle and the working fluid. In transcritical cycles, their design becomes more complex and is key to the efficient operation of the cycle [18].

- **Primary heat exchanger**

  In this element the heat exchange takes place between the waste heat source used and the cold working fluid. The working fluid comes from the condensate well generally located at the bottom of the condenser, and is evaporated within the primary heat exchanger. There is a wide variety of heat exchangers, and their selection will depend on the application in question. However, their design is another key aspect of the cycle, due to the impact of this element on cost.

- **Expander**

  The expander is the most important element of the cycle, since it is in it where the process by which the mechanical energy is generated, takes place. It is so important that the rest of the thesis will focus on evaluating its behaviour and analyzing the losses that can reduce its performance. There are different types of expanders:

  - Volumetric expanders: this type of expanders is out of the scope of this thesis.
  - Turbomachinery: this type of expanders will be presented in sections 2.4 and 2.5.

- **Condenser**

  Condensers have the purpose of cooling and condensing the gas stream leaving the expander. As with SRCs, the cooling fluids are usually water or air.

2.3.2 Organic working fluids

When selecting the working fluid for this type of cycles, it is important to know what impact the properties of the fluid will have on it, as they will determine its optimum arrangement and the best design of each of its components [18]. These properties are closely related to the performance and cost of the cycle, and are summarized as follows:

- Molecular weight: this property has a direct impact on the compactness of the turbine. As the molecular weight of the compound increases, both the speed of sound and the enthalpy drop in expansion decrease so that fewer stages will be required.

- Molecular complexity: determines the behaviour of the fluid during the adiabatic expansion of dry steam. Depending on this behaviour, the fluid can be dry, isentropic or wet, and the associated expansion process is as shown in Figure 2.7.

  Dry fluids present a positive slope of the saturation vapour curve, while wet fluids present a negative slope and isentropic fluids an infinite slope.

- Critical properties: they have an impact on the size and volume of the cycle. The higher the critical temperature, the larger the size [18].

  Moreover, since organic working fluids present lower critical pressures than water, lower evaporation and condensing temperatures are required. This thermodynamic advantage not only reduces the need of super heating but guarantees dry expansion [18].

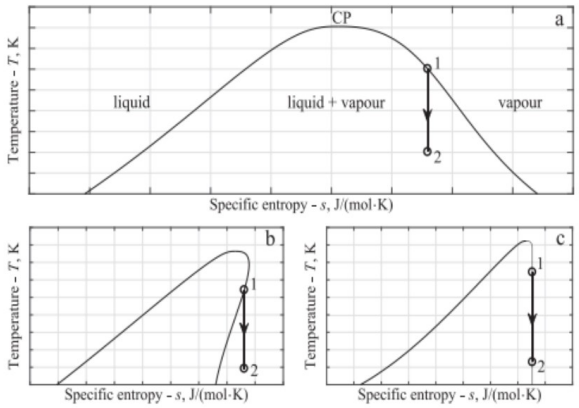

Figure 2.7: Classification of organic working fluids on T-s diagram: dry, wet and isentropic, respectively [19].

2.3.3 ORC configurations and plant layouts

The different configurations in which the Organic Rankine cycle can be used are presented in Figure 2.8. This scheme has been extracted from R. Agromayor in [8], and further details of each configurations are provided in his work.

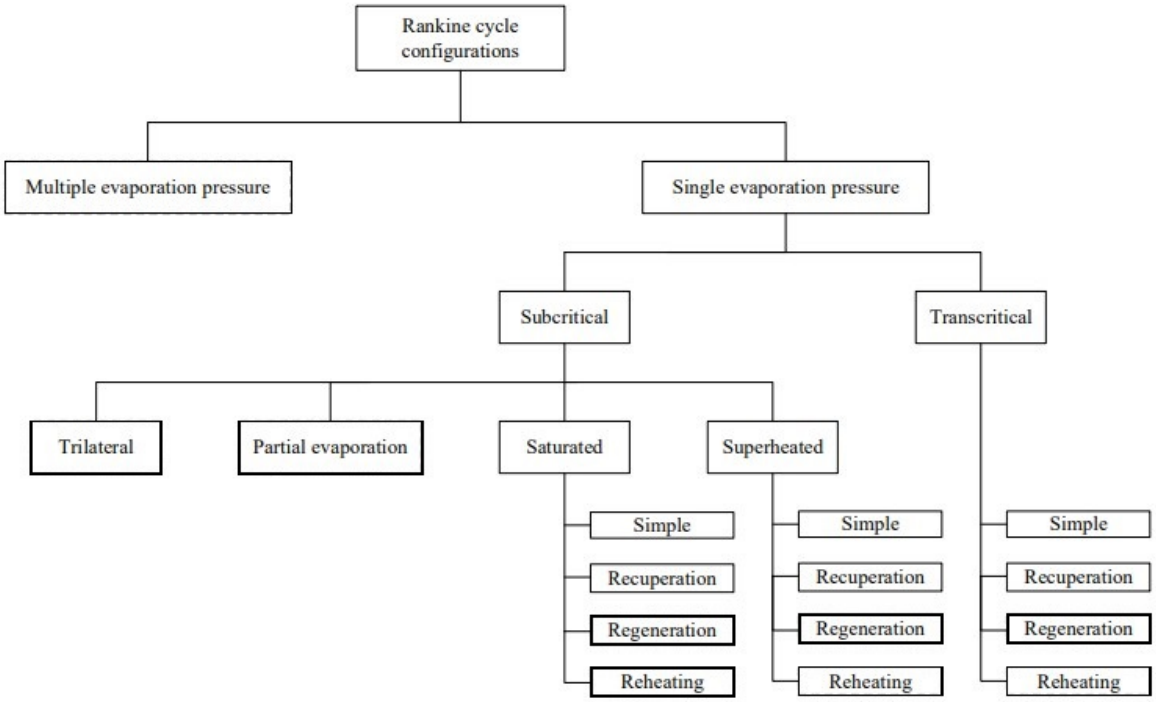

Figure 2.8: ORC configurations [8].

2.3.4 Main differences between Steam and Organic Rankine Cycles

Figure 2.9 shows the T-s diagrams of a Steam Rankine cycle (a) and an Organic Rankine cycle (b), respectively.

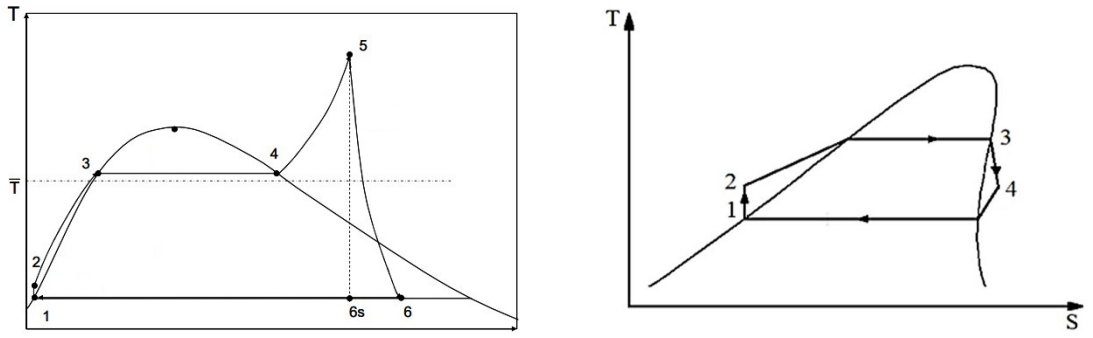

(a) Steam Rankine Cycle

(b) Organic Rankine Cycle

Figure 2.9: T-s diagrams for Steam and Organic Rankine cycles

The main differences between these cycles, as listed in [8] and [20] are:

- Slope of the saturation vapour curve.
- Maximum temperatures: ORC present source temperature levels below $350°C$.

- Back work ratio.
- Condensing pressure
- Specific enthalpy difference.
- Expander design.

Summarizing, the fact of using organic fluids that present a higher molecular weight, allows reaching lower enthalpic drops than in SRC, so that a lower number of stages is necessary, and a higher compactness of the expander is achieved. This will consequently have an impact on the cost. However, the use of this cycle also has its disadvantages when the flow through the expander blades is in the transonic or supersonic regime.

2.4 Thermofluid-dynamic concepts relevant to the study of thermal turbomachines

It has been explained above that the expander is the most important element of the cycle, since it is where the conversion of heat into mechanical energy takes place. This mechanical energy will then be transformed into electricity, generally by means of a generator coupled to the same shaft.

In order to be able to study in more detail the performance of the expander, it is convenient first to present and introduce the principle of operation of turbomachines and the different types that exist, and then to focus the study on one of them. For this, it is necessary to previously introduce the most relevant thermodynamic and fluid mechanics concepts for the study of turbomachines.

2.4.1 Turbomachines: definition, types and working principle

A turbomachine is a device in which energy is transferred either to, or from, a continuously flowing fluid by the dynamic action of one or more moving blade rows [21]. It could be either open, characterized by acting on an infinite extent of fluid, or closed, which acts on a finite quantity of fluid that passes through a casing. In this project, closed turbomachines in which the moving blade rows are attached to a freely rotating shaft will be considered.

The aforementioned fluid is generally a compressible fluid or a fluid that acts as such, and which on its passage through the machine undergoes both, a variation of enthalpy and kinetic energy — according to the first principle of thermodynamics —, and a variation of the amount of kinetic momentum — according to the laws of mechanics. These variations are translated into an exchange of work and mechanical energy with the outside.

Moreover, as it passes through the machine, the compressible fluid, as its name suggests, varies significantly in volume. This variation, together with that of enthalpy and fluid velocity, is strongly related to the design of the machine. Hence the great importance of optimizing the design of a turbomachine in order to obtain a good performance.

Two main types of turbomachines can be distinguished:

- Turbomachines that communicate energy to the fluid by increasing its pressure while absorbing power. Examples of these machines are compressors, pumps and fans.
- Those in which the fluid communicates energy to the machine by expanding the fluid to lower pressure [21], and therefore, power is produced. Steam and gas turbines are some examples of this type of turbomachines.

From here on, the literature review will be focused and the whole subsequent study will be characterized for this last type of turbomachines: turbines.

The one-stage turbine is formed by two main elements in which the expansion process takes place:

- **The rotor** is a cascade of rotating blades that exchanges the mechanical and thermal energy of the fluid passing through the turbine with the mechanical energy of the shaft. As explained, the energy of the fluid decreases producing energy on the shaft.
- **The stator or nozzle section** is a cascade of stationary blades that allows to modify the kinetic energy of the current, increasing it to make it available to the rotor, in the case of a turbine.

The single stage turbine is depicted in Figure 2.10. The fluid moves through the turbine by passing through the ducts that form two consecutive blades, the outer casing and the shaft, resulting in the expansion of the fluid as well as in changes in its velocity. As it can be seen, in a turbine, the stator is followed by a rotor in which the energy exchange takes place.

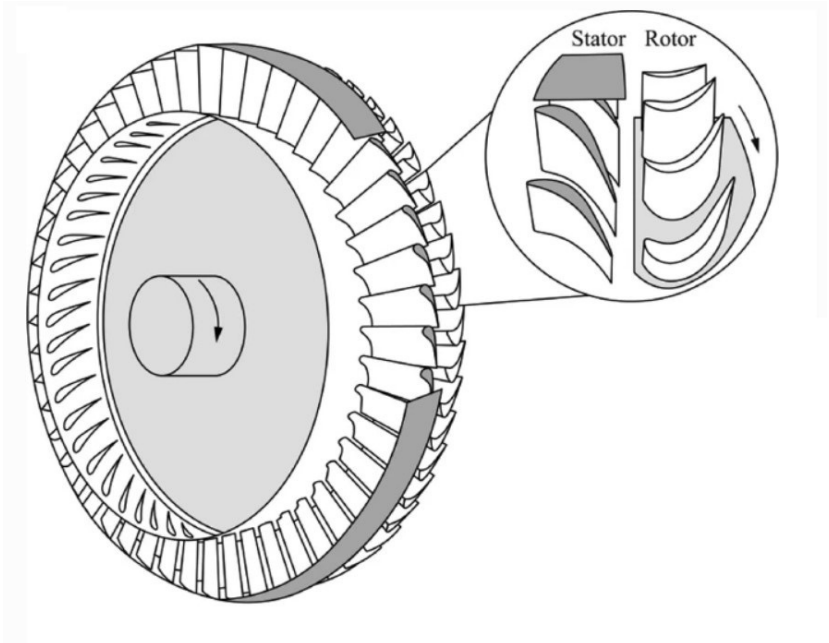

Figure 2.10: Single stage turbine [22].

Since each cascade is formed by equal vanes that give rise to identical passageways, it is sufficient to analyze the evolution of the fluid in a generic inter-vane duct [23]. However, when turbines operate with high enthalpy drops, they need to be structured as a set of single stage turbines placed in series, i.e., as a staggered set. The entire study presented below is based on single-stage staging, due to the compactness required by ORC. It is important to note that this will result in high expansion ratios and may lead to supersonic flows which must be taken into account.

2.4.2 Fundamental laws of mechanics and thermodynamics

Equation of continuity

If a stationary and uniform flow is considered, the mass flow rate, $\dot{m}$ can be related to the density, ρ , the velocity of the fluid on a cross section, c, and the area of the cross section, A, as shown in eq.(2.3):

$$\dot{m} = \rho \cdot c_n \cdot A \tag{2.3}$$

where c_n is the projection of the fluid velocity on the normal of the cross section.

By application of the principle of conservation of mass, the mass flow at the inlet of a control volume, in this case the one formed by the turbine casing, shaft and stage blade rows, is the same as the flow at the outlet.

Even though turbomachines are characterized by having a periodic flow, the approach of stationary and uniform flow (steady flow) can be accepted only if a one-dimensional flow simplification is considered. This simplification consists in regarding as constant the different flow properties across each section of a passage [21], and gives rise to a method of analysis which will be presented and explained in Section 2.7.

First law of thermodynamics

The first law of thermodynamics applied to steady flows between the inlet (1) and outlet (2) of a control volume, yields:

$$\dot{Q} - \dot{W} = \dot{m} \cdot [(u_{spe,1} + p_1 \cdot v_{spe,1} + \frac{c_1^2}{2} + g \cdot z_1) - (u_{spe,2} + p_2 \cdot v_{spe,2} + \frac{c_2^2}{2} + g \cdot z_2)] \tag{2.4}$$

where $\dot{Q}$ is the heat transfer rate in the surroundings of the control volume, $\dot{W}$ is the work rate obtained in the shaft from the fluid expansion, $\dot{m}$ is the mass flow rate, u_{spe} stands for the specific internal energy of the fluid, the product of pressure and specific volume $(p \cdot v_{spe})$ stands for the flow work, $c^2/2$ is the kinetic energy per unit mass and $(g \cdot z)$ is the potential energy per unit mass.

The specific enthalpy is defined as the sum of the specific internal energy and the flow work:

$$h = u_{spe} + p \cdot v_{spe} \tag{2.5}$$

and the stagnation enthalpy, that is the enthalpy of the reference state that the fluid would acquire if it were isentropically braked, is given by:

$$h_0 = h + \frac{c^2}{2} \tag{2.6}$$

If the above equation (Eq. 2.4) is rewritten considering the potential energy negligible, introducing the definitions just presented in Eq. (2.5) and Eq. (2.6), and dividing by the mass flow rate, the following expression is obtained:

$$q - w = h_{01} - h_{02} \tag{2.7}$$

If it is also assumed that the turbine is adiabatic ($q = 0$), a reasonable assumption with respect to what happens in reality in most cases, it is reached that the specific work developed by the turbine is equal to the stagnation enthalpy drop that takes place in the turbine.

$$w = h_{01} - h_{02} \tag{2.8}$$

Second law of thermodynamics

From the second law of thermodynamics, entropy can be defined as:

$$s_2 - s_1 = \int_1^2 \frac{dq_{rev}}{T} \tag{2.9}$$

where q_{rev} stands for the transferred heat in a reversible process. However, if the process presents any irreversibility, the entropy is given by:

(2.10)

It can be concluded from equations (2.9) and (2.10) that if the process is adiabatic and reversible, in other words, in the ideal case of an isentropic process, the entropy remains constant, while the entropy increases in case of an adiabatic and irreversible process [21].

The equations of Gibbs (2.11) and (2.12), which relate state variables and thus can be used in either reversible or irreversible processes, are derived from the entropy definitions given above.

$$T \cdot ds = du_{spe} + p \cdot dv_{spe} \tag{2.11}$$

$$T \cdot ds = dh - v_{spe} \cdot dp \tag{2.12}$$

Assessing the entropy generation within a system is quite important in order to determine the performance parameters. However, "the value of entropy production for a given process does not have much significance by itself" [24]. Real turbines are far from experimenting ideal processes, indeed, irreversibilities are characteristic of turbomachines. To evaluate the entropy generation within the expansion process in a turbine, these irreversibilities (internal and external) are accounted as losses, that can be calculated in different ways. A whole section (2.8) will be devoted to explain the losses in turbines.

Momentum equation

As mentioned in the introduction to this section, not only does the fluid undergo variations in enthalpy and velocity as it passes through the turbine, but it also undergoes a variation in the amount of kinetic momentum.

The momentum equation for a control volume through which a steady flow passes, "relates the sum of the external forces acting on the fluid element to its acceleration or to the rate of change of momentum in the direction of the resultant external force" [21]. It is given by:

$$\sum F_x = \dot{m} \cdot (c_{x2} - c_{x1}) \tag{2.13}$$

Nevertheless, it is when Newton's second law is applied to the moments of forces that the Euler equation of turbomachinery (essential for the study of these machines) can be obtained, through the conservation of angular momentum. This will be presented in detail in Section 2.4.5.

2.4.3 Expansion process and definition of efficiency

As a consequence of the first principle of thermodynamics, it has been seen that in the case of adiabatic turbomachines, the enthalpy variation experienced is equal to the work exchanged with the fluid per unit mass. And if the process is also reversible, the heat exchanged with the outside is equal to the integral of Tds. Therefore, it is reasonable to use T-s and h-s diagrams to represent the different thermodynamic processes that take place in turbines and, in general, in turbomachines.

The stagnation enthalpy, the definition of which has been obtained from the first principle of thermodynamics, can be represented on this diagram as shown in Figure 2.11 (a). In the same way, the expansion process that takes place between two pressures (p_1 and p_2) can be seen in Figure 2.11 (b). If the expansion takes place at constant entropy, i.e. isentropically, in an adiabatic and reversible process, the point 2s is reached. However, the actual expansion process in a turbine follows an irreversible process in which entropy is generated, so that by means of a polytropic curve, point 2 is reached.

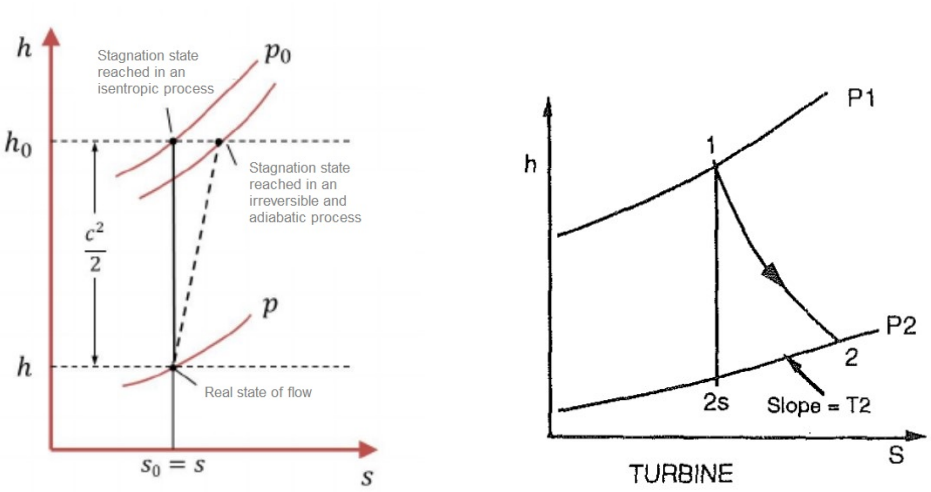

(a) Stagnation enthalpy [23]. (b) Expansion process [25]

Figure 2.11: h-s diagram

Considering the points:

- **1 and 01**: as the entry point to the blade of a cascade and its respective stagnation point.
- **2 and 02**: as the exit point of the vane (and entry point to the next vane, if there is one) and its respective stagnation state.

and by studying the processes presented in Figure 2.11 on the same diagram, one arrives at the diagram in Figure 2.12 in which the complete expansion process through a turbine blade is shown.

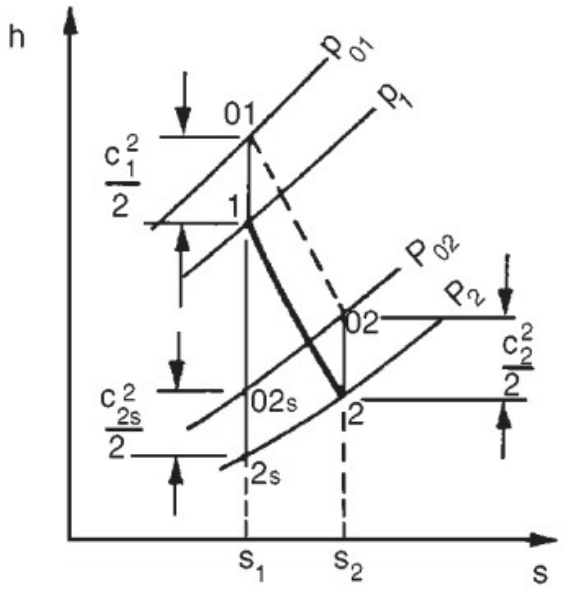

Figure 2.12: Complete turbine expansion process on h-s chart [21].

From this graph, the isentropic or internal efficiency of a turbine can be defined as:

$$\eta_i = \frac{h_1 - h_2}{h_1 - h_{2s}} = \frac{w}{w_{max}} \tag{2.14}$$

where w_{max} is the maximum work output, obtained by an isentropic process.

2.4.4 Compressible fluid and speed of sound

It has already been said in Section 2.4.1 that the fluid that expands in a turbine is generally compressible or acts as such.

Real gasses effects, which involve complex processes "usually take place at the first stages of the expansion in Rankine cycles" [8]. The compressibility factor, z, given by Eq. (2.15) is the thermodynamic property that tells how much a real gas deviates from the ideality. Values of $z < 1$ imply higher density than that of the ideal gas, whereas $z > 1$ implies having a gas with lower density than the ideal gas.

$$z = \frac{p}{\rho \cdot R \cdot T} \tag{2.15}$$

Where R is given by:

$$R = \frac{8.3144598 \ \frac{J}{mol \cdot K}}{M} \tag{2.16}$$

and M is the molar mass of the fluid.

On the other hand, the regime in which flow travels along the turbine depends on the Mach number (Eq.(2.17)), defined as the ratio between fluid velocity, v, and speed of sound, a, given by Eq.(2.18).

$$Ma = \frac{v}{a} \tag{2.17}$$

$$a = \sqrt{\gamma \cdot R \cdot T} \tag{2.18}$$

Where γ is the heat capacity ratio given by:

$$\gamma = \frac{c_p}{c_v} \tag{2.19}$$

Mach numbers larger than 1 imply supersonic flows, in which the fluid's thermodynamic properties change highly towards small changes in velocity due to compressible

effects [8]. This occurs in a convergent-divergent passage, as in order to satisfy the continuity equation the area of the passage must increase towards an increase in the fluid's volume due to a rapid acceleration. This aforementioned convergent-divergent passage is shown in Figure 2.13 under different flow conditions.

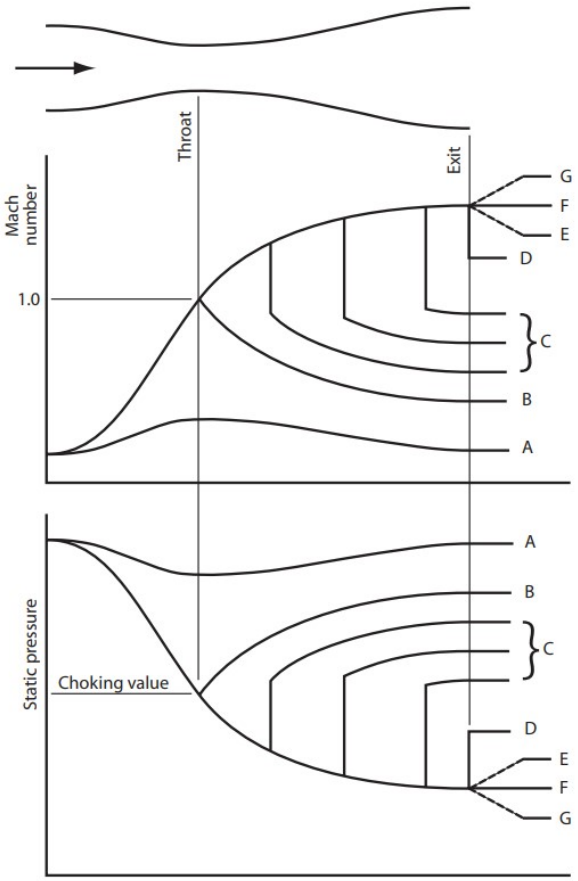

Figure 2.13: Static pressure and Mach number variations in accelerating flow in a straight convergent-divergent passage [26].

As seen in Figure 2.13 the smallest area section is known as the throat and is characterized by the fact that the fluid reaches the speed of sound (Ma=1) and is said to be chocked. This situation of chocked throat is also known as critical condition, and it depends on the turbine's inlet conditions [26].

2.4.5 Energy transformation in thermal turbines: Euler's equation of turbomachinery and rothalpy

In order to understand the fundamental equation of turbomachines, it is necessary to introduce a series of concepts related to the velocities of the flow through the machine.

Two reference systems can be distinguished when analyzing the flow through a stage. An inertial reference system, used to analyze the flow velocities in the stator, which are absolute velocities, and a non-inertial reference system, used to analyze the relative

velocities of the rotor.

The system of absolute stator velocities, generally represented by the letter c, although in this work it will be denoted by the letter v, can be broken down into the following cylindrical components:

- Axial component - v_x
- Radial component – v_r
- Tangential component – v_θ

The relationship between these components is given by:

$$v^2 = v_x^2 + v_r^2 + v_\theta^2 \tag{2.20}$$

The same for the relative rotor speeds, denoted by the letter w.

The relative and absolute velocities are related by means of the blade speed velocity u, given by Eq. (2.21), as shown in Eq. (2.22).

$$u = \Omega \cdot r \tag{2.21}$$

$$\vec{v} = \vec{w} + \vec{u} \tag{2.22}$$

If the angular momentum principle is applied to the control volume formed by two consecutive blades, the casing and the shaft, it is obtained that the torque on the shaft, τ is:

$$\tau = \dot{m} \cdot (r_2 \cdot v_{\theta,2} - r_1 \cdot v_{\theta,1}) \tag{2.23}$$

The torque in the machine will be in the opposite direction:

$$\tau = \dot{m} \cdot (r_1 \cdot v_{\theta,1} - r_2 \cdot v_{\theta,2}) \tag{2.24}$$

From the torque it is possible to obtain the power of the machine, P_i:

$$P_i = \Omega \cdot \tau = \dot{m} \cdot (\Omega \cdot r_1 \cdot v_{\theta,1} - \Omega \cdot r_2 \cdot v_{\theta,2} = \dot{m} \cdot (u_1 \cdot v_{\theta,1} - u_2 \cdot v_{\theta,2}) \tag{2.25}$$

The power can also be expressed as the product of mass flow and specific work w_i:

$$P_i = \dot{m} \cdot w_i \tag{2.26}$$

From this the Euler equation or fundamental equation of turbomachines is derived:

$$w_i = u_1 \cdot v_{\theta,1} - u_2 \cdot v_{\theta,2} \tag{2.27}$$

If this equation is expressed in terms of energy, then:

$$w_i = \frac{v_1^2 - v_2^2}{2} + \frac{u_1^2 - u_2^2}{2} + \frac{w_2^2 - w_1^2}{2} \tag{2.28}$$

On the other hand, from the First Principle of Thermodynamics it has been found that:

$$w_i = h_{01} - h_{02} = \left(h_1 + \frac{v_1^2}{2}\right) - \left(h_2 + \frac{v_2^2}{2}\right) = \frac{v_1^2 - v_2^2}{2} + (h_1 - h_2) \tag{2.29}$$

If equations (2.28) and (2.29) are equated, it follows that:

$$h_1 - h_2 = \frac{u_1^2 - u_2^2}{2} + \frac{w_2^2 - w_1^2}{2} \tag{2.30}$$

It can be seen from equation (2.29) that the specific work originates from the decrease in kinetic energy in the stator and the decrease in enthalpy in the rotor. This decrease in enthalpy in the rotor, given by equation (2.30), in the case of an axial machine in which the radius is conserved, is due exclusively to the acceleration of the relative flow during expansion.

If equation (2.30) is rewritten as follows:

$$h_1 + \frac{w_1^2}{2} + \frac{u_2^2 - u_1^2}{2} = h_2 + \frac{w_2^2}{2} \tag{2.31}$$

as well as the absolute stagnation enthalpy was defined in Eq. (2.6), the relative stagnation enthalpy can be defined considering relative velocity instead of absolute velocity, and by rewriting, one can arrive at the definition of the rothalpy, which remains constant for a flow line along the whole turbomachine as long as the process is adiabatic:

$$h_{01R} - \frac{u_1^2}{2} = h_{02R} - \frac{u_2^2}{2} \tag{2.32}$$

If in addition an axial machine is considered ($u_1 = u_2$), it follows that the relative stagnation enthalpy is conserved:

$$h_1 + \frac{w_1^2}{2} = h_2 + \frac{w_2^2}{2} \rightarrow h_{01R} = h_{02R} \tag{2.33}$$

2.4.6 Degree of reaction

The degree of reaction for a turbine is defined as the ratio between the energy transferred as a consequence of the thermodynamic evolution of the fluid in the rotor and the static enthalpy variation of the stage [21]. It is given by:

$$\Lambda = \frac{h_2 - h_3}{h_1 - h_3} \tag{2.34}$$

If the absolute inlet and outlet velocities at the stage are conserved, the following is obtained:

$$\Lambda = \frac{h_2 - h_3}{h_{01} - h_{03}} = \frac{h_2 - h_3}{h_{02} - h_{03}} \tag{2.35}$$

Reaction influences both "the design of the blades and the performance characteristics of the stage" [27], as it will be seen in the next sections.

2.5 Classification of turbines

There are different types of turbines depending on the architecture or turbine structure, and also depending on the degree of reaction of the stages. In this section, the classification of turbines will be presented. The following sections will focus on one of the types presented below.

2.5.1 According to the architecture and technology

Due to the large number of turbines' applications, different configurations are currently available in the market. Since the cycle that is being studied in this project is the Organic Rankine Cycle, the following classification will be specified for them, as detailed in [17].

- Radial turbines.

  In this type of turbines, the axial component of the velocity is negligible compared to the rest velocity components. They can be classified into:

  - Radial-inward or centripetal turbines.
    In this type of turbines the flow enters the expander in the radial direction and exits in the axial direction. They are usually characterized by having large expansion ratios and low degree of reaction, which leads to highly supersonic flows at the centripetal stator exit [17]. Critical converging and diverging designs are needed, however, relatively low performances are reached within the ORC.

  - Radial-outward or centrifugal turbines.
    This type of turbines in which the flow enters in the axial direction and exits the expander in the radial direction, are "a valid alternative over the classical and traditional solutions" [17]. Some of the advantages of this configuration are for instance, the better capacity to cope with the large expansion ratios, and the capacity of presenting a large number of stages while remaining compact.

- Axial turbines.

  These turbines are characterized by having a radial component of the velocity that is zero or negligible compared to the rest of the components. Thus, the flow enters in the axial direction, or with a certain angle.

  Axial turbines are suitable for low power ranges or small-scale applications, where the specific speed and mass flow rate through the machine are increased. Since increasing the number of stages leads to small entropy drops and thus small power ratings, the number of stages will remain small, leading to high expansion ratios, which may adversely affect the performance of the expanders.

- Hybrid turbine architectures.

  Hybrid architectures combine radial centrifugal or centripetal and axial stages in order to obtain better performances. However, these configurations are still under study.

2.5.2 According to the degree of reaction

Turbines can be classified according to the reaction degree of each stage into:

- Impulse turbines: characterized by having no pressure drop in the rotor, as all the expansion takes place in the stator [27]. $\Lambda \leq 0$.
  - Zero reaction turbines: relative flow is neither accelerated nor decelerated.
- Reaction turbines: in these turbines the relative flow is accelerated. $\Lambda > 0$.

2.6 Axial Turbine fundamentals

The study will focus on axial turbines, since the model that has been used to carry out the thesis has been designed for this type of turbines. Some of the reasons why this configuration was selected are the maturity and development of the technology, and the power ranges used for waste heat recovery applications with ORC.

In order to understand the methodology that has been followed to develop this Master's thesis, some axial turbine fundamentals must be introduced and explained first.

2.6.1 Blade geometry and turbine stage parameters

To begin with, Figure 2.14 shows some of the geometrical parameters of a turbine blade. It is important to know all the variables involved in the design of a blade, since this will determine the amount of work extracted by the turbine and consequently its performance, as explained in Section 2.4.1.

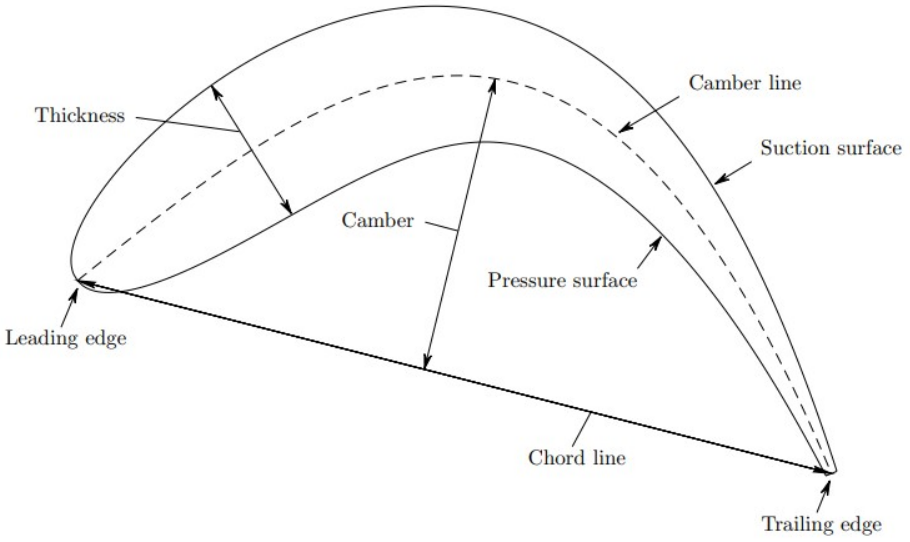

Figure 2.14: Geometry of a turbine blade [8].

A blade is a profiled distribution of thicknesses around a midline, which generally presents a curvature in order to deflect the flow as it passes through the blade. This midline is known as camber line, arc of circumference whose length, l, extends from the leading edge to the trailing edge. The straight line that joins the leading and trailing edges is known as chord line or chord, c, and perpendicular to this line, the distance between chord and camber line is known as camber. The angle between the tangents to the leading and trailing edges is the blade camber angle $\Delta\theta$, which is given by:

$$\Delta\theta = |\theta_{in} - \theta_{out}| \tag{2.36}$$

and is shown in Figure 2.15. In Eq. (2.36), θ_{in} and θ_{out} are the blades' methal angles, angle between the tangential component of the camber line and the axial direction. The blade thickness, t, is the distance between the pressure and suction surfaces of the blade, normal to the camber line [8]. The maximum thickness, t_{max}, and the trailing edge thickness, t_{te}, are also important variables in order to determine the turbines' performance parameters.

The axial chord, c_{ax} is the chord in the axial direction, and it is given by the expression below:

$$c_{ax} = c \cdot cos(\xi) \tag{2.37}$$

where ξ is the stagger angle, angle between the chord line and axial direction, in turn given by:

$$\xi = \frac{1}{2} \cdot (\theta_{in} + \theta_{out}) \tag{2.38}$$

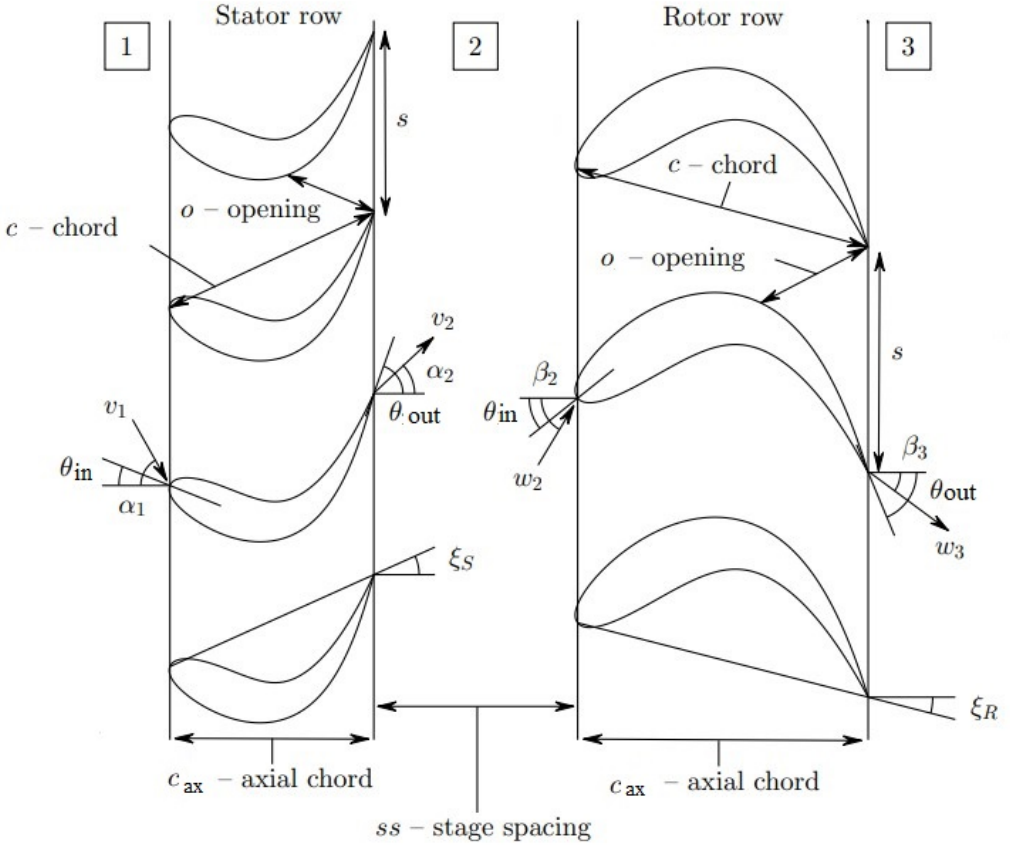

Figure 2.15: Geometry of a turbine stage [8].

The distance between two adjacent blades is known as pitch, s, and the distance between the trailing edge (TE) and the suction surface of the adjacent blade — perpendicular to the outlet methal angle [28]—, is called the opening, o, and can be calculated by using the next expression:

$$o \approx s \cdot cos(\theta_{out}) \tag{2.39}$$

The distance between two adjacent stages is known as the stage spacing, ss, also depicted in Figure 2.15. Another geometrical parameter that derives from the ones described above is the maximum thickness to chord ratio, t_{max}/c, which compares the blade's maximum vertical thickness to its chord, and is important to assess the performance of the blade when it is working at transonic speeds. This variable can be approximated by using the definition provided by Kacker and Okapuu [28]:

$$\frac{t_{max}}{c} = \begin{cases} 0.15 & \text{if } \Delta\theta \leq 40° \\ 0.15 + 1.25 \cdot 10^{-3} \cdot (\Delta\theta - 40) & \text{if } 40° < \Delta\theta < 120° \\ 0.25 & \text{if } 120° \leq \Delta\theta \end{cases} \tag{2.40}$$

Not only variables in the cross-sectional shape of the blades are relevant to the performance analysis of a turbine, but also some geometrical variables in the radial direction have to be considered, and thereby, they are presented in Figure 2.16.

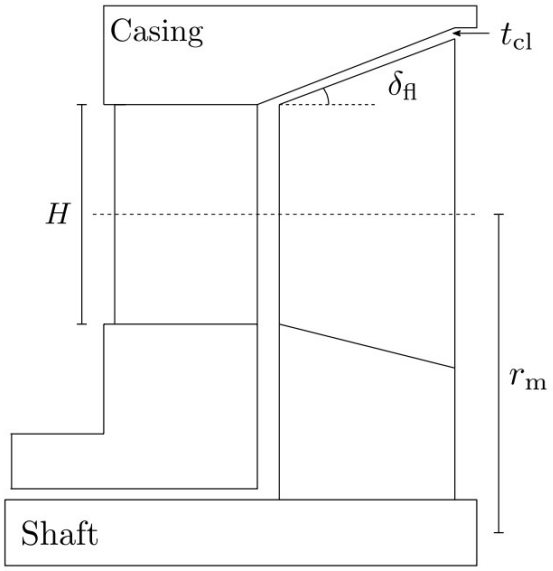

Figure 2.16: Geometry of turbine blades in radial direction [28].

The mean radius, r_m, is the distance between the shaft and blade mean line, and it is considered constant in axial turbines. On the other hand, the mean blade height is given by H, and it is used to obtain the inlet and outlet blade heights. Since the expansion process leads to lower pressure and fluid density, the volume increases significantly, thus, the blade height increases from the inlet through the outlet. This variation is given by the flaring angle, δ_{fl}.

For the stator, the inlet and exit blade heights are given by:

$$H_{in,s} = H_s - tan(\delta_{fl,s}) \cdot c_{ax,s} \tag{2.41}$$

$$H_{out,s} = H_s + tan(\delta_{fl,s}) \cdot c_{ax,s} \tag{2.42}$$

The rotor inlet blade height equals the stator exit blade height ($H_{r,in} = H_{s,out}$), and this equity can be used to obtain the rotor flaring angle as:

$$\delta_{fl,r} = arctan(\frac{H_r - H_{out,s}}{c_{ax,r}}) \tag{2.43}$$

Finally, in the same way as for the stator, the rotor oulet blade height is given by:

$$H_{out,r} = H_r + tan(\delta_{fl,r}) \cdot c_{ax,r} \tag{2.44}$$

Another variable that can be seen in Figure 2.16 is the tip clearance, t_{cl}, gap between the tip of the rotating blade and stationary part of the machine. Only the rotor tip clearance is being considered in this thesis.

Some important ratios towards the analysis of turbine performance are: the pitch to chord ratio, s/c, also known as blade solidity when expressed as c/s, the trailing edge to opening ratio, t_{te}/o, the aspect ratio, H/c, and the hub-to-tip ratio, that is given by:

$$r_{ht} = \frac{r_h}{r_t} = \frac{r_m - H/2}{r_m + H/2} \tag{2.45}$$

Finally, the area at each blade station is given by:

$$A_{station} = 2 \cdot \pi \cdot r_m \cdot H_{station} \tag{2.46}$$

and if the considered station is the blade throat, the expression will be:

$$A_{throat} = A_{station} \cdot cos(\theta_{out}) \tag{2.47}$$

Furthermore, in view of Figure 2.15 it can be noted that the stator inlet is represented by point 1, and point 01 denotes its corresponding stagnation state. Point 2 determines both the output of the stator and the input to the rotor, with 02 being its corresponding stagnation state. Finally, point 3 is reserved for the rotor output.

The stator flow angles are denoted by α_i, where i can be 1, 2 or 3 depending on the turbine station; while the rotor flow angles are denoted by β_i. Note that $\alpha_2 = \beta_2$, since the flow exits the stator at the same angle it enters the rotor.

Some important parameters in the study of turbines that derive from these angles are as follows:

- **Incidence**: in the stator or in the rotor is given by the difference between the flow angle at the blade inlet and the inlet methal angle.

$$i_{st} = \alpha_1 - \theta_{in,s} \tag{2.48}$$

$$i_{rot} = \beta_2 - \theta_{in,r} \tag{2.49}$$

  When axial flow entering the stator is considered, the incidence yields zero.

- **Deviation**: for stator and rotor, it is given by the difference between the flow exit angle and outlet methal angle.

$$\delta_{st} = \alpha_2 - \theta_{out,s} \tag{2.50}$$

$$\delta_{rot} = \beta_3 - \theta_{out,r} \tag{2.51}$$

- **Deflection**: also in stator and rotor, it is given by the difference between inlet and outlet flow angles. The bigger the deflection, the higher the power output.

$$\varepsilon_{st} = \alpha_1 - \alpha_2 \tag{2.52}$$

$$\varepsilon_{rot} = \beta_2 - \beta_3 \tag{2.53}$$

Stage parameters

Together with the reaction degree, Λ, the most important stage parameters used to design the turbine blades which will lead to a specific power output are the flow coefficient, Φ and loading or work coefficient, ψ .

- **Flow coefficient** Φ: "ratio of the meridional velocity to the blade speed" [8]. The meridional velocity v_m is given by:

$$v_m^2 = v_x^2 + v_r^2 \tag{2.54}$$

  and for a purely axial turbine it equals the axial velocity.

  The flow coefficient is given by:

$$\Phi = \frac{v_x}{u} \tag{2.55}$$

  Low flow coefficients imply high deflections and highly loaded blades, which decreases efficiency but requires less stages.

- **Loading coefficient** ψ: ratio of the stagnation enthalpy change across the stage to the square of the blade speed [8]. It is given by:

$$\psi = \frac{\Delta h_0}{u^2} \tag{2.56}$$

2.6.2 Velocity triangles

Based on the design of the velocity triangles, a turbine blade is designed. In other words, the geometry of a blade — which responds to the degree of reaction —, gives rise to what is known as a velocity triangle because it conditions the flow throughout the blades. Figure 2.17 shows a stator and rotor cascade, with its correspondent velocity triangles.

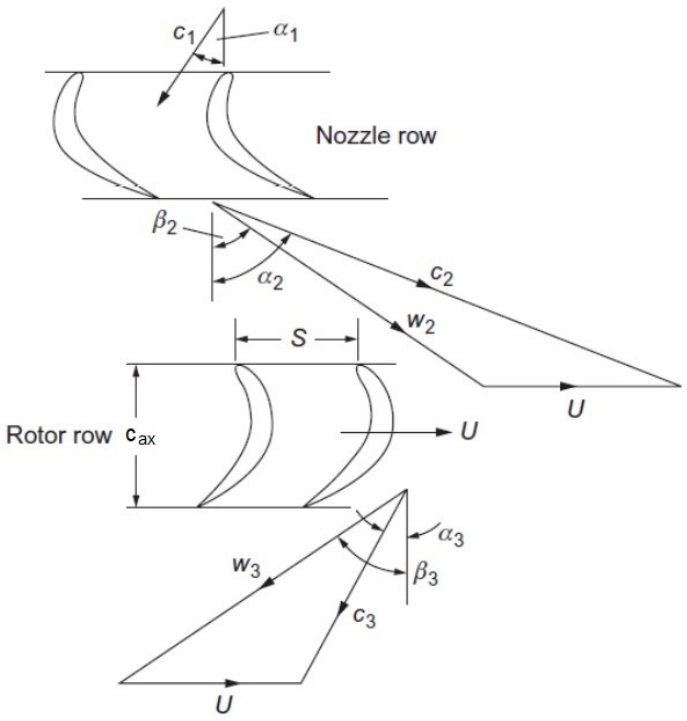

Figure 2.17: Velocity triangles of an axial turbine stage [21].

From the angles described in the previous section and a series of geometric relations, these speeds can be obtained, as indicated below, in order to adapt the nomenclature to that used in the project:

$$v_m = v \cdot cos(\alpha) \tag{2.57}$$

$$v_\theta = v \cdot sin(\alpha) \tag{2.58}$$

$$w_m = w \cdot cos(\beta) \tag{2.59}$$

$$w_\theta = w \cdot sin(\beta) \tag{2.60}$$

2.6.3 Thermodynamic fundamentals and performance parameters

The expansion process taking place within an axial turbine stage can be represented in a h-s diagram as shown in Figure 2.18. This diagram represents both, the blades and the velocity triangles in Figure 2.17 for the same stage, as the h-s diagram of the expansion of a turbine includes both the speeds (absolute and relative) and the main thermodynamic conditions of pressure and temperature. The performance parameters to be defined below can also be represented on this diagram.

An important thermodynamic parameter in the evaluation of turbines is the pressure or expansion ratio. Depending on the considered pressures this ratio can be named differently. The total to static pressure ratio is given by:

$$PR_{ts} = \frac{p_{01}}{p_3} \tag{2.61}$$

Another important thermodynamic parameter, as was explained in Section 2.3 is the inlet stagnation temperature, temperature at which the fluid enters the turbine, represented by T_{01}.

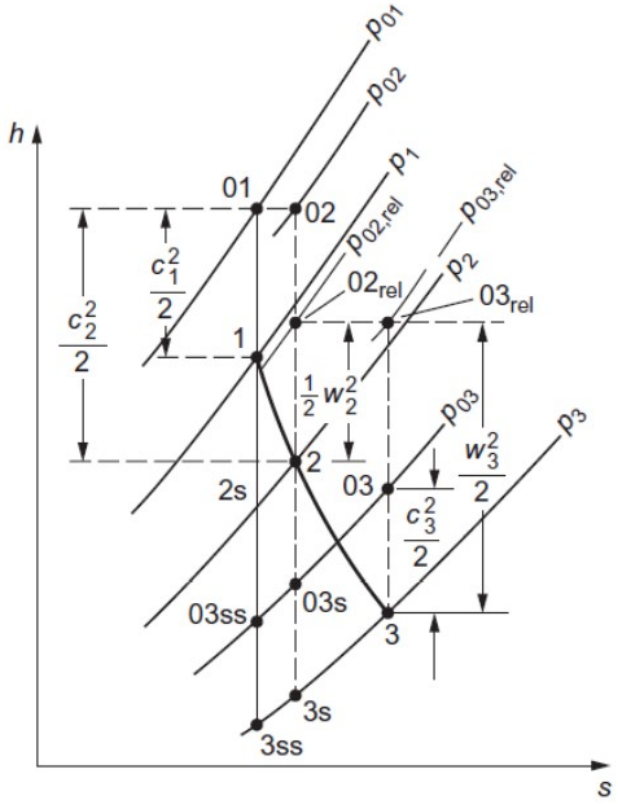

Figure 2.18: h-s diagram of an axial turbine [21].

From this graph the different performance parameters of the turbine can be defined:

- Work Output:

$$w_i = h_{01} - h_{03} \tag{2.62}$$

- Power Output:

$$P_i = \dot{m} \cdot w_i = \dot{m} \cdot (h_{01} - h_{03}) \tag{2.63}$$

- Total to total efficiency:

$$\eta_{tt} = \frac{\text{actual work output}}{\text{ideal work output operating to same back pressure}} = \frac{h_{01} - h_{03}}{h_{01} - h_{03ss}} \tag{2.64}$$

- Total to static efficiency:

$$\eta_{ts} = \frac{h_{01} - h_{03}}{h_{01} - h_{3ss}} \tag{2.65}$$

2.7 Mean-line modelling in preliminary design

Nowadays, there is a growing need to develop accurate models in order to predict important aspects in the study of a given technology. Models are not only used as a strategy for problem solving, but also to enable a systematic understanding of the system that is being modelled [29]. When it comes to the design of an expander for organic working fluids, difficulties can be found due to the number of ORC applications and the large number of available technologies to develop this type of cycle. The use of mathematical modelling "allows for improved design accuracy and the use of modern computer capabilities" [29].

So, the first step in turbomachinery design is to select both, the working fluid — taking into account the properties explained in Section 2.3.2—, and the machine architecture — from the options shown in Section 2.5. Given the power range of ORC applications (few kW_{el} up to some MW_{el}), axial turbines are the best fit for this purpose. After selecting the machine configuration, the design will be driven by fluid-dynamic concepts. The complete schematic of an axial turbine design can be seen in Figure 2.19.

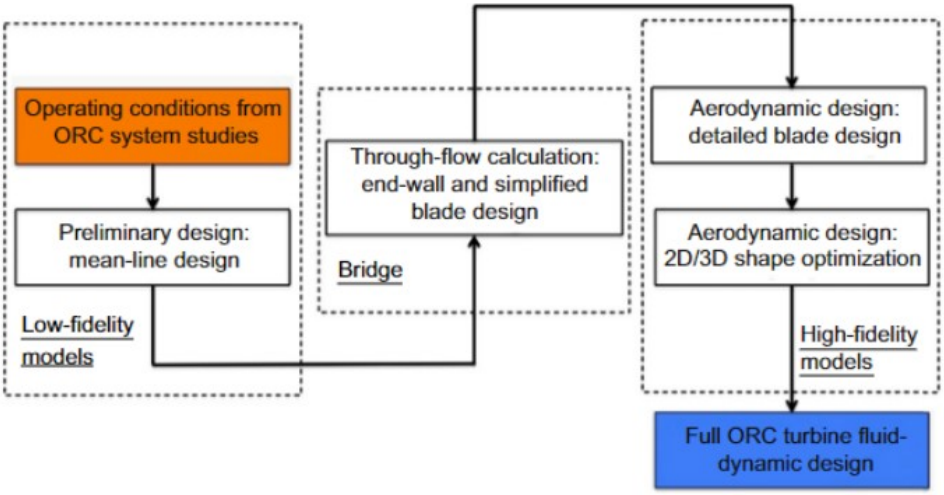

Figure 2.19: Schematic of the fluid-dynamic design process for an Organic Rankine Cycle (ORC) turbine [17].

Different steps have to be followed in order to carry out a complete fluid-dynamic design, and several stages can be distinguished. Each of these stages is characterized by different types of models, which in view of Figure 2.19 are:

- **Low-fidelity models**: characterized by a preliminary mean-line design. This type of models uses simplifications, loss and flow angle correlations, and allows to obtain a reliable turbine design.
- **High fidelity models**: based on an aerodynamic design in which the flow characteristics are predicted by complex schemes.
- **The through-flow model**: is the bridge between the two previous ones.

As the title of this chapter suggests, the present study is focused on the preliminary design, which will be carried out by means of a mean-line model. This type of modelling tool involves a one-dimensional flow simplification that considers all the fluid properties along a blade cascade uniform and averaged at a mean streamline located at the blades' midspans, as depicted in Figure 2.20.

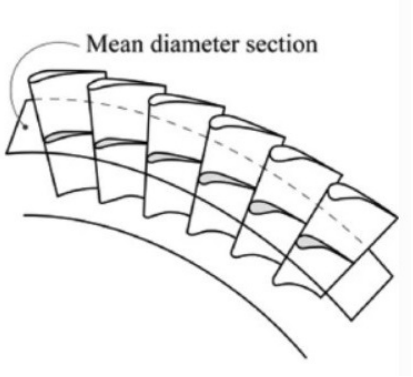

Figure 2.20: Mean diameter section [22].

Before explaining how this one-dimensional analysis is conducted, it is necessary to detail the purpose of the preliminary design and outline the possible starting points taking into account the effects that parameters under consideration have on design.

As Baines detailed in [27], preliminary design is intended to provide a first estimate of the key dimensions in the turbine geometry, as well as the type and number of stages that give a reasonable prediction of turbine performance at design and off-design conditions. Since a detailed knowledge of the turbine geometry is not available at this stage of design, this first estimate should not stray far from the optimum point in order to inspire confidence and achieve an effective tool.

The starting point of the preliminary design depends on the situation the designer is facing. If the starting point is a design that already existed, two cases can occur:

- The design does not require major modifications because the new turbine is similar to the existing one in terms of size, operation and applications. In this case, the preliminary design is reduced to obtaining reasonable predictions of the turbine's performance.
- That it requires major modifications given the significant differences in operating conditions or working fluid of the new turbine, intended to cover slightly different applications than the existing design. In this case, geometric scaling in consistency with the principles of dimensional analysis yields an appropriate and cost-effective modelling technique.

  Scaling has several limitations due to the influence on turbine performance of important conditions related to Reynolds number and other geometrical effects [27]. These limitations require the use of assumptions and empirical correlations that give rise to some uncertainty. Nevertheless, it can be considered an acceptable and useful first estimate in the preliminary design.

On the other hand, if there is no previous design to make changes to and therefore starting from scratch, the preliminary design must begin by considering performance and other requirements [27]. In this case there are also different possibilities of proceeding, all of them assuming the one-dimensional flow simplification. It is very convenient to use the one-dimensional flow simplification in the preliminary design of an axial turbine whenever the ratio between the blade height and the mean blade diameter (shown in Figure 2.21) is small (in the order of $\frac{1}{8} - \frac{1}{10}$).

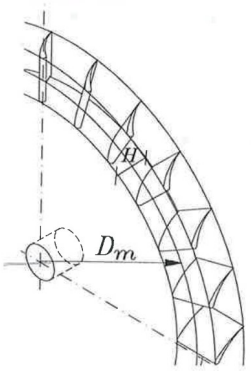

Figure 2.21: Blade cascade [21].

The most widespread way to proceed is the use of mean-line models, which are essential for preliminary design when it comes to predict the turbine performance and obtain an accurate first solution [30].

2.7.1 One-dimensional analysis conducted by a mean-line model

Even though mean-line modelling is the most commonly used technique, not many textbooks include a comprehensive formulation of the preliminary design problem [30], only some scientific publications do. In [30], R. Agromayor carried out a non-exhaustive survey of mean-line axial turbine models in the open literature, which is shown in Figure 2.22.

Reference	Optimization [a]	Stages [b]	Repeating [c]	Diffuser [d]	Properties [e]	Validation [f]
Balje and Binsley [12]	Direct	1	No	No	Incompressible	Exp.
Macchi and Perdichizzi [13]	Direct	1	No	Fixed	Perfect gas	No
Lozza et al. [14]	Direct	1, 2, 3	No	Fixed	Perfect gas	No
Astolfi and Macchi [15]	Direct	1, 2, 3	No	Fixed	Real gas	No
Tournier and El-Genk [16]	No	Any	Yes	No	Real gas	Exp.
Da Lio et al. [17]	No	1	Yes	Fixed	Real gas	No
Da Lio et al. [18]	No	1	Yes	Fixed	Real gas	No
Meroni et al. [19]	Direct	1	No	Fixed	Real gas	Exp./CFD
Meroni et al. [20]	Direct	Any	No	Fixed	Real gas	Exp./CFD
Bahamonde et al. [21]	Direct	Any	No	No	Real Gas	CFD
Talluri and Lombardi [22]	Direct	1	Yes	No	Real gas	No
Denton [8]	No	Any	Optional	No	Perfect gas	CFD
Present work	Gradient	Any	Optional	1D model	Real gas	Exp.

[a] If applicable, type of optimization algorithm used (gradient-based or direct search). [b] Number of turbine stages that the model can handle. [c] Whether or not the model uses the repeating-stage assumption (this reduces the design space significantly). [d] Whether the model accounts for the influence of the diffuser or not. The models that accounted for the diffuser assumed a *fixed fraction* of kinetic energy recovery and did not model the flow within the diffuser. [e] Equation of state used to compute the properties of the fluid. [f] Whether or not the model has been validated with experimental data or CFD simulations.

Figure 2.22: Non-exhaustive survey of axial turbine mean-line models [30].

This leads to the conclusion that there is no single best mean-line model. The choice of one or another will depend on the particular circumstances under consideration due to the assumptions that must be taken accordingly. However, in general a mean-line model can easily be adapted to other situations.

To start with, the diagram in Figure 2.23 shows in a general way the different inputs and outputs of a mean-line model. Depending on the input parameters considered, one or other output variables will be obtained. The model used in this thesis work, unlike the one shown in the diagram, evaluates the kinetic parameters by taking the thermodynamic variables at inlet and outlet as inputs, but this will be further detailed in Section 3.

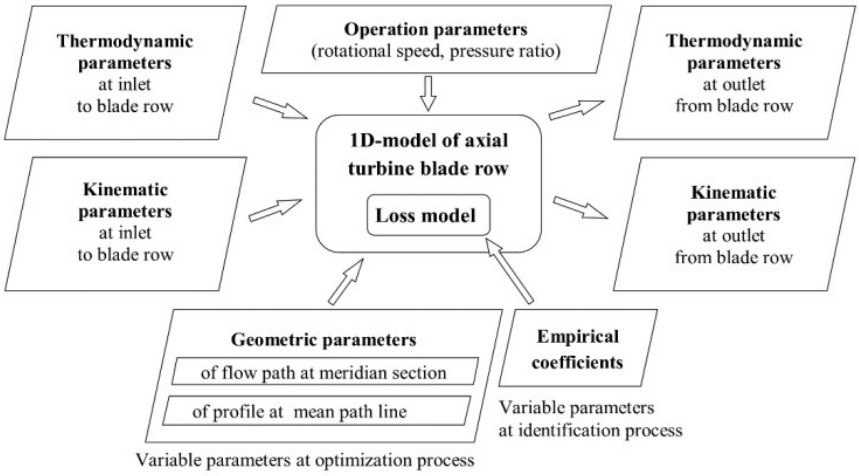

Figure 2.23: Example of preliminary design with a mean-line model of an axial turbine blade row [31].

Mean-line models are characterized by calculating and assessing performance at three stations along the mean streamline: upstream and downstream of the turbine, and between blade rows, as if different control volumes around each blade row were analyzed. This is depicted in Figure 2.24. The advantage of using this analysis tool is that the solution is independent of what happens inside the control volume, so it is not necessary to know the geometry of the blades to be able to give a first prediction of the performance [27].

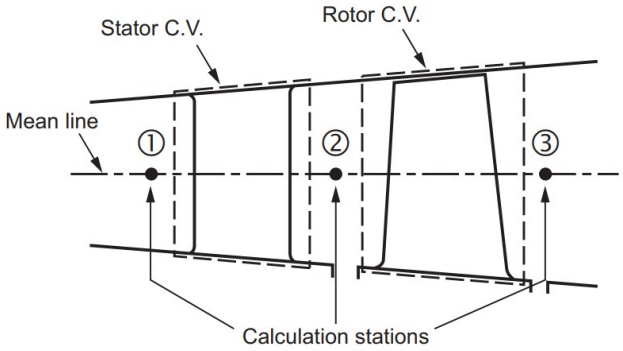

Figure 2.24: Turbine stage mean-line and control volumes [27].

As seen from Figure 2.24, stator and rotor are the two assessed control volumes, being the stations:

1. Stator inlet
2. Stator exit = Rotor inlet → No variation in flow properties between adjacent blade rows is considered.
3. Rotor exit

In each of these stations, once the input parameters have been determined and set, the turbine performance is assessed by means of the following:

- **Equations of state or libraries**

  The equations of state that should be used to compute the different thermodynamic properties in Rankine cycles (density, speed of sound, pressure, dynamic viscosity, entropy, enthalpy, etc.) are the multiparameter equations of state, since they are more accurate and complex and therefore provide greater reliability to the model [8]. Among the different multiparameter equations, those that use temperature-density as an independent variable and "are explicit in the Helmholtz energy function" [8], are being increasingly used for this purpose. They are known as fundamental Helmholtz-energy-explicit equations of state (HEOS).

  In order to compute these aforementioned thermodynamic properties, different libraries containing these HEOS and other models for transport properties [8], such as CoolProp, REFPROP or FluidProp can be used.

- **Balance equations**

  As it had already been introduced in Section 2.4.2, balance equations, also known as conservation laws have to be assessed and satisfied in each stage of the turbine. These are:

  - Equation of continuity or conservation of mass (Eq.(2.3)).
  - Conservation of energy, from the first law of thermodynamics, presented in Section 2.4.2.
  - Conservation of momentum, described in sections 2.4.2 and 2.4.5.

- **Euler equation for turbomachinery and velocity triangles**

  The Euler equation of turbomachinery (Eq.(2.27)) and velocity triangles (Eqs.(2.57-2.60)), also must be evaluated. With the latter, the different flow angles can be obtained.

- **Loss correlations**

  A whole section (2.8.10) within the next chapter is devoted to explain the different approaches to loss modelling. Among the different approaches, loss correlations can be highlighted since they represent an effective way of evaluating the losses through a turbine stage, essential in order to assess its performance. Thereby, they will be further explained in Section 2.9 rather than being presented now.

2.7.2 Examples of mean-line models

Once explained how the one-dimensional analysis is carried out by using mean-line models, two different examples are going to be described in order to introduce the model that has been used for developing the present work (presented in Section 3).

However, before this, it has been decided to include a method that offers a first approximation of the design without resorting to the iteration, characteristic of these models in order to find an optimal solution. Therefore, the options to be discussed are:

- Starting the turbine stage design from reaction, stage loading and flow coefficients.
- Two different examples of mean-line models.

With the aim of not extending this section more than necessary, it has been decided not to include the list of equations used in each of the presented cases here, although the procedure to be followed in each one will be briefly commented.

Starting the turbine stage design from reaction, loading and flow coefficients

Since loading and flow coefficients are related to the specific work output of a turbine stage and the flow rate respectively, they can be considered as useful starting points in preliminary design, together with the degree of reaction, which influences velocity triangles and blade profiles, as explained in Section 2.6.2.

This procedure, detailed by Nicholas Baines in [27], can be considered one of the easiest ways of starting the preliminary design from scratch, since it uses very simple mathematics and no iteration is needed. The design of a turbine stage consists of determining the flow angles and the main dimensions of the blades (radii, chord, etc.), as well as giving a reasonable estimate of efficiency. The estimated value of efficiency can be later updated by using 1D methods or CFD analysis.

From fixed values of the aforementioned dimensionless coefficients, the flow angles can be obtained without knowing the turbine geometry, from the equations presented below (eqs.(2.66-2.69)). However, the main dimensions of the turbine cannot be obtained from these coefficients alone, as it has been shown that they depend on the mass flow rate and other properties of the fluid, such as the density in case it is compressible. Hence, in order to start the preliminary design following this procedure, in addition to the ψ, Φ and Λ coefficients, a series of boundary conditions including the working fluid and the operating point, (i.e. the thermodynamic variables that are determined by the cycle, as well as the blade speed), are necessary.

The energy in the working fluid available for conversion to useful work is fixed by the inlet and exit state. Since all of the energy in the working fluid is available at the inlet, the total state is used for the inlet conditions. For the exit conditions the static state is used instead. This is because "the exit kinetic energy of the fluid is not used in the stage" [27]. Thereby, the boundary conditions that have to be considered are: inlet total stagnation temperature, inlet total stagnation pressure, exit static pressure, and mass flow rate.

In case the power output of the turbine application is specified, one of the aforementioned boundary conditions must be relaxed and calculated from the efficiency estimate. This estimate is obtained from the Smith chart, used as loss correlation, since the starting points are the dimensionless coefficients. Baines proposed a table with the required actions for preliminary sizing of a turbine stage depending on the operating input parameters available in each case. This table is shown in Figure 2.25.

The operating point is not only given by the thermodynamic variables, but also by the blade speed, u, which affects the flow capacity and specific work output and also influences the size of the turbine. It is usually obtained from the rotational speed, which can be either specified or chosen. In the latter case, the choice must be made within a range of rotational speeds that complies with the blade speed limits imposed by the centrifugal stress in the rotating parts [27].

Finally, the blade angles must be determined. Even though blade angles differ slightly from flow angles, it is common assuming perfect guidance in the preliminary design stage, so blade angles will take the same value as flow angles. These are obtained as follows:

- At stator inlet and exit:

$$\alpha_1 = atan\left(\frac{\frac{\psi}{2} - R + 1}{\Phi}\right) \tag{2.66}$$

$$\alpha_2 = atan\left(\frac{\frac{\psi}{2} + R - 1}{\Phi}\right) \tag{2.67}$$

- At rotor inlet and exit:

$$\beta_2 = atan\left(\frac{\frac{\psi}{2} + R}{\Phi}\right) \tag{2.68}$$

$$\beta_3 = atan\left(-\frac{\frac{\psi}{2} - R}{\Phi}\right) \tag{2.69}$$

Baines noted the importance of selecting the dimensionless coefficients, boundary conditions and blade speed on a common radius, often the mean radius. The remaining kinetic and geometric variables that make up the turbine design can then be calculated by means of the equations presented in Sections 2.6.1 and 2.6.2.

This method is not sufficient to provide an accurate preliminary design, since it is based on an estimated efficiency value. Ideally, an iterative process should be carried out in which the efficiency value is refined. This leads to the commonly used method for preliminary design, the mean-line modelling method. Some examples will be presented in the following.

Compressible working fluids		
Case	*Operating point parameters available*	*Action required*
4	p_{01}, T_{01}, p_3, m	None
5	p_{01}, T_{01}, m, P	Estimate efficiency and calculate p_3 from power, mass flow rate and efficiency $\frac{T_{03}}{T_{01}} = 1 - \frac{P}{mC_p T_{01}}$ $p_3 = p_{01}\left\{1 - \frac{1}{\eta_{ts}}\left[1 - \left(\frac{T_{03}}{T_{01}}\right)\right]\right\}^{k/(k-1)}$
6	T_{01}, p_3, m, P	Estimate efficiency and calculate p_{01} from power, mass flow rate and efficiency $\frac{T_{03}}{T_{01}} = 1 - \frac{P}{mC_p T_{01}}$ $p_{01} = p_3\left\{1 - \frac{1}{\eta_{ts}}\left[1 - \left(\frac{T_{03}}{T_{01}}\right)\right]\right\}^{k/(1-k)}$
7	p_{01}, T_{01}, p_3, P	Estimate efficiency and calculate specific work from pressure ratio and efficiency, then mass flow rate from power and specific work $\Delta h_0 = C_p T_{01} \eta_{ts}\left[1 - \left(\frac{p_3}{p_{01}}\right)^{(k-1)/k}\right]$ $m = P/\Delta h_0$

Figure 2.25: Input parameters required for preliminary sizing of a turbine stage for compressible working fluids [27].

Different mean-line models available in the open literature

The first example to be considered is the model proposed by Marco Gambini and Michela Vellini in [22], which develops the Baines approximation, presented above, in order to obtain a more reliable prediction of turbine performance. In addition to using the same input variables, the authors propose the most appropriate ranges for the selection of the dimensionless parameters, as can be seen in Figure 2.26. The full model, which uses the same equations as those mentioned above (in the Baines approach), takes into account the losses occurring in the duct between two consecutive blades to calculate the efficiency, by means of empirical correlations — that are used to compensate mean-line modelling simplifications, such as inviscid flow—, and which will be presented later in Section 2.9. The complete model is shown in the schematic in Figure 2.27.

Parameter	Range
Flow coefficient φ	0.4–0.8
Work coefficient ψ	1.0–1.4
Degree of reaction R	≈0.5
Stage efficiency (starting value)	$\eta_p = f(SP)$

Figure 2.26: Input parameters to M.Gambini and M.Vellini's model [22].

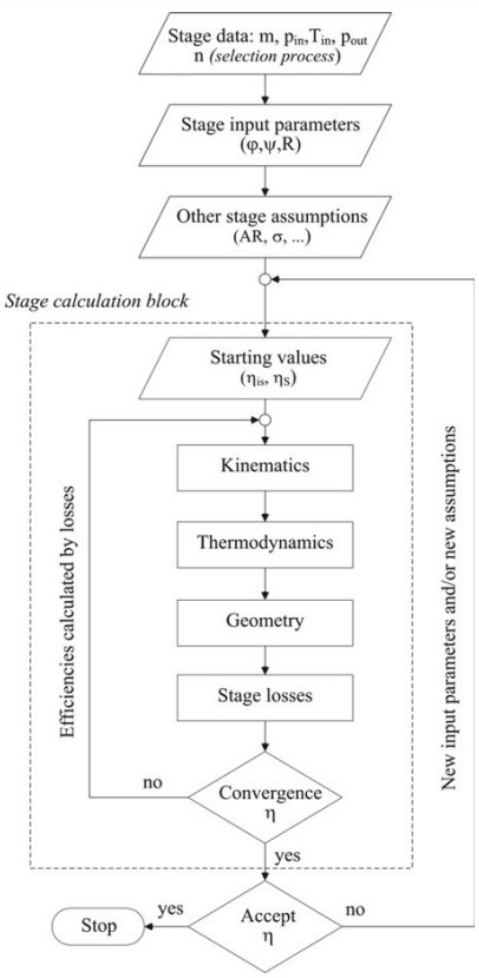

Figure 2.27: Stage calculation block diagram in M.Gambini and M.Vellini's model [22].

On the other hand, similarly to the previous models, the formulation presented by Macchi and Astolfi in [17] distinguishes three categories of input variables as can be seen in Figure 2.28. These authors propose a model for designing ORC turbines. The peculiarity of this type of turbines is the working fluid, which will give rise to arbitrary thermodynamic behaviour [17]. Therefore, they suggest using external libraries such as RefProp or CoolProp, among others, instead of implementing the corresponding equations of state, as well as formulating the balance equations in a general form in order to treat properly subsonic and supersonic flows.

Boundary conditions	**Geometrical constraints**	**Design variables**
Inlet/outlet TD conditions	Blade minimum thickness	Reaction degree
Mass flow rate	Maximum flaring angle	Blade angle/throat
Stage expansion ratio	Hub/tip clearance	Blade chord
Target power	Stator/rotor gap	Angular speed

Figure 2.28: Main input data for mean-line model of a turbine stage [17].

The boundary conditions in this model include the inlet and outlet thermodynamic conditions, mass flow rate and stage expansion ratio, obtained from the thermodynamic assessment. As explained by Baines, the target power can also be a design specification, in which case one of the above boundary conditions must be relaxed, as shown in Figure 2.25.

Geometric constraints must be taken into account, as they represent blade limitations that will negatively influence turbine performance if they are not met.

Finally, there are some design variables such as blade chord, blade angles and throat, angular speed and reaction degree. The choice of reaction is not a completely free variable as it is given to some extent by the constraints and requirements of the application, in particular the flow rate and pressure available [27].

The model proposed by these authors is characterized by the fact that based on the assignment of the main geometrical variables, the flow is evaluated by calculating the different kinetic variables. Finally, if the cascade model is combined with a loss model, as detailed in [17], the following results are obtained: velocity diagrams, meridional channel shape and stage performance prediction.

Furthermore, if the described model is combined with a systematic optimization algorithm, with the different performance parameters as objective function, it results in a highly flexible design tool.

2.7.3 Mean-line modelling solution requirements

As in any model used to predict the response of a system, and even more so in the field of computational fluid mechanics — where it is common to assume a number of hypotheses and simplifications that can lead to considerable errors and uncertainties —, the accuracy of the numerical solution is of great importance. This is because the usefulness of this solution depends on its ability to model the physical problem under study.

The simple fact of developing a numerical model of greater or lesser complexity does not guarantee the accuracy and predictability of the answer. It is necessary to verify that the assumptions used during modelling give rise to acceptable predictions. This is done by comparing the model predictions with reference data. Verification consists of ensuring that the algebraic equations and algorithms used to implement the model, work correctly, taking into account any possible discretization errors [32].

However, model verification is not sufficient to draw a conclusion from the results obtained with the model. It is necessary to check whether the equations used are adequate to represent the real physical problem. This is done by validating the model. Some comments on model validation will be done after presenting the different losses that take place in an axial turbine blade passage and in the methodology section. It is very important to understand the flow patterns and losses that arise in a turbine duct as a consequence of their complexity, for modelling purposes. For this reason an extensive literature review has been carried out in this topic, and a summary will be presented in Section 2.8.

2.7.4 Optimization

This section, in which the basics of optimization are going to be presented, should be included in order to make the mean-line model an efficient and powerful tool for design. To optimize is to seek the best way for carrying out something. When combined with mathematical models, the previous definition takes on a slightly different nuance. To optimize a mathematical model is to seek the best way for solving the problem for which the model is being used. Furthermore, is seeking the variables that lead to the best possible solution. This can be easily done by means of optimization algorithms.

Naturally, the optimization problem in the present work is the preliminary design of ORC single-stage axial turbines. It can be set as any other optimization problem by first selecting that "best possible solution" in terms of an objective function, that could be either maximized or minimized. It is to be expected that those variables that lead to the sought maximal or minimal solution also have to be selected. It is also necessary in any optimization problem to restrict the search space for these solutions in order to avoid spending in the optimization more time than required. This is normally done by means of bounds and constraints, which together with the above presented elements of optimization will be explained in the following.

- **Objective function**

  The objective function f is the variable to be optimized. As detailed in [8], optimization algorithms are usually designed to find the minimal value for the objective function, however, this can be easily changed to maximize the objective function by using a minus sign, as shown:

  $$\text{Minimize} \hookrightarrow f \tag{2.70}$$

  $$\text{Maximize} \hookrightarrow -f \tag{2.71}$$

- **Degrees of freedom**

  The degrees of freedom in an optimization problem are those variables that are going to be studied and varied independently [8], in order to find the best combination that optimizes the objective function. It is important to keep the number of variables as low as possible, since the complexity and computational cost of the problem increase exponentially with the degrees of freedom. For this purpose, sensitivity analyses are highly appreciated, since they give an idea of how the different variables in the model are related and may lead to efficient choices of degrees of freedom. They are usually provided in a vector, for instance $\mathbf{x}$.

- **Constraints**

  As explained above, constraints are used to limit the search space — which also increases with the number of independent variables —, and reduce the time and cost invested in the optimization. There are different types of constraints. The simplest case is to establish lower and upper bounds (lb and ub respectively) for each of the variables that make up the degrees of freedom of the problem [33], as they are computationally more easily handled than the other types of constraints, namely equality and inequality constraints.

While inequality constraints (c_{ineq}) are characterized by establishing boundaries that must not be violated when looking for the optimal solution [8], equality constraints (c_{eq}) can be seen as conditions that the optimal solution must fulfill to be considered feasible. The latter are always active (by definition), since they are necessary to be able to "accept" the provided solution. However, inequality constraints are active when, being the constrained variable in the limit, the equality sign is satisfied, as explained in [8].

With this, an optimization problem may look as the one presented below [18]:

$$\min f(\mathbf{x}) = \begin{cases} lb \leq \mathbf{x} \leq ub \\ c_{ineq}(\mathbf{x}) \leq 0 \\ c_{eq}(\mathbf{x}) = 0 \end{cases} \tag{2.72}$$

- **Algorithms**

  Algorithms are often used to address the above presented optimization problem. Depending on the nature of the problem two different types of algorithms can be used:

  - Gradient-based algorithms:
    They are used for models with smooth constraints and objective function. Gradient-based algorithms are characterized by a short convergence time, not being independent from the initial guess provided for the degrees of freedom and for providing optimal local solutions rather than global [8].
  - Direct search methods:
    This type of algorithms is often used when the computational model is not smooth [8]. Unlike gradient-based algorithms, these methods operate independently of the gradient of the objective function and are noted for their speed in identifying candidate regions within the search space. Even though global optimal solutions are more likely to be found, the speed of convergence is often considerably slower than that of gradient-based methods.

The settings for the optimization problem considered within this work will be presented in Section 3.1.3.

2.8 Flow and losses in an axial turbine blade passage

Although the study presented so far has used the simplification of one-dimensional flow, the flow through the blades of an axial turbine is not only three-dimensional, but also highly viscous and unstable [34]. It is controlled by two main influences and some secondary effects that apply to all turbines and working fluids [26], both of them being responsible for changes in pressure forces due to the occurrence of a normal pressure gradient influencing the static pressure. These are:

- **Fluid acceleration**: which originates from the changes in passage area normal to the flow direction, in turn dependent on the degree of reaction.
- **Streamline curvature**: which depends on the shape of the blade passage.

The complexity of the flow is accentuated due to the effects of viscosity and fluid compressibility. Thus, different flow regimes (subsonic, transonic, supersonic), and different regions of laminar and turbulent flow, subject to these large pressure gradients can give rise to phenomena such as shock waves, flow rotation and boundary layers, among others. Some of them will be introduced in the following.

These aforementioned flow effects along the turbine blade can be seen in Figure 2.29. The main consequence of flow complexity is the negative impact on turbine performance, as the work output decreases significantly. These phenomena are called losses, and must be considered individually to be able to understand how they particularly influence the turbine. However, "loss-generating processes are interrelated and interact" [26], thus, any division is artificial and implies several simplifications that will lead to some uncertainty when calculating the turbine performance.

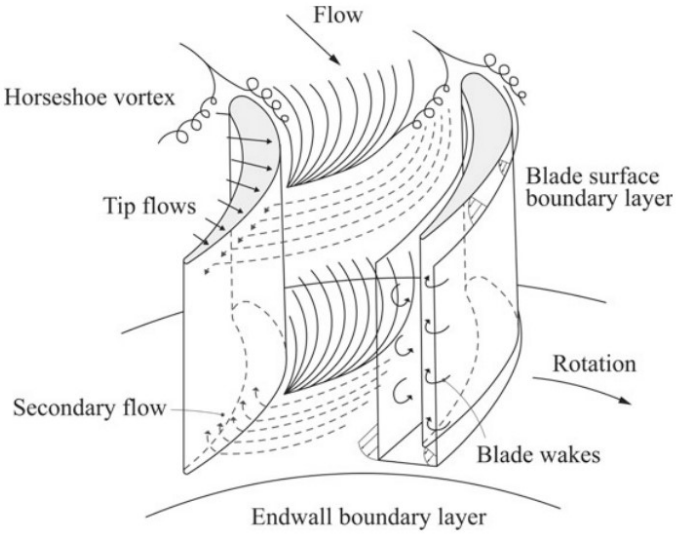

Figure 2.29: Flow along a turbine blade [22].

Losses can be classified into two groups: first and second type of losses. The first, also known as internal losses, is the one that takes place within the turbine annulus and accounts for entropy generation, hence for the decrease in power output due to the aforementioned irreversible flow effects; while the second, external losses, accounts for power output reduction due to mechanical features related to the turbine construction. Since this type of losses does not have any influence on the isentropic efficiency [8], only internal losses are going to be discussed individually, although both occur simultaneously while the flow passes through the duct of the turbine stage, and must therefore be included when predicting the stage or the whole turbine performance.

In order to quantify losses within a turbine blade passage, a loss coefficient is used. Several loss coefficients have been defined but, for the present work, the pressure loss

coefficient has been considered in order to assess the performance of the turbine and will be introduced in Section 2.8.9.

The overall loss coefficient used to account for internal losses is generally divided into: profile, secondary or endwall, tip clearance and trailing edge losses. However, there are other losses that greatly influence turbine performance when the operating conditions are not precisely the design conditions. Examples of these are incidence and shock wave losses, which will be also discussed in this chapter, due to their importance in ORC turbines.

2.8.1 Profile loss

It has been previously mentioned that as the flow passes through a row of blades, due to the effects of compressibility and viscosity, boundary layers can be generated on the pressure and suction faces of the blade, as shown in Figure 2.30 (a). Blade boundary layers start to form at the leading edge and are characterized by a gradient of streamwise velocity in the normal direction [26], as can be seen in Figure 2.30 (b), from zero at the surface to free stream velocity at the outer limit.

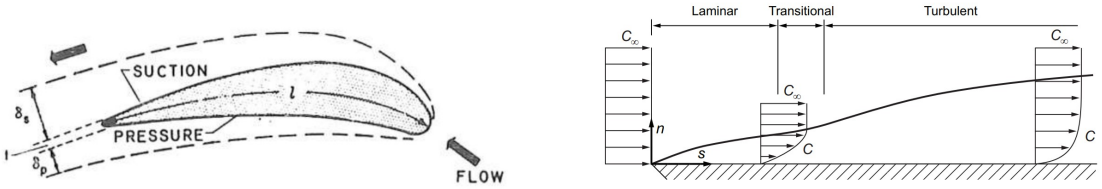

(a) Blade boundary layers [35].

(b) Boundary layer development and transition [26]

Figure 2.30: Origin of profile losses

Flow in boundary layers can be either laminar or turbulent, differing essentially in boundary layer thickness, flow velocity gradient, and in the various effects that result from these characteristics, such as wall shear stress or frictional drag. The development and transition of blade boundary layers from one state to another is complex since it is subject to many influences, such as blade surface velocity distribution, curvature and roughness, incidence angles, Mach and Reynolds numbers and free stream turbulence, among others. Laminar boundary layers are thinner and give less blockage than turbulent boundary layers, which present higher wall shear stress and frictional drag than the former, due to the variation in the velocity profile [26], also seen in Figure 2.30 (b).

At the beginning of the chapter it was said that both, degree of reaction (for its influence on blade passage area and flow acceleration) and surface curvature, had an effect on the pressure gradient along the blade. Adverse pressure gradients — due to blade loading and high angles of incidence —, and skin friction on the blade surface, lead to entropy generation and give rise to the well-known profile losses which occur in the inner part of the boundary layers, also known as primary region, with greater influence on the suction surface, as depicted in Figure 2.31. On the other hand, the outer regions of the boundary layer are mainly affected by streamwise pressure gradients, which lead to

secondary flows and are much more frequent in turbines than adverse pressure gradients [26]. However, the higher the blade loading, the higher the work output and the more likely these adverse pressure gradients are. And the higher the adverse pressure gradient, the higher the profile losses. In the case of a reaction turbine stage, where expansion takes place in the rotor, the relative flow is accelerated while the pressure decreases in the flow direction. Hence, the profile losses will be lower in reaction stages than in equivalent impulse stages.

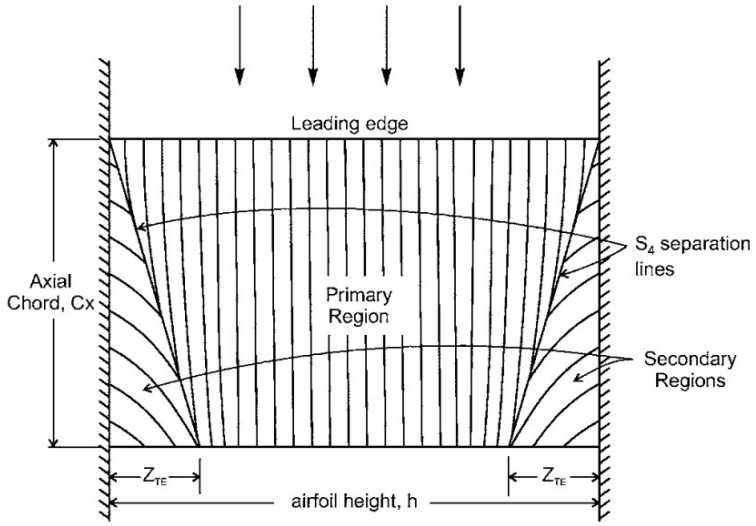

Figure 2.31: Different regions of the boundary layer on the suction blade surface [36].

It is not easy to control the state of the boundary layer at any part of the blade as the above mentioned influences on the transition are interrelated and have a complex effect on losses. Some of these influences are shown in Figure 2.32.

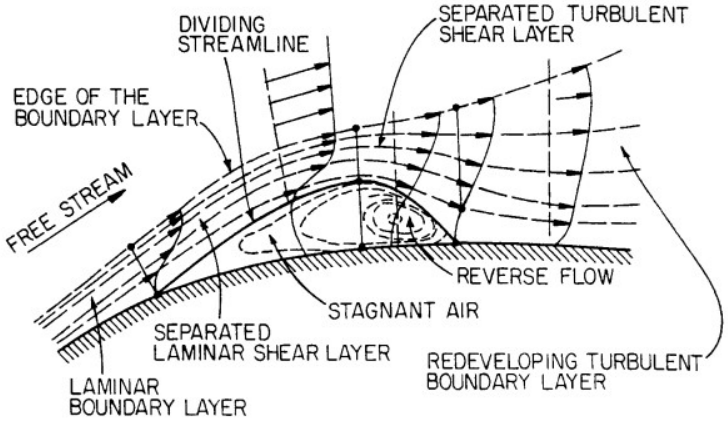

Figure 2.32: Influences and effects in laminar and turbulent boundary layers [34].

Wall shear stress increases with the increase in the normal velocity gradient, as a consequence of a raise in the free stream velocity. This increase in velocity in turn increases the Reynolds number, and the bigger the Reynolds number, the smaller the wall shear stress. From this it can be concluded that simplifications and assumptions are needed when it comes to model the development of the boundary layer.

The dividing streamline in Figure 2.32, indicates stall and the beginning of the separation of the boundary layer. It starts at the point in which the innermost flow within the boundary layer comes to rest, after decreasing its velocity when facing an adverse pressure gradient. As the flow separates it originates a region of reverse and stagnant flow that causes the growth of the boundary layer thickness and drag force [26]. Once stall and separation take place, the flow can undergo two processes. The first is that the flow reattaches to the blade surface due to a change in the pressure gradient, forming a so-called separation bubble. The state of the flow once reattached is difficult to predict. On the other hand, the separation can reach the trailing edge of the blade, causing a considerable loss of momentum due to the thickness of the wake. This will be considered further below.

Another consideration is the significant dependence of profile losses on Reynolds number and surface roughness, depicted in Figure 2.33, in which the Reynolds number has been calculated by using the blade chord as characteristic length and fluid conditions at the outlet [22].

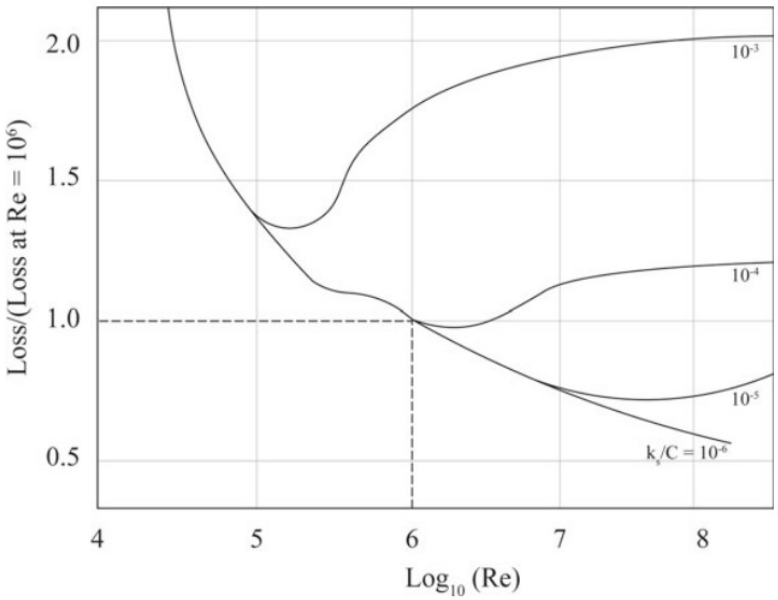

Figure 2.33: Variation of profile loss with Reynolds number and surface roughness [22].

It can be said from Figure 2.33, that for low Reynolds numbers (within the laminar region of the boundary layer), losses are high, whereas in the turbulent region (high Reynolds numbers), losses are greatly affected by the surface roughness — also calculated to the blade chord —. For this reason, the blade chord is considered as one of the geometrical parameters that affect profile losses. Other important and influential parameters are the blade pitch and thickness, as they have a considerable effect on the flow incidence and deflection.

2.8.2 Secondary or endwall loss

As can be seen in Figure 2.29 and as just discussed above, primary flow through the blades, as subject to boundary layer viscous effects, is deflected and turned inwards towards the blade suction surface side of the passage [26], giving rise to a secondary flow. This secondary flow, driven mainly by static pressure gradients, generates a series of losses in the suction surface endwall corner where the so-called annulus or endwall losses also take place.

These two sources of loss are the most difficult to predict, since unlike the flow that causes the profile loss component, the secondary flow is an inviscid phenomenon, and therefore does not give rise to entropy generation per se. The secondary flow is caused by the falling cross-passage pressure gradient due to the turning of the flow when entering the blade passage. The vorticity of the flow is in turn a direct result of viscous shear at the endwalls [25], as shown in Figure 2.34, which is caused due to the endwall boundary layers. For this reason, both sources of loss are usually considered together for modelling purposes and are known as secondary losses or preferable endwall losses. In turbines, they typically account for 1/3 of the total losses. Although they are often considered together, they are going to be explained separately in order to facilitate the understanding of the mechanisms deriving from each of them.

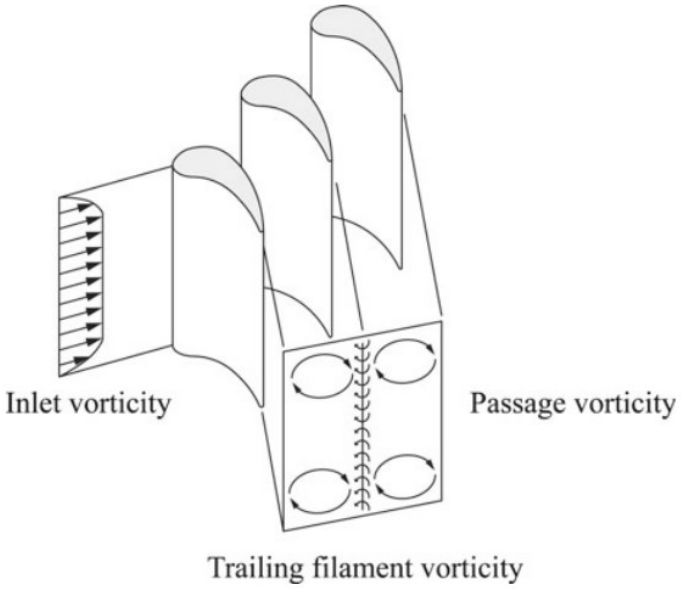

Figure 2.34: Vortices on a plane perpendicular to the main flow [22].

The reason why the secondary flow rotates inwards towards the suction surface side of a blade passage when facing a cross-passage pressure gradient is the difference in radii of curvature between the streamlines at the endwall and the free stream, in turn due to the difference in velocities, shown in Figure 2.30 (b). As the secondary flow rolls up it forms a passage vortex that moves along the duct and tends to stay close to the suction surface endwall corner. The vortex formation and movement along the blade passage is illustrated in Figure 2.35.

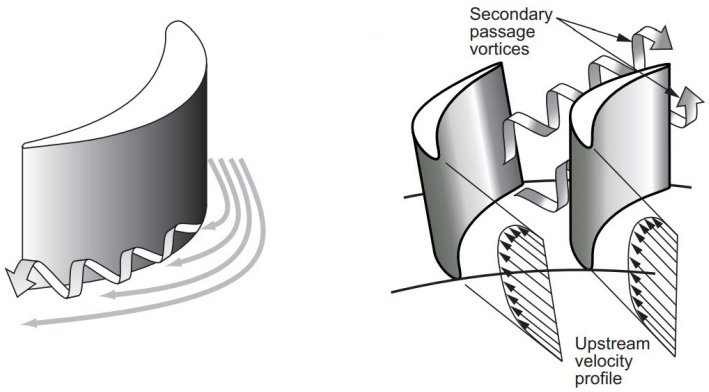

Figure 2.35: Schematic diagram of secondary flow vortex formation and passage vortices [26].

On the other hand, the endwall boundary layer surrounds the leading edge of the blade also rolling up into a vortex consisting of two legs. This vortex also suffers the effect of the pressure gradient that crosses the passage. As it can be seen in Figure 2.36, the leg in the pressure side of the passage is driven towards the suction surface of the adjacent blade removing big part of the boundary layer fluid [26], while it mixes with the passage vortex; whereas the leg in the suction side is kept close to the suction surface. As it can also be seen from the figure, the suction and pressure legs of the vortex created by the endwall boundary layer rotate in opposite direction. This leads the suction side vortex to delay mixing, being able to last until the trailing edge. This two-legged vortex is known as horseshoe vortex, due to shape it forms in a section perpendicular to the endwall, as it can be seen in the right schematic in Figure 2.36.

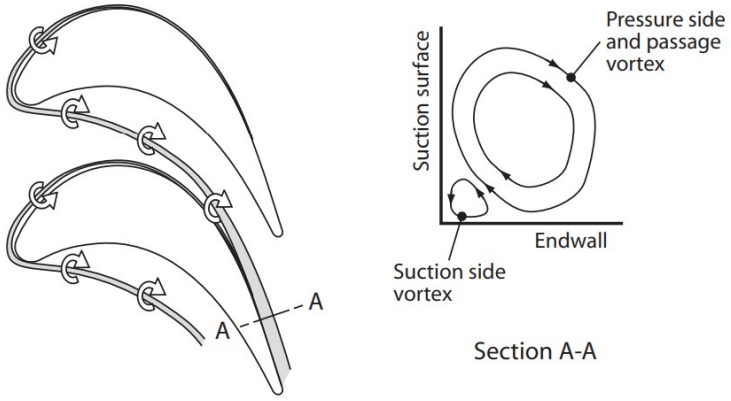

Figure 2.36: Schematic diagram of horseshoe vortex formation and effects [26].

As explained, passage vortices interact with the horseshoe vortex at the suction surface endwall corner, where the mixing process takes place. This phenomenon is what causes the secondary losses to form, generating entropy. As detailed in [26], this energy dissipation may continue downstream of the trailing edge, where the vortices merge the mainstream flow, as will be explained in Section 2.8.4. These interactions can be understood by taking a look to Figure 2.37.

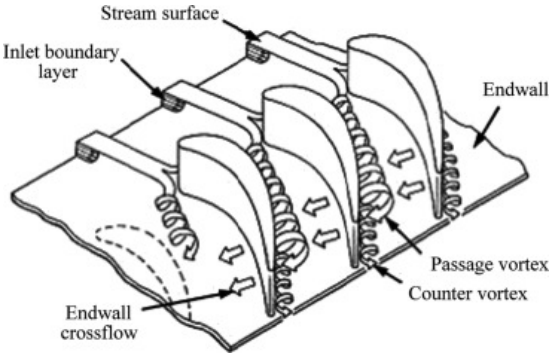

Figure 2.37: Secondary flow vortices [37].

As it can be deduced from the figure above, the parameters that most influence endwall losses are the thickness of the inlet boundary layer, which may have started upstream the leading edge [26], the Mach number and some geometrical parameters of the blade, such as aspect ratio, pitch to chord ratio and turning angle. The latter has an important effect on secondary losses, and introduces a considerable deviation as the endwall boundary layer moves between stator and rotor rows.

When the turning angle is high, the pressure gradient increases, and as mentioned before, the secondary flow increases consequently causing in turn an increase in the blade load. Blade loading acts on the strength of the pressure gradient [26], and it is also affected by the pitch to chord ratio. On the other hand, an increase in the aspect ratio causes the secondary flow at the endwall to increase, decreasing secondary losses, since it influences the extent of fluid affected by the passage vortex. Something similar happens when the Mach number is high: the thickness of the boundary layer is reduced and the effect of these losses in the boundary layer is diminished [38], keeping the vortices near the endwall.

2.8.3 Tip clearance loss

The turbine tip clearance gap — interface between the casing and blade tips — leads to a leakage flow that originates the well-known tip clearance losses, generally in the rotor blades since no tip clearance is considered in the stator when stator blades are attached to stationary annuli at tip and hub [27].

The proximity of the leakage to the turbine casing can cause the interaction of this type of losses with the just explained endwall losses, as shown in Figure 2.38. A tip leakage vortex is formed and driven by the cross-passage pressure gradient into the blade passage leading to very complex flow patterns. The leakage flow is an important source of inefficiency in turbine performance since it does not only not contribute to the expansion process, but it also reduces the flow through the blade passage, in turn reducing the work output. Moreover, tip leakage flow causes changes in the flow conditions at the blade exit, as well as in the flow capacity of the blade row [27].

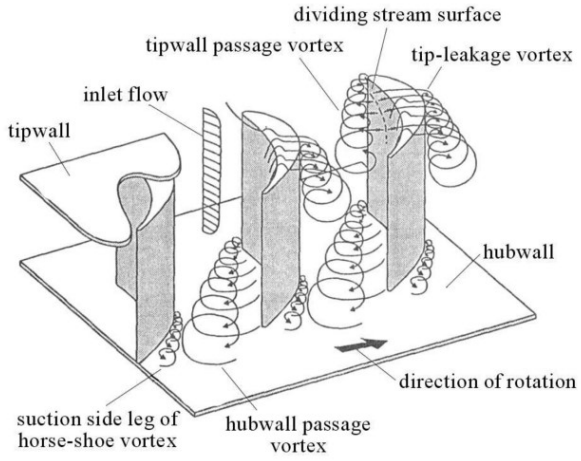

Figure 2.38: Tip leakage and passage vortices at the tip endwall with a clearance [39].

As expected, tip clearance losses increase with both, tip clearance thickness and aspect ratio, which depend on the turbine design and construction. Sometimes, shrouds are incorporated to the tip of the blades in order to reduce the leakages, however, centrifugal losses are increased due to higher stresses. Figure 2.39 shows a shrouded and unshrouded blade.

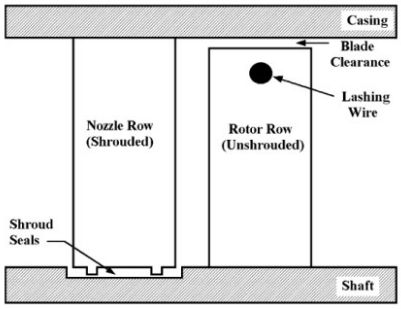

Figure 2.39: Axial turbine stage with shrouded and unshrouded cascades [40].

As it can be seen in Figure 2.40, losses in these two types of blades are different. In shrouded blades (a), a jet is formed once the leakage flow in its path from the leading to the trailing edge, passes through a fin seal used to limit the flow rate [26]. This jet mixes in the clearance space within an irreversible process that causes a reduction in the meridional component of velocity without influencing the tangential component. The difference between these two components in velocity due to a direct pressure ratio across the blade row [26], will lead to a swirl when the leakage flow meets again the main flow, in turn leading to additional mixing losses [39].

On the other hand, with unshrouded blades (b) as explained, the tip leakage flow separates from the endwall leading to a tip leakage vortex due to an adverse pressure gradient on the suction blade surface [39]. Mixing processes and losses also take place while the leakage flow passes through the tip clearance gap, as secondary flows are created and the work output is reduced. However, unlike tip clearance losses in shrouded blades, these mixing process are only a part of tip clearance losses in unshrouded blades. Blade loading and shape influence the leakage flow in this type of blades.

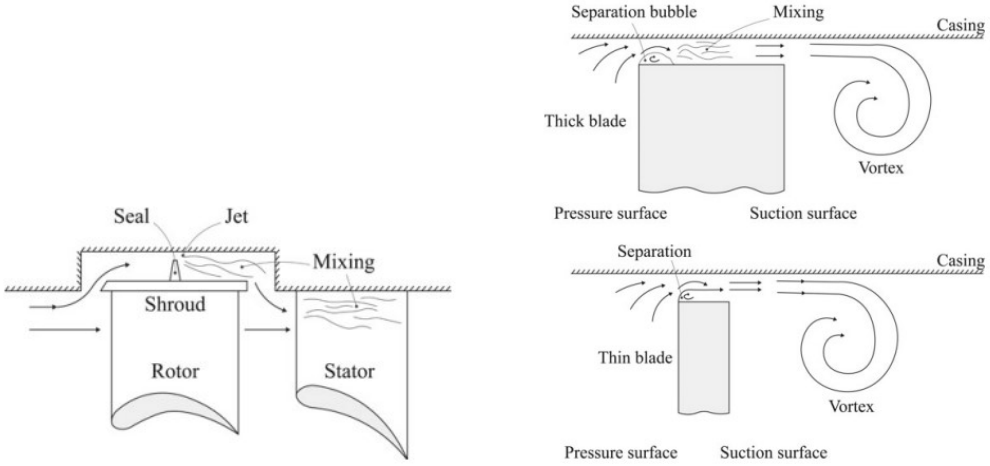

(a) Over a shrouded tip seal [22].

(b) Over tip gap of an unshrouded blade [22].

Figure 2.40: Mixing processes depending on the turbine geometry

2.8.4 Trailing edge loss

Trailing edge losses appear when the boundary layers of flow at the exit of the blade pressure and suction surfaces merge downstream of the base region created beyond the separation points shown in Figure 2.41, giving rise to a set of alternating vortices called Karman vortex street (depicted in Figure 2.42) which generates entropy as it moves downstream.

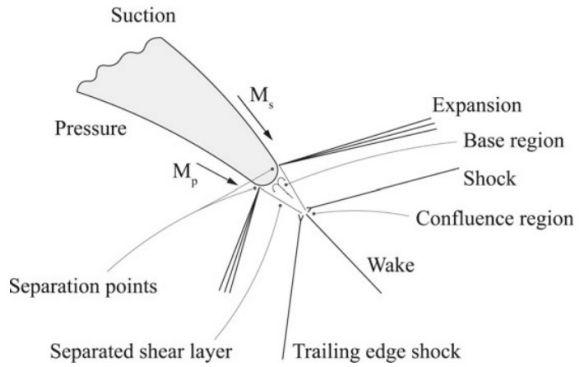

Figure 2.41: Trailing edge mixing processes and loss [22].

Figure 2.42: Visualization of a Karman vortex street forming at the trailing edge of a blade and moving downstream [26].

A detail of the flow at the exit of the trailing edge is shown in Figure 2.43. The base region that starts from the separating points is characterized by having almost constant pressure. This pressure together with the trailing edge thickness strongly influence the source of loss that arises when the boundary layers unify the base region forming a wake of low momentum fluid [26], and mixes with the main stream until uniform flow conditions are reached.

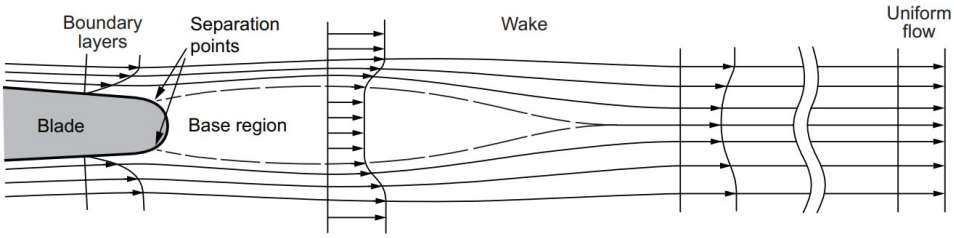

Figure 2.43: Boundary layer and wake [26].

As it was explained in Section 2.8.1, if the stall and separation occurred before reaching the trailing edge, the low momentum wake at this point would be considerably bigger and would lead to greater losses.

Having understood this type of losses, which take into account wake, sudden expansion loss and mixing processes, it can be noted that not only the trailing edge thickness, but also the outlet flow angle, pitch and opening are some parameters that impact their value. The Mach number also affects when it comes to the shock waves that can be produced at this point of the blade with supersonic flows, as it will be explained below.

2.8.5 Shock wave losses

This type of losses are caused by transonic or supersonic flows usually at the trailing edge, as shown in Figure 2.44. Shock waves involve significant irreversibility leading to concentrated entropy generation [22].

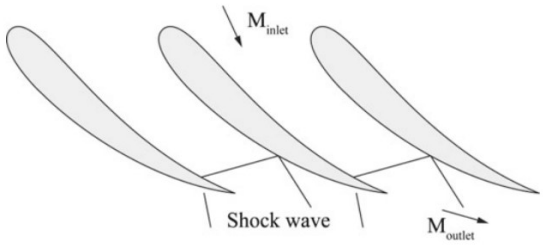

Figure 2.44: Shock wave losses at the trailing edge [22].

These losses can be included in the estimation of the profile loss since they are highly affected by the influence of Mach and Reynolds numbers, which also have an important role in the latter.

ORC turbines are prone to suffer the effects of supersonic flows, as it has been mentioned along the technical background of this thesis. In order to allow supersonic expansion without a limitation of work output, the idealization of a convergent-divergent blade passage introduced and presented in Section 2.9.6 must be slightly modified. The throat must be located upstream of the trailing edge, leaving a diverging zone downstream, where the flow is allowed to expand supersonically and turn [26], as it can be seen in Figure 2.45.

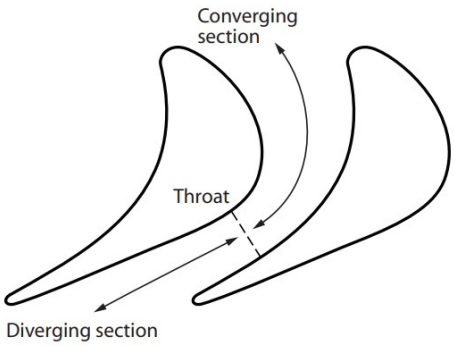

Figure 2.45: Convergent-divergent turbine blade passage [26].

Shock waves appear as the supersonic flow beyond the blade passage throat turns. They can arise for different reasons, such as the boundary layer effects discussed in the previous sections, separation of the flow at the trailing edge and changes in curvature [26]. These changes in curvature can lead to different types of shock waves, such as oblique shock waves or Mach shock waves, which can be either compression or expansion waves. Each of them lead to different flow effects, since Mach waves are weaker than oblique shock waves, but they all contribute to reduce the turbine efficiency to some extent. They can be seen in Figure 2.46.

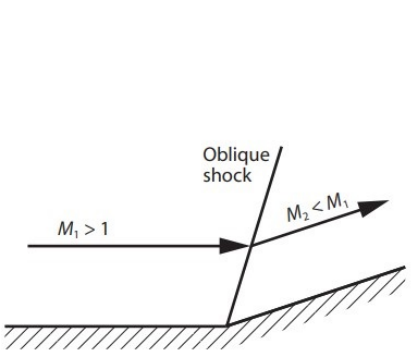

(a) Oblique shock wave at a sharp corner [26].

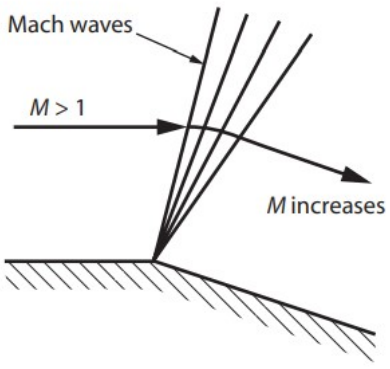

(b) Expansion Mach waves at a sharp corner [26].

Figure 2.46: Supersonic expansion and compression phenomena [26].

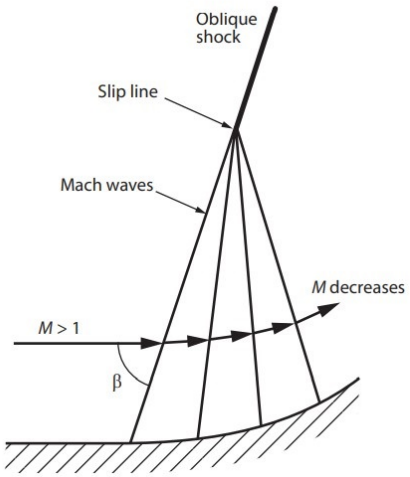

(c) Compression Mach waves at a concave surface [26].

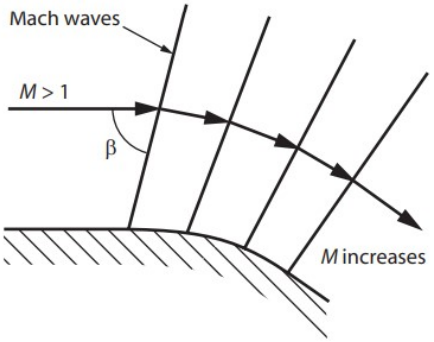

(d) Expansion Mach waves at a convex surface [26].

Figure 2.46: Supersonic expansion and compression phenomena (cont.) [26].

2.8.6 Incidence loss

An additional and important source of loss has to be considered when the turbine undergoes off-design operating conditions. Incidence loss can be considered as a component of the explained profile and secondary losses because it leads to the growth of boundary layers and flow separation from the blade surface [27].

Incidence losses account for the mismatch between the incoming flow and inlet blade angles. As it was explained in Section 2.7.2, for purposes of preliminary design, flow and blade angles are considered to be equal, so the flow is assumed to be perfectly guided. In reality this does not happen since blade loading has an important influence and work has to be done to turn the fluid into the blade passage [27]. The induced incidence — incidence when the turbine is operating under design conditions and therefore losses are minimum —, is normally 2°- 4° in reaction blades.

However, as for the losses explained in the previous section, ORC turbines are required to perform under a wide range of operating conditions, usually far from the design point. Thus, incidence losses are an important source of inefficiency within these machines, and must be considered in order to build a valid an efficient tool for preliminary design.

Different behaviours can be observed depending on the sign of the incidence. From Figure 2.47 it can be noticed that profile losses decrease their value with an increase of incidence up to a point of positive incidence. Beyond this point profile losses soar.

The reason why off-design incidence losses soar at positive incidence angles is the growth of the suction surface boundary layer thickness due to flow acceleration. It has been explained that profile losses are strongly affected by the effects of boundary layers, being these bigger on this blade surface. This over-acceleration takes place because positive incidence angles displace the stagnation point towards the pressure surface, being usually followed by a fast deceleration [27].

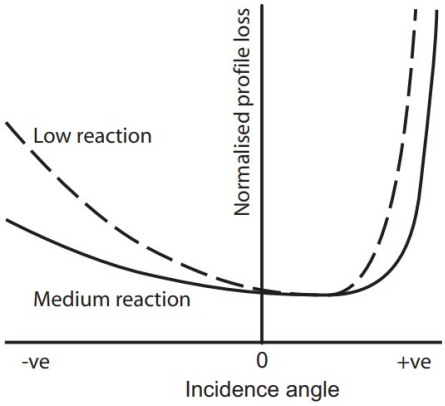

Figure 2.47: Rotor incidence loss characteristic for stages of different reactions [27].

On the other hand, negative incidence angles lead to a rapid deceleration of the flow, followed by a fast acceleration on the blade pressure surface, which has less influence on profile losses. It is important to note that either with negative or positive incidence angles, reaching stall and separation increases the losses.

It is believed and it has been proven that the leading edge geometry is a key parameter affecting incidence losses. Other important parameters are the ones that affect the profile losses, and sometimes secondary losses, which have been presented in the precedent sections.

2.8.7 Influential parameters on turbine losses

Having presented the different sources of loss within a turbine blade passage, this section tries to summarize for the reader the different parameters — mentioned in the previous sections —, that influence these losses to a greater or lesser extent. Without losing sight of the objective of this thesis — to improve the optimization mode of the mean-line model used for the preliminary design of an ORC axial turbine, and try to understand if this model makes sense —, it is very interesting to know at a glance which of these parameters are influencing or not the different loss components, because this will give an idea of which parameters should be studied in more detail. The aim of this work is to see how big this influence is, thereby a sensitivity analysis of the different design variables used with one of the loss models that will be introduced in Section 2.9 will be carried out and presented in Section 2.10. Moreover, when it comes to this type of turbines, characterized by facing a wide range of operating conditions, parameters influencing incidence losses should be identified and the effects predicted, in order to design turbines that are more tolerant to incidence and off-design conditions.

For this purpose, a series of tables have been drawn up from a literature review of different papers such as [27] and [36], explaining how each of these parameters affects each loss component. It must be noted that tailoring a table like this is not easy, since all of the effects are interrelated as it has been seen. Finally, a chart in which it can be seen which of the parameters simultaneously affect several loss components will be presented. A first hypothesis for the analysis that can be carried out is to assume that those parameters

affecting several components will have a greater influence on the performance of the turbine, but this will be developed further in Section 3.

Table 2.2: Influential parameters on the different components of turbine losses (I)

Profile Losses		
Parameter	Symbol	Effects
Degree of reaction	R	It influences the passage area and therefore flow acceleration and pressure gradients. Higher degrees of reaction lead to lower profile losses than the equivalent impulse turbines.
Blade curvature	$\Delta\theta$	It leads to the difference in pressure gradients and pressure forces over blade surfaces and turning of the flow.
Blade surface roughness	ε	The higher the surface roughness, the higher the skin friction, thus, the higher the profile losses.
Blade loading	ψ	The higher the blade loading, the more likely adverse pressure gradients and the higher the pressure gradients, the higher the profile losses.
Blade and flow angles	$\theta_{s/r}$, α, β	They have an effect on incidence. The higher the incidence angles, the higher the profile losses.
Mach number	Ma	It takes into account compressibility effects, as it influences the flow acceleration, shock waves at the leading edge and supersonic drag.
Reynolds number	Re	It influences the state of the boundary layer.
Inlet boundary layer thickness	δ	The thicker the boundary layers, the more likely to have flow separation and the bigger the profile losses.
Pitch-to-chord ratio	s/c	Either blade pitch or chord influence the boundary layers, flow acceleration, etc.
Blade thickness	t	It has an effect on incidence and deflection.
Secondary Losses		
Parameter	Symbol	Effects
Blade loading	ψ	It influences the strength of the cross-passage pressure gradient.
Aspect ratio	H/c	It influences the extent of flow affected by the vortices within the blade passage.
Inlet and exit methal angles	$\theta_{s/r}$	They have an effect on deflection and turning of the flow, which in turn affect the blade loading.
Pitch-to-chord ratio	s/c	It also affects the blade loading.
Mach number	Ma	It influences the flow acceleration and as it increases, the secondary flow decreases since the growth of the boundary layer is limited.
Inlet boundary layer displacement thickness	δ^*	It influences the penetration depth of the separation line between the different regions of flow and therefore it influences the secondary flow.
Tip clearance Losses		
Parameter	Symbol	Effects
Degree of reaction	R	It affects the cross-passage pressure gradient and therefore the leakage flow. Lower degrees of reaction lead to lower leakage flows.
Blade loading	ψ	It also affects the pressure gradient and leakage flow.
Pitch-to-chord ratio	s/c	Not a great influence in tip clearance losses but influences the shape of the blade.
Aspect ratio	H/c	Not a great influence in tip clearance losses but influences the shape of the blade.
Tip clearance	t_{cl}	The bigger the clearance gap, the bigger the leakage flow and loss.
Trailing edge Losses		
Parameter	Symbol	Effects
Boundary layer thickness	δ	It depends on the degree of reaction and influences the pressure base coefficient at the separation points.
Reynolds number	Re	It influences the state of the boundary layers and influences the losses due to stagnation and separation.
Mach number	Ma	It also influences the pressure base coefficient and may lead to shock waves at the trailing edge.
Blade loading	ψ	It influences the Mach number difference across the trailing edge.
Trailing edge thickness	t_{te}	It influences the pressure base coefficient, which affects the mixing and vortices downstream of the trailing edge.
Trailing edge wedge angle	We_{te}	It also influences the Mach number difference across the trailing edge.
Shock wave Losses		
Parameter	Symbol	Effects
Mach number	Ma	It influences the flow regime, giving rise to supersonic flows when Ma > 1.
Reynolds number	Re	Has an influence on the boundary layers which also affect shock waves at trailing edge.
Blade curvature	$\Delta\theta$	Changes in curvature lead to different types of shock waves.

Table 2.3: Influential parameters on the different components of turbine losses (II)

Incidence Losses		
Parameter	Symbol	Effects
Blade loading	ψ	It displaces the stagnation point towards the pressure surface side of the blade passage and favours incidence to appear.
Leading edge wedge angle	We	It influences the incidence losses since it stands for an approximation of curvature discontinuities. The higher the wedge angle the lower the discontinuities.
Leading edge diameter	d	It has an influence on incidence losses even if not significantly. It is believed that larger diameters can handle a wider range of incidence angles incurring losses.
Convergence ratio	CR	It stands for the channel acceleration and influences the secondary flow and therefore part of the incidence losses.
Exit Mach number	Ma_{exit}	Compressibility effects also affect incidence losses.
Incidence angles	Δi	The higher the angles the higher the incidence (profile losses).

Considering from these parameters those that are easily accessed during turbine or cascade testing, specially the thermodynamic and geometrical variables that influence in a way the rest parameters, the chart in Table 2.4 can be created. Moreover, it can be seen that the degree of reaction and blade loading affect the different existing losses. Therefore, the tables in Figure 2.48 and Figure 2.49, extracted from [27], show the influential parameters on these two variables.

Table 2.4: Chart with the most significant variables influencing losses within a turbine blade passage

	Re	Ma	s/c	H/c	t_{te}	t_{cl}	α, β	$\theta_{in/out,s/r}$	We
Profile losses	×	×	×	×			×	×	×
Secondary losses		×	×	×				×	
Tip clearance losses			×	×		×		×	
Trailing edge losses	×	×			×			×	
Shock wave losses	×	×						×	
Incidence losses		×					×	×	×

Parameter	**Influence on reaction**
U/C_0 at design	Favours a particular reaction
Specific work W_x/U^2	Low reaction for high specific work
Fluid temperature	Low reaction for low rotor inlet temperature
Aspect ratio	High aspect ratio leads to high spanwise reaction change
Platform fit	Low hub reaction may create assembly problems
Axial thrust	Low reaction reduces axial thrust
Tip leakage	Low tip reaction reduces tip leakage for shrouded blades. For unshrouded blades, low tip reaction accompanied by higher loading may increase the tip leakage
Exit swirl	Limits on rotor exit swirl may limit choice of reaction

Figure 2.48: Influence parameters on reaction [27].

Parameter	Influence on blade loading
Trailing edge thickness	Minimum thickness limited by manufacturing, fatigue resistance and internal cooling. Large TE reduces blade number, increases loading
Throat width	Minimum throat width set by manufacturing limitations and crowding of the blades at the hub. Large throat width reduces blade number, increases loading
Blade number	Increasing blade number increases profile loss, reduces diffusion loss and loading
Turning angle	Increasing turning angle increases secondary flow and endwall losses, increases loading and diffusion loss
Aspect ratio	Large aspect ratio limits secondary loss but reduces pitch and increases loading
Chord	Minimise for size and weight, maximise for manufacturing. Both influence solidity and blade loading
Platform fit	High turning angle make it more difficult to fit the blades on the hub platforms
Reaction	Controls passage acceleration and diffusion loss, and influences the distribution of blade loading.

Figure 2.49: Influence parameters on blade loading [27].

2.8.8 Second type of losses: external losses

External losses are those which, without altering the thermodynamic state of the fluid, reduce the turbine power by dissipating mechanical energy through friction in bearings and rotating parts [22]. Mass losses also contribute to the dissipation of mechanical energy. External losses are also known as parasitic losses and can be divided into bypass loss, disk friction loss, bearing loss, and clearance gap windage loss, being this one the most significant. Some of them can be seen in Figure 2.50.

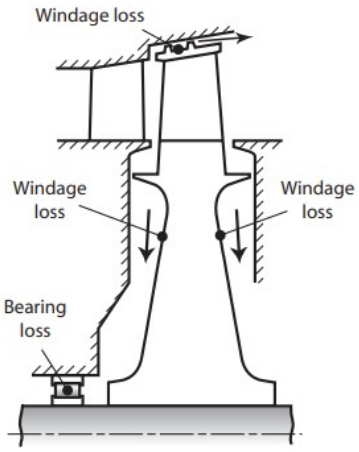

FIGURE 1.23. External losses in a turbine.

Figure 2.50: External losses in a turbine [26].

2.8.9 Definition of overall loss coefficient: Total pressure loss coefficient

Among the different definitions of overall loss coefficient, the total pressure loss coefficient offers an effective way to express the losses considered in the sections above. It is defined as the ratio of the total pressure of the cascade (difference between the pressure at inlet and outlet) to the dynamic pressure at the cascade exit [8]:

- **For the stator:**

$$Y_s = \frac{p_{01} - p_{02}}{p_{02} - p_2} \tag{2.73}$$

- **For the rotor:**

$$Y_r = \frac{p_{02,rel} - p_{03,rel}}{p_{03,rel} - p_3} \tag{2.74}$$

Unlike the enthalpy, velocity and entropy loss coefficients, the total pressure loss coefficient is entirely defined from measurable quantities that can be obtained directly from test data [27]. Moreover, this loss coefficient depends on the working fluid and its properties. Therefore it is commonly used. Another reason is that the other loss coefficients require an isentropic exit state that has to be calculated before the application of test data.

2.8.10 Approaches to loss modelling

To evaluate the performance of a turbine using a mean-line model, as it was explained in Section 2.7, the losses presented above must be taken into account in some way. There are different approaches to loss modelling. They will be presented in the following, however, only one will be further explained in the section below (Section 2.9). These are:

- **Single parameter approach**

  This approach is characterized by modelling the overall loss coefficient while ignoring the various sources of loss into which it can be decomposed. It is the simplest approach since it requires very basic data, but it is strictly limited to a range of parameters. Furthermore, a considerable drawback is the lack of accuracy, as more or less efficient designs can be assumed to be valid when using this approach.

  In order to improve accuracy and enlarge the range of applicability, overall blade loss correlations including geometric, thermodynamic and flow parameters were developed [27]. Some of these are:

  - Smith Chart

    Smith developed a tool to plot efficiency as a function of stage loading and flow coefficients. Nowadays it can be used to describe performance trends in trade-off studies or when comparing different design candidates, as it is based on pre-1965 turbines and would not provide accurate solutions for modern turbines [27].

- Soderburg's correlation

  Soderburg developed a correlation with test data from subsonic and high-speed turbines that proved to be fast and useful for preliminary design, as it included important blade geometry parameters [27]. However, like Smith's chart, the correlation is limited and may not be applicable to modern turbines.

- Latimer's correlation

  In 1978 Latimer developed a correlation that estimated stage efficiency not only in terms of stage loading and flow coefficients, but also of blade geometry. He also correlated efficiency at off-design conditions with its inherent limitations.

- **Loss models**

  This approach consists of identifying and separately modelling the various loss-generating mechanisms, so that:

$$\text{Overall Loss} = \sum_i \text{Individual loss}_i \tag{2.75}$$

  To account for each source of loss, a set of loss model correlations is needed. Different steps have to be followed in order to develop a loss model:

  1. Airfoil cascade data collection and creation of database: the airfoils have to cover a variety of geometric parameters and have to be tested over wide ranges of operating conditions.
  2. Parameter's selection: based on their dominant influence on losses and availability of test results.
  3. Correlation development
  4. Creation of a similar database: of stage and turbine test data in order to prove the ability of the prediction method.
  5. Calibration: in which corrections and multiplying factors are included to show the differences between cascade and turbine data.

- **CFD Analysis**

  Although CFD analysis provides a valid and acceptable procedure to assess losses, it is more commonly used at later and more advanced stages of design rather than at the preliminary design stage.

- **Physical and fundamental approach**

  This theoretically satisfying approach that considers physical mechanisms such as entropy generation within and around a blade passage, develops mathematical models that are generally applicable but not enough developed, since it relies on information that may not be available for the design [27].

2.9 Correlations for axial turbine losses - Loss models

Loss models have been criticized for being inaccurate when small databases are available, as the relationship between influential parameters and loss mechanisms is based on observation. However, these empirical mathematical correlations, developed and improved to predict turbine entropy generation, are the most widely used approach, as they have been studied over the years and are the most comprehensive tool available in the open literature.

There are different correlations to evaluate turbine losses. Some of them are those proposed by Soderberg in 1949, Ainley & Mathieson in 1951, Baljé & Binsley in 1968, Muktharov & Krichakin in 1969, Craig & Cox in 1970, Dunham & Came also in 1970, Traupel in 1977, Kacker & Okapuu in 1982, Moustapha et al in 1990, Denton in several years (1987, 1990 and 1993), Benner in 1997 and 2006 and Aungier in 2006, among others.

Practical difficulties may arise when attempting to correlate the different losses, as existing models are not able to account for all influences at the required level of detail. However, there are some fair approaches that lead to an ongoing need to review these correlations.

Since the aim of the mean-line model used for this thesis is to contemplate design and off-design conditions in the preliminary design phase of a single-stage axial turbine, only some of the above-mentioned models will be introduced. The Ainley & Mathieson loss model was developed for axial turbines and has been updated with new experimental data several times since the first version of the method was published [30]. It has probably been the most widely used system since both, design and off-design conditions can be analyzed when evaluating the turbine performance with it. This model was refined by the one provided by Dunham & Came and further improved by Kacker & Okapuu in what concerns to the design-point correlations. Hence, a detailed description of each of these models will be presented in the following. Some of the other mentioned correlations evaluate losses in a more complex way than mean-line models [8], being out of the scope of the preliminary design of a turbine, however, further refinements of these models have been done. Moustapha et al. reviewed the available correlations for profile and secondary losses at off-design conditions, comparing them with more recent measurements [41]. Their model was in turn verified and improved by Benner et al. who proposed a new loss breakdown scheme and other correlations to be used in profile and secondary losses at off-design conditions.

After presenting the aforementioned models — based on the work presented in [8] and following a very similar structure pursuing consistency —, a brief comparison will be done in Section 2.9.6, in order to set the basis for the sensitivity analysis. It has to be noted that since this work derives from previous projects, the notation had to be adapted in order to be consistent with the model that has been used.

2.9.1 Ainley & Mathieson

This method assesses turbine losses at the reference diameter, common diameter throughout each stage of the turbine [39] that can be obtained by taking the mean value between the hub and tip diameters.

The total loss coefficient for Ainley & Mathieson (AM) takes into account the profile, secondary, tip clearance and trailing edge loss components, and is defined as:

$$Y = (Y_p + Y_{sec} + Y_{cl}) \cdot y_{te} \tag{2.76}$$

where Y_p stands for the profile loss coefficient, Y_s stands for the secondary loss coefficient, Y_{cl} stands for the tip clearance loss coefficient and y_{te} stands for a multiplication factor that is used to account the trailing edge losses [8]. In the following, it is going to be explained how each coefficient is deducted.

Profile loss coefficient Y_p

The profile loss with the Ainley & Mathieson model is calculated at zero incidence, for both, impulse and reaction blades, and is later corrected for blades working at certain incidence by determining the stalling incidence of the blade, angle at which the profile loss doubles the profile loss at zero incidence [39]. Different charts have been provided by Ainley & Mathieson in order to obtain the profile loss at stalling incidence and will be presented below.

With this consideration in mind, the profile loss coefficient at zero incidence is given by:

$$Y_p = \left[Y_{p,reaction} + \left(\frac{\beta_2}{\beta_3} \right)^2 \cdot (Y_{p,impulse} - Y_{p,reaction}) \right] \cdot \left(\frac{t_{max}/c}{0.20} \right)^{-\frac{\beta_2}{\beta_3}} \tag{2.77}$$

The first term of the equation interpolates the profile loss coefficient of impulse and reaction blades, $Y_{p,impulse}$ and $Y_{p,reaction}$ respectively, which can be obtained from the charts provided by the authors and presented in Figure 2.51 (a) and (b). As it can be seen in the figure, the profile loss coefficient depends on the exit flow angle and on the pitch to chord ratio, presenting a minimum value that often matches the optimum pitch to chord ratio.

- $Y_{p,impulse}$ is the profile loss coefficient of an impulse cascade in which the inlet flow angle is opposite to the outlet flow angle. In the case of the stator $\alpha_1 = -\alpha_2$ and in the case of the rotor $\beta_2 = -\beta_3$.
- $Y_{p,reaction}$ is the profile loss coefficient of a reaction cascade in which flow enters in the axial direction, being $\alpha_1 = 0$ for the stator and $\beta_2 = 0$ for the rotor.

The maximum blade thickness has to be limited and the second term of Eq. (2.77) is used for this purpose. The maximum thickness to chord ratio has to be within the range of 0.15 and 0.25, adopting the limit values in case of being out of it.

From Figure 2.51 it can also be seen that a mean Reynolds number of $2 \cdot 10^5$ has been used. This average value is used all along the loss coefficient calculations within the Ainley & Mathieson model [39], so results obtained for any other Reynolds number must be corrected by using:

$$(1-\eta) = \left(\frac{Re}{2 \cdot 10^5}\right)^{-\frac{1}{5}} \cdot (1-\eta)_{Re=2\cdot 10^5} \tag{2.78}$$

where Re stands for the average Reynolds number between stator and rotor.

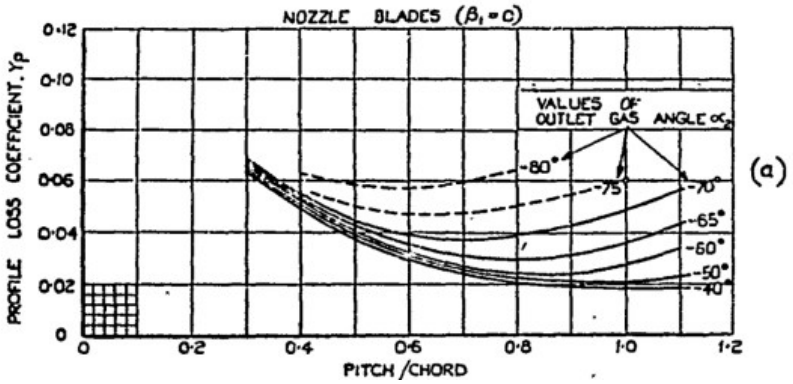

(a) Profile loss of reaction blades [42].

Figure 2.51: : Profile loss coefficients for conventional section blades at zero incidence. (t/c = 20%; Re = 2×10^5; Ma < 0.6.) [39].

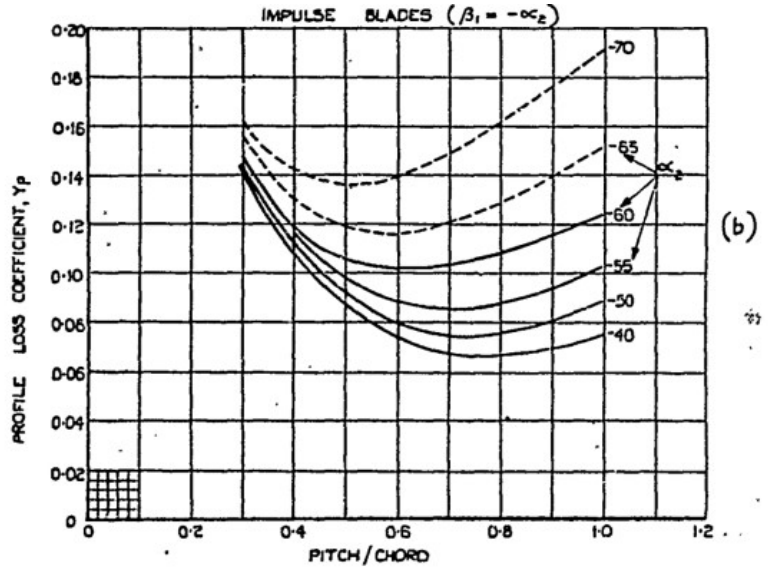

(b) Profile loss of impulse blades[42]

Figure 2.51: : Profile loss coefficients for conventional section blades at zero incidence. (t/c = 20%; Re = 2×10^5; Ma < 0.6) (cont.) [39].

When it comes to evaluate the profile losses when the incidence is different from zero, as it was explained above, the stalling incidence i_{stall} must be determined from the graphs presented in Figure 2.52.

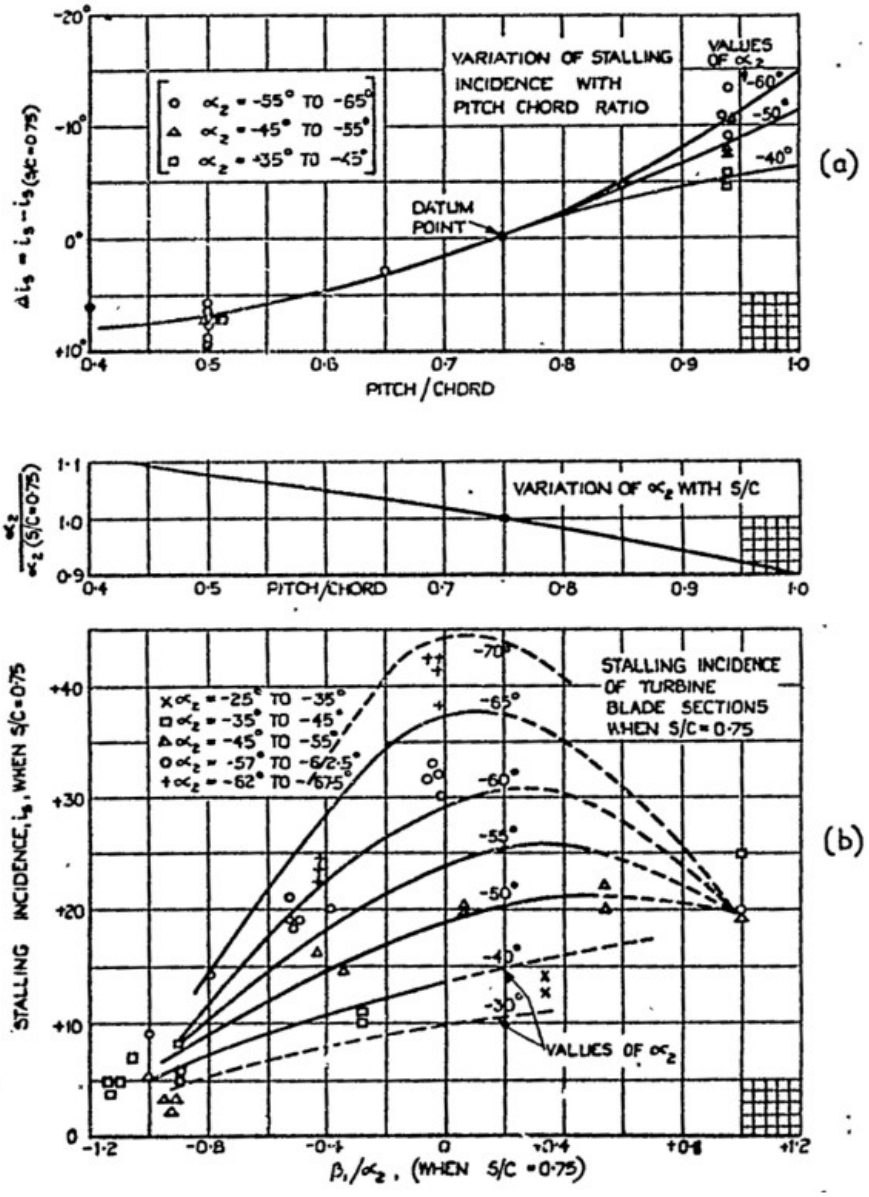

Figure 2.52: Positive stalling incidences of cascades of turbine blades. (Re = 2 x 10^5; Ma < 0.6 [39].

As it can be seen, the stalling incidence of the studied cascade can be obtained from Figure 2.52 (a). This graph can be used once the exit angle of this cascade with pitch-to-chord ratio of 0.75 is corrected with the graph in the middle, and the reference stalling incidence — for a cascade with pitch-to-chord ratio of 0.75 —, has been determined from Figure 2.52(b).

Once the profile losses at zero incidence and the stalling incidence have been determined, the profile losses at any incidence are given in the graph of Figure 2.53. This graph has been built assuming that $Y_p/Y_{p(i=0)}$ is a function of i/i_{stall} [39]. The curve is

used in the -1.5 < i/i_{stall} < 1.0 frame, and outside it, the secondary losses occurring at incidence take on the values corresponding to the extreme values for the incidence ratio in stead of applying a correction factor [43].

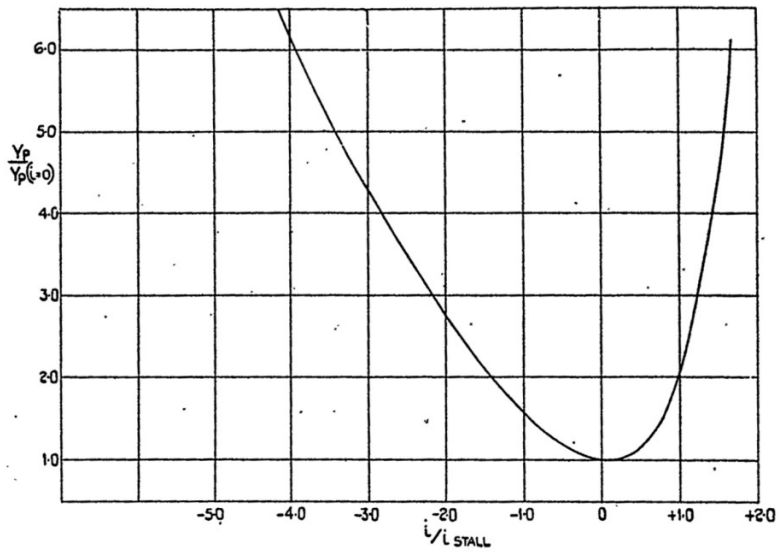

Figure 2.53: Variation of profile loss with incidence for typical turbine blading [39].

Later authors expose some shortcomings of this correlation for off-design conditions. One major is the fact that the shape of the leading edge does not affect the stalling incidence as it has been deducted. However, it was seen in Section 2.8.1 that stalling and separation of the flow are due to the effects that boundary layers suffer in velocity close to the leading edge.

Secondary loss coefficient Y_{sec}

The secondary loss coefficient is given by:

$$Y_{sec} = \lambda \cdot Z \tag{2.79}$$

representing the drag that secondary flows produce on the blades.

- λ is a geometric parameter that depends on the hub-to-tip ratio. It also depends on the fluid degree of acceleration [39]. It is given by the expression below and the chart in Figure 2.54.

$$\lambda = \lambda \cdot \left[\frac{\left(\frac{A_3 \cdot cos(\beta_3)}{A_2 \cdot cos(\beta_2)} \right)^2}{1 + r_{ht}} \right] \tag{2.80}$$

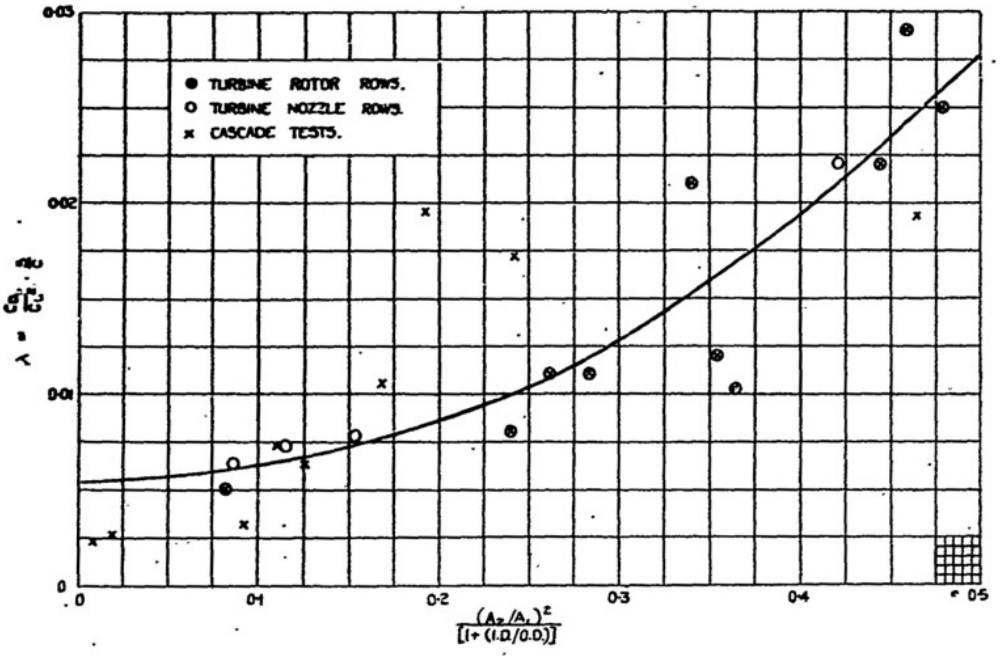

Figure 2.54: Secondary losses in turbine blade rows [42].

- Z is the Ainley loading parameter which takes into account the lift coefficient based on the mean velocity and is given by the following expressions:

$$Z = \left(\frac{C_L}{s/c}\right)^2 \cdot \frac{cos(\beta_3)^2}{cos(\beta_{mid})^3} \tag{2.81}$$

$$\left(\frac{C_L}{s/c}\right) = 2 \cdot cos(\beta_{mid}) \cdot [tan(\beta_2) - tan(\beta_3)] \tag{2.82}$$

$$\beta_{mid} = arctan\left(\frac{1}{2} \cdot [tan(\beta_2) - tan(\beta_3)]\right) \tag{2.83}$$

  as detailed in [8]. This lift coefficient C_L is usually approximated and can be used strictly if the constant meridional velocity and constant radius assumption is used [27].

Tip clearance loss coefficient Y_{cl}

The tip clearance loss coefficient is given by a linear relation between the blade loading factor and the clearance to span ratio:

$$Y_{cl} = B \cdot Z \cdot \left(\frac{t_{cl}}{H}\right) \tag{2.84}$$

where:

- B stands for the blockage factor, an empirical parameter that equals:

$$B = \begin{cases} 0 & \text{for stator blades} \\ 0.25 & \text{for shrouded rotor blades} \\ 0.5 & \text{for rotor blades with radial tip clearance} \end{cases} \tag{2.85}$$

- Z is the loading parameter in eqs. (2.81-2.83), H is the blade mean height and t_{cl} the blade tip clearance gap.

Trailing edge loss multiplication factor y_{te}

The trailing edge multiplication factor used by Ainley & Mathieson to compute the total loss coeficient is given by the expression:

$$y_{te} = y_{te} \cdot \left(\frac{t_{te}}{s}\right) \tag{2.86}$$

and can be taken from the graph in Figure 2.55. Ainley and Mathieson's correlations were based on blades with a trailing edge to pitch ratio equal to 0.02. For different ratios a correction factor was applied [27].

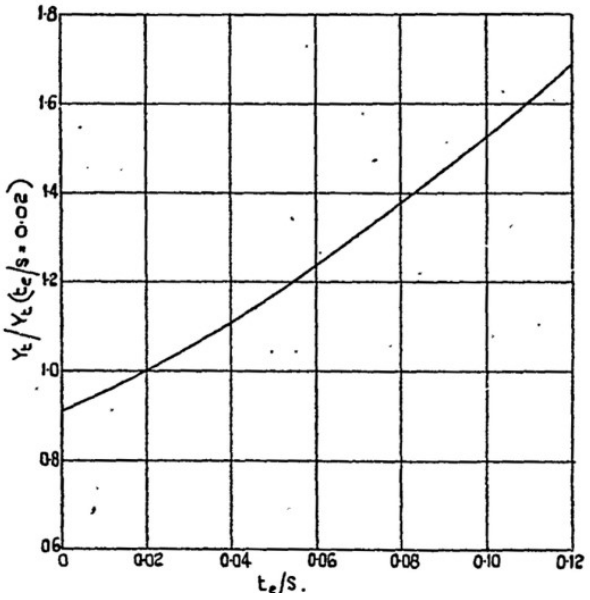

Figure 2.55: Trailing edge multiplication factor [42].

2.9.2 Dunham & Came

The Dunham & Came loss model (DC) is a refinement of Ainley's & Mathieson's work. Some corrections have been introduced in order to calculate the total loss coefficient that is given by:

$$Y = (f_{Re} \cdot f_{Ma} \cdot Y_p + f_{Re} \cdot Y_{sec} + Y_{cl}) \cdot y_{te} \tag{2.87}$$

As it can be seen in Eq. (2.87), the profile and secondary loss coefficients are affected by a Reynolds correction factor, given by Eq.(2.88) in which the Reynolds number has been calculated at the rotor outlet.

$$f_{Re} = \left(\frac{Re}{2 \cdot 10^5} \right)^{-0.20} \tag{2.88}$$

The profile loss is in turn corrected by a factor that accounts the rise of supersonic drag due to shock waves with supersonic flows. The Mach correction factor is calculated as:

$$f_{Ma} = \begin{cases} 1 & \text{for } Ma_{3,rel} \leq 1 \\ 1 + 60 \cdot (Ma_{3,rel-1})^2 & \text{for } Ma_{3,rel} > 1 \end{cases} \tag{2.89}$$

where $Ma_{3,rel}$ is the relative Mach number at the exit of the rotor cascade. This variation has been reproduced from [8] in Figure 2.56.

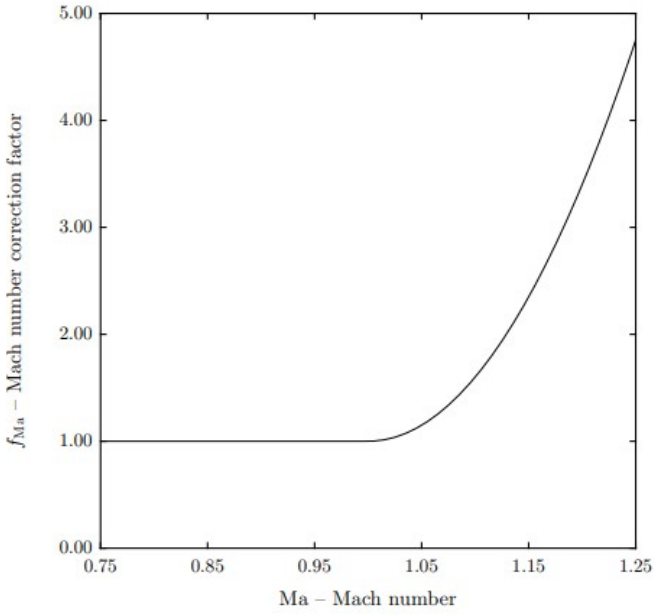

Figure 2.56: Mach correction factor [8].

Here relies the main weakness of the Dunham and Came model, since the Mach correction factor is independent from the blade exit angle and it implicitly ignores the limit loading of the blades [27].

Profile loss coefficient Y_p

The profile loss coefficient in the Dunham and Came model is the same as for the Ainley and Mathieson model, presented in Eq. (2.77).

Secondary loss coefficient Y_{sec}

The secondary loss coefficient varies slightly from the one presented by Ainley and Mathieson, taking into account other geometrical parameters, such as the aspect ratio. It is given by the following equation:

$$Y_{sec} = 0.0334 \cdot Z \cdot \frac{cos(\beta_3)}{cos(\beta_2)} \cdot \left(\frac{c}{H}\right) \tag{2.90}$$

The numerical constant 0.0334 is accounted to estimate the effect of the inlet boundary layer thickness, which depends on the blade shape, in turn dependent on the aspect ratio [39]. The loading of the blade Z is calculated as for the Ainley and Mathieson model by using eqs. (2.81), (2.82) and (2.83).

Tip clearance loss coefficient Y_{cl}

Dunham & Came changed the linear dependence on clearance ratio to an exponent of 0.78 and also took into account the aspect ratio when calculating the tip clearance loss coefficient, which is given by:

$$Y_{cl} = B \cdot Z \cdot \left(\frac{c}{H}\right) \cdot \left(\frac{t_{cl}}{H}\right)^{0.78} \tag{2.91}$$

but in this case, the blockage B acquires the following values:

$$B = \begin{cases} 0 & \text{for stator blades} \\ 0.37 & \text{for rotor blades with shrouded tips} \\ 0.47 & \text{for rotor blades with plain tip} \end{cases} \tag{2.92}$$

Trailing edge loss multiplication factor y_{te}

The trailing edge loss multiplication factor is obtained as presented in Eq. (2.86) for the AM loss model.

2.9.3 Kacker & Okapuu

The Kacker and Okapuu loss model (KO) is also a mean-line model, but as said, unlike the models provided by Ainley & Mathieson and Dunham & Came it is used for assessing axial turbines performance only at design conditions. Another difference with respect to the previous models is the way in which the trailing edge losses are accounted for. The Kacker and Okapuu loss model provides a trailing edge loss coefficient that is added to the coefficients of the rest loss components, instead of using a multiplication factor. The total loss coefficient for this model is given by:

$$Y = f_{Re} \cdot f_{Ma} \cdot Y_p + Y_{sec} + Y_{cl} + Y_{te} \tag{2.93}$$

It can be seen that the profile losses are also corrected with two factors accounting the Reynolds and Mach numbers, as in the Dunham & Came model, but the secondary losses are not affected by the Reynolds correction factor in this case. The Kacker and Okapuu loss model is a further refinement of the Ainley and Mathieson model presented above [8].

The Reynolds correction factor differs slightly from the ones used in the previous models. It can take different values depending on the state of the boundary layer, in turn dependent on Reynolds number, as shown in Eq. (2.94). However, the Mach correction factor is the same as the one used in the DC model, shown in Eq. (2.89).

$$f_{Re} = \begin{cases} \left(\frac{Re}{2 \cdot 10^5}\right)^{-0.40} & \text{for } Re < 2 \cdot 10^5 \\ 1 & \text{for } 2 \cdot 10^5 < Re < 1 \cdot 10^6 \\ \left(\frac{Re}{1 \cdot 10^6}\right)^{-0.20} & \text{for } Re > 1 \cdot 10^6 \end{cases} \tag{2.94}$$

Profile loss coefficient Y_p

Kacker and Okapuu have introduced several modifications to the original profile loss coefficient calculation. First, the profile loss coefficient that has been used in the previous models is corrected by a constant factor equal to 2/3, in order to obtain more accurate results with modern blades, and by a coefficient known as acceleration parameter, K_p, that accounts the fluid compressibility effects with subsonic flows [39]. On the other hand, the shock wave losses discussed in Section 2.8.5, are included within the profile losses in this model, Y_{shock}.

The profile loss coefficient is given by:

$$Y_p = 0.914 \cdot \left(\frac{2}{3} \cdot Y'_p \cdot K_p + Y_{shock}\right) \tag{2.95}$$

The 0.914 factor is used for correcting the profile loss to blades with no trailing edge thickness [8], since the trailing edge coefficient is being considered individually.

The profile loss coefficient Y'_p is almost the same as the profile loss coefficient of the previous models, however, positive angles at stator inlet and negative angles at rotor inlet are allowed by incorporating the following term $|\beta_2/\beta_3|$, as shown:

$$Y'_p = \left[Y_{p,reaction} - \left(\frac{\beta_2}{\beta_3}\right) \cdot \left|\frac{\beta_2}{\beta_3}\right| \cdot (Y_{p,impulse} - Y_{p,reaction})\right] \cdot \left(\frac{t_{max}/c}{0.20}\right)^{-\frac{\beta_2}{\beta_3}} \tag{2.96}$$

And the acceleration parameter, K_p, used to account the limitation in the growth of boundary layers and the suppression of flow separation when inlet Mach numbers are slightly lower than exit Mach numbers [27], is given by:

$$K_p = 1 - K_2 \cdot (1 - K_1) \tag{2.97}$$

where:

$$K_1 = \begin{cases} 1 & \text{for } Ma_{3,rel} \geq 0.20 \\ 1 - 1.25 \cdot (Ma_{3,rel} - 0.20) & \text{for } 0.20 < Ma_{3,rel} < 1 \\ 0 & \text{for } Ma_{3,rel} \leq 1 \end{cases} \tag{2.98}$$

and:

$$K_2 = \left(\frac{Ma_{2,rel}}{Ma_{3,rel}} \right)^2 \tag{2.99}$$

The shock wave losses are accounted with the Y_{shock} coefficient, given by Eq. (2.100), taken from R.Agromayor's work in [8] after operating with the equations provided by Kacker and Okapuu.

$$Y_{shock} = 0.75 \cdot (f_{hub} \cdot Ma_{2,rel} - 0.40)^{1.75} \cdot r_{ht} \cdot \left(\frac{p_{02,rel} - p_2}{p_{03,rel} - p_3} \right) \tag{2.100}$$

The hub-to-tip ratio is taken into account, as well as the f_{hub} term, due to the greater effects of shock wave losses near the hub. The latter term can be obtained from Figure 2.57.

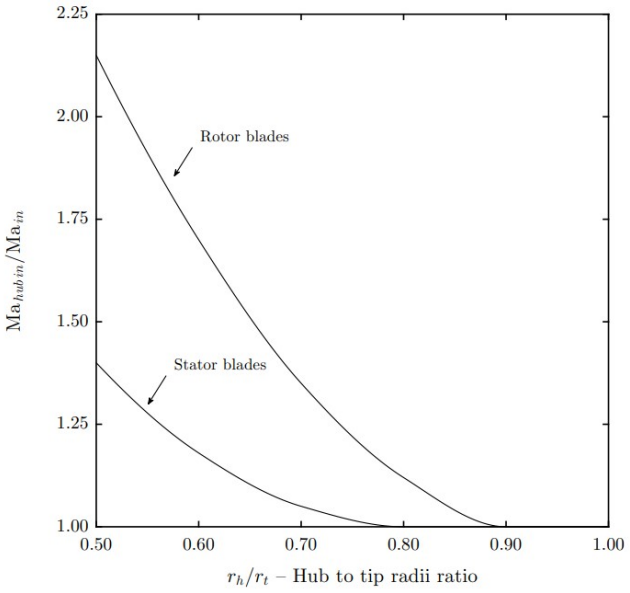

Figure 2.57: Ratio of Mach number at the hub to Mach number at the mean radius [8].

A structural weakness of this model, as noted in [27], is that for pure impulse blades the profile losses would be independent of the blade profile shape and fluid flow angles, completely represented by the shock losses.

Secondary loss coefficient Y_{sec}

The secondary loss coefficient is calculated as:

$$Y_{sec} = 1.2 \cdot K_s \cdot \left[0.0334 \cdot f_{AR} \cdot Z \cdot \left(\frac{cos(\beta_3)}{cos(\beta_2)} \right) \right] \tag{2.101}$$

Similarly to the profile loss coefficient calculation, the 1.2 factor corrects the secondary loss coefficient to blades with no trailing edge thickness; and K_s or subsonic Mach correction factor has the same purpose as K_p in the profile loss correlation. It is given by:

$$K_s = 1 - K_3 \cdot (1 - K_p) \tag{2.102}$$

where:

$$K_3 = \left(\frac{1}{H/b} \right)^2 \tag{2.103}$$

Not only compressibility fluid effects are accounted with this variable within subsonic flows, but also the axial aspect ratio is being considered, since b stands for axial chord, previously introduced as c_{ax}.

The loading of the blade Z is calculated as in the other models (eqs.(2.81-2.83)), and the f_{AR} coefficient takes into account the aspect ratio, due to its influence in secondary losses. However, Kacker and Okapuu provided a more complex function since they considered that the effect of aspect ratio was overestimated for small values of this parameter. It is given by:

$$f_{AR} = \begin{cases} \frac{1-0.25 \cdot \sqrt{2-H/c}}{H/c} & \text{for } H/c < 2 \\ \frac{1}{H/c} & \text{for } H/c > 2 \end{cases} \tag{2.104}$$

Tip clearance loss coefficient Y_{cl}

The tip clearance loss coefficient is calculated with the same equation presented by Dunham & Came, Eq. (2.91). However, it was noticed by these authors that B = 0.47 for blades with plain tips gave bigger predictions than expected [8].

Trailing edge loss coefficient Y_{te}

Kacker and Okapuu incorporated a trailing edge loss coefficient instead of a multiplication factor, calculated as:

$$Y_{te} \approx \zeta = \frac{1}{\Phi^2} - 1 = \frac{1}{1 - \Delta\phi^2} - 1 \tag{2.105}$$

where the energy coefficient, $\Delta\phi^2$, is in turn obtained as follows:

$$\Delta\phi^2 = \Delta\phi^2_{reaction} - \left(\frac{\beta_2}{\beta_3}\right) \cdot \left|\frac{\beta_2}{\beta_3}\right| \cdot (\Delta\phi^2_{impulse} - \Delta\phi^2_{reaction}) \tag{2.106}$$

These energy coefficients particularized for impulse and reaction blades, can be taken from the chart in Figure 2.58, depending on the trailing edge thickness to opening ratio, t_{te}/o.

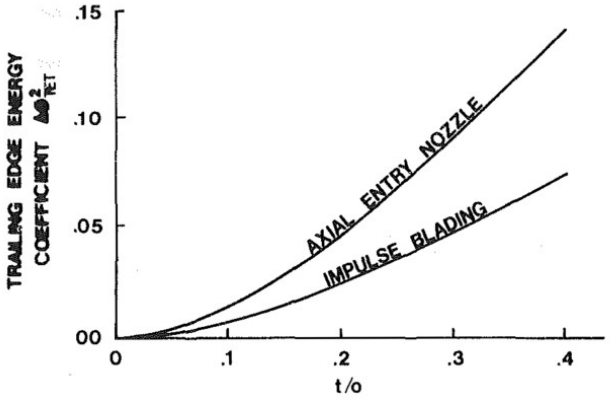

Figure 2.58: Trailing edge loss energy coefficient correlated against the trailing edge thickness to throat opening ratio [39].

In the case of supersonic exit velocities trailing edge losses are included in the term that accounts for supersonic drag rise in profile losses [27].

2.9.4 Moustapha et al.

Moustapha et al. reviewed Ainley and Mathieson's and Mukhtarov and Krichakin's incidence loss correlations and proposed improved correlations for profile and secondary losses at off-design conditions. These correlations were given in order to calculate the kinetic energy loss coefficient, ϕ. However, the authors proposed Eq. (2.107) to convert the energy loss coefficient into total pressure loss coefficient, taking into account the exit Mach number.

$$Y = \frac{\left[1 - \frac{\gamma-1}{2} \cdot Ma_2^2 \cdot \left(\frac{1}{\phi^2} - 1\right)\right]^{\frac{-\gamma}{\gamma-1}-1}}{1 - \left(1 + \frac{\gamma-1}{2} \cdot Ma_2^2\right)^{\frac{-\gamma}{\gamma-1}}} \tag{2.107}$$

Profile loss coefficient $\mathbf{Y}_p$

The proposed correlation for obtaining the profile kinetic energy loss coefficient is given by:

$$\Delta\phi_p^2 = \begin{cases} 0.078 \cdot 10^{-5}\chi' + 0.56 \cdot 10^{-7}\chi'^2 + 0.4 \cdot 10^{-10}\chi'^3 + 2.054 \cdot 10^{-19}\chi'^6 & \text{for } 0 < \chi' < 800 \\ -5.1734 \cdot 10^{-6}\chi' + 7.6902 \cdot 10^{-9}\chi'^2 & \text{for -800} < \chi' < 0 \end{cases} \tag{2.108}$$

where the incidence parameter χ' is given by:

$$\chi' = \left(\frac{d}{s}\right)^{-0.16} \cdot \left(\frac{\cos\,\beta_1}{\cos\,\beta_2}\right)^{-2} \cdot [\alpha_1 - \alpha_{1(des)}] \tag{2.109}$$

This correlation is based on the one provided by Mukhtarov and Krichakin in 1969, who correlated profile losses considering the following influential factors: incidence, convergence ratio, leading edge diameter and compressibility. The whole correlation for obtaining the kinetic energy loss coefficient is presented in eqs. (2.110-2.111).

$$[(1-\phi^2) = (1-\phi^2)_{\alpha_1=\alpha_{1(des)}} + \Delta(1-\phi^2)]_p \tag{2.110}$$

$$\Delta(1-\phi^2)_p = \Delta\phi_p^2 \tag{2.111}$$

The first term in Eq. (2.110) is the profile loss at the design inlet flow angle — sum of friction and trailing edge losses [43]—. The correlations used to obtain this value included Mach and Reynolds number corrections. The second term represents the profile loss at off-design conditions and is the one that Moustapha et al. modified with respect to Mukhtarov and Krichakin's correlation. As it can be seen from Eq. (2.109), the former authors retained some of the influential parameters considered by the latter, such as the influence of the leading edge geometry, accounted with the diameter to pitch ratio, or the incidence and convergence ratio, which accounts for the flow acceleration in the blade passage [43]. However, they neglected the effect of compressibility and Reynolds number, as they considered it was enough accounting them by using the corrections to profile losses proposed by Kacker and Okapuu (eqs.(2.89) and (2.94)).

Secondary loss coefficient $\mathbf{Y}_s$

In a similar way, the secondary loss coeffient at off-design conditions is given by the next correlation:

$$\left(\frac{Y}{Y_{(des)}}\right)_{sec} = \begin{cases} \exp\,(0.9\chi'') + 13\chi''^2 + 400\chi''^4 & \text{for } 0 < \chi'' < 0.3 \\ \exp\,(0.9\chi'') & \text{for -0.4} < \chi'' < 0 \end{cases} \tag{2.112}$$

where

$$\chi'' = \frac{\alpha_1 - \beta_1}{180 - (\beta_1 + \beta_2)} \cdot \left(\frac{\cos\,\beta_1}{\cos\,\beta_2}\right)^{-1.5} \cdot \left(\frac{d}{s}\right)^{-0.3} \tag{2.113}$$

Unlike Mukhtarov and Krichakin, Moustapha et al. considered also the effect of the leading edge diameter in secondary losses, since they believed it had an influence on the horseshoe vortex at the leading edge [43]. These off-design correlations together with the Kacker and Okapuu design-point correlations form a complete loss system.

2.9.5 Benner

Benner et al. revised and verified Moustapha et al.'s correlation for profile losses, in order to check and study in more detail the effect of the leading edge geometry. Their study ended with an improved correlation for off-design profile losses, in 1997, however, years later a new correlation for off-design secondary losses was developed by the hand of a new loss breakdown scheme. This new way of decomposing losses required other correlations that will be presented within this section. As for Moustapha's correlation, Eq. (2.107) is used for converting the kinetic energy loss coefficient into total pressure loss coefficient.

Profile loss coefficient

The profile loss coefficient is obtained from Eq. (2.114):

$$\Delta\phi_p^2 = \begin{cases} a_8\chi^8 + a_7\chi^7 + a_6\chi^6 + a_5\chi^5 + a_4\chi^4 + a_3\chi^3 + a_2\chi^2 + a_1\chi & \text{for } \chi \geq 0 \\ 1.358 \cdot 10^{-4}\chi^2 - 8.720 \cdot 10^{-4}\chi & \text{for } \chi < 0 \end{cases} \tag{2.114}$$

where

$$\begin{aligned} a_8 &= 3.711 \cdot 10^{-7}, \quad a_7 = -5.318 \cdot 10^{-6}, \; a_6 = 1.106 \cdot 10^{-5}, \; a_5 = 9.017 \cdot 10^{-5} \\ a_4 &= -1.542 \cdot 10^{-4}, \; a_3 = -2.506 \cdot 10^{-4}, \; a_2 = 1.327 \cdot 10^{-3}, \; a_1 = -6.149 \cdot 10^{-5} \end{aligned} \tag{2.115}$$

and

$$\chi = \left(\frac{d}{s}\right)^{-0.05} \cdot We^{-0.2} \cdot \left(\frac{\cos\,\beta_1}{\cos\,\beta_2}\right)^{-1.4} \cdot [\alpha_1 - \alpha_{1(des)}] \tag{2.116}$$

Unlike the incidence parameter presented by Moustapha et al. in Eq. (2.109), the one presented by Benner et al. in Eq. (2.116) includes the effect of the wedge angle and reduces the influence that leading edge diameter had on profile losses. This is because after studying several airfoils with different leading edge diameters a small and almost negligible influence was appreciated. Instead, the influence of wedge angle in profile losses is considerably big, since it approximately measures the curvature discontinuity at the leading edge blend points, as depicted in Figure 2.59, which affects the boundary layers and therefore the losses. Convergence ratio and incidence are still considered influential parameters in this correlation.

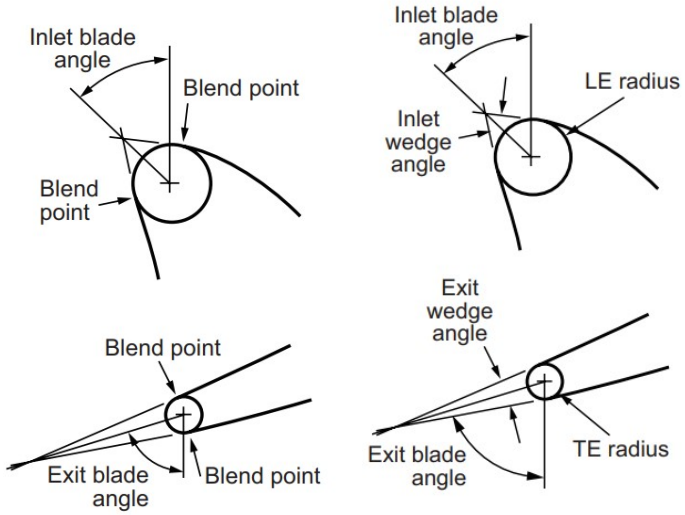

Figure 2.59: Blade leading and trailing edge geometry [44].

New loss breakdown scheme

Although it has already been introduced somehow in sections 2.8.1 and 2.8.2, when it came to study the off-design secondary losses, Benner et al. developed a new loss breakdown scheme that required several correlations and which will be explained in the following. The main reason for developing this new scheme was that the old one considered the losses due to boundary layers to be uniform across the span of the airfoil [36]. Moreover, the conventional loss breakdown scheme failed at high incidence, where secondary losses became negative. Therefore, the new scheme presented in Eq. (2.117) takes into account the effects of boundary layers on profile and secondary losses considering two different regions across the airfoil span, the primary and the secondary regions divided by the separation lines, as it was explained in the aforementioned sections and depicted in Figure 2.31.

$$Y_{total} = Y_{mid} \cdot \left(1 - \frac{Z_{TE}}{h}\right) + Y_{sec} + Y_{cl} \tag{2.117}$$

From the previous equation, it can be said that profile losses are nothing but the product of the midspan loss, Y_{mid} and the extent of surface within the primary region shown in Figure 2.31. This weight factor requires the development of a correlation for the spanwise penetration depth of the passage vortex separation line at the trailing edge, which will be introduced below. The midspan loss is meant to be obtained with the previous correlation — for off-design conditions —, and with the Kacker and Okapuu's correlation when operating at design point [36]. On the other hand, the secondary losses, now accounted with less influence than profile losses over the span of the airfoil, will be deducted from a correlation that the authors proposed in 2006. However, the overall loss coefficient is deducted at zero tip clearance, important detail when assessing airfoils with non-zero clearance.

Penetration depth correlation

Benner et al. improved the existing correlation for penetration depth proposed by Sharma and Butler. It was correlated against the parameters believed to influence the size of the passage vortex, which in turn determines the distance that the separation line of the secondary region penetrates at the trailing edge. These parameters are: convergence ratio — since the penetration depth diminishes with increasing the channel convergence [36]—, the inlet boundary layer displacement thickness — with cascade geometry-independent effects —, and, unlike the Sharma and Butler correlation, aspect ratio and tangential blade loading. The penetration depth non-dimensionalized by the blade height is given by:

$$\frac{Z_{TE}}{h} = \frac{0.10 \cdot (F_t)^{0.79}}{\sqrt{CR} \cdot (\frac{h}{c})^{0.55}} + 32.70 \cdot \left(\frac{\delta^*}{h}\right)^2 \tag{2.118}$$

where the convergence ratio is obtained as:

$$CR = \frac{\cos\ \alpha_1}{\cos\ \alpha_2} \tag{2.119}$$

excluding flaring, and the tangential loading parameter is given by:

$$F_t = 2 \cdot \left(\frac{s}{C_x}\right) \cdot \cos^2\alpha_{mid} \cdot (\tan\ \alpha_1 - \tan\ \alpha_2) \tag{2.120}$$

as a function of pitch-to-axial chord ratio and flow turning, and where α_m is calculated as:

$$\tan\ \alpha_{mid} = 0.5 \cdot (\tan\ \alpha_1 + \tan\ \alpha_2) \tag{2.121}$$

Benner et al. neglected the effect of stagger angle in the penetration depth after carrying out a sensitivity analysis which concluded the insensitivity of this parameter.

Secondary loss coefficient

Finally, the correlation proposed by Benner et al. for calculating secondary losses within the new loss breakdown scheme is given by:

$$Y_{sec} = \begin{cases} \frac{0.038+0.41\cdot\tanh\ (1.20)\cdot(\frac{\delta^*}{h})}{\sqrt{\cos\ \bar{\xi}}\cdot(CR)\cdot\left(\frac{h}{c}\right)^{0.55}\cdot\left(\frac{c\cdot\cos\ \alpha_2}{C_{ax}}\right)^{0.55}} & \text{for } \frac{h}{c} \leq 2.0 \\ \\ \frac{0.052+0.56\cdot\tanh\ (1.20)\cdot(\frac{\delta^*}{h})}{\sqrt{\cos\ \bar{\xi}}\cdot(CR)\cdot\left(\frac{h}{c}\right)\cdot\left(\frac{c\cdot\cos\ \alpha_2}{C_{ax}}\right)^{0.55}} & \text{for } \frac{h}{c} > 2.0 \end{cases} \tag{2.122}$$

Two cases were distinguished depending on the aspect ratio, since the loss trend strays from the previous correlations for high values of this parameter. Therefore, for aspect ratios bigger than 2 a slightly different correlation was provided.

From Eq. (2.122) it can be seen that the main parameters influencing secondary losses selected by Benner et al. after conducting different studies were the inlet boundary layer displacement thickness to height ratio, the loading-distribution parameter accounting the stagger angle, the convergence ratio, the height-to-axial chord ratio (blade axial aspect ratio) and the aspect ratio as expected. The skin friction, believed to have an influence on secondary losses was discarded after the sensitivity analysis.

It has to be said that even though the authors presented an improved system of correlations they identified other influential parameters that still have to be studied such as Reynolds and Mach numbers, among others.

2.9.6 Comparison of loss models

Having presented the most significant existing correlations for the development of this thesis, a brief and summarized comparison will be performed. It is important to understand the differences between the correlations in order to choose the best one when assessing the turbine performance.

Cascade or rotating turbine database

The first and probably the most relevant difference between the loss correlations above presented is the source from which the databases have been created. Ainley and Mathieson, Dunham and Came and Kacker and Okapuu calibrated their correlations towards data from rotating turbines, whereas the correlations proposed by Moustapha and Benner were cascade test-based. As detailed in [43], turbine cascade tests, performed in facilities such as the one presented in Figure 2.60, provide a successful basis for estimating losses besides being simple, cost-effective and flexible, as they enable the independent study of profile and secondary incidence losses.

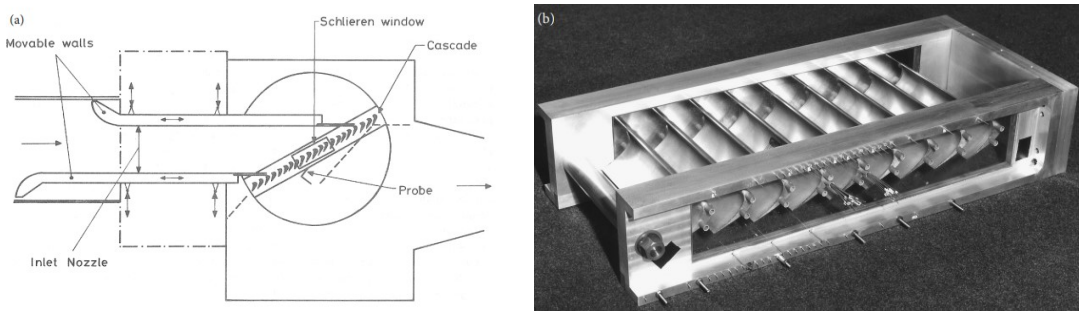

Figure 2.60: Turbine cascade facility and blade cascade prepared for testing [45].

However, the difference between both methods leads to mismatches in results when analyzing one correlation with the wrong database. Thereby, scaling factors are used in order to convert one type of correlations to the other for purposes of comparison. Benner

applied a scaling factor of 0.23 — which still led to scattered results—, to convert the Kacker and Okapuu/Moustapha correlation in order to compare them and present the improvements of the new developed correlation.

Angles convention

Another important consideration is the angles convention for the different models, which is presented in Figure 2.61, changing from the Ainley & Mathieson and Dunhan & Came to the Kacker & Okapuu, Moustapha and Benner loss models.

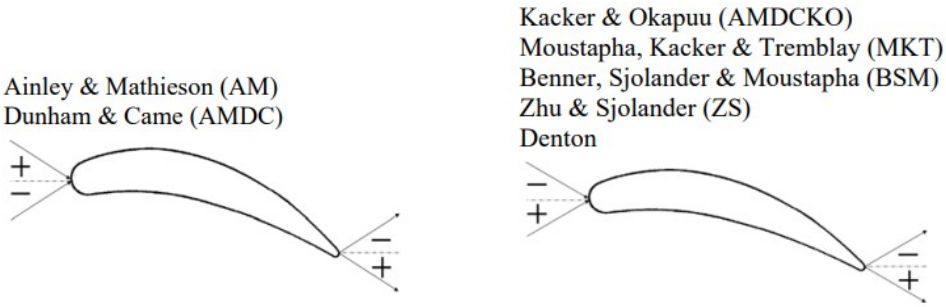

(a) Ainley & Mathieson and Dunham & Came [38].

(b) Kacker & Okapuu [38]

Figure 2.61: Angles convention for the different loss models

Main differences in loss components correlations

Summarizing and comparing the main aspects of the models presented, it can be said that:

- Regarding the profile losses, when it comes to the design point, the DC and KO models incorporate a correction of this coefficient in order to consider the effects caused by the Reynolds number, i.e. by the flow regime (laminar or turbulent) and by the Mach number (subsonic, transonic or supersonic flow). On the other hand, KO is the only one that also accounts for the effects of shock waves at the leading edge, by means of a coefficient included within the profile loss coefficient. When considering incidence in off-design conditions, Moustapha improved the AM off-design correlation and the Mukhtarov and Krichakin by including the effect of the leading edge diameter within the incidence profile losses, however, Benner further improved their correlation by reducing this effect and including the effect of the wedge angle.
- As for secondary losses, AM takes into account by means of a geometrical parameter some blade area ratios, as well as flow angles, while DC and KO additionally consider the aspect ratio, given the importance of its influence on the creation of vortices at the endwall, as was seen in Section 2.8.2. In addition, DC incorporates to the secondary loss coefficient from the AM model a correction to account for Reynolds number, however, KO does not consider it, but at the time of calculating the coefficient it takes into account the effects due to subsonic flow. Off-design secondary losses in Moustapha's correlation also included the effect of leading edge

diameter, however the Benner correlation was developed within a new loss breakdown scheme in which secondary losses where accounted with a lower weight than profile losses. Inlet boundary layer displacement thickness, convergence and aspect ratios and blade loading are important parameters affecting these losses.

- Leakage losses have been calculated similarly for the three models analyzed at the design point. While AM considers a linear correlation that takes into account parameters such as tip clearance gap, pitch or chord [39], the model presented by DC considers a non-linear relationship and proposes a coefficient to calculate such losses in more specific cases. KO warns that one of the values given by DC for this coefficient, the blockage factor B, overestimates the losses [8]. Neither Moustapha nor Benner propose a correlation for tip clearance losses in off-design conditions since they are cascade test-based and no tip clearance can be accounted.

- Finally, the way of accounting trailing edge losses differs between the two first presented models and the KO for design operating conditions. AM and DC consider a multiplication factor in order to obtain the total loss coefficient by accounting a trailing edge thickness different from the one of a default blade, in which $t_{te} = 0.02 \cdot s$ [39]. Whereas KO define a trailing edge loss coefficient which takes into account the boundary layers at this part of the blade. Moustapha and Benner consider trailing edge effects within the profile loss correlation.

2.9.7 Loss model verification and validation

As explained in the Section 2.7.3, despite verifying the correct application of the equations within a mathematical model against representative and reliable test data, to complete a loss modelling system it is necessary to validate that the equations best represent the physical problem. Validation of the loss model serves not only to quantify the uncertainty of the model due to the adopted simplifications, but also to improve its accuracy by using the above-mentioned scaling factors or other empirical coefficients [26]. To this end, the predominant choice when validating a loss model is to use the overall loss coefficient instead of the individual loss components, since any splitting in the former is artificial, as mentioned above, and is also a major source of uncertainty.

From this a general rule is derived, "it is better to use a set of models from a single source than to mix models from different sources", as explained in [26]. The fact of using a single source favours that the underestimates of any loss coefficient offset the overestimates in another loss coefficient, hence no significant difference will be found in the overall loss coefficient. However, even though the validation were to be carried out in a proper way, it has to be said that "there is no one loss modelling system that gives performance estimates within a guaranteed accuracy for all the types of turbines, and no chance of such a system being developed" [26].

In the following, several graphs from the papers of the authors of the various correlations will be presented. The aim of these graphs is, after verifying the model in question, comparing it with previous models and demonstrating the reached improvements. Note by that the only available datasets in the open literature with enough detail to separate the overall loss coefficient into the individual components come from turbine cascades

rather than from rotating turbines.

First, Figure 2.62 compares the Ainley and Mathieson and the Dunham and Came correlations. It is shown how after verifying the model, the efficiency prediction is more accurate once the corrections proposed by Dunham and Came (figure on the right) were applied to the Ainley and Mathieson original model (figure on the left). Both models have a tolerance of ± 2%.

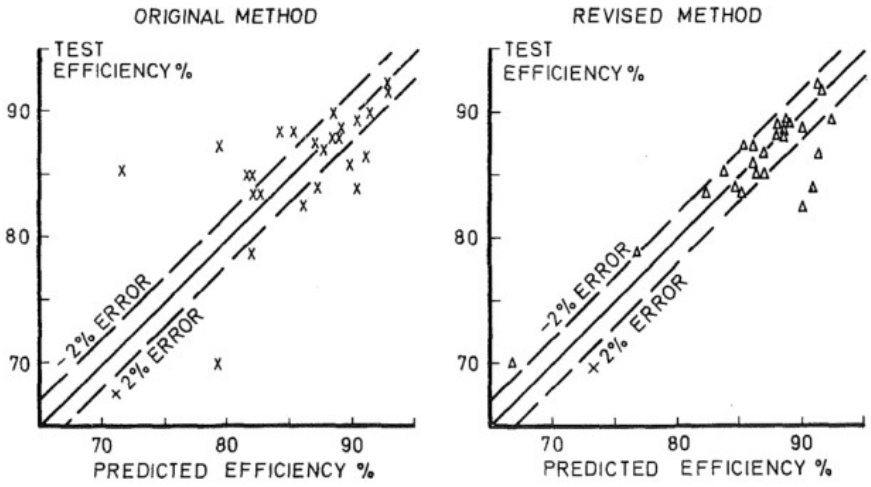

Figure 2.62: Ainley & Mathieson and Dunham & Came models' verification and comparison [39].

In the same way, by looking at Figure 2.63 in which the AMDC and KO correlations are compared, the higher accuracy of the model proposed by Kacker and Okapuu is justified, as it is a further refinement of the original model and takes into account influential parameters in the various losses considered. The results for the KO loss model are given within a tolerance of ± 1.5%.

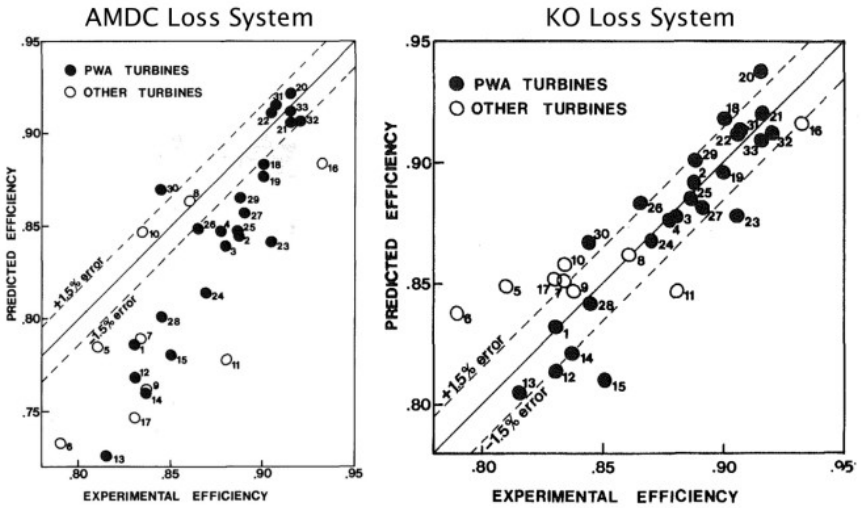

Figure 2.63: Ainley & Mathieson -Dunham & Came and Kacker & Okapuu model's verification and comparison [39].

Unlike the design-point correlations, compared in the graphs above in terms of efficiency, the graphs presented in [41], [43] and [46] compare the measured and predicted kinetic energy loss coefficient. From Figure 2.64 the improvements of the off-design profile loss correlation from Moustapha et al. (bottom) compared to the off-design Ainley and Mathieson correlation (left) and the Mukhtarov and Krichakin correlation (right) can be seen. The scattered points in the latter correlations are better predicted in the former, however, it can be seen that Moustapha et al.'s correlation still fails for some cascades.

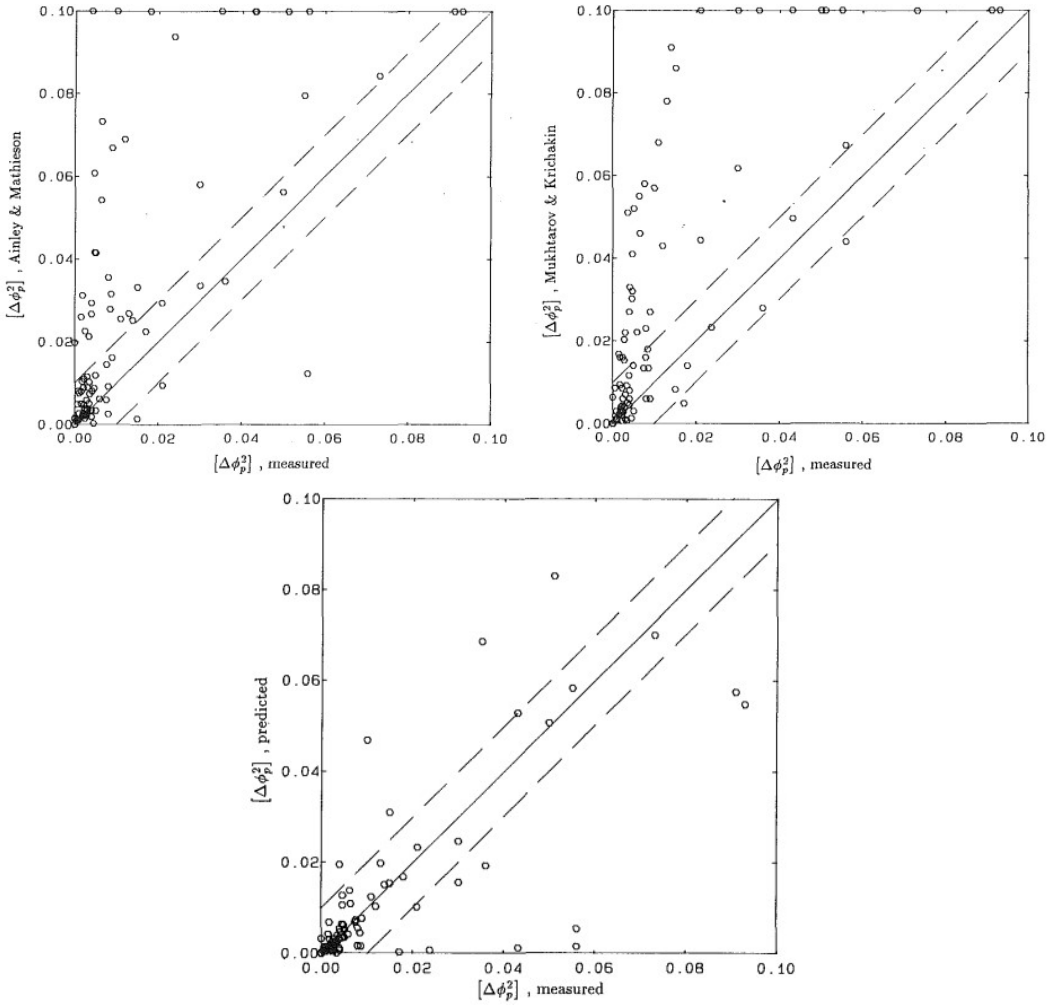

Figure 2.64: Comparison of the Ainley & Mathieson, Mukhtarov & Krichakin and Moustapha et al. off-design profile loss correlation [43].

The same conclusions are obtained for the off-design secondary loss correlation proposed by Moustapha et al. (bottom) compared to the off-design Ainley and Mathieson (top) and Mukhtarov and Krichakin (middle) correlations, as seen in Figure 2.65.

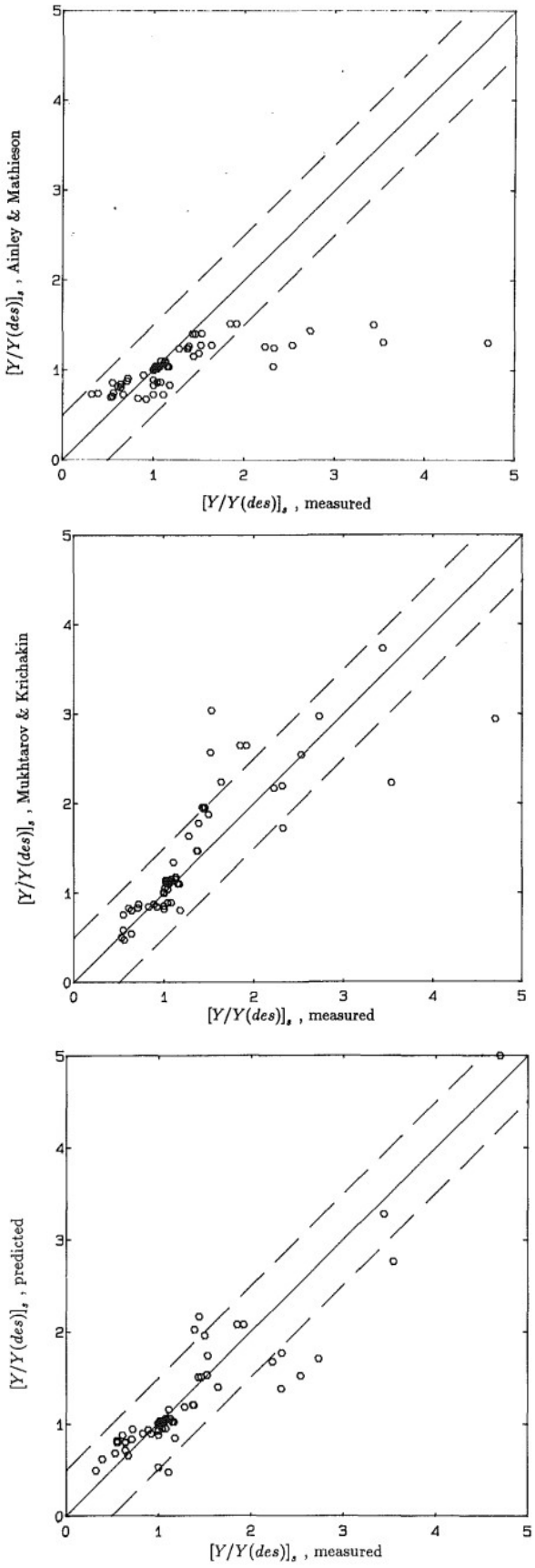

Figure 2.65: Comparison of the Ainley & Mathieson, Mukhtarov & Krichakin and Moustapha et al. off-design secondary loss correlation [43].

On the other hand, Figure 2.66 compares the Ainley and Mathieson off-design profile loss correlation (left) based on cascade data of 1940s and 1950s [41], with the Moustapha et al. profile loss correlation (right) and the Benner correlation (bottom), both for recent cascades. This may explain the inaccuracy of Ainley and Mathieson's correlation, improved by Moustapha et al.'s correlation and further improved by Benner's when including the effect of the wedge angle and reducing the effect of the leading edge diameter. The latter correlation fails for a few cascades but only for large incidence angles.

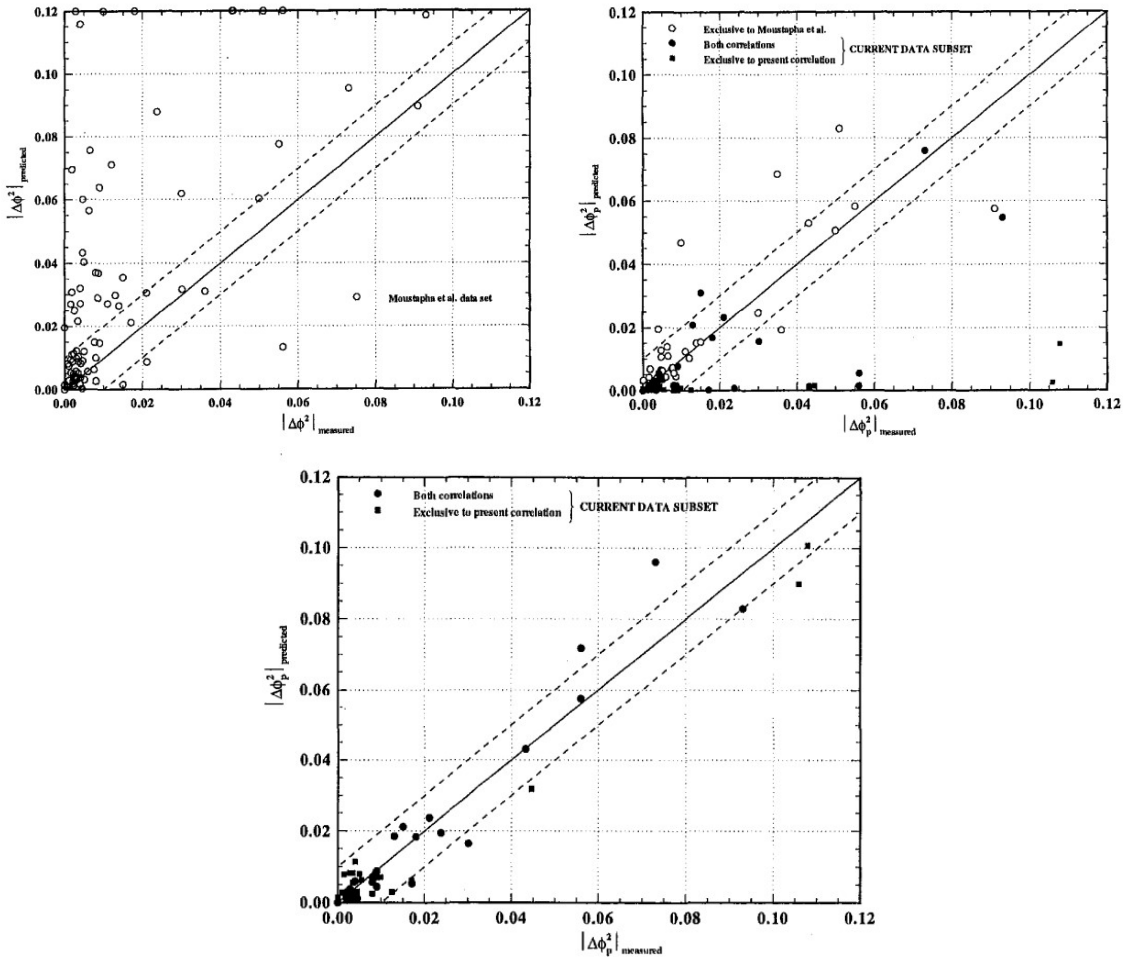

Figure 2.66: Comparison of the Ainley & Mathieson, Moustapha et al. and Benner off-design profile loss correlation [41].

Finally, Benner's secondary off-design loss correlation (right) within the new loss breakdown scheme was compared to the Kacker and Okapuu-Mousthapa et al. correlation (left), within the conventional breakdown scheme and based on a rotating turbine database. For this purpose, as mentioned before and as shown in the graph, the latter was scaled by a factor of 0.23. It can be noticed that Benner's correlation gave a better prediction, however, the scaling factor used for comparison purposes is empirical and should be considered as a source of inaccuracy to be studied in more depth.

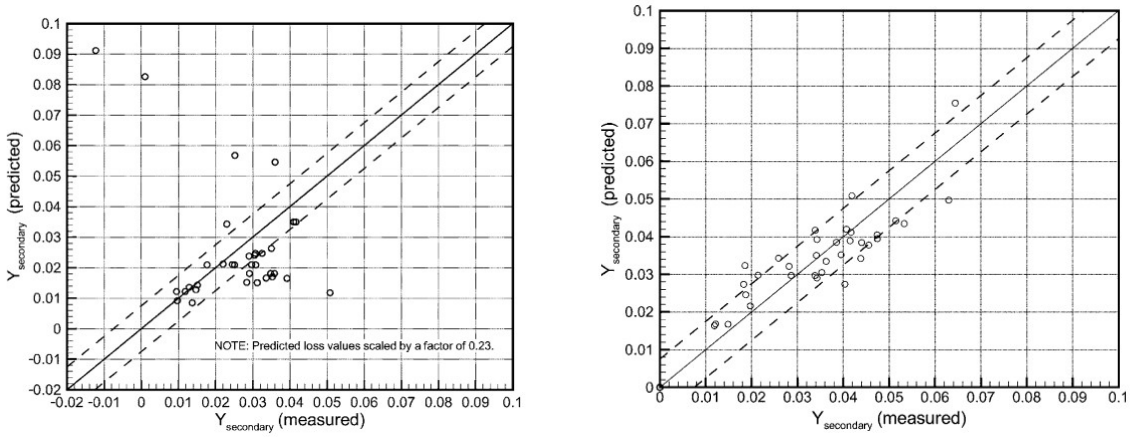

Figure 2.67: Comparison of the Kacker and Okapuu/Moustapha et al. and Benner off-design secondary loss correlation [46].

2.10 Sensitivity analysis and Design of Experiments

As it was introduced at the beginning of the thesis and reminded in Section 2.8.7, the target of this work is analyzing and quantifying the effect that the different design variables have on the turbine performance, by influencing the above presented loss components.

Sensitivity analysis (SA) is the tool that best fits for this purpose as it is precisely used to assess the impact and effect that changes in one or more input variables have on the output of a model, as well as to understand if the model is behaving correctly, before it is validated. It is important to note that a model is not validated by performing a sensitivity analysis on it. As it is explained in [47], "the only way to validate a model is to collect real-world data for both its input and output, and see whether the model fits reality once it is tested on that data".

But, sensitivity analysis has other advantages in addition to providing insight into model functioning and assessing the impact of parameter variation. By also knowing how the different variables interact, key parameters and irrelevant inputs to the model can be identified [47]. This can be used to improve and optimize the model performance, which in turn will allow better decisions to be made. It therefore provides an objective judgement criterion before moving on to the next stage of the model-building process, which was summarized in Figure 2.19. SA can be also used to test the robustness of the model and its reliability, as it can identify weaknesses in the face of uncertainty.

Among the different methods available to address sensitivity analysis, it has been decided to use the design of experiments for the development of this thesis. According to [33], design of experiments (DOE) is an encompassing term for the different techniques that are used to guide the choice and design of the experiments to be carried out for the purpose of a particular study. An experiment is precisely a set of tests in which these aforementioned variations to the variables of the model are performed in order to assess what has been explained so far in the preceding paragraphs.

The results provided by the different DOE techniques are usually combined with statis-

tical analysis methods, in order to account for the noise that data subject to experimental error may introduce [33].

These DOE techniques are characterized by seeking to ensure that experiments are carried out as efficiently as possible, i.e. in a way that the most information is obtained in the shortest time and at the lowest cost. Or, in other words, with as few factors involved as possible.

It seems natural that the selection of these factors is for this reason a key issue in conducting experiments, as they will allow the design space to be explored efficiently if they are strategically chosen and set with the remaining conditions of the experiment. However, despite the number of factors, the sample size is different for each DOE technique. In the following, only three of them will be briefly presented and explained, given their relationship and relevance to the thesis' work. But first, following the structure of the accessed source ([33]), it seems convenient to introduce the basic terminology used in the design of experiments:

- Factors: (input) variables of the model that are going to be studied.
- Design space: region covered in the experiment by varying the selected factors between a lower and upper bound.
- Levels: number of values that are going to be assigned to each variable. In other words, number of points at which the variables are going to be analyzed.
- Response variable: objective function, (output) variable for which the sensitivity analysis is to be carried out.
- Sample size or space: set of experiments or number of runs within an experiment in order to obtain results as efficiently as possible.

2.10.1 Full factorial design

Full factorial is one of the most known orthogonal DOE techniques for carrying out experiments if sufficient resources are available, as it provides the results of evaluating each level of each factor in all possible combinations [33]. In other words, every level of each factor is tested in conjunction with all the levels of the other factors. This allows to examine not only the main effects, but also the interaction effects between them, with the advantage that they are not confounded.

The sample size is given by the equation below:

$$N = L^k \tag{2.123}$$

where k is the number of factors and L is the number of levels per factor. The number of levels may differ from one factor to another.

It can be seen from Eq.(2.123) that the number of samples increases rapidly with the number of factors, which can lead to a very expensive and difficult to implement design. For this reason, the number of levels is also usually small, for instance 2 (low and high), or 3 (low, medium and high). These mentioned full factorial designs have been presented in Figure 2.68 (extracted from [33]) for two factors (a) and (b), and three factors (c), all with the same number of levels.

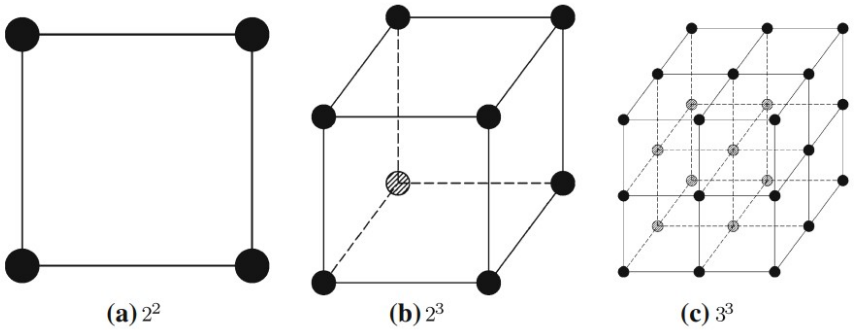

Figure 2.68: L^k full factorial experimental design [33].

The value for the low level, commonly denoted by "l", is "-1", whereas the value for the high level ("h") is "+1". The mean value ("m") for the above presented medium level is "0", and it stands for the average between the factor's low and high levels [33].

When assessing all the possible combinations of factors at all levels, a table can be built. As an example, the simplest case of 2-levels 2-factors table has been drawn up and presented in Table 2.5.

Table 2.5: 2^2 full factorial experimental design.

Runs	Factor level		Response variable	2-way interaction
	X_1	X_2		$X_1 \cdot X_2$
1	-1 (l)	-1 (l)	$y_{l,l}$	+1 (h)
2	-1 (l)	+1 (h)	$y_{l,h}$	-1 (l)
3	+1 (h)	-1 (l)	$y_{h,l}$	-1 (h)
4	+1 (h)	+1 (h)	$y_{h,h}$	+1 (l)

The main and interaction effects are calculated as "the difference between the average of the response variable at the high level and at the low level runs and the difference between the average of the response variable at the high and low level runs of the interaction effects" [33], as it is shown in Eqs. (2.124) and (2.125) respectively.

$$M_{X_i} = \frac{\sum_i y_i(h) - \sum_i y_i(l)}{2} \tag{2.124}$$

$$M_{X_{ij}} = \frac{\sum_{ij} y_{ij}(h) - \sum_{ij} y_{ij}(l)}{2} \tag{2.125}$$

Being for the example presented:

$$M_{X_1} = \frac{y_{h,l} + y_{h,h} - y_{l,l} - y_{l,h}}{2} \tag{2.126}$$

$$M_{X_2} = \frac{y_{l,h} + y_{h,h} - y_{l,l} - y_{h,l}}{2} \tag{2.127}$$

$$M_{X_{12}} = \frac{y_{l,l} + y_{h,h} - y_{l,h} - y_{h,l}}{2} \tag{2.128}$$

Insight into how each of the factors involved affects the response variable can be gained by studying the values obtained for the above effects, and it is — as said—, one of the main purposes for carrying out these experiments.

2.10.2 Fractional factorial design

In the case of having limited resources, carrying out a full factorial experimental design may not be the most efficient solution. Fractional factorial design instead selects a smaller set of all the possible combinations considered in the full factorial design. This still allows to study the factor's main effects but only some of the key interactions.

The sample size of the fractional factorial design is given by:

$$N = L^{k-p} \tag{2.129}$$

where L is the number of levels, k is the number of factors and p is the fraction factor that will determine the number of combinations that will be included in the design.

This fraction factor may often be set to 1 or 2, so the sample size will be respectively a half or a quarter of the full factorial sample size [33], but it is important that it is selected appropriately according to the restrictions being faced when performing the experiments, the number of factors, the number of levels of each factor and the available sample size, among others. As detailed in the source cited earlier in this paragraph, the fractional factorial sample size is properly selected as long as the samples are orthogonal (as in the full factorial design) and balanced, meaning that every factor has an equal number of samples for all of its levels.

A drawback of not studying all the possible combinations is that main and some interaction effects are aliased. This depends on the design resolution, which gives an idea of "how badly the design is confounded" [33]. The resolution of the design in turn depends on the accuracy of the definition of the words. A word or generator in a fractional factorial design specifies the particular combinations of factor levels that are aliased with each other within the design. The better the word is selected, the higher the resolution and the better the results can be expected. p words are required in an N-samples design.

The most common resolutions are the ones presented below:

- **Resolution III**: design that has aliasing between main effects a two-factor interactions. The former are clearly estimable whereas the latter are confounded with main effects and each other.
- **Resolution IV**: design in which higher orders of factors are aliased. Main effects and some two-factor interactions can be estimated but other two-factors interactions are confounded with each other and main effects are aliased with three-factor interactions [33].
- **Resolution V**: Main effects are aliased with four-factor interactions, and two-factor interactions are confounded with three-factor interactions.

As for the previous DOE technique, some graphical examples are provided in Figure 2.69 while the table for a 2^{3-1} design (2 levels, 3 factors and 1 word) is presented in Figure 2.70.

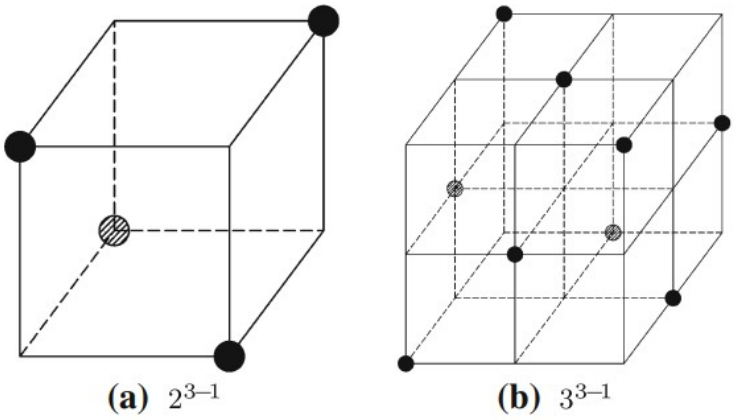

Figure 2.69: Examples of fractional factorial experimental designs [33].

Experiment number	Factor level X_1 (A)	X_2 (B)	$X_3 = X_1 \cdot X_2$ (C)	$I = X_1 \cdot X_2 \cdot X_3$
1	−1	−1	+1	+1
2	−1	+1	−1	+1
3	+1	−1	−1	+1
4	+1	+1	+1	+1

Figure 2.70: Example of 2^{3-1} fractional factorial experimental design [33].

From this last example it can be seen that the third factor's main effect is aliased with the 2-factors interaction, as it is a Resolution III design.

2.10.3 Central composite design

The last DOE technique that is being presented is the Central composite design (CCD), also known as Box and Wilson design. This design is usually a 2^k full factorial or resolution V fractional factorial, to which axial or star points and centre points are added [48].

These designs are widely known and used to fit second-order models in response surface methodology when quadratic effects are to be detected and taken into account, by considering these additional aforementioned points. The sample size of a Central Composite design when a 2^k full factorial is being used is given by:

$$N = 2^k + 2 \cdot k + n_c \tag{2.130}$$

where k is the number of factors, $2k$ are the star points and n_c the number of centre points.

The star points in this type of designs are the sample points outside or inside the experiment's domain in which all the factors except one are set at the mean level ("m"). It was seen in Section 2.10.1 that the levels of the sample points of the factorial design are -1 and 1, low and high respectively. Similarly, the levels of a design including the star points are $\pm\alpha$, with $|\alpha| \geq 1$ [49]. The value of the above mentioned remaining factor not set to the mean value is set to α, which — as detailed in [33]—, "is given in terms of distance from the central point".

There are different types of central composite designs according to this distance, which determines the quality and accuracy of the estimations together with the selection of the number of centre points. The three main types of CCD have been collected in Figure 2.71 and will be explained below. Moreover, Table 2.6 has been created in order to show an example of a central composite experimental design.

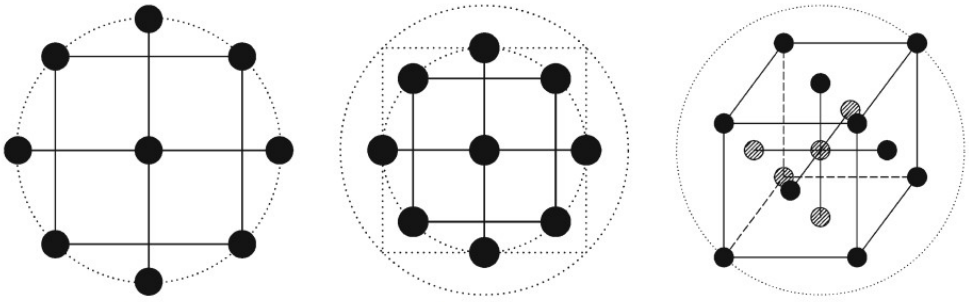

Figure 2.71: Examples of central composite experimental designs [33].

Looking at Figure 2.71 and normalizing the distance between the central point and each point of the full factorial (also known as cube points) to 1, the three different designs presented are obtained. As said, they are characterized by the different distance from the central point to the star points. These are:

- **Central composite circumscribed design - (CCC)**

  This first design, seen in Figure 2.71 (a), is commonly used for a spherical region of interest, since all the samples (cube and axial points) are located on a hypersphere equidistant from the central point when α is set to 1. As it can be seen, axial points are located outside the experiment's domain.

In this type of designs it is usual to replicate the centre point from 3 to 5 times in order to achieve a balanced and consistent variation in the predicted response [48]. Five levels are required for each factor in the CCC design: "ll", "l", "m", "h" and "hh".

- **Central composite inscribed design - (CCI)**

  If the region of interest is spherical but the limits of the higher and lower levels cannot be violated, the central composite inscribed design (Figure 2.71(b)) is frequently used. By scaling down the previous design (CCC) and setting all the samples at a distance of $\frac{\sqrt{k}}{k}$ from the central point, this is achieved.

  Five levels are also required for every factor in the CCI design, but now these are: "l", "lm", "m", "mh" and "h".

- **Face-centered central composite design - (CCF)**

  The last design shown in Figure 2.71(c) is the face-centered central composite design. By setting α to $\frac{\sqrt{k}}{k}$ the star points are being located in the middle of the faces of the cube that represents the experiment's domain.

  Unlike the previous two designs, only three levels are required in the CCF design: "l","m" and "h". For this reason it is often preferred to the other two options, but it has a disadvantage compared to them that must be taken into account in the subsequent analysis of the results. This drawback will be commented below. The number of centre points required in this design to provide a stable variance in the predicted response is also smaller than in CCC and CCI.

Table 2.6: 2^k and 2 factors Central Composite experimental design.

Runs	Factor level		2-way interaction	Quadratic effects	
	X_1	X_2	$X_1 \cdot X_2$	X_1^2	X_2^2
0	0	0	0	0	0
1	+1	+1	1	1	1
2	+1	-1	-1	1	1
3	-1	+1	-1	1	1
4	-1	-1	1	1	1
5	α	0	0	α^2	0
6	-α	0	0	α^2	0
7	0	α	0	0	α^2
8	0	-α	0	0	α^2

From Table 2.6 it can be seen that run 0 stands for the central point, runs 1-4 are the cube points and runs 5-8 are the star points. These are allowing to distinguish the different quadratic effects, which would be aliased in case no axial points were being considered and the experiment was reduced to a factorial design.

Regarding the aforementioned drawback in the CCF design, it is to be said that while CCC and CCI are rotatable designs, CCF is not. Rotatability is the property by which

the variance of the predicted response is said to be constant for all the points that are at the same distance from the central point within the design space. This property is important towards the selection of a response surface as precision is sought in order to locate the surface's optimum.

It was said at the beginning of this subsection that central composite designs are usually employed within the response surface methodology as they can fit second-order models without confounding quadratic effects if a proper regression model is selected in order to analyze the results. Further comments on response surface methodology (RSM) and on some of the statistical methods that are often combined with these presented DOE techniques will be done in Section 3.2.4.

3 Methodology

In this section, the methods that have been used for developing this thesis are going to be described. First, the mean-line model that is going to be employed as design tool will be presented, followed by the loss model selection and implementation, necessary in order to obtain and assess the performance of the turbine. The different bounds and constraints that have been defined for the optimization are also going to be introduced. Next, a sensitivity analysis will be carried out in order to check that the implemented model makes sense and gives reasonable results, with the underlying aim of improving the optimization mode of the model by knowing how the main design variables affect the turbine efficiency.

The sensitivity analysis will be performed in different steps. First, a non-rigorous factorial analysis will be carried out in order to choose the factors that will be studied within the selected design of experiments technique: the face-centered central composite design. All the necessary variables will be introduced in order to use the above technique and carry out the desired experiments. From these experiments — which will be described in detail—, the main, interaction and quadratic effects of the chosen factors over the selected output will be obtained and analyzed with different statistical techniques that will also be mentioned.

Finally, the optimization will be run before and after the sensitivity analysis with some modifications derived from the extracted conclusions. Both, the mean-line model and sensitivity analysis have been carried out by using the Python programming language. Limitations in the model while performing the experiments will be also introduced within this section and Section 4, once the results have been presented.

3.1 Mean-line model for performance assessment and preliminary design of one stage axial turbines

The model that has constituted the basis for the previous project and the current thesis offers a two-fold method for assessing the performance of one stage axial turbines and for optimizing its preliminary design.

The low efficiency and potential of the current ORC expanders, expected to work best at the design point towards a series of variable input conditions, have led to the purpose of this method: providing a solid tool for evaluating these turbines over a wide range of operating conditions, thereby for both, design and off-design operating points.

The workflow of the mathematical model that will be presented next is shown in Figure 3.1. Even though the same model is used for the two aforementioned purposes, both modes are formulated differently and can operate separately. As it can be seen in the flowchart, from the input data to the model, the performance analysis is performed first. Then, the preliminary design is completed with the optimization routine. It is important to note that both modes have to be consistent in order to obtain valid results.

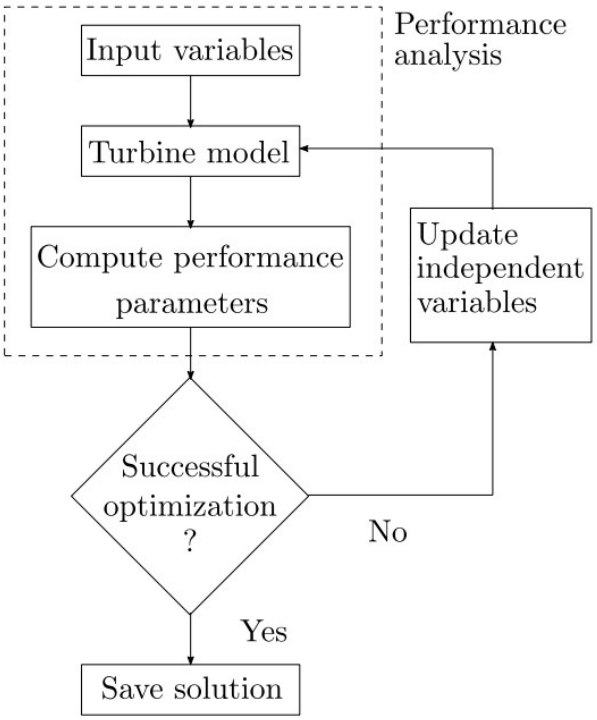

Figure 3.1: Model's flowchart for the preliminary design optimization process and performance evaluation [28].

The objective of each mode is as follows:

- **For the performance assessment:** given the geometry and design point, characterized by the working fluid, loss model and thermodynamic boundaries, obtaining the performance of the turbine, in turn characterized by parameters such as the efficiency, mass flow rate or work output among others. This is done by solving a system of equations set from determining some kinetic and thermo-physical unknown variables (velocity and static pressure inputs) [28].
- **For the optimization mode**: given the design point— characterized by the thermodynamic boundaries, loss model and working fluid—, and given the design variables, obtaining the values of the geometrical variables that optimize the objective function. This function has been set to the total to static efficiency, however it can be changed to any other performance parameter [28]. This is reached by using an optimization algorithm in Python that gives values to the geometric variables, rotational speed and input velocity and static pressure until the optimal is found. A more detailed explanation will be given in Section 3.1.3.

Different versions of the model presented below have been used during the thesis work. The most recent one presents these two modes independently. The performance mode is accessed through a class object called "Turbine class"; while the optimization mode is accessed through "Optimal turbine", a child class of Turbine class. Both modes will be presented in detail.

3.1.1 Mathematical model for performance assessment

The mathematical model developed for the preliminary design is based on the assumption of uniform flow in the circumferential and spanwise directions [28], since the turbine performance is calculated along the flow path mean line. As explained in Section 2.7, the mean-line approach assumes that the passage conditions through the stage of a turbine are averaged at the mean streamline [50].

In order to determine the expanders' overall characteristics for specific input parameters with the mean-line approach, different stations of the expander must be assessed. This model stands out for evaluating the turbine performance at three stations, not only inlet and exit, as most of other available methods, but also at the throat. The evaluation is done for each blade row. Additionally, the model is able to predict which of these blade rows are chocked by using a novel numerical treatment of flow chocking [28].

According to the performance analysis mode, it has been said that these particular input parameters to the Turbine class are a design point or condition (given by thermodynamic boundaries and working fluid) and the main design variables which are essentially geometric. On the other hand, the aforementioned unknown kinetic and thermo-physical variables are obtained by assessing the velocity triangles and equations of state at each station of the turbine. An initial guess for these variables is required as it is crucial for the convergence of the model. Moreover, in order to obtain from this mode the turbine's overall performance parameters, the losses must also be accounted by selecting a loss model to predict the overall loss coefficient. This loss model is selected within the condition provided as input parameter to this mode of the model.

The workflow in Figure 3.2 has been created to summarize the process within the dashed line of the performance analysis mode in Figure 3.1.

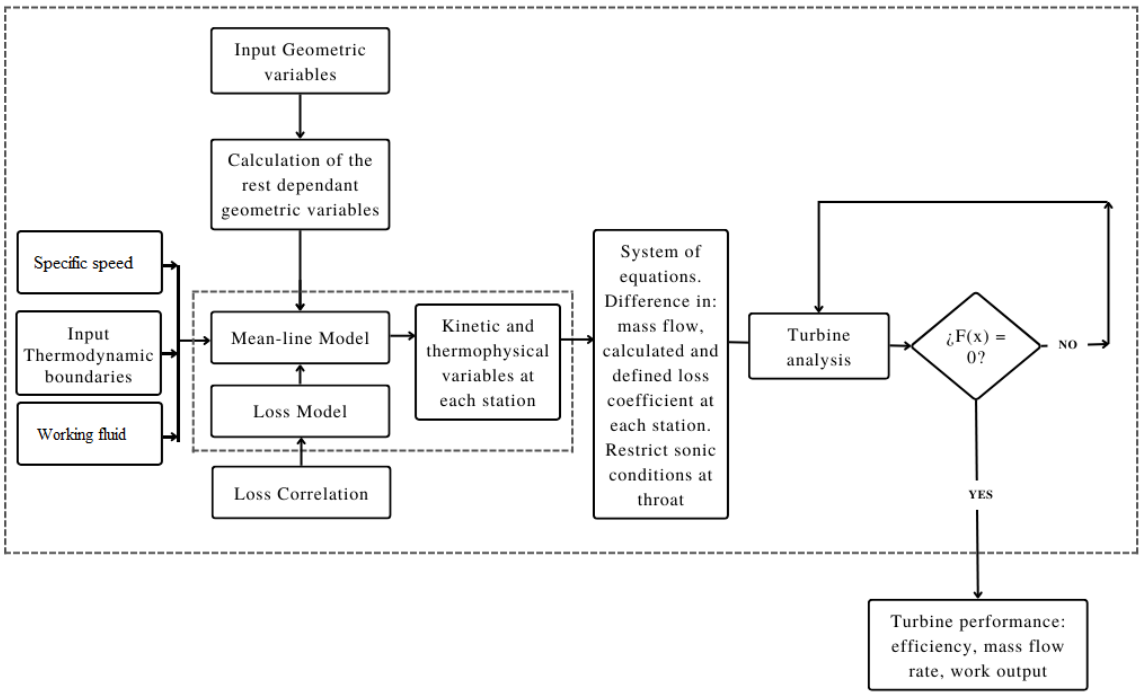

Figure 3.2: Workflow for the performance analysis mode.

As said and depicted in the workflow, not all geometrical variables are given as inputs. In order to make it easier for the optimization algorithm to perform the relevant calculations, a better option is to make use of equations relating some of these variables, so that they can be calculated from the minimum number of independent variables required. These variables are listed in Table 3.1 and are related to the cross sectional shape of the blades, to the distance between adjacent blades and extent in radial direction [28]. As for every turbomachine, stator and rotor have to be considered separately.

To avoid redundancy, the equations of the model that have been previously introduced in the technical background have been omitted in this section. However, they have been referred to where it has been convenient.

Table 3.1: Geometric variables of the axial turbine set as input to the model [28].

Variable	Stator	Rotor
Specific diameter	d_{spe}	d_{spe}
Aspect ratio (AR)	$(H/c)_s \equiv AR_s$	$(H/c)_r \equiv AR_r$
Blade solidity (BS)	$(c/s)_s \equiv BS_s$	$(c/s)_r \equiv BS_r$
TE thickness to opening ratio	$(t_{te}/o)_s$	$(t_{te}/o)_r$
Inlet methal angle	$\theta_{in,s} \equiv \theta_1$	$\theta_{in,r} \equiv \theta_4$
Outlet methal angle	$\theta_{out,s} \equiv \theta_3$	$\theta_{out,r} \equiv \theta_6$
Inlet hub-to-tip ratio	$r_{ht_{in,s}} \equiv r_{ht_1}$	$r_{ht_{in,r}} \equiv r_{ht_4}$
Exit hub-to-tip ratio	$r_{ht_{out,s}} \equiv r_{ht_3}$	$r_{ht_{out,r}} \equiv r_{ht_6}$

From the specific diameter, the initial guess for mass flow rate, and the thermodynamic conditions at inlet and exit, the mean radius is obtained as:

$$r_{mid} = d_{spe} \cdot \frac{\sqrt{\frac{\dot{m}_{guess}}{\rho_{6,is}}}}{\sqrt[4]{\frac{h_{01}-h_{6,is}}{2}}} \tag{3.1}$$

Note that the blade converges and diverges in the same way at the inner and outer wall of the flow passage, as shown in Figure 2.16, therefore, the mean radius is considered constant [28]. The stator inlet flow angle is 0° since the flow enters in the axial direction, and even though it is not included within the design variables it is convenient to remind that no tip clearance is considered in the stator.

By using some of the equations presented in Section 2.6, the following geometrical variables are obtained:

- Stator inlet and outlet heights, $H_{in,s}$ and $H_{out,s}$ from Eq.(2.45)
- Rotor inlet and outlet heights, $H_{in,r}$ and $H_{out,r}$ also from Eq.(2.45)
- Blade chord for stator, c_s, and rotor, c_r, from the aspect ratio (AR)
- Blade pitch for stator, s_s, and rotor, s_r, from the blade solidity (BS)

- Blade camber for stator, $\Delta\theta_s$, and rotor, $\Delta\theta_r$, from Eq.(2.36)
- Blade axial chord for stator, c_{ax_s}, and rotor, c_{ax_r}, from Eq.(2.37)
- Stagger angle for stator, ξ_s, and rotor, ξ_r, from Eq.(2.38)
- Blade opening for stator, o_s, and rotor, o_r, from Eq.(2.39)
- Blade trailing edge thickness for stator, te_s, and rotor, te_r, from the trailing edge thickness to opening ratio
- Blade maximum thickness for stator, t_{max_s}, and rotor, t_{max_r}, from Eq.(2.40)
- Area at each station, A_{in} and A_{out} from Eq.(2.46) and A_{throat} from Eq.(2.47)
- Stator and rotor flaring angle, $\delta_{fl,s}$ and $\delta_{fl,r}$ from Eqs.((2.41) and (2.43)) and from the mean blade height.
- Mean blade height for stator, H_s, and rotor, H_r, given by the equations below (Eq.(3.2) and Eq.(3.3))

$$H_s = \frac{H_1 + H_3}{2} \tag{3.2}$$

$$H_r = \frac{H_4 + H_6}{2} \tag{3.3}$$

The next input variables to the model are the thermodynamic boundaries listed in Table 3.3, which together with the working fluid and loss model constitute the design point or condition. These boundaries comprise the inlet stagnation temperature, since it is in the turbine inlet where stagnation is specified; inlet stagnation pressure and outlet static pressure. The working fluid in this particular study will be Pentafluoroethane R125. The selection of the loss model will be commented in Section 3.1.2. In the case of selecting the Benner loss model, the variables listed in Table 3.2 must be added to the design variables in Table 3.1.

Table 3.2: Extra design variables to compute the Benner loss model.

Variable	Stator	Rotor
Wedge angle	We_s	We_r
Leading edge thickness to pitch ratio	$(le/s)_s$	$(le/s)_r$

As it can be expected, the leading edge thickness for the stator blade, le_s, and for the rotor blade, le_r are obtained from the blade pitch and the leading edge thickness to pitch ratio presented in Table 3.2.

Table 3.3: Design point for the turbine [28].

Variable	Symbol
Inlet stagnation temperature	$T_{0,in} \equiv T_{0,1}$
Inlet stagnation pressure	$p_{0,in} \equiv p_{0,1}$
Outlet static pressure	$p_{out} \equiv p_6$
Working fluid	-
Loss model	-

From the input variables in Table 3.3, kinetic and thermophysical variables must be assessed along the different stations of the stage: inlet, throat and outlet in this case. For the implementation of the model, stator inlet, throat and exit are accounted as stations 1, 2 and 3 respectively. Similarly, stations 4, 5 and 6 are respectively rotor inlet, throat and exit.

CoolProp is the library of thermophysical properties that has been used to calculate variables such as the fluid density, ρ, speed of sound, a, pressure, p and dynamic viscosity, μ, at the inlet of the turbine, as a function of entropy and enthalpy at that station; and fluid density, speed of sound, entropy and dynamic viscosity through the rest of the turbine, as a function of static pressure and enthalpy.

Throughout the turbine, the enthalpy is calculated as explained in Section 2.4.2 with Eq.(2.6), whereas the pressure has to be set as an input to the model for every evaluated station (initial guess provided except for static exit pressure). Moreover, the entropy generation is predicted by means of a loss coefficient in order to enable the performance analysis. This loss coefficient can be either predicted by using the correlations presented in Section 2.9, or calculated by using its definition (Eqs.(2.73) and (2.74)). There should not be any difference between the results obtained for each method. For each blade row, the entropy and consequently, the loss coefficient are assessed at the throat and at the exit, even though the loss models are thought to predict losses between the inlet and exit [28].

To compute the unknown kinetic variables, the velocity triangles described in Section 2.6.2 also have to be assessed at each station. Thus, another parameter required for this purpose is the rotational speed, Ω. It is obtained from the specific speed (Ω_{spe}) — set as input to the model together with the design variables in Table 3.1—, the initial guess for mass flow rate and other thermo-physical variables, as shown in Eq.(3.4).

$$\Omega = \Omega_{spe} \cdot \frac{\sqrt[4]{(h_{01} - h_{6,is})^3}}{\sqrt{\frac{\dot{m}_{guess}}{\rho_{6,is}}}} \tag{3.4}$$

Blade speed is also consequently calculated as the product of mean radius and rotational speed, as shown:

$$u = \Omega \cdot r_{mid} \tag{3.5}$$

From the equations of the velocity triangles in Section 2.6.2 (eqs.(2.57)-(2.60)) and from assuming no deviation between the throat and exit, the rest of the unknown angles can be calculated. These unknown kinetic variables together with the thermo-physical aforementioned variables are gathered in Table 3.4.

Table 3.4: Kinetic and thermo-physical variables computed from the input variables [28].

Variable	Symbol	
Stator inlet velocity	$v_{in,s}$	$\equiv v_1$
Stator throat velocity	$v_{throat,s}$	$\equiv v_2$
Stator exit velocity	$v_{out,s}$	$\equiv v_3$
Rotor throat relative velocity	$w_{throat,r}$	$\equiv w_5$
Rotor exit relative velocity	$w_{out,r}$	$\equiv w_6$
Stator exit absolute flow angle	$\alpha_{out,s}$	$\equiv \alpha_3$
Rotor exit relative flow angle	$\beta_{out,r}$	$\equiv \beta_6$
Stator throat static pressure	$p_{throat,s}$	$\equiv p_2$
Stator exit static pressure	$p_{out,s}$	$\equiv p_3$
Rotor throat static pressure	$p_{throat,r}$	$\equiv p_5$

Once the variables in Table 3.4 have been computed, the mass flow rate, and Reynolds and Mach numbers can be evaluated along the stage. This, together with the two methods for obtaining the loss coefficient (definition and loss model), leads to the following system of equations, that must be satisfied in order to provide a physical solution:

$$\begin{cases} \dot{m}_{in} - \dot{m}_{throat} = 0 \\ \dot{m}_{in} - \dot{m}_{out} = 0 \\ Ma_{throat,rel} - min(1, Ma_{out,rel}) = 0 \\ (Y_{def} - Y_{loss})_{throat} = 0 \\ (Y_{def} - Y_{loss})_{exit} = 0 \end{cases} \tag{3.6}$$

These equations state that the mass flow rate must be constant along the stage, Mach number must be restricted to 1 at the throat, and there should be no difference between the defined and calculated loss coefficient, as explained before. The mean-line model predicts the optimal performance parameters that satisfy the system in Eq. (3.6). For this purpose, a root finder is used. A tolerance of 10^{-5} in the residuals provided by the root finder has been set to accept the obtained optimal solution. These overall performance parameters are:

- Total to static efficiency, η_{ts}
- Total to total efficiency, η_{tt}
- Mass flow rate, $\dot{m}$
- Power output, $\dot{W}$

For the user's information, the model has been implemented in a way that it has a default initial guess, in case no values are specified when initializing the turbine analysis mode.

It is also to be said that previous versions of this model have been validated against a numerical case and three different experimental cases, achieving in all of them values for the performance parameters that are within, or almost within the limits set by the author of the loss model that was chosen for accounting the losses. The present model still needs to be validated. Lack of databases and a delay in the availability of the test rig of the

department's laboratory have prevented it from being carried out within the framework of this work. It will be discussed in more detail in Section 5.

3.1.2 Loss model selection

Having already presented the model's performance analysis mode, the next step is selecting the loss model that will be used to account for the entropy generation within the turbine blade passages during the expansion process.

A comparison of the different loss models used for design conditions and introduced in Section 2.9 (AM, DC and KO), had been carried out as a previous study. No significant conclusions could be extracted since the model was not validated using all these mentioned loss models. Conversely, the trends followed by each loss model were observed, compared and commented. What could be concluded from that previous study, as seen and discussed in the technical background, was that none of the analyzed models were suitable for off-design conditions. Ainley and Mathieson had developed an off-design loss correlation, as explained, but it was not implemented in Python.

Therefore, in order to address the objective of providing a valid tool for conditions far from the design point, it was necessary to implement in Python a more advanced loss model to account for incidence losses. Two different options have been presented in Section 2.9, the Moustapha et al. and Benner et al. loss models, both of them — unlike the previous three —, cascade test-based. From the comparison in Section 2.9.6 and the discussion in Section 2.9.7, it was seen that the Benner loss model — which was developed within a new and more precise loss breakdown scheme —, further improved the previous correlations, providing more accurate results after being verified. The fact of being a cascade test-based model and thereby being subject to a scaling factor when comparing results with rotating turbine-based models is still a drawback, since this scaling factor cannot be obtained but empirically. However, the Benner loss model is the one that has been selected to characterize and carry out the analysis that will be presented hereafter.

The Benner loss model was implemented in the Python programming language as a function called within the mean-line performance analysis mode to obtain the calculated total loss coefficient. The function is called by providing the kinetics and geometrical variables of the turbine described in Section 3.1.1. From these variables, the ones that are loaded to calculate the different loss coefficients are respectively gathered in Table 3.5 and Table 3.6, for both stator and rotor.

Table 3.5: Kinetic variables loaded from the turbine for the Benner loss model.

Variable	Symbol
Exit flow angle	α_{out}/β_{out}
Inlet flow angle	α_{in}/β_{in}
Boundary layer displacement thckness to blade height ratio	δ
Exit relative Mach number	$\mathrm{Ma}_{rel,out}$
Heat capacity ratio	γ

Table 3.6: Geometric variables loaded from the turbine for the Benner loss model.

Variable	Symbol
Pitch	s
Chord	c
Inlet methal angle	θ_{in}
Exit methal angle	θ_{out}
Axial chord	c_{ax}
Mean blade height	H
Stagger angle	ξ
Leading edge thickness	le
Wedge angle	We
Tip clearance	t_{cl}
Cascade type	Stator or rotor

The total loss coefficient, Y_{tot}, is calculated by using Eq.(2.117) in Section 2.9.5, where the different components are calculated as follows:

- Y_{mid} is calculated as the sum of the incidence losses Y_{inc}, obtained from the conversion of the energy loss coefficient, by using eqs.(2.107), (2.114) and (2.116); and in turn, the sum of the Kacker and Okapuu corrected profile loss and trailing edge loss coefficients, given respectively by the product of eqs.(2.89), (2.94) and (2.95), and Eq.(2.105).
- $\frac{Z_{TE}}{H}$ is calculated by using Eq.(2.118).
- Y_{sec} is calculated by means of Eq.(2.122).
- Y_{cl} is also calculated as for the DC and KO loss models with Eq.(2.91), since Benner did not define any correlation for these losses as his model is cascade test-based and no clearance is considered.

The different loss components can be accessed either individually or computed into the total loss coefficient, as expected.

3.1.3 Mean-line model optimization mode

The second mode that the model offers is the optimization mode. An "Optimal turbine class" was created as a child of the already presented "Turbine class", meaning that it is initialized with the same design variables and conditions used to initialize the previous mode and that it inherits its attributes and methods.

In the following, the optimization problem is going to be described in accordance with the structure presented in Section 2.7.4.

Since a comparison between the optimal turbine before and after the sensitivity analysis that will be presented in the section below has been carried out, two different optimizations must be described. The decisions that were taken for the post-sensitivity analysis

optimization are derived from the conclusions drawn from the sensitivity analysis. Therefore, no deeper explanation than the one provided below will be given until the results from the sensitivity analysis are discussed (Section 4.3).

- **Objective function**

  First, the objective function had to be set from among the turbine overall performance parameters gathered in Section 3.1.1. It has been chosen to maximize the total to static efficiency, η_{ts}, given by Eq.(2.65), but any of the other parameters could have been selected, as it has already been said. This yields as shown:

  $$\text{Minimize} \hookrightarrow -\eta_{ts}(\mathbf{x}) \tag{3.7}$$

  and will be the same for both optimal turbines.

- **Fixed parameters**

  Before establishing the degrees of freedom of the optimization problem, a careful study of the input variables to the model is recommended in order to carry out the optmization efficiently. From this study, the decision of not wanting to include in the optimization all the input variables to the model may arise. For this purpose, some of them can be fixed in order to save their associated time and computational cost within the optimization. In addition to this, the variables included in the design point (Table 3.3) are fixed parameters in the model.

  - For the optimal turbine pre-sensitivity analysis: no parameters were fixed.
  - For the optimal turbine post-sensitivity analysis, the following parameters were fixed:
    - Stator aspect ratio, AR_s
    - Stator TE thickness to opening ratio, $(t_{te}/o)_s$
    - Stator leading edge thickness to height ratio, $(le/s)_s$
    - Stator wedge angle, We_s
    - Rotor aspect ratio, AR_r
    - Rotor TE thickness to opening ratio, $(t_{te}/o)_r$
    - Rotor leading edge thickness to height ratio, $(le/s)_r$
    - Rotor wedge angle, We_r

    The values that are going to be set to fix each of the reported variables will be presented in Section 4.4.

- **Degrees of freedom**

  Regarding the degrees of freedom, some differences between both optimal turbines can also be found.

  - For the optimal turbine pre-sensitivity analysis: all the design variables collected in Table 3.1 and Table 3.2 have been set as degrees of freedom to optimize.

– For the optimal turbine post-sensitivity analysis: all the design variables in Table 3.1 and Table 3.2 except the ones that have been fixed (presented above) have been set as degrees of freedom to optimize.

- **Optimization constraints**

  The optimization mode has been implemented in order to account for any equality or inequality constraint set by the user. Lower and upper bounds for each of the design variables and kinetic and thermo-physical variables provided as initial guess are set as default. These bounds have been selected according to R. Agromayor's previous work, based on a thorough literature review and are shown in Table 3.7.

Table 3.7: Lower and upper bounds for scaling the required variables

Cascade Type	Stator		Rotor	
Bound	Lower	Upper	Lower	Upper
Specific diameter, d_{spe}	0.1	10	0.1	10
Aspect ratio, $(H/c)_s$	1	2	1	2
Blade solidity, (c/s)	0.9	3.5	0.9	3.5
Inlet hub-to-tip ratio, $r_{ht_{in}}$	0.5	0.9	0.5	0.9
Exit hub-to-tip ratio, $r_{ht_{out}}$	0.5	0.9	0.5	0.9
TE thickness to opening ratio, (t_{te}/o)	0.05	0.4	0.05	0.4
Inlet methal angle, θ_{in}	-15 $\cdot\frac{\pi}{180}$ rad	15 $\cdot\frac{\pi}{180}$ rad	-15 $\cdot\frac{\pi}{180}$ rad	-15 $\cdot\frac{\pi}{180}$ rad
Outlet methal angle, θ_{out}	40 $\cdot\frac{\pi}{180}$ rad	80 $\cdot\frac{\pi}{180}$ rad	-80 $\cdot\frac{\pi}{180}$ rad	-40 $\cdot\frac{\pi}{180}$ rad

Bound	Lower	Upper
Specific speed, Ω_{spe}	0.1	10
Stator inlet absolute velocity, v_1	0.01	0.2
Stator throat absolute velocity, v_2	0.3	0.9
Stator exit absolute velocity, v_3	0.3	0.9
Stator exit flow anlge, a_3	40 °	80 °
Rotor throat absolute velocity, w_5	0.4	0.9
Rotor exit relative velocity, w_6	0.4	0.9
Rotor exit flow angle, b_6	-80 °	-40 °
Stator throat static pressure, p_2	0.4	0.9
Stator exit static pressure , p_3	0.4	0.9
Rotor throat static pressure, p_5	0.3	0.8

In addition to these bounds, the closure equations (Eq.(3.6)) are specified in the model as a set of equality constraints to guarantee a physical solution [28].

No additional constraints have been considered to evaluate the turbine before and after the sensitivity analysis, as the main objective is to see how for the same conditions the sensitivity analysis affects the results. However, in the case of using the model to design a single-stage axial turbine, some of the equality constraints that can be added are those related to the mass flow rate or flaring angle, among others.

- **Optimization algorithm**

  A gradient-based algorithm has been used to tune the selected degrees of freedom in order to reach the optimal value of the objective function respecting the bounds and constraints presented above [28]. This algorithm is the sequential quadratic

programming (SQP) algorithm, which is available in the Python's Scipy library [51].

Robust optimization mode

The model has a third mode, which provides the optimal turbine obtained from robust optimization. In order not to extend the memory of the thesis more than necessary, as this function has not been used, no further details will be given. It has been mentioned just to show the completeness of the model being used.

3.1.4 Case study for analysis and comparison of the optimization results

Although the model cannot be used to predict or reproduce a case study without prior validation, at this point it is necessary to define a particular case on which the sensitivity analysis will be based, and for which the comparison between this case and optimal turbines will be carried out. This case study is currently set by L.B. Anderson in his model as default case, based on the previous work of R.Agromayor. The values for the design variables and condition and kinetic and thermo-physical inputs for the initial guess are shown in Table 3.8, Table 3.9 and Table 3.10, respectively.

Table 3.8: Values for the input geometrical variables and specific speed for performance analysis

Cascade Type	Stator		Rotor	
Variable	Symbol	Value	Symbol	Value
Specific diameter	d_{spe}	2,26	d_{spe}	2,26
Aspect ratio (AR)	$(H/c)_s$	1.5	$(H/c)_r$	2
Blade solidity (BS)	$(c/s)_s$	1.6	$(c/s)_r$	1.5
Inlet hub-to-tip ratio	r_{ht_1}	0.6	r_{ht_4}	0.6
Exit hub-to-tip ratio	r_{ht_3}	0.6	r_{ht_6}	0.55
TE thickness to opening ratio	$(t_{te}/o)_s$	0.05	$(t_{te}/o)_r$	0.05
Inlet methal angle	θ_1	0	θ_4	-14.32 °
Outlet methal angle	θ_3	80.21 °	θ_6	-77.35 °
Specific speed	Ω_{spe}	0.9	Ω_{spe}	0.9

Table 3.9: Design point for performance analysis.

Variable	Value
Inlet stagnation temperature, $T_{0,in}$	428.15 K
Inlet stagnation pressure, $p_{0,in}$	$3.618{\cdot}10^6$ Pa
Outlet static pressure, p_{out}	$1.585{\cdot}10^6$ Pa
Working fluid	R125
Loss model	Benner

Table 3.10: Kinetic and thermo-physical input variables for initial guess of velocity triangles and pressure

Variable	Value	
Stator inlet absolute velocity, v_1	0.1	
Stator throat absolute velocity, v_2	0.7	
Stator exit absolute velocity, v_3	0.7	$\equiv v_2$
Stator exit flow anlge, a_3	80.21 °	$\equiv \theta_{out,s}$
Rotor throat absolute velocity, w_5	0.7	
Rotor exit relative velocity, w_6	0.7	$\equiv w_5$
Rotor exit flow angle, b_6	-76.77 °	$\equiv \theta_6$
Stator throat static pressure, p_2	0.7	
Stator exit static pressure, p_3	0.7	$\equiv p_2$
Rotor throat static pressure, p_5	0.4	

The velocities and pressures among the variables presented in Table 3.10 are normalized with the spouting velocity and the inlet stagnation pressure respectively. The actual values are obtained as soon as the initial guess is fed to the mean-line model.

3.2 Sensitivity analysis by means of DOE and regression models

Once the different functions that make up the mean-line model — which, as explained above, is intended to be used as an effective tool for the preliminary design of axial turbines — have been explained, and once the selection of the loss model to be used to evaluate the performance parameters of the turbine in question has been justified, it is necessary to carry out a first pre-validation to indicate that the model makes sense and provides coherent and reasonable results.

For this purpose, as introduced in Section 2.10, a sensitivity analysis will be carried out to see how the design variables (input variables to the model) influence the chosen output variable, since in the case of axial turbines, relying on intuition is not very useful to understand how a variation in the former affects the latter. The conclusions drawn from this sensitivity analysis will not only serve to make sense of the model, but will also be used to try to improve the optimization mode, with the aim of obtaining the maximum information in the shortest possible time, and therefore, at the lowest possible cost.

In this subsection, both the design of experiments technique used and its set-up will be presented. The factors chosen for the analysis will be justified and the code used to obtain the design of experiments will be explained. Subsequently, the regression model used to quantitatively obtain the coefficients with which the factors (with their main, interaction and quadratic effects) affect the turbine efficiency will be presented. Finally, a statistical analysis has been carried out to see the significance of these coefficients and their variability intervals.

3.2.1 Design of experiments technique selection

The first step in carrying out this study was to choose from among the different design of experiments techniques the one that best suited the purpose of the project, which is the same as that sought with optimization: to obtain the maximum information with the smallest possible number of experiments, since, as it has been seen, an experiment involves time, cost and may even require sophisticated technological resources.

With this objective in mind, it was necessary to choose a technique that could be developed on the student's computer, that would not take an inordinate amount of time and that would allow the evaluation of curvature points.

Among the techniques presented in Section 2.10, the one that best meets these requirements is the central composite design, since, as explained, the advantages of this technique over the others are: it provides information on the sensitivity of the study variable to more than one input variable, with a slight higher number of required experiments than the full factorial and fractional factorial designs — as a few more samples than the ones required for bilinear interpolation on the 2^k design space are being considered [33]—, but it allows estimating the non-linear effects, which are important to consider in the design of a turbine.

However, the selection does not end here as it has been shown that there are different types of CCDs and that it is necessary to choose one in order to configure the settings for the experiments. The face-centred CCD has been chosen because — with all the samples within the experiment domain—, it only requires 3 levels for each factor, being a simpler and more cost-effective option, as sufficient information is obtained in relatively few runs. It is important to remind that despite the advantages mentioned above, as a trade-off, this type of technique provides a non-rotatable design, meaning that the variances of the output variable are not constant throughout the design space as the design space is not symmetric around the central point. For the moment it is only necessary to consider this, further comments will be made later.

Once the DOE technique has been selected, a series of steps must be followed in order to carry out the experiments. First, the most important factors for the study must be chosen. This will be explained in the next section. Then, the remaining information needed for the setup will be detailed: the levels and the number of samples. Finally, the code used to carry out the experiments will be explained.

3.2.2 Non-rigorous factorial analysis for factors selection in the face-centered central composite design

The potential factors to be considered to initiate the experiments are the model design variables presented in tables 3.1 and 3.2. It is important to make a careful selection of the most relevant parameters for the study, as it is not interesting to analyze factors that do not provide significant information. It has already been seen in Section 2.10 that the greater the number of factors, the greater the number of runs and therefore the greater the time invested and the more money spent, as happens within optimization. But it is

also important not to leave out any of the parameters that can make a difference in the conclusions.

To this end, it was initially planned to carry out a one at a time analysis, common for this type of studies, in which — as its name suggests—, keeping all the design variables fixed at a time, the value of one in question is modified, taking it to its upper limit and then to its lower limit, in order to observe how its variation affects the output variable. The disadvantage of this type of analysis is that it does not provide the complete sought information, as several of the factors may have a considerable interaction effect on the output variable which would not be reflected.

Therefore, it was decided to use a non-rigorous factorial analysis, in which each geometrical parameter was fixed one by one at 3 different levels and observed to vary with the static exit pressure at 6 different levels. That is to say, with 2 factors for each experiment (a geometrical variable and the pressure), 3 levels for the former and 6 levels for the latter.

The reason for taking into account the interaction of each design variable with the exit pressure set in the turbine study condition (Table 3.3) is the same as repeated so far: to take into account the variability in the inlet conditions of the axial turbine designed for ORC applications that will have an impact on the thermodynamic outlet conditions. In the following, the factors screening will be illustrated and the rationale for the selection of the study factors will be presented.

The first parameter that has been discarded is the specific speed (Ω_{spe}), since it is correlated with the specific diameter (d_{spe}) through the blade speed (u), as can be seen from the equations (3.1), (3.4) and (3.5). It can be seen from Figure 3.3, that both vary in the same way.

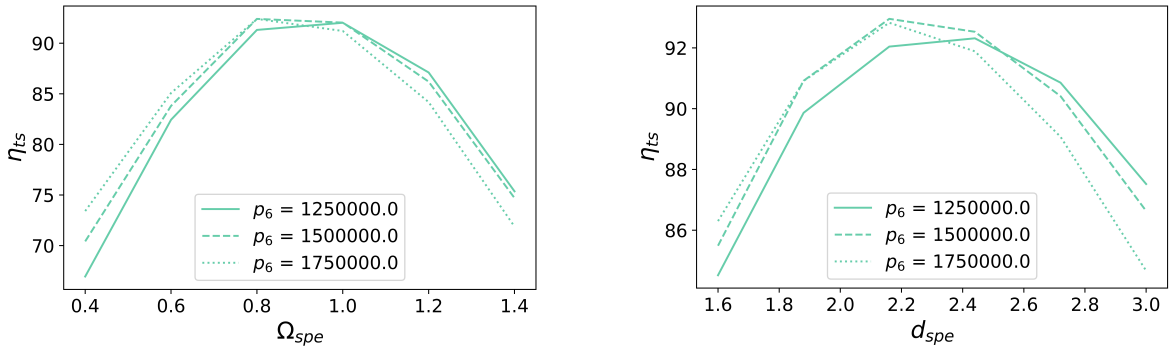

(a) Total-to-static efficiency vs. specific speed (Ω_{spe}) for different values of static exit pressure (p_6)

(b) Total-to-static efficiency vs. specific diameter (d_{spe}) for different values of static exit pressure (p_6)

Figure 3.3: Screening of specific speed (Ω_{spe}) and specific diameter (d_{spe}) in non-rigorous factorial analysis.

The design variables related to the chosen loss model have also been discarded, since their variation has a negligible effect on the turbine efficiency and therefore they would not be contributing relevant information to the study, but would be consuming resources. This can be seen in Figure 3.4.

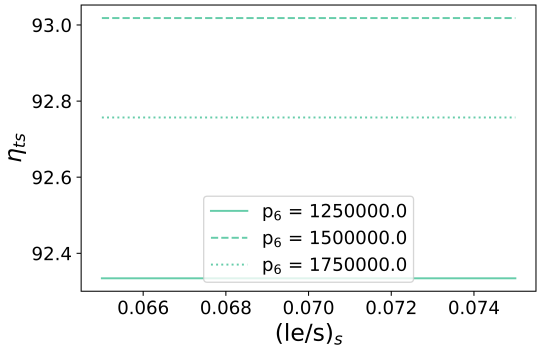

(a) Total-to-static efficiency vs. stator leading edge diameter to pitch ratio ($(le/s)_s$) for different values of static exit pressure (p_6)

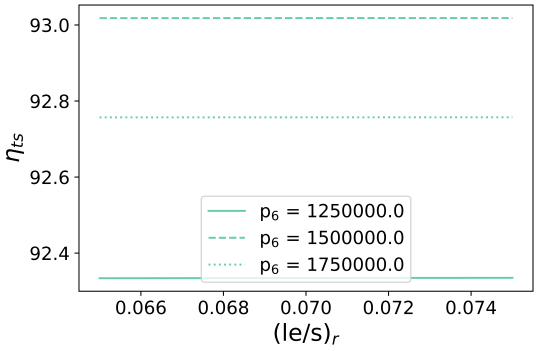

(b) Total-to-static efficiency vs. rotor leading edge diameter to pitch ratio $(le/s)_r$ for different values of static exit pressure p_6

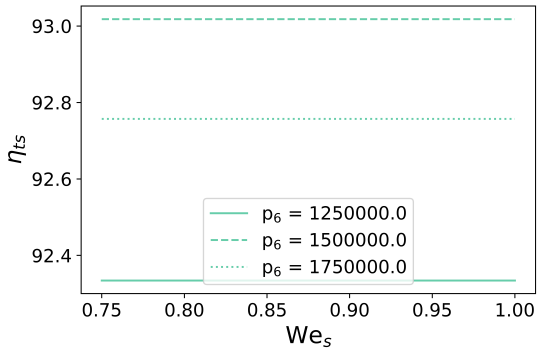

(c) Total-to-static efficiency vs. stator wedge angle (We_s) for different values of static exit pressure (p_6)

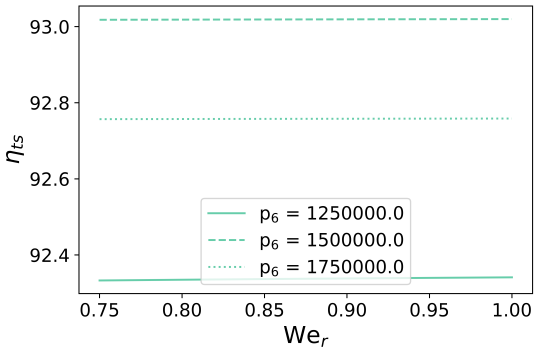

(d) Total-to-static efficiency vs. rotor wedge angle (We_r) for different values of static exit pressure (p_6)

Figure 3.4: Screening of the Benner loss model design variables in non-rigorous analysis.

As seen so far, the aim of this first study is not only discarding the variables with little influence on the response variable but also those that are correlated, since for the subsequent analysis of the results, techniques that assume the independence of the factors will be used, and introducing correlated factors would add uncertainty to the results. The effect of the variation of the other factors has been captured in Figure 3.5.

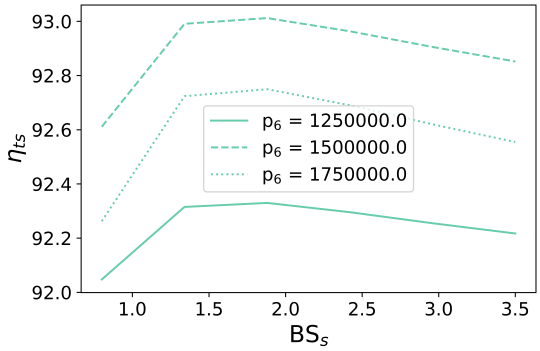

(a) Total-to-static efficiency vs. stator blade solidity (BS_s) for different values of static exit pressure (p_6)

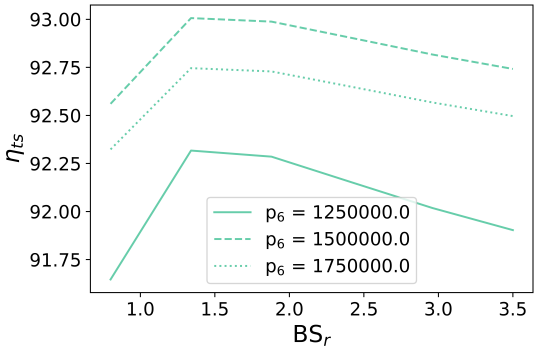

(b) Total-to-static efficiency vs. rotor blade solidity (BS_r) for different values of static exit pressure (p_6)

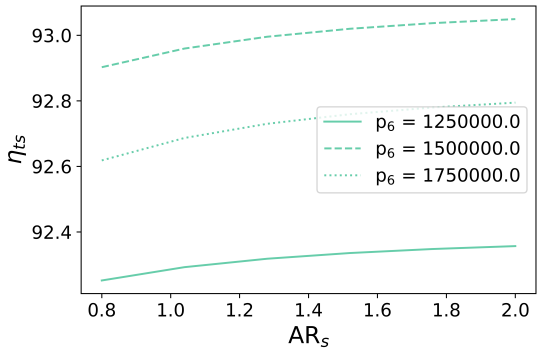

(c) Total-to-static efficiency vs. stator aspect ratio (AR_s) for different values of static exit pressure (p_6)

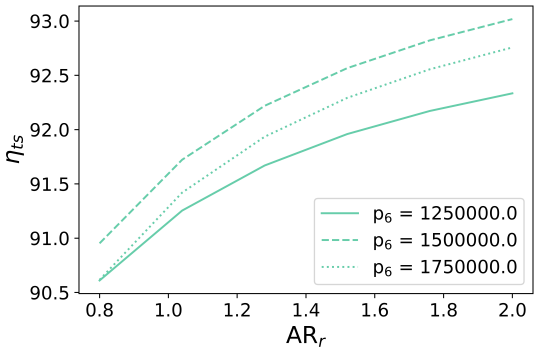

(d) Total-to-static efficiency vs. rotor aspect ratio (AR_r) for different values of static exit pressure (p_6)

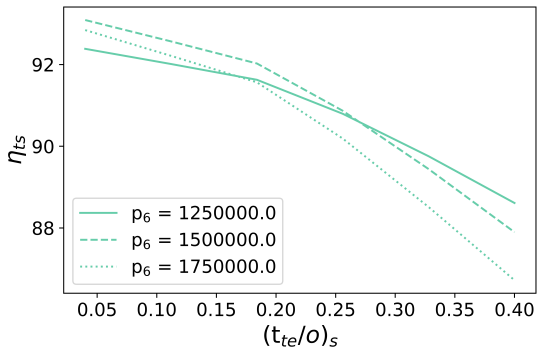

(e) Total-to-static efficiency vs. stator TE thickness to opening ratio ($(t_{te}/o)_s$) for different values of static exit pressure (p_6)

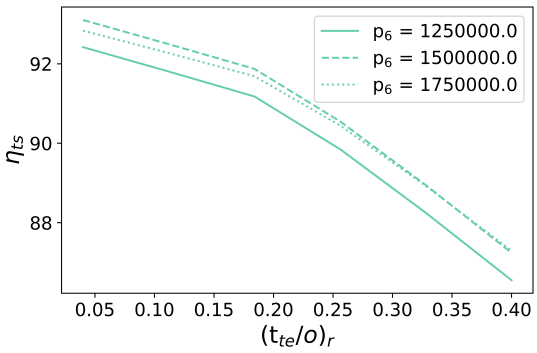

(f) Total-to-static efficiency vs. rotor TE thickness to opening ratio ($(t_{te}/o)_r$) for different values of static exit pressure (p_6)

Figure 3.5: Screening of the remaining design variables in non-rigorous factorial analysis.

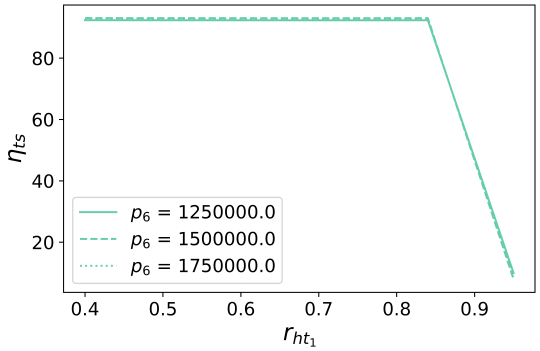

(g) Total-to-static efficiency vs. stator inlet hub-to-tip ratio (r_{ht_1}) for different values of static exit pressure (p_6)

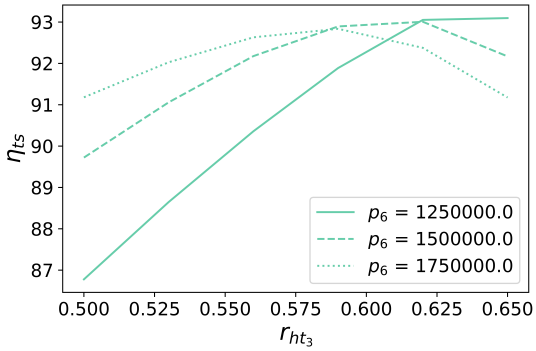

(h) Total-to-static efficiency vs. stator exit hub-to-tip ratio (r_{ht_3}) for different values of static exit pressure (p_6)

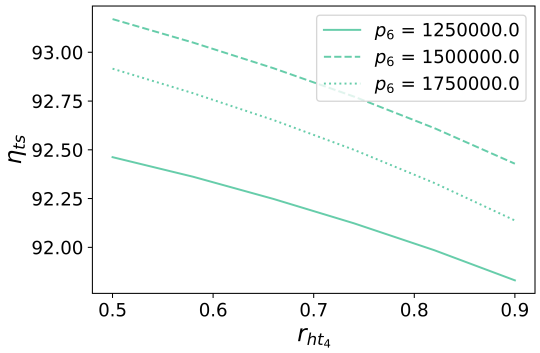

(i) Total-to-static efficiency vs. rotor inlet hub-to-tip ratio (r_{ht_4}) for different values of static exit pressure (p_6)

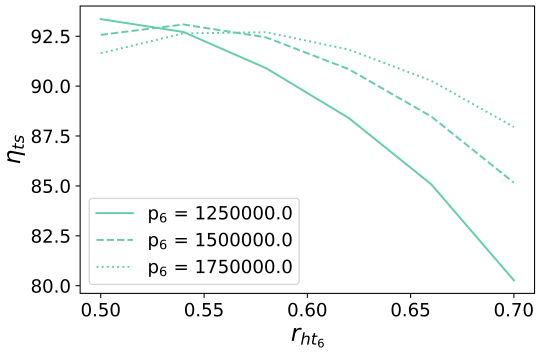

(j) Total-to-static efficiency vs. rotor exit hub-to-tip ratio (r_{ht_6}) for different values of static exit pressure (p_6)

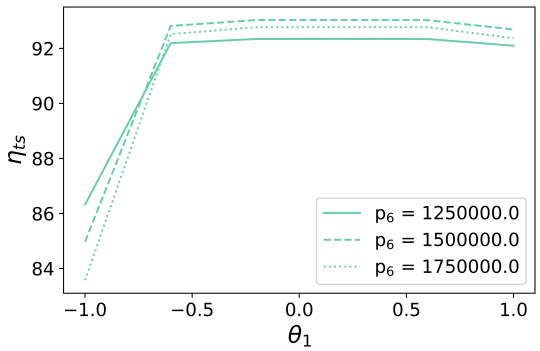

(k) Total-to-static efficiency vs. stator inlet methal angle (θ_1) for different values of static exit pressure (p_6)

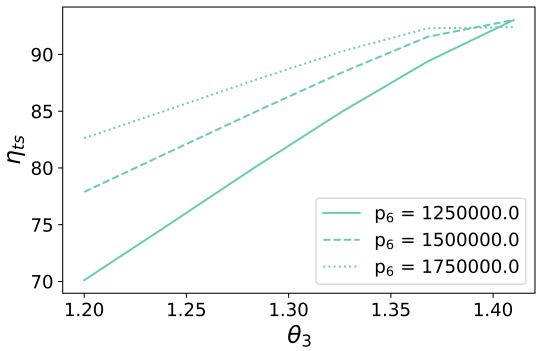

(l) Total-to-static efficiency vs. stator exit methal angle (θ_3) for different values of static exit pressure (p_6)

Figure 3.5: Screening of the remaining design variables in non-rigorous factorial analysis (cont.).

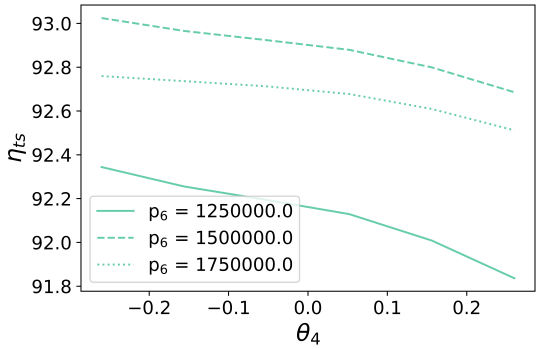

(m) Total-to-static efficiency vs. rotor inlet methal angle (θ_4) for different values of static exit pressure (p_6)

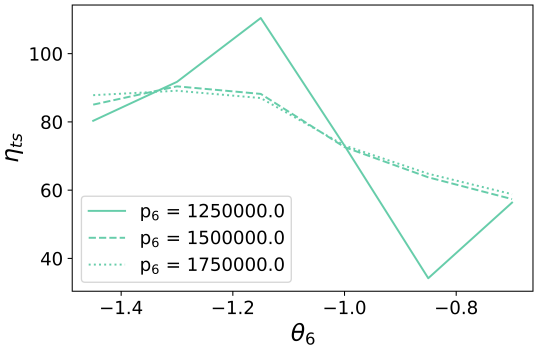

(n) Total-to-static efficiency vs. rotor exit methal angle (θ_6) for different values of static exit pressure (p_6)

Figure 3.5: Screening of the remaining design variables in non-rigorous factorial analysis (cont.).

From Figure 3.5 it can be seen that a priori, some factors seem to have a greater impact on the performance than others, but as was seen in Section 2.8.7, the different factors to be studied have an effect on the different loss components, giving rise to a complex problem as all these effects are related. For this reason, it has been decided to introduce in the experiment the 14 design variables presented in the figure above, together with the specific diameter and the exit pressure, p_6, as a thermodynamic condition over which some control can be exercised.

3.2.3 Experiment settings and Python code

Next, the setup of the main variables necessary for the experiments will be presented, and the code implemented in Python, with the help of the student's co-supervisor, to carry them out will be explained.

To set up each experiment, it is first necessary to indicate which of the 15 design variables presented above are to be considered in the experiment, and the same for the thermodynamic condition. The number of factors to be considered in each experiment will therefore be given by the sum of the design variables and the pressure condition if it is being introduced.

Next, the output variable to be analyzed must be selected from among the different variables that make up the set of the turbine's overall performance parameters. This study has been carried out to evaluate the influence of the design and pressure variables on the turbine's total to static efficiency, also set as objective function for the optimization.

Once the number of factors is known, the structure of the matrix that characterizes the selected DOE technique (which includes only main effects) has to be prepared. For this purpose, use has been made of a Python function that constructs a 2-level full factorial design by providing the number of factors to be studied. This constitutes the cube points presented in Table 2.6. To these points, as seen in the theory, different axial points (in

which α acquires the value of 1 given that the CCF design has been chosen) and a central point have to be incorporated.

From the number of factors, the sample size must be calculated by means of Eq.(2.130), in order to assign the variables their corresponding values from the matrix. But, before explaining how this allocation has been carried out, a comment must be made concerning the number of levels. It has been seen that the chosen technique uses three levels: low, medium and high. The low and high levels are given by the lower and upper bounds of each variable, while the medium level is the average between these bounds. In order to establish the different levels in each run, the lower and upper bounds have been provided in two Python dictionaries, respectively, for all the design variables, regardless of whether they are being introduced in the experiment or not, since in order to be able to execute the turbine analysis function within the model's performance mode, all design variables presented in Table 3.1 and Table 3.2 must be taken into account. In the same way, another dictionary containing the deign point must be incorporated. This is the one given in Table 3.9.

By means of a for loop, the considered design variables and the thermodynamic condition have to be separately decoded and updated within each run to fit the design, and simulate all samples. This decoding is done with the equation presented below:

$$\text{Variable}_i = 0.5 \cdot (x+1) \cdot \text{ub}_{variable_i} + 0.5 \cdot (1-x) \cdot \text{lb}_{variable_i} \tag{3.8}$$

where x is the coded variable in the CCF matrix, *ub* stands for upper bound and *lb* for lower bound.

Once they have been decoded, within each run the turbine analysis function is called and the total to static efficiency is stored in an array as the results provided by the experiment.

To these main effects, 2-way interaction and quadratic effects are added. With this, the complete matrix of the face-centered central composite design —in which every factor has been assessed in every possible combination of the three levels of each of the other factors—, is obtained and ready to analyze.

The bounds that have been used will be presented in Section 3.3 for each of the performed analyses. The regression model and the statistical analysis carried out to interpret the results provided by the experiment are going to be presented in the following.

3.2.4 Response surface methodology, regression models and confidence intervals

This section aims to briefly present the regression model used and the statistical analysis performed, and to justify its selection.

It has been seen in Section 2.10 that the central composite design is often used in response surface methodology because it fits well to second order models when considering the curvature of the different factors.

Response Surface Methodology or RSM is a set of mathematical and statistical techniques used to model and analyze problems in which a response of interest is influenced by several quantitative factors, with the objective of optimizing the response by determining the optimal values of the factors involved.

Before explaining how the present study has been carried out, it is necessary to point out that the selection of the RSM technique with which the chosen DOE technique is to be combined — when working with response surfaces—, can significantly influence the results, as detailed in [33].

Since the aim of the present work is not to optimize the response surface, but to analyze the influence of each of the factors involved quantitatively, not all the phases of the RSM have been performed, but only to fit the model and obtain the coefficients by means of regression, that is, only the first phase after the factor screening.

The full second order model to which the design has been fitted is given by:

$$y = \beta_0 + \sum_{i}^{k} \beta_i x_i + \sum_{i<} \sum_{j} \beta_{ij} x_i x_j + \sum_{i}^{k} \beta_{ii} x_i^2 + \varepsilon \tag{3.9}$$

in which β_0 is the intercept, that has not been considered in this work; β_i are the coefficients for the main effects, β_{ij} are the coefficients for the 2-factor interactions, β_{ii} are the coefficients for the quadratic effects and ε is the statistical error term.

Quadratic effects in second order models are generally correlated between with each other and with the intercept term [52], while interaction and main effects are not correlated. For this reason, multiple lineal regression (MLR) is usually used to estimate second order models, as the model is still linear in the parameters. The coefficients have been obtained by using the linear least squares method, which provides the minimum sum of squared residuals at all the different points assessed during the experiment:

$$S = \sum_{i=1}^{N} \varepsilon_i^2 \tag{3.10}$$

where the residuals are given by "the difference between the experimental responses and the value predicted by the model function at the locations x_i in the design space" [33], as:

$$\varepsilon_i = y_i - \hat{f}(x_i, \beta), \quad \text{i} = 1,2,...,\text{N} \tag{3.11}$$

and in the linear least squares method, the $\hat{f}$ function is given by:

$$\hat{f}(x_i, \beta) = \beta_0 + \sum_{j=1}^{k} x_{i,j} \beta_j \tag{3.12}$$

In the matrix form the problem yields:

$$\mathbf{y} = \mathbf{X}\beta + \varepsilon \tag{3.13}$$

where the different components are given by the expressions shown in Figure 3.6.

$$\mathbf{y} = \begin{pmatrix} y_1 \\ y_2 \\ \vdots \\ y_N \end{pmatrix}, \quad \mathbf{X} = \begin{pmatrix} 1 & x_{1,1} & \dots & x_{1,k} \\ 1 & x_{2,1} & \dots & x_{2,k} \\ \vdots & \vdots & \ddots & \vdots \\ 1 & x_{N,1} & \dots & x_{N,k} \end{pmatrix}, \quad \boldsymbol{\beta} = \begin{pmatrix} \beta_0 \\ \beta_1 \\ \vdots \\ \beta_k \end{pmatrix}, \quad \boldsymbol{\epsilon} = \begin{pmatrix} \epsilon_1 \\ \epsilon_2 \\ \vdots \\ \epsilon_N \end{pmatrix}$$

Figure 3.6: Terms in the matrix form of the least square method's equation.

By solving in β the minimum of Eq.(3.10), the following is obtained:

$$\beta = \left(X^T X\right)^{-1} X^T y \tag{3.14}$$

being the response of the fitted model:

$$\hat{y} = X\beta \tag{3.15}$$

Once the coefficients of the different effects were obtained, their corresponding 95% confidence intervals were built in order to study their significance on the output. This was done by means of the t-distribution.

First, the mean squared error (average squared residual) was obtained as:

$$MSE = \frac{\sum (y_i - \hat{y}_i)^2}{2} \tag{3.16}$$

Later, the standard error and the t_{crit} value for α equal to 5% were calculated for each run by means of a python function, and the confidence intervals were provided as:

$$CI = (\hat{\beta} - t_{crit} \cdot SE, \hat{\beta} + t_{crit} \cdot SE) \tag{3.17}$$

Those intervals not containing 0 meant the significance of the corresponding factor, which with 95% confidence will be between those limits.

Finally, it is very important to note that although MLR is often used to address the problem being studied, it is not the best technique to employ due to the aforementioned disadvantage of the rotatability of the chosen technique. This may lead to obtain the main and interaction coefficients with certain bias that has to be taken into account. Further comments will be done after presenting all the results.

3.3 Methodology for performing the experiments

This section will present the methodology followed to carry out the experiments that make up this work, which has been summarized in the workflow in Figure 3.7.

Two main analyses have been carried out due to limitations found in the model, mainly differing in the size of the design space. Between the two analyses, a couple of experiments have been carried out to verify the hypotheses put forward in view of the limitations found at the end of the first analysis. Finally, two other sets of experiments within the local sensitivity analysis have been carried out to analyze the remaining factors not included in the previous experiments due to these limitations, however, these will be directly presented in the results section.

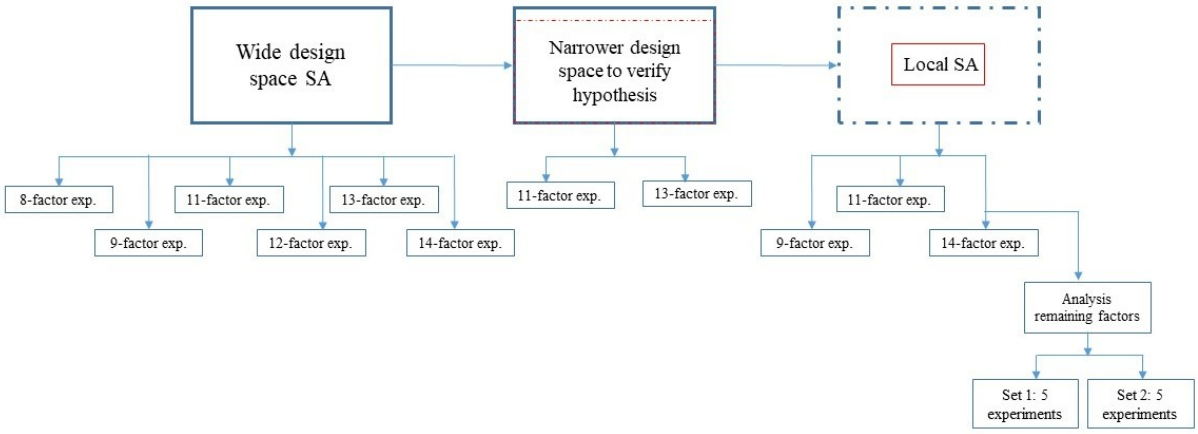

Figure 3.7: Workflow of the methodology followed for carrying out experiments.

3.3.1 Experiments with wide design space

The first analysis intended to study a wide design space in order to see how off-design conditions, far from the design and optimal point, affected the turbine performance.

A total of 6 experiments have been performed within this analysis. From the first one to the last one the number of factors has been gradually increased in order to understand the effect that their introduction in the experiment has, not only on η_{ts}, but also on the other factors.

The lower and upper bounds have been chosen based on the factorial analysis presented above in Section 3.2.2 and on the results of the optimization pre-SA, for the case study being used presented in Section 3.1.4. They are shown in Table 3.11. The different factors considered in each experiment will be introduced in the Results section (4.1).

Table 3.11: Lower and upper bounds for factors in Wide sensitivity analysis

Factor	Lower Bound	Upper Bound
Ω_{spe}	0.7	1.2
BS_s	1	3
BS_r	0.9	3.5
AR_s	0.8	2
AR_r	0.8	2
r_{ht_1}	0.5	0.9
r_{ht_3}	0.5	0.65
r_{ht_4}	0.5	0.9
r_{ht_6}	0.5	0.7
$(t_{te}/o)_s$	0.05	0.33
$(t_{te}/o)_r$	0.05	0.3
d_{spe}	2.1	2.3
θ_1 [°]	-34.37	17.18
θ_3 [°]	69.90	81.36
θ_4 [°]	-15	15
θ_6 [°]	-80	-71.72
p_6 [Pa]	1448000	1707547.17

Limitations in the experiments above 14 factors were found. This is why in Table 3.11 two variables have been shaded in grey, as they have not been considered together with the other factors. The reason why these experiments failed was that they arrived at non-physical values of some thermodynamic variables, such as molar density. This is nothing more than the root-finder being unstable and running wild as it is not being able to handle the whole design space with reasonable bounds.

In addition, efficiency outliers have also been found, which could be introducing uncertainty in the results. All of this will be presented and explained in more detail in Section 4.

Given these efficiency outliers, the choice of reducing the design space was made. Other options could have been to reduce the number of factors and thus obtain less information, or to remove the problematic runs from the matrix, with the drawback that some of the interaction effects would be aliased.

The two mentioned intermediate experiments have been carried out with the same bounds as the wide sensitivity analysis, but the design space has been slightly reduced for the trailing edge thickness to opening ratios, as shown in Table 3.12.

Table 3.12: Lower and upper bounds for trailing edge thickness to opening ratios in the narrower SA

Factor	Lower Bound	Upper Bound
$(t_{te}/o)_s$	0.02	0.25
$(t_{te}/o)_r$	0.02	0.25

3.3.2 Local sensitivity analysis

The repeated occurrence of efficiency atypical values has led the student to carry out a local sensitivity analysis in the surroundings of the case study considered so far. It has been decided to vary all the factors in the same proportion, with a ε of 5 % to facilitate the subsequent analysis. The bounds used for this second analysis are given in Table 3.13.

For each of the experiments carried out in this and the previous analysis, the value of t_{crit}, the standard error, SE, and with them their corresponding confidence intervals have been calculated, as presented in Section 3.2.4, in order to analyze the significance of the coefficients obtained from the regression.

In addition, a Python script has been developed to check the tolerance that the model is using to provide the results, by decoding the variables of the runs analyzed and executing the turbine analysis function.

Table 3.13: Lower and upper bounds for local sensitivity analysis

Factor	Lower Bound	Upper Bound
Ω_{spe}	0.855	0.945
BS_s	1.52	1.68
BS_r	1.425	1.575
AR_s	1.425	1.575
AR_r	1.9	2.1
r_{ht_1}	0.57	0.63
r_{ht_3}	0.57	0.63
r_{ht_4}	0.57	0.63
r_{ht_6}	0.523	0.578
$(\mathrm{t}_{te}/\mathrm{o})_s$	0.048	0.053
$(\mathrm{t}_{te}/\mathrm{o})_r$	0.048	0.053
d_{spe}	2.147	2.373
θ_1 [°]	-2.86	2.86
θ_3 [°]	76.20	84.22
θ_4 [°]	-15.47	-13.64
θ_6 [°]	-81.36	-73.51
p_6 [Pa]	1505750	1664250

3.4 Comparison between optimizations

Finally, as mentioned above, the last thing that has been carried out with the conclusions drawn from the last of the sensitivity analyses is a slightly different optimization to the one prior to the SA. Some of the factors —those discarded in the first analysis and those that were found to always have the same effect on performance—, have been set to their upper or lower bounds. To give more information on the factor's effects, several bar graphs have been made comparing the losses of the three turbines analyzed, the one before the SA, the one in the case study and the one after the SA. These will be presented together with the results obtained in Section 4.4.

4 Results and discussion

This section will present the most relevant results obtained from the two different analyses carried out to study the influence of the design variables of the model on the performance of the turbine. The significance of the differences found between both analyses (extensive and local) will be discussed and, from the latter, conclusions will be drawn to summarize the student's work.

The section is divided into four subsections. First of all, the different experiments carried out for the extensive study, from which the conclusions for the work were initially intended to be drawn, will be presented. Next, the results of two other experiments will be shown, carried out by slightly varying the conditions of the extensive study, with the aim of obtaining more precise results. Afterwards, the local sensitivity analysis will be presented. Finally, the results of the comparison of the optimal turbine before and after the sensitivity analysis will be analyzed.

4.1 Results from the sensitivity analysis for a wide design space

As explained in Section 3.3, the first study carried out tries to cover a wide design space since the aim of the thesis is to understand how the variation of the design variables affects the output variable of the model, when the turbine inlet conditions are far from the optimal design point (a situation that frequently occurs in ORC turbines, given the low stability of these conditions).

The study comprises six different experiments in which the number of factors has gradually been increased up to 14. The results from the first five experiments are presented in Appendix A, however, the main information will be commented and compared below, to end with a deeper discussion of the results from the last experiment. Limitations in the model and the reliability of the results will be commented afterwards.

In order to be able to comment on the obtained results, it has been decided to adopt the following criterion of importance among the factors that have turned out to be significant after the study:

- **Important effect**: 10^0 - coefficients of the order of unity.
- **Considerable effect**: 10^{-1} - coefficient of the order of one tenth.
- **Minor effect**: 10^{-2} - coefficient of the order of one hundredth.

In addition, (+) and (-) have been used to express if a significant factor increases or decreases, respectively, the output variable, in this case, the total to static efficiency.

4.1.1 Experiment 1: 8 factors

The first experiment was carried out by analyzing the next eight factors: stator and rotor blade solidity — BS_s and BS_r—, stator and rotor aspect ratio — AR_s and AR_r—, and stator and rotor inlet and exit hub-to-tip ratios— r_{ht_1}, r_{ht_3}, r_{ht_4} and r_{ht_6}. The number of runs, invested time and minimum and maximum efficiency obtained in the experiment are shown in Table 4.1.

Table 4.1: Data from experiment 1

Number of runs	Time [s]	η_{min} [%]	η_{max} [%]
273	185.76	58.18	92.04

The coefficients for the main, interaction and quadratic effects of the considered factors have been obtained from the multiple linear regression of the face-centered CCD results and gathered in Table A.1 in Appendix A.1. Moreover, a confidence interval has been calculated for each of these coefficients in order to state which of them are significant to the turbine performance. These confidence intervals and relevance are given for the main, quadratic and interaction effects in Tables A.2, A.3 and A.4 respectively.

Only four of the eight studied factors prove to have a significant main effect, which are in order of importance r_{ht_6}(-), r_{ht_3}(+), AR_r(+) and r_{ht_4}(-). The first and the last seem to decrease the efficiency whereas the other two factors seem to increase it. There are also some significant interaction effects to be highlighted between these four factors and between the stator inlet hub-to-tip ratio, r_{ht_1}, and the stator exit and rotor exit hub-to-tip ratios. The latter shows a significant negative quadratic effect.

4.1.2 Experiment 2: 9 factors

The second experiment was carried out by adding the static pressure to the previous eight factors. The nature of this factor is a little different from the others since it is a thermodynamic condition rather than a geometric variable, but as it has been mentioned in Section 3.2.2, it is possible to have some control over it. Therefore it is being considered as a design variable.

As for the previous experiment, the number of runs, invested time and minimum and maximum efficiencies are gathered in Table 4.2.

Table 4.2: Data from experiment 2

Number of runs	Time [s]	η_{min} [%]	η_{max} [%]
531	361.52	54.06	92.25

It can be seen that the invested time has been doubled by only adding one factor. This gives a first idea of the importance of the correct selection of the factors to be studied in order to carry out the work efficiently. It can also be noticed that a lower minimum and

higher maximum efficiency have been achieved. Even though 50% efficiency is low for an axial turbine, it is possible if the turbine is not optimized.

The coefficients for the different effects and confidence intervals have been presented in Appendix A.2. The fact that pressure has been introduced into the study has slightly modified the result obtained from the previous experiment. The factors that were significant before are still significant and important now and show practically the same trend as earlier. The stator inlet hub-to-tip ratio, that had significant interaction effects but not a significant main effect in the previous experiment, proves to have a significant and considerable main effect now, decreasing the efficiency. The static pressure main effect also seems to be significant, considerable and positive. So, in order of importance, the significant factors are: r_{ht_6} (-), r_{ht_3} (+), AR_r (+), r_{ht_4} (-), p_6 (+) and r_{ht_1} (-).

Regarding the interactions, static pressure and stator exit hub-to-tip ratio, as well as static pressure and rotor exit hub-to-tip ratio, together with the significant interaction effects from the previous experiment, also show a significant effect on the turbine performance. No significant quadratic effects have been found in this analysis.

4.1.3 Experiment 3: 11 factors

The next experiment was performed by considering the previous nine factors and the stator and rotor trailing edge thickness to opening ratios. The number of runs for analyzing these eleven factors, as well as the time that the experiment took and the minimum and maximum efficiencies achieved are presented in Table 4.3.

Table 4.3: Data from experiment 3

Number of runs	Time [s]	η_{min} [%]	η_{max} [%]
2071	1172.81	13.31	92.24

Following the same trend as above, it can be said that increasing the number of factors leads to a greater amount of significant effects. From this experiment it can be seen that the two added factors seem to be significant and important, the rotor blade solidity, until now not significant, has not only become significant but considerable, and the stator inlet hub-to-tip ratio has become not significant once more. In order of importance the significant factors are: r_{ht_6} (-), r_{ht_3} (+), AR_r (+), $(\mathrm{t}_{te}/\mathrm{o})_r$ (-), $(\mathrm{t}_{te}/\mathrm{o})_s$ (-), r_{ht_4} (-), p_6 (+) and BS_r(-).

Since the significant effects vary depending not only on the number of factors, but also on which of them are being considered, rather than explaining the different interaction effects (which will be done for the last experiment as it provides the most information) the focus will be on a more interesting outcome. The tables collecting the coefficients and confidence intervals for the different effects (Tables A.9, A.10, A.11 and A.12) are presented in Appendix A.3.

While an efficiency of 50% may be possible if the turbine in question is not optimized, the minimum achieved efficiency of 13% is remarkable for its low value. As explained in

the methodology section (3.1.1), to perform the turbine analysis, a series of equations have to be satisfied, for which an error tolerance of 10^{-5} has been set. With the code explained in Section 3.3 and created to carry out the tolerance check of the obtained results, it has been observed after analyzing the anomalous runs, that despite converging and finding a physically possible solution for the efficiency, the residuals for the set of equations are provided with an order of magnitude greater than that established (10^{-4}, 10^{-3}).

This result raises several issues. Firstly, the fact of having introduced these two factors in particular has caused the model to find invalid values during the execution of the experiment. This could be attributed to the boundary conditions being used for the study, conditions which, as explained above, have been chosen based on the non-rigorous factorial analysis and the optimal turbine. It can be seen how for the nature of the DOE technique being used, the bounds of the factors are being reached, which requires the model to be good and robust. On the other hand, the fact that the results of the anomalous runs are being provided with the indicated tolerance does not mean that the whole study is invalid, but rather that the results obtained present some uncertainty since the thermodynamical variables may be non-physical despite having a positive value of efficiency. The tolerance of the results provided by the runs that gave higher values of efficiency were also checked. It was seen that these runs respected the convergence tolerance condition.

The problem lies in the fact that the uncertainty of these outliers affects the assignment of weights to the coefficients that are being obtained with the multiple linear regression for the different effects. How reliable these results are in order to extract conclusions is something that has to be cautiously taken into account. Having this in mind, the experiments were extended to 12, 13 and 14 factors, which will be presented in the following.

4.1.4 Experiment 4: 12 factors

To the previous 11-factor experiment, the specific diameter d_{spe} was added. The number of runs and devoted time raise as expected for this 12-factor experiment being considered. The minimum and maximum efficiency are gathered in Table 4.4. A similar reasoning as above can be followed to justify the low value of the minimum efficiency achieved.

Table 4.4: Data from experiment 4

Number of runs	Time [s]	η_{min} [%]	η_{max} [%]
4121	2519	13.15	92.19

After evaluating the confidence intervals of the coefficients obtained from the MLR of the results from the present experiment, in order of importance the significant factors are: r_{ht_6} (-), r_{ht_3} (+), AR_r (+), $(t_{te}/o)_r$ (-), $(t_{te}/o)_s$ (-), r_{ht_4} (-), d_{spe} (-), p_6 (+), BS_r(-) and r_{ht_1} (-).

As it can be noticed, the introduced factor, d_{spe} has a significant main effect over the turbine performance. This effect is considerable and decreases the efficiency. Another interesting observation is that introducing the specific diameter in the experiment has

led to the stator inlet hub-to-tip ratio to become significant again. From this it can be interpreted that there are certain interaction effects that have a strong impact on the output and that make that one not significant factor turns to be significant.

Tables A.13, A.14, A.15 and A.16 in Appendix A.4 show the results for the coefficients, confidence intervals and relevance of the main, quadratic and interaction effects.

4.1.5 Experiment 5: 13 factors

The fifth experiment was carried out with the previous twelve factors and the stator inlet methal angle, θ_1. The number of runs, invested time and minimum and maximum efficiency, as for the experiments presented so far, have been gathered in Table 4.5.

Table 4.5: Data from experiment 5

Number of runs	Time [s]	η_{min} [%]	η_{max} [%]
8219	5210.61	13.18	92.21

The stator inlet methal angle resulted not significant, and its consideration has led to the same significant factors as for the previous experiment, in order of importance: r_{ht_6} (-), r_{ht_3} (+), AR_r (+), $(t_{te}/o)_r$ (-), $(t_{te}/o)_s$ (-), r_{ht_4} (-), d_{spe} (-), p_6 (+), BS_r(-) and r_{ht_1} (-). The effect over the efficiency has not changed either and the values for each of the main effect coefficients have practically remained constant.

The results from the MLR are presented in Table A.17, and the confidence intervals and relevance of the different effects are shown in tables A.18, A.19 and A.20, all of them in Appendix A.5.

4.1.6 Experiment 6: 14 factors

The sixth and last experiment carried out successfully within the analysis that considers a wide design space is the one that analyzed 14 of the 16 selected factors for the study. It has been decided to include within this subsection the principal results, since they are going to be carefully discussed, and since no further experiments could be finished. This will be commented after presenting the results.

As for the rest of experiments, the number of runs, devoted time, and minimum and maximum efficiencies obtained are gathered in Table 4.6.

Table 4.6: Data from experiment 6

Number of runs	Time [s]	η_{min} [%]	η_{max} [%]
16413	9396.86	12.97	92.22

Looking at the table above it can be seen that the problem with the low value of efficiency persists. Therefore it has to be said that any discussion derived from the results

of this experiment is subject to the same uncertainty that was mentioned in the previous experiments.

To start with, the coefficients of the main effects that have been obtained from the multiple linear regression within the experiment are presented together with their confidence interval lower and upper bounds and relevance in Table 4.7. Those factors that have resulted significant have been highlighted in grey.

Table 4.7: Confidence interval and relevance of the main effects in experiment 6. Significant effects highlighted in grey.

Main effect	IC lower bound	Coefficient	IC upper bound	Relevance
$\mathbf{BS}_s$	-0.0391	0.0154	0.0699	Not significant
$\mathbf{BS}_r$	-0.2122	-0.1577	-0.1032	Significant
$\mathbf{AR}_s$	-0.0383	0.0162	0.0707	Not significant
$\mathbf{AR}_r$	1.7885	1.843	1.8975	Significant
$\mathbf{r}_{ht1}$	-0.222	-0.1675	-0.113	Significant
$\mathbf{r}_{ht3}$	3.7047	3.7592	3.8137	Significant
$\mathbf{r}_{ht4}$	-0.9047	-0.8501	-0.7956	Significant
$\mathbf{r}_{ht6}$	-4.7322	-4.6777	-4.6232	Significant
$(\mathbf{t}_{te}/\mathbf{o})_s$	-1.2955	-1.241	-1.1865	Significant
$(\mathbf{t}_{te}/\mathbf{o})_r$	-1.796	-1.7415	-1.687	Significant
$\mathbf{d}_{spe}$	-0.8307	-0.7761	-0.7216	Significant
θ_1	-0.0537	0.0009	0.0554	Not significant
θ_4	-0.2528	-0.1983	-0.1438	Significant
$\mathbf{p}_6$	0.47	0.5245	0.579	Significant

From the table it can be seen that the new considered factor, stator exit methal angle (θ_4), is significant to the output and decreases its value, but, unlike the specific diameter, d_{spe}, that was the last factor that proved to be significant, it introduces no change in the relevance of the other factors. In order of importance the significant factors are: r_{ht_6} (-), r_{ht_3} (+), AR_r (+), $(t_{te}/o)_r$ (-), $(t_{te}/o)_s$ (-), r_{ht_4} (-), d_{spe} (-), p_6 (+), θ_4 (-), r_{ht_1} (-) and BS_r(-). However, by adding θ_4 to the study, the coefficient of the main effect of the stator inlet hub-to-tip ratio has increased in terms of absolute value, and has become greater than the rotor blade solidity coefficient, also in terms of absolute value.

The first thing that may come to mind when observing and starting to analyze the results is to ask oneself whether they make sense or not, and to question some of the following aspects: why for the same variable opposite results are obtained between stator and rotor (as in the case of BS and AR)? What influence does the selected boundary conditions have on the result? What would happen if all 16 factors could have been considered simultaneously?

In order to answer these questions a wider sight than the one provided by the data in Table 4.7 is needed. Even though the main effects are the most relevant to the purpose of evaluating the coherence of the used mean-line model, to be able to understand better the results, interaction and quadratic effects should also be considered.

Therefore, the following table (Table 4.8) has been built. The coefficients of the main effects are presented at the top. Beneath these coefficients, the 2-way interactions between the different factors have been included, and at the bottom, the coefficients of the quadratic effects are shown. Those coefficients that have proven to be significant after evaluating the confidence intervals (presented for quadratic and interaction effects in Tables A.21 and A.22 in Appendix A.6), have been highlighted in pink.

Table 4.8: Results of Experiment 6 - Faced central composite design with 14 factors. Significant effects highlighted in pink.

Main effects													
$\mathbf{BS}_s$	$\mathbf{BS}_r$	$\mathbf{AR}_s$	$\mathbf{AR}_r$	$\mathbf{r}_{ht1}$	$\mathbf{r}_{ht3}$	$\mathbf{r}_{ht4}$	$\mathbf{r}_{ht6}$	$(\mathbf{t}_{te}/\mathbf{o})_s$	$(\mathbf{t}_{te}/\mathbf{o})_r$	$\mathbf{d}_{spe}$	θ_1	θ_4	$\mathbf{p}_6$
$1.5409{\cdot}10^{-2}$	$-1.5773{\cdot}10^{-1}$	$1.6204{\cdot}10^{-2}$	1.8430	$-1.6751{\cdot}10^{-1}$	3.7592	$-8.5014{\cdot}10^{-1}$	-4.6777	-1.2410	-1.7415	$-7.7614{\cdot}10^{-1}$	$8.5731{\cdot}10^{-4}$	$-1.9832{\cdot}10^{-1}$	$5.2447{\cdot}10^{-1}$
Interaction effects													
	$\mathbf{BS}_s\mathbf{BS}_r$	$\mathbf{BS}_s\mathbf{AR}_s$	$\mathbf{BS}_s\mathbf{AR}_r$	$\mathbf{BS}_s\mathbf{r}_{ht1}$	$\mathbf{BS}_s\mathbf{r}_{ht3}$	$\mathbf{BS}_s\mathbf{r}_{ht4}$	$\mathbf{BS}_s\mathbf{r}_{ht6}$	$\mathbf{BS}_s(\mathbf{t}_{te}/\mathbf{o})_s$	$\mathbf{BS}_s(\mathbf{t}_{te}/\mathbf{o})_r$	$\mathbf{BS}_s\mathbf{d}_{spe}$	$\mathbf{BS}_s\theta_1$	$\mathbf{BS}_s\theta_4$	$\mathbf{BS}_s\mathbf{p}_6$
	$-2.7256{\cdot}10^{-3}$	$1.2863{\cdot}10^{-2}$	$-1.6394{\cdot}10^{-2}$	$-2.0679{\cdot}10^{-2}$	$3.96{\cdot}10^{-3}$	$1.6698{\cdot}10^{-2}$	$6.4485{\cdot}10^{-3}$	$-2.5477{\cdot}10^{-2}$	$1.6438{\cdot}10^{-2}$	$1.6505{\cdot}10^{-2}$	$-4.3760{\cdot}10^{-2}$	$-8.4398{\cdot}10^{-3}$	$1.4905{\cdot}10^{-2}$
		$\mathbf{BS}_r\mathbf{AR}_s$	$\mathbf{BS}_r\mathbf{AR}_r$	$\mathbf{BS}_r\mathbf{r}_{ht1}$	$\mathbf{BS}_r\mathbf{r}_{ht3}$	$\mathbf{BS}_r\mathbf{r}_{ht4}$	$\mathbf{BS}_r\mathbf{r}_{ht6}$	$\mathbf{BS}_r(\mathbf{t}_{te}/\mathbf{o})_s$	$\mathbf{BS}_r(\mathbf{t}_{te}/\mathbf{o})_r$	$\mathbf{BS}_r\mathbf{d}_{spe}$	$\mathbf{BS}_r\theta_1$	$\mathbf{BS}_r\theta_4$	$\mathbf{BS}_r\mathbf{p}_6$
		$-2.5156{\cdot}10^{-3}$	$7.3377{\cdot}10^{-2}$	$-5.2418{\cdot}10^{-3}$	$9.667{\cdot}10^{-2}$	$-1.9563{\cdot}10^{-2}$	$-1.0785{\cdot}10^{-1}$	$-1.476{\cdot}10^{-2}$	$-9.3216{\cdot}10^{-2}$	$-3.3046{\cdot}10^{-2}$	$8.6072{\cdot}10^{-3}$	$5.7933{\cdot}10^{-2}$	$-2.3326{\cdot}10^{-2}$
			$\mathbf{AR}_s\mathbf{AR}_r$	$\mathbf{AR}_s\mathbf{r}_{ht1}$	$\mathbf{AR}_s\mathbf{r}_{ht3}$	$\mathbf{AR}_s\mathbf{r}_{ht4}$	$\mathbf{AR}_s\mathbf{r}_{ht6}$	$\mathbf{AR}_s(\mathbf{t}_{te}/\mathbf{o})_s$	$\mathbf{AR}_s(\mathbf{t}_{te}/\mathbf{o})_r$	$\mathbf{AR}_s\mathbf{d}_{spe}$	$\mathbf{AR}_s\theta_1$	$\mathbf{AR}_s\theta_4$	$\mathbf{AR}_s\mathbf{p}_6$
			$8.1701{\cdot}10^{-4}$	$1.8275{\cdot}10^{-3}$	$1.6323{\cdot}10^{-2}$	$-1.1715{\cdot}10^{-3}$	$8.8593{\cdot}10^{-3}$	$2.9895{\cdot}10^{-3}$	$-3.9316{\cdot}10^{-4}$	$-6.3041{\cdot}10^{-4}$	$-7.3597{\cdot}10^{-3}$	$-6.7907{\cdot}10^{-3}$	$4.0242{\cdot}10^{-3}$
				$\mathbf{AR}_r\mathbf{r}_{ht1}$	$\mathbf{AR}_r\mathbf{r}_{ht3}$	$\mathbf{AR}_r\mathbf{r}_{ht4}$	$\mathbf{AR}_r\mathbf{r}_{ht6}$	$\mathbf{AR}_r(\mathbf{t}_{te}/\mathbf{o})_s$	$\mathbf{AR}_r(\mathbf{t}_{te}/\mathbf{o})_r$	$\mathbf{AR}_r\mathbf{d}_{spe}$	$\mathbf{AR}_r\theta_1$	$\mathbf{AR}_r\theta_4$	$\mathbf{AR}_r\mathbf{p}_6$
				$-3.8316{\cdot}10^{-2}$	-1.1037	$7.4114{\cdot}10^{-1}$	1.0462	$5.3470{\cdot}10^{-2}$	$2.2120{\cdot}10^{-1}$	$6.0898{\cdot}10^{-1}$	$-1.5121{\cdot}10^{-2}$	$6.4305{\cdot}10^{-2}$	$2.2337{\cdot}10^{-1}$
					$\mathbf{r}_{ht1}\mathbf{r}_{ht3}$	$\mathbf{r}_{ht1}\mathbf{r}_{ht4}$	$\mathbf{r}_{ht1}\mathbf{r}_{ht6}$	$\mathbf{r}_{ht1}(\mathbf{t}_{te}/\mathbf{o})_s$	$\mathbf{r}_{ht1}(\mathbf{t}_{te}/\mathbf{o})_r$	$\mathbf{r}_{ht1}\mathbf{d}_{spe}$	$\mathbf{r}_{ht1}\theta_1$	$\mathbf{r}_{ht1}\theta_4$	$\mathbf{r}_{ht1}\mathbf{p}_6$
					$1.8394{\cdot}10^{-1}$	$3.3992{\cdot}10^{-2}$	$1.8665{\cdot}10^{-1}$	$1.9958{\cdot}10^{-2}$	$4.6420{\cdot}10^{-2}$	$1.6850{\cdot}10^{-2}$	$-2.6512{\cdot}10^{-2}$	$6.6556{\cdot}10^{-3}$	$-3.6996{\cdot}10^{-3}$
						$\mathbf{r}_{ht3}\mathbf{r}_{ht4}$	$\mathbf{r}_{ht3}\mathbf{r}_{ht6}$	$\mathbf{r}_{ht3}(\mathbf{t}_{te}/\mathbf{o})_s$	$\mathbf{r}_{ht3}(\mathbf{t}_{te}/\mathbf{o})_r$	$\mathbf{r}_{ht3}\mathbf{d}_{spe}$	$\mathbf{r}_{ht3}\theta_1$	$\mathbf{r}_{ht3}\theta_4$	$\mathbf{r}_{ht3}\mathbf{p}_6$
						$4.7326{\cdot}10^{-1}$	4.3723	$-3.7391{\cdot}10^{-1}$	$4.7867{\cdot}10^{-1}$	$6.5948{\cdot}10^{-1}$	$9.4796{\cdot}10^{-3}$	$1.6499{\cdot}10^{-1}$	$-6.0925{\cdot}10^{-1}$
							$\mathbf{r}_{ht4}\mathbf{r}_{ht6}$	$\mathbf{r}_{ht4}(\mathbf{t}_{te}/\mathbf{o})_s$	$\mathbf{r}_{ht4}(\mathbf{t}_{te}/\mathbf{o})_r$	$\mathbf{r}_{ht4}\mathbf{d}_{spe}$	$\mathbf{r}_{ht4}\theta_1$	$\mathbf{r}_{ht4}\theta_4$	$\mathbf{r}_{ht4}\mathbf{p}_6$
							$-4.6774{\cdot}10^{-1}$	$-6.7275{\cdot}10^{-2}$	$-1.8136{\cdot}10^{-1}$	$-3.619{\cdot}10^{-1}$	$1.5467{\cdot}10^{-2}$	$-7.801{\cdot}10^{-2}$	$-1.8795{\cdot}10^{-1}$
								$\mathbf{r}_{ht6}(\mathbf{t}_{te}/\mathbf{o})_s$	$\mathbf{r}_{ht6}(\mathbf{t}_{te}/\mathbf{o})_r$	$\mathbf{r}_{ht6}\mathbf{d}_{spe}$	$\mathbf{r}_{ht6}\theta_1$	$\mathbf{r}_{ht6}\theta_4$	$\mathbf{r}_{ht6}\mathbf{p}_6$
								$5.1679{\cdot}10^{-1}$	$-5.2752{\cdot}10^{-1}$	$-4.8385{\cdot}10^{-1}$	$-4.0399{\cdot}10^{-3}$	$-2.0725{\cdot}10^{-1}$	1.1059
									$(\mathbf{t}_{te}/\mathbf{o})_s(\mathbf{t}_{te}/\mathbf{o})_r$	$(\mathbf{t}_{te}/\mathbf{o})_s\mathbf{d}_{spe}$	$(\mathbf{t}_{te}/\mathbf{o})_s\theta_1$	$(\mathbf{t}_{te}/\mathbf{o})_s\theta_4$	$(\mathbf{t}_{te}/\mathbf{o})_s\mathbf{p}_6$
									$-5.2771{\cdot}10^{-2}$	$-1.2083{\cdot}10^{-1}$	$-1.0637{\cdot}10^{-1}$	$1.4613{\cdot}10^{-2}$	$-2.5553{\cdot}10^{-1}$
										$(\mathbf{t}_{te}/\mathbf{o})_r\mathbf{d}_{spe}$	$(\mathbf{t}_{te}/\mathbf{o})_r\theta_1$	$(\mathbf{t}_{te}/\mathbf{o})_r\theta_4$	$(\mathbf{t}_{te}/\mathbf{o})_r\mathbf{p}_6$
										$-2.093{\cdot}10^{-1}$	$1.5089{\cdot}10^{-2}$	$-4.2248{\cdot}10^{-2}$	$-2.8251{\cdot}10^{-1}$
											$\mathbf{d}_{spe}\theta_1$	$\mathbf{d}_{spe}\theta_4$	$\mathbf{d}_{spe}\mathbf{p}_6$
											$1.4997{\cdot}10^{-2}$	$-9.8013{\cdot}10^{-2}$	$-4.3079{\cdot}10^{-1}$
												$\theta_1\theta_4$	$\mathbf{theta}_1\mathbf{p}_6$
												$2.1414{\cdot}10^{-2}$	$1.1592{\cdot}10^{-2}$
													$\theta_4\mathbf{p}_6$
													$-7.3776{\cdot}10^{-2}$
Quadratic effects													
$\mathbf{BS}_s^2$	$\mathbf{BS}_r^2$	$\mathbf{AR}_s^2$	$\mathbf{AR}_r^2$	$\mathbf{r}_{ht1}^2$	$\mathbf{r}_{ht3}^2$	$\mathbf{r}_{ht4}^2$	$\mathbf{r}_{ht6}^2$	$(\mathbf{t}_{te}/\mathbf{o})_s^2$	$(\mathbf{t}_{te}/\mathbf{o})_r^2$	$\mathbf{d}_{spe}^2$	θ_1^2	θ_4^2	$\mathbf{p}_6^2$
$-2.3842{\cdot}10^{-1}$	$-3.6075{\cdot}10^{-1}$	$-1.8324{\cdot}10^{-1}$	$-5.4963{\cdot}10^{-1}$	$-1.7897{\cdot}10^{-1}$	$-8.8517{\cdot}10^{-1}$	$-2.2918{\cdot}10^{-1}$	-2.1985	$-6.2323{\cdot}10^{-1}$	$-8.429{\cdot}10^{-1}$	$-2.7209{\cdot}10^{-1}$	$-1.9601{\cdot}10^{-1}$	$-2.3611{\cdot}10^{-1}$	$-5.2595{\cdot}10^{-1}$

Starting by analyzing the result for the thermodynamic pressure condition which, with 95% confidence, seems to have a positive effect on efficiency — increasing its value—, the following comments can be made. From a previous study it has been confirmed that an increase in the expansion ratio not necessarily increases the efficiency as it presents an optimum point after which the efficiency drops. As explained in the technical background, pressure ratio is given by the ratio between the stagnation pressure and static exit pressure. So, an increase in the exit pressure for a fixed stagnation pressure will decrease the pressure ratio. Thereby, the result obtained from this experiment means that design space being considered for this variables is located at the right of this maxima. The variation of total to static efficiency with exit static pressure has been plotted in Figure 4.1.

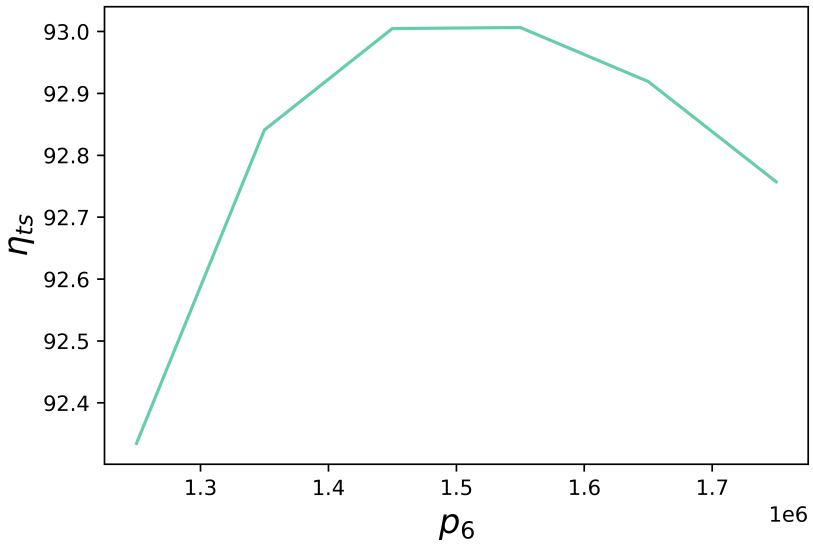

Figure 4.1: Variation of total to static efficiency with static exit pressure.

There is a strong quadratic effect that is not being considered by looking at the experiment results. Surprisingly, any of the quadratic effects seem to be significant. This is a first concern, since from the factorial analysis that had been carried out for selecting the factors it was seen that some of them had a strong curvature, that would certainly affect the output. However, the interaction effects — which are the ones that were properly analyzed in the aforementioned analysis—, do seem to reflect significance on the output.

The results obtained for the geometric design variables are now going to be discussed. The specific diameter is another variable that has to be optimized, since it also presents a strong curvature. An increase in specific diameter may lead to an increase in efficiency as it increases the area of the flow passage and may allow better flow conditions, reducing blockage effects and losses, but it can also lead to a decrease in the turbine efficiency due to structural limitations and high blade loading. However, it should not be considered independently since it has significant interaction effects with other important parameters, as it can be seen from Table 4.8.

The hub-to-tip ratio increases the efficiency when it is set to its minimum, in other words, an increase in hub-to-tip ratio decreases the efficiency. This is because an increase in hub-to-tip ratio implies a decrease in the blade height, which for a fixed value of aspect

ratio will lead to lower values of blade chord increasing profile losses, as explained in [30]. It can be seen that the provided results are in accordance with this reasoning for the stator inlet hub-to-tip ratio and rotor inlet and exit hub-to-tip ratio, unlike the stator exit hub-to-tip ratio that stands out for its important and significant positive effect on the turbine efficiency. The reason for this unexpected result may be the significant interaction effect that, according to the experiment results, this factor has with almost all the others.

As it was seen in Section 2.8.2, the aspect ratio influences the extent of fluid affected by the passage vortex. Therefore, an increase in aspect ratio usually decreases the endwall region and thereby the secondary losses are limited. On the contrary, increasing the aspect ratio increases the blade loading, which leads to greater profile losses. However, small aspect ratios means having small blades and in these cases the turbine performance is affected by tip clearance losses. The results for these two factors within the experiment show to increase the efficiency, although only the rotor aspect ratio seems to be significant.

The trailing edge thickness to opening ratio also decreases the efficiency as it has an effect on the wake that will lead to the formation of secondary flows. A bigger trailing edge thickness to opening ratio will also increase leakage losses between adjacent blade rows, also decreasing the efficiency. From the experiment results it can be seen that both, stator and rotor trailing edge thickness to opening ratio have a negative effect on the efficiency.

Regarding blade solidity, as for the pitch-to-chord ratio, there is an optimum value for which the profile losses are minimum and efficiency is increased. This optimum value is calculated as a function of gas angles, and was presented by Ainley and Mathieson in the graph shown in Figure 4.2. The greater the gas deflection required, the smaller must be the optimum pitch to chord ratio to control the gas adequately [53]. Note that this optimum is also dependent of flow compressibility and working fluid, as explained in [54], a study carried out for ORC turbines.

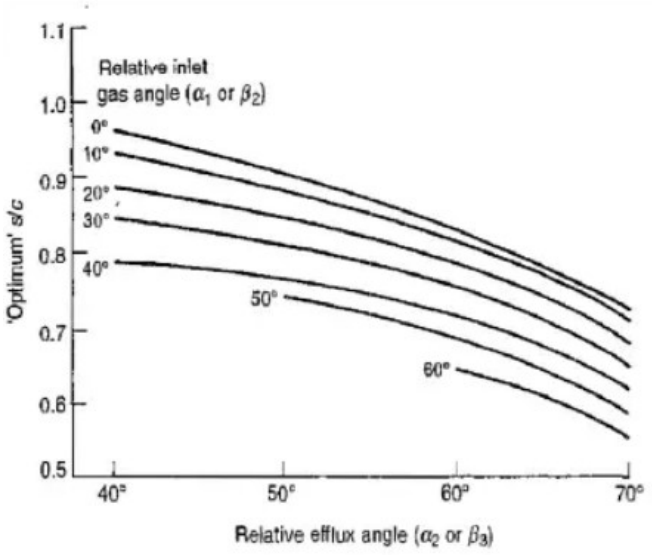

Figure 4.2: Optimum pitch to chord ratio [53].

From the results it can be seen that stator and rotor blade solidities give opposite

effects over the turbine performance.

The last factors to be analyzed are the stator inlet and exit methal angles. These angles have an important role since they give the blade's curvature and have to be set to minimize incidence losses. It can be seen from the results that while the inlet methal angle of the rotor is significant to the efficiency, the inlet methal angle of the stator is not. For the reason just mentioned it was believed that the inlet methal angle of the stator as well as the exit methal angle of the rotor would be the significant factors due to their effect on incidence and deviation, although the latter has not been included in the present experiment as explained.

Therefore, in order to answer the questions posed for analysis, it can be said that the reason why some of the variables present a significant effect and some do not, may be due to the different significant interaction effects that take place during the expansion process in an axial turbine, which may be slightly different between stator and rotor since they present distinct functions within this process. Furthermore, the fact of selecting the bounds in order to cover a wide design space is having a strong influence in the analysis. This can be confirmed by the low values of efficiency achieved in several runs within the last three experiments.

Looking a little deeper into the efficiency results achieved, the following information should be pointed out:

- 65 out of the 16413 runs (0.39% of the runs) gave an efficiency lower than 13.34%, but also lower than 39.66%
- 4689 out of 16413 runs (28.56% of the runs) gave an efficiency under 80%

From this it can be said that there is not a big amount of "failed" runs, but enough to introduce some uncertainty in the results, since the coefficients that are being analyzed could have been assigned according to these atypical runs. As this problem arises from the bounds that have been considered, they should be studied in order to seek more precise results. This is what has led to perform the next analysis by narrowing some of the initial bounds, which will be commented in Section 4.2.

Finally, it has been found that introducing a factor to the experiment has an effect on the results. This was precisely the purpose of progressively increasing the number of factors in the experiments that have been conducted. So, results do not only depend on the bounds, but also on the number and selection of the studied factors. Including the two remaining factors, θ_3 and θ_6, would certainly introduce some changes in the relevance of the other factors and in the coefficients of the different effects. Conducting this full experiment would have provided much more information than the presented above, but some limitations in the model, which will be commented below, have not made it possible.

4.1.7 Limitations in the experiments and discussion

A complete face-centered central composite design was intended to be carried out by analyzing within the same experiment the sixteen selected factors from the previous non-

rigorous factorial analysis presented in Section 3.2.2. As it has been said, limitations were found in the model, which made the experiment fail, not allowing to see how all those factors affect the efficiency when being considered together.

This failure arose when either θ_3, θ_6 or both simultaneously were introduced in the experiment. Several tries by changing the specific diameter for the specific speed led to the same error. The fact of analyzing the turbine in points that are that far from the optimum design point makes it difficult for the model to converge and find a right and coherent solution. The reason why the experiment failed in all the different tries was an non-physical value reached among the thermodynamic equations of state, a negative molar density which disabled the solver to continue.

A comment to be made at this point is that the attempt of the various failed experiments has resulted in a large amount of time spent and therefore, in the case of a real experiment, it would have resulted in a great amount of money lost. With this, the advantages of working with numerical simulation, previously discussed in Section 2.7, have been experienced.

Since it is considered that the factors that could not be analyzed in the set of design variables are important for the design, it has been decided to continue the analysis by trying to solve the first of the problems encountered at the present study. As discussed in Section 3.3, the wide range analysis has been repeated by reducing the field of study of the variables that first introduced uncertainty in the results ($(t_{te}/o)_s$ and $(t_{te}/o)_r$). The main results will be presented in the next section.

4.2 Results from the sensitivity analysis for a narrower design space and discussion

Two different experiments have been conducted by narrowing the design space of the factors that first led to anomalous values of low efficiency. As explained in Section 3.3 the purpose was to try to reduce the uncertainty in the results by easing the model to converge in a more coherent solution. The main information from each experiment (11-factor and 13-factor) will be respectively presented in Section 4.2.1 and Section 4.2.2. A further discussion concerning the limitations found within the present analysis will be presented in Section 4.2.3.

4.2.1 Experiment 1: 11 factors

The first experiment that has been conducted within this new analysis is the 11-factor experiment presented in Section 4.1.3, with a narrower design space for $(t_{te}/o)_s$ and $(t_{te}/o)_r$, as it has been shown in Section 3.3. In Table 4.9, the main information of the experiment has been collected. Comments on the reliability of this experiment will be done later in Section 4.2.3, together with other comments related to the second performed experiment.

Number of runs	Time [s]	η_{min} [%]	η_{max} [%]
2071	1165.4	52.27%	91.22%

Table 4.9: Data from 11-factor experiment

In order to verify some of the hypotheses posed in the just presented section, the following table (Table 4.10) has been drawn up. It compares the coefficients obtained for the main effects in the narrower SA to the coefficients for the main effects in the wide design space SA. Those effects that have proven to be significant after evaluating their corresponding confidence intervals have been highlighted in grey. These confidence intervals for the main, interaction and quadratic effects have been included in Appendix B.1, presented respectively in Table B.23, Table B.24 and Table B.25.

Table 4.10: Comparison of the main effect coefficients between the narrower 11-factor and wide 11-factor sensitivity analysis. Significant effects highlighted in grey.

Main effect	Coefficient Narrower SA	Relevance	Coefficient Wide SA	Relevance
$\mathbf{BS}_s$	0.0056	Not significant	-0.0039	Not significant
$\mathbf{BS}_r$	-0.1088	Significant	-0.1635	Significant
$\mathbf{AR}_s$	0.0133	Not significant	0.0091	Not significant
$\mathbf{AR}_r$	1.9889	Significant	2.169	Significant
$\mathbf{r}_{ht1}$	-0.2044	Significant	-0.0575	Not significant
$\mathbf{r}_{ht3}$	3.9057	Significant	3.9723	Significant
$\mathbf{r}_{ht4}$	-0.8798	Significant	-1.0474	Significant
$\mathbf{r}_{ht6}$	-4.7306	Significant	-4.7438	Significant
$(\mathbf{t}_{te}/\mathbf{o})_s$	-0.7457	Significant	-1.314	Significant
$(\mathbf{t}_{te}/\mathbf{o})_r$	-1.2951	Significant	-1.7388	Significant
$\mathbf{p}_6$	0.662	Significant	0.4069	Significant

Different things can be seen from Table 4.10. The first one is that by reducing the design space of the mentioned factors, the stator inlet hub-to-tip ratio, r_{ht_1}, appears to be significant. This result confirms — as it was seen in previous experiments —, that this factor is sensitive to the other factors considered for the study. In order of importance and in absolute value the significant factors for the present experiment are: r_{ht_6} (-), r_{ht_3} (+), AR_r (+), $(\mathrm{t}_{te}/\mathrm{o})_r$ (-), r_{ht_4} (-), $(\mathrm{t}_{te}/\mathrm{o})_s$ (-), p_6 (+), r_{ht_1} (-) and BS_r (-). The importance of the trailing edge thickness to opening ratios for the stator and rotor has been reduced by shortening their design space. Only the static exit pressure presents a bigger coefficient among the significant factors. Among the not significant factors it can also be seen that the aspect ratio of the stator presents a bigger coefficient than the previous one and that the blade solidity of the stator has changed its effect on the efficiency from negative to positive, proving also to be sensitive to changes in the bounds, despite its relevance to the output in the experiment in question.

4.2.2 Experiment 2: 13 factors

The second experiment carried out within the narrower analysis included the same 13 factors that the ones included in the experiment presented in Section 4.1.5, but instead

of introducing the specific diameter, the rotor inlet methal angle was considered. This change was done in order to avoid the warning messages that appeared during this 13-factor experiment within the wide design space analysis due to the specific diameter, as it was commented above. The minimum and maximum efficiencies reached in the experiment are shown in Table 4.11.

Number of runs	Time [s]	η_{min} [%]	η_{max} [%]
8219	5231.2	51.80%	92.63%

Table 4.11: Data from 13-factor experiment

A similar table to the one presented above has been drawn up in order to compare the results for the coefficients of the main effects for the aforementioned experiments. It has been built presenting 14 factors, but results for the 13 factors considered in each of the experiments. Those factors that resulted significant when analyzing the 95% confidence intervals (included in Appendix B.2 in Table B.26, Table B.27 and Table B.28) have been highlighted in grey.

Table 4.12: Comparison of the main effect coefficients between the narrower 13-factor and wide 13-factor sensitivity analysis. Significant effects highlighted in grey.

Main effect	Coefficient narrower SA	Relevance	Coefficient wide SA	Relevance
$\mathbf{BS}_s$	0.016	Not significant	0.029	Not Significant
$\mathbf{BS}_r$	-0.0748	Significant	-0.1934	Significant
$\mathbf{AR}_s$	0.0141	Not significant	0.02	Not significant
$\mathbf{AR}_r$	2.0093	Significant	1.8162	Significant
$\mathbf{r}_{ht1}$	-0.202	Significant	-0.1628	Significant
$\mathbf{r}_{ht3}$	4.04	Significant	3.5772	Significant
$\mathbf{r}_{ht4}$	-0.9168	Significant	-0.8101	Significant
$\mathbf{r}_{ht6}$	-4.9037	Significant	-4.4552	Significant
$(\mathbf{t}_{te}/\mathbf{o})_s$	-0.7222	Significant	-1.2291	Significant
$(\mathbf{t}_{te}/\mathbf{o})_r$	-1.2387	Significant	-1.7346	Significant
$\mathbf{d}_{spe}$	—	—	-0.7189	Significant
θ_1	0.0391	Not significant	-0.0073	Not significant
θ_4	-0.2377	Significant	—	—
$\mathbf{p}_6$	0.6558	Significant	0.5592	Significant

As for the previous experiment, the coefficients for the factors whose bounds are being modified ($(t_{te}/o)_s$ and $(t_{te}/o)_r$) are lower in absolute value, but in this case, all the factors present the same effect on the efficiency and the same relevance as before. Comparing the narrower 13-factor SA to the 11-factor SA a slight difference is introduced in the coefficients by adding these two new factors, θ_1 and θ_4.

4.2.3 Limitations in the experiments and discussion

It has been seen that changes in the design bounds do not only influence the results for the multiple linear regression coefficients of the different effects, but also the results for

the efficiency. From the above experiments it can be said that by narrowing the design space, the model converges in a more coherent solution, with greater values of minimum efficiency, as seen in Table 4.9 and Table 4.11. However, these values are as reliable as the ones of 13% efficiency obtained for the wide design space analysis. This has been checked by using the already described script in Python, which tells the tolerance the model is using to provide the solution. This tolerance is greater than the one set for relying on the results (10^{-5}). Hence, even though the efficiency is greater than the one obtained in the first analysis, the results are uncertain, therefore, no further experiments within this analysis have been conducted. But, from this it can be said that it is more likely to obtain good results if a smaller design space is considered — as a less robust model is required —, and how this design space is set may also affect the output and coefficients results. This has led to the third and last sensitivity analysis, a local sensitivity analysis that assesses the influence of the design variables variation on the efficiency in the surroundings of the case study point. It will be presented in the section below.

4.3 Results from the local sensitivity analysis and discussion

The results obtained from the local sensitivity analysis — carried out in view of the uncertainty in the results of the experiments that contemplate a wider design space, in the studies just reported— , will be presented below. As in the case of the latter, several experiments have been carried out in which the number of factors involved has been progressively increased. It has been decided to present in this section only the 14-factor experiment, since it is the last one that could be carried out due to limitations of the model, and it is the one that therefore provides the most information. Since it was not possible to analyze all the selected factors together in the same experiment, the remaining factors have been examined separately in order to add a series of comments on their importance, not least because they were not introduced in the study. The experiments that were carried out up to the 14-factor experiment (9-factor and 11-factor) have been included in full in Appendix C (Ap. C.1 and Ap. C.2).

The information of the experiment has been collected in Table 4.13: number of runs, time invested and minimum and maximum efficiencies obtained. Since this is a local sensitivity analysis in which the design space is reduced to ± 5% of the value of each of the input variables, the variation in efficiency is expected to be small. The fact of varying all the factors the same percentage rather than each in a different way also eases the analysis.

Number of runs	Time [s]	η_{min} [%]	η_{max} [%]
16412	9380.9	89.587	93.187

Table 4.13: Data from local sensitivity analysis

The results obtained from the experiment have been gathered in two different tables, as in the 14-factor experiment presented in the wide design space section. The first table shows the coefficients of the main effects obtained from the linear multiple regression, together with the lower and upper limits of the 95% confidence interval calculated for

these coefficients, and their significance on the output variable. On the other hand, the second table shows not only these main effects, but also the interaction and quadratic effects, shaded in pink those that, after studying the corresponding confidence interval (shown in Appendix C.3 for the interaction and quadratic effects), have been found to be significant.

In view of Table 4.14, the first thing to note is that the two factors that have not been included in the study are the exit methal angles of the stator and rotor blades. The reason why they have not been included in the analysis is a limitation found in the model after various attempts at experiments, as it happened in the wide SA. This limitation will be detailed at the end of the section. However, the non-inclusion of these two factors does not imply their lesser importance; on the contrary, it is believed that both factors are not irrelevant to the conclusions of the study, in accordance with the corresponding efficiency variation graphs of the first non-rigorous factorial analysis presented in Section 3.2.2. Therefore, as mentioned above, once the other results have been discussed, the effect of these two factors will be analyzed in more detail.

Table 4.14: Confidence interval for the main effects in local sensitivity analysis. Significant effects highlighted in grey.

Main effect	IC lower bound	Coefficient	IC upper bound	Relevance
$\mathbf{BS}_s$	0.0015	0.0024	0.0033	Significant
$\mathbf{BS}_r$	-0.0008	0.0001	0.0011	Not significant
$\mathbf{AR}_s$	0.006	0.007	0.0079	Significant
$\mathbf{AR}_r$	0.0746	0.0755	0.0765	Significant
$\mathbf{r}_{ht1}$	-0.005	-0.0041	-0.0032	Significant
$\mathbf{r}_{ht3}$	-0.0799	-0.079	-0.078	Significant
$\mathbf{r}_{ht4}$	-0.0458	-0.0449	-0.044	Significant
$\mathbf{r}_{ht6}$	0.0209	0.0219	0.0228	Significant
$(\mathbf{t}_{te}/\mathbf{o})_s$	-0.0202	-0.0192	-0.0183	Significant
$(\mathbf{t}_{te}/\mathbf{o})_r$	-0.0205	-0.0196	-0.0186	Significant
$\mathbf{d}_{spe}$	-0.1274	-0.1264	-0.1255	Significant
θ_1	-0.0073	-0.0064	-0.0054	Significant
θ_4	-0.0016	-0.0007	0.0003	Not significant
$\mathbf{p}_6$	-0.1481	-0.1471	-0.1462	Significant

The following observation by looking at the table above is that only two of the fourteen studied factors seem not to be significant when analyzing a small design space. These are the rotor blade solidity and rotor inlet methal angle. In order of importance and in absolute value, the significant factors in the local sensitivity analysis are: p_6 (-), d_{spe} (-), r_{ht_3} (-), AR_r (+), r_{ht_4} (-), r_{ht_6} (+), $(t_{te}/o)_r$ (-), $(t_{te}/o)_s$ (-), AR_s (+), θ_1 (-), r_{ht_1} (-) and BS_s (+). As it can be observed, these results are quite different from the ones obtained for the wide design space sensitivity analysis presented in Section 4.1.6. In order to gain insight and understand a bit better what is happening in the proximities of the design point, the interaction and quadratic effects are required, since they will help to see why some factors are more important or sensitive than others, as it is known that all of them are to be considered somehow when designing an axial turbine.

Furthermore, knowing the loss breakdown when assessing the performance of the tur-

bine with the selected loss model for the case study, which has also been used for carrying out the experiments, will aide to explain the impact that some of these factors would have on the efficiency (positive or negative), by its effect on the losses. Therefore, a bar-chart showing the different components in which the stator and rotor loss coefficients are divided has been created: Kacker and Okapuu profile loss coefficient for design conditions, secondary loss coefficient, tip clearance loss coefficient and incidence loss coefficient for off-design conditions. It has to be noted that the total loss coefficient is calculated taking into account the penetration depth, as it was introduced in Section 2.9.5 and explained in Section 3.1.2. Further comments on this graph will be made in Section 4.4, where it will be illustrated once the coefficients and relevance of the different mentioned effects (interaction and quadratic) have been presented and discussed.

With this aim, Table 4.15 has been built. As for the 14-factor experiment within the wide design space sensitivity analysis, the main effects of the studied factors — already presented in Table 4.14—, are located at the top. Beneath them the different interaction effects have been collected, and finally, at the bottom the quadratic effects are shown. Those coefficients that resulted significant when evaluating the corresponding confidence intervals are highlighted in pink.

Table 4.15: Results of local SA - Faced central composite design with 14 factors. Significant effects highlighted in pink.

Main effects													
$\mathbf{BS}_s$	$\mathbf{BS}_r$	$\mathbf{AR}_s$	$\mathbf{AR}_r$	$\mathbf{r}_{ht1}$	$\mathbf{r}_{ht3}$	$\mathbf{r}_{ht4}$	$\mathbf{r}_{ht6}$	$(\mathbf{t}_{te}/\mathbf{o})_s$	$(\mathbf{t}_{te}/\mathbf{o})_r$	$\mathbf{d}_{spe}$	θ_1	θ_4	$\mathbf{p}_6$
0.0024	0.0001	0.007	0.0755	-0.0041	-0.079	-0.0449	0.0219	-0.0192	-0.0196	-0.1264	-0.0064	-0.0007	-0.1471
Interaction effects													
	$\mathbf{BS}_s\mathbf{BS}_r$	$\mathbf{BS}_s\mathbf{AR}_s$	$\mathbf{BS}_s\mathbf{AR}_r$	$\mathbf{BS}_s\mathbf{r}_{ht1}$	$\mathbf{BS}_s\mathbf{r}_{ht3}$	$\mathbf{BS}_s\mathbf{r}_{ht4}$	$\mathbf{BS}_s\mathbf{r}_{ht6}$	$\mathbf{BS}_s(\mathbf{t}_{te}/\mathbf{o})_s$	$\mathbf{BS}_s(\mathbf{t}_{te}/\mathbf{o})_r$	$\mathbf{BS}_s\mathbf{d}_{spe}$	$\mathbf{BS}_s\theta_1$	$\mathbf{BS}_s\theta_4$	$\mathbf{BS}_s\mathbf{p}_6$
	-0.0	0.0001	0.0	0.0	0.0004	-0.0	-0.0003	-0.0	-0.0	0.0001	-0.0001	0.0	0.0002
		$\mathbf{BS}_r\mathbf{AR}_s$	$\mathbf{BS}_r\mathbf{AR}_r$	$\mathbf{BS}_r\mathbf{r}_{ht1}$	$\mathbf{BS}_r\mathbf{r}_{ht3}$	$\mathbf{BS}_r\mathbf{r}_{ht4}$	$\mathbf{BS}_r\mathbf{r}_{ht6}$	$\mathbf{BS}_r(\mathbf{t}_{te}/\mathbf{o})_s$	$\mathbf{BS}_r(\mathbf{t}_{te}/\mathbf{o})_r$	$\mathbf{BS}_r\mathbf{d}_{spe}$	$\mathbf{BS}_r\theta_1$	$\mathbf{BS}_r\theta_4$	$\mathbf{BS}_r\mathbf{p}_6$
		-0.0	0.0001	0.0	-0.0002	0.0	0.0002	0.0	-0.0	0.0002	0.0	0.0003	0.0001
			$\mathbf{AR}_s\mathbf{AR}_r$	$\mathbf{AR}_s\mathbf{r}_{ht1}$	$\mathbf{AR}_s\mathbf{r}_{ht3}$	$\mathbf{AR}_s\mathbf{r}_{ht4}$	$\mathbf{AR}_s\mathbf{r}_{ht6}$	$\mathbf{AR}_s(\mathbf{t}_{te}/\mathbf{o})_s$	$\mathbf{AR}_s(\mathbf{t}_{te}/\mathbf{o})_r$	$\mathbf{AR}_s\mathbf{d}_{spe}$	$\mathbf{AR}_s\theta_1$	$\mathbf{AR}_s\theta_4$	$\mathbf{AR}_s\mathbf{p}_6$
			0.0	-0.0001	0.0012	-0.0	-0.001	-0.0	-0.0	0.0004	-0.0001	0.0	0.0007
				$\mathbf{AR}_r\mathbf{r}_{ht1}$	$\mathbf{AR}_r\mathbf{r}_{ht3}$	$\mathbf{AR}_r\mathbf{r}_{ht4}$	$\mathbf{AR}_r\mathbf{r}_{ht6}$	$\mathbf{AR}_r(\mathbf{t}_{te}/\mathbf{o})_s$	$\mathbf{AR}_r(\mathbf{t}_{te}/\mathbf{o})_r$	$\mathbf{AR}_r\mathbf{d}_{spe}$	$\mathbf{AR}_r\theta_1$	$\mathbf{AR}_r\theta_4$	$\mathbf{AR}_r\mathbf{p}_6$
				-0.0	-0.0034	0.0018	0.0049	-0.0	-0.0001	-0.0038	-0.0	0.0	-0.0004
					$\mathbf{r}_{ht1}\mathbf{r}_{ht3}$	$\mathbf{r}_{ht1}\mathbf{r}_{ht4}$	$\mathbf{r}_{ht1}\mathbf{r}_{ht6}$	$\mathbf{r}_{ht1}(\mathbf{t}_{te}/\mathbf{o})_s$	$\mathbf{r}_{ht1}(\mathbf{t}_{te}/\mathbf{o})_r$	$\mathbf{r}_{ht1}\mathbf{d}_{spe}$	$\mathbf{r}_{ht1}\theta_1$	$\mathbf{r}_{ht1}\theta_4$	$\mathbf{r}_{ht1}\mathbf{p}_6$
					-0.0013	0.0	0.0006	-0.0	0.0	-0.0002	-0.0	-0.0	-0.0003
						$\mathbf{r}_{ht3}\mathbf{r}_{ht4}$	$\mathbf{r}_{ht3}\mathbf{r}_{ht6}$	$\mathbf{r}_{ht3}(\mathbf{t}_{te}/\mathbf{o})_s$	$\mathbf{r}_{ht3}(\mathbf{t}_{te}/\mathbf{o})_r$	$\mathbf{r}_{ht3}\mathbf{d}_{spe}$	$\mathbf{r}_{ht3}\theta_1$	$\mathbf{r}_{ht3}\theta_4$	$\mathbf{r}_{ht3}\mathbf{p}_6$
						-0.0009	0.5897	-0.0034	0.0025	-0.247	-0.0012	0.0094	-0.3184
							$\mathbf{r}_{ht4}\mathbf{r}_{ht6}$	$\mathbf{r}_{ht4}(\mathbf{t}_{te}/\mathbf{o})_s$	$\mathbf{r}_{ht4}(\mathbf{t}_{te}/\mathbf{o})_r$	$\mathbf{r}_{ht4}\mathbf{d}_{spe}$	$\mathbf{r}_{ht4}\theta_1$	$\mathbf{r}_{ht4}\theta_4$	$\mathbf{r}_{ht4}\mathbf{p}_6$
							-0.0026	0.0	0.0	0.0045	0.0	-0.0001	0.0005
								$\mathbf{r}_{ht6}(\mathbf{t}_{te}/\mathbf{o})_s$	$\mathbf{r}_{ht6}(\mathbf{t}_{te}/\mathbf{o})_r$	$\mathbf{r}_{ht6}\mathbf{d}_{spe}$	$\mathbf{r}_{ht6}\theta_1$	$\mathbf{r}_{ht6}\theta_4$	$\mathbf{r}_{ht6}\mathbf{p}_6$
								0.0028	-0.002	0.213	0.001	-0.0088	0.2628
									$(\mathbf{t}_{te}/\mathbf{o})_s(\mathbf{t}_{te}/\mathbf{o})_r$	$(\mathbf{t}_{te}/\mathbf{o})_s\mathbf{d}_{spe}$	$(\mathbf{t}_{te}/\mathbf{o})_s\theta_1$	$(\mathbf{t}_{te}/\mathbf{o})_s\theta_4$	$(\mathbf{t}_{te}/\mathbf{o})_s\mathbf{p}_6$
									0.0	-0.001	0.0	-0.0	-0.0018
										$(\mathbf{t}_{te}/\mathbf{o})_r\mathbf{d}_{spe}$	$(\mathbf{t}_{te}/\mathbf{o})_r\theta_1$	$(\mathbf{t}_{te}/\mathbf{o})_r\theta_4$	$(\mathbf{t}_{te}/\mathbf{o})_r\mathbf{p}_6$
										-0.0006	0.0	0.0	-0.0001
											$\mathbf{d}_{spe}\theta_1$	$\mathbf{d}_{spe}\theta_4$	$\mathbf{d}_{spe}\mathbf{p}_6$
											-0.0003	-0.0075	-0.2804
												$\theta_1\theta_4$	$\theta_1\mathbf{p}_6$
												-0.0	-0.0006
													$\theta_4\mathbf{p}_6$
													-0.0021
Quadratic effects													
$\mathbf{BS}_s^2$	$\mathbf{BS}_r^2$	$\mathbf{AR}_s^2$	$\mathbf{AR}_r^2$	$\mathbf{r}_{ht1}^2$	$\mathbf{r}_{ht3}^2$	$\mathbf{r}_{ht4}^2$	$\mathbf{r}_{ht6}^2$	$(\mathbf{t}_{te}/\mathbf{o})_s^2$	$(\mathbf{t}_{te}/\mathbf{o})_r^2$	$\mathbf{d}_{spe}^2$	θ_1^2	θ_4^2	$\mathbf{p}_6^2$
0.0024	0.0021	0.0036	0.0057	0.0041	-0.3737	0.0031	-0.2679	0.004	0.004	-0.1803	0.0085	0.0042	-0.1263

The first thing that stands out by looking at the table above is that four of the twelve factors with a significant main effect have also a significant quadratic effect. These are: static exit pressure, p_6, specific diameter, d_{spe}, stator exit hub-to-tip ratio, r_{ht_3}, and rotor exit hub-to-tip ratio, r_{ht_6}. The quadratic effects provide information about the sensitivity of the factors, in this case to a small variation, as they indicate the existence of curvature.

Comparing this first observation with the results obtained for the first analysis, which showed no significant quadratic effects, it can be seen that the present analysis captures more reliably what can be verified by means of a simple graph of efficiency against each of these factors. The presence of a strong curvature in the efficiency vs. pressure graph was already shown in Figure 4.1. In the same way, it can be seen from Figure 4.3 that the results provided by the experiment are not misleading, since the three other factors also show a considerable curvature.

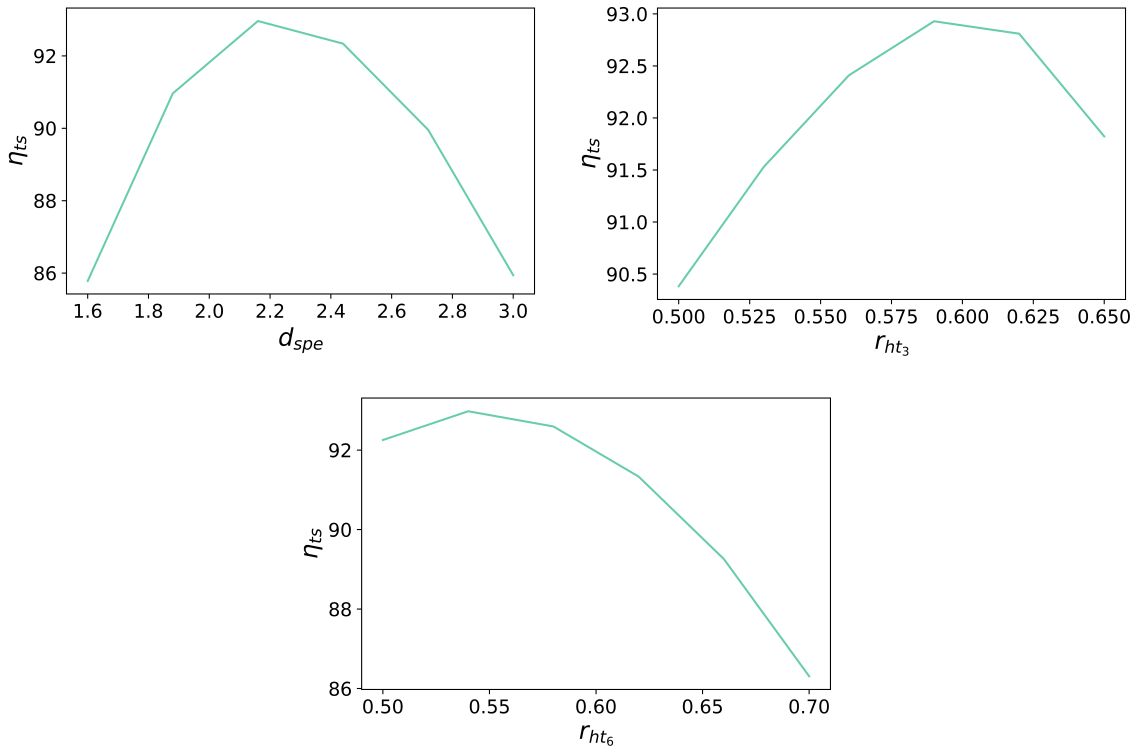

Figure 4.3: Significant quadratic effects in local sensitivity analysis: Total to static efficiency vs. specific diameter, stator and rotor exit hub-to-tip ratios respectively

The positive and negative effect of these four factors on the efficiency can also try to be explained from the graphs in Figure 4.1 and Figure 4.3 above. Taking into account the bounds that are being used for the local sensitivity analysis, gathered in Table 3.13, it can be seen that the variation range for the static pressure is behind the optimum point, so a negative effect might be expected. However, the variation range for the specific diameter, stator hub-to-tip ratio and rotor hub-to-tip ratio contains the optimum point. It is therefore necessary to resort to the various interaction effects in order to continue the analysis. The interaction effects between the static exit pressure and the rest of the factors have already been presented in Section 3.2.2, since they were used to make a first selection of the relevant design variables. Thereby, they will not be discussed again.

Starting by analyzing the interactions of the other three factors under consideration, it is to be expected that the effect between them is considerable, given their significance. Indeed, by taking a look at Table 4.15 it can be seen that among the interaction effects, those that present a bigger coefficient are the combined effects of r_{ht_3}&r_{ht_6}, r_{ht_3}&d_{spe} and r_{ht_6}&d_{spe}, apart from the combination of each of the three factors and static pressure. These three main interaction effects have been plotted and presented below in Figure 4.4.

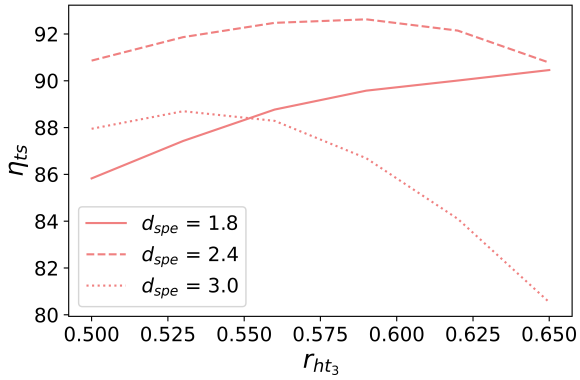

(a) Interaction effect between stator exit hub-to-tip ratio and specific diameter (r_{ht_3}&d_{spe}).

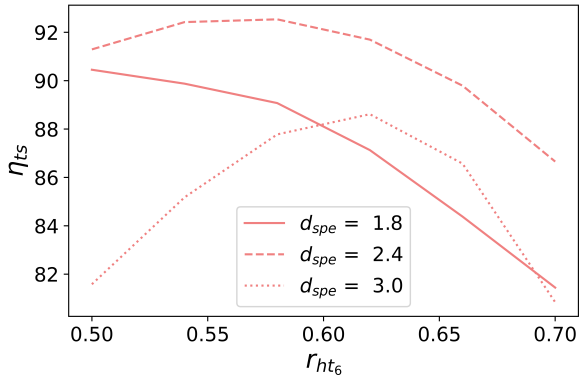

(b) Interaction effect between rotor exit hub-to-tip ratio and specific diameter (r_{ht_6}&d_{spe}).

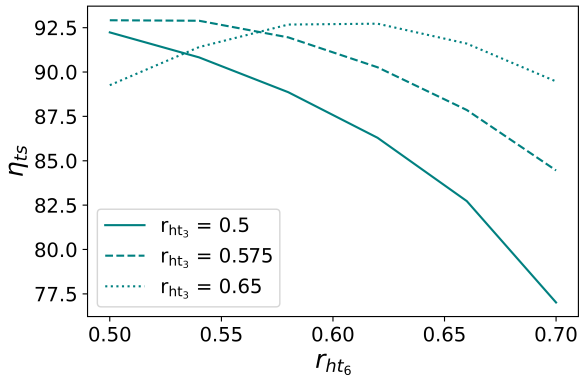

(c) Interaction effect between rotor exit hub-to-tip ratio and stator exit hub-to-tip ratio (r_{ht_6}&r_{ht_3}).

Figure 4.4: Principal interaction effects

Something curious to be noted is that even though the rotor exit hub-to-tip ratio has an important and significant quadratic and main effect, as well as interesting interaction effects with some of the factors (as seen from above), two other factors appear to have a greater main effect coefficient. These are the rotor aspect ratio and rotor inlet hub-to-tip ratio. They have not proven to present significant quadratic effects in the experiment, however, this has been tested using the same simple graph as for the factors already analyzed, and is presented below in Figure 4.5.

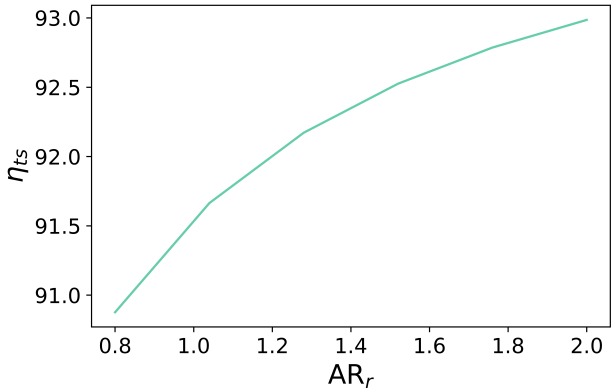

(a) Total to static efficiency vs. rotor aspect ratio (AR_r)

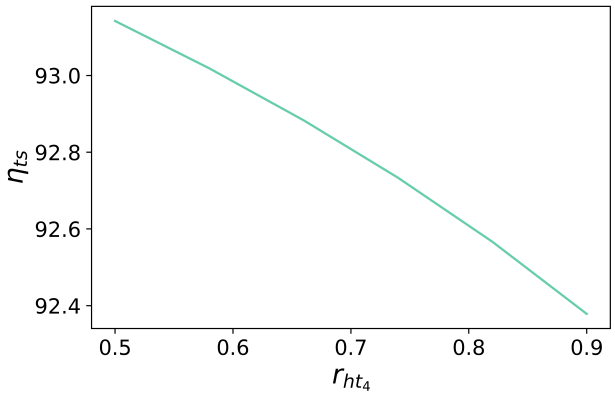

(b) Total to static efficiency vs. rotor inlet hub-to-tip ratio (r_{ht_4})

Figure 4.5: Deeper analysis of the main effect of some factors

From the figure above it can be seen that the experiment is giving coherent results since almost a linear trend is found when varying their values. The advantage of performing this kind of experiments is that cautious decisions may be taken, as there is more information than the one provided by the graphs above. By only looking at these graphs it is not unreasonable to say that the rotor aspect ratio could be set to its upper bound whereas the rotor inlet hub-to-tip ratio could be set to its lower bound, as it is how they lead to higher values of efficiency. However, this should be checked by analyzing the interaction effects. From Table 4.15 it is seen that the rotor aspect ratio has a significant interaction with r_{ht_6}, d_{spe}, r_{ht_3} and r_{ht_4} in order of importance. This seems to be in accordance with the discussion that has been made so far. The first three interaction effects have been plotted and gathered in Figure 4.6 in order to confirm the hypothesis above.

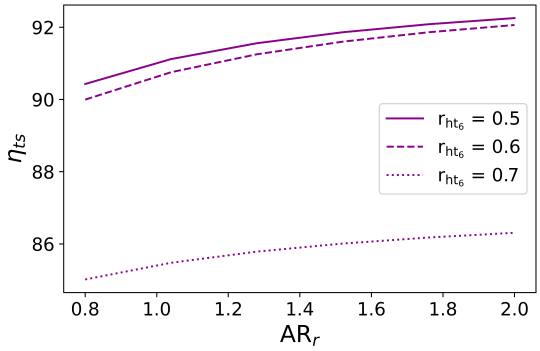

(a) Interaction effect between rotor aspect ratio and rotor exit hub-to-tip ratio (AR_r&r_{ht_6}).

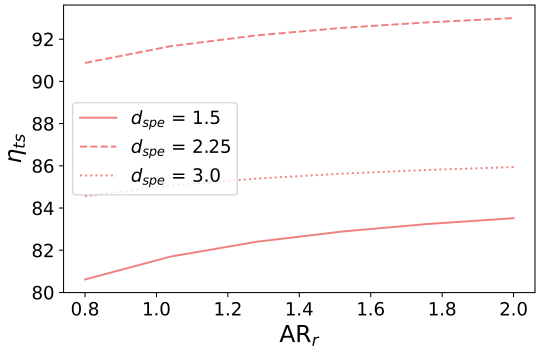

(b) Interaction effect between rotor aspect ratio and specific diameter (AR_r&d_{spe}).

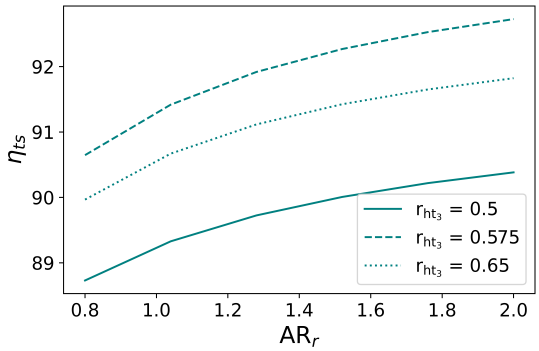

(c) Interaction effect between rotor aspect ratio and stator exit hub-to-tip ratio (AR_r&r_{ht_3}).

Figure 4.6: Principal interaction effects of the rotor aspect ratio (AR_r)

There is not any unexpected behaviour among the interactions of rotor aspect ratio and each of the three principal factors. An increase in the former will always have a positive impact on the efficiency, so this will be one of the conditions for the further comparison between the optimization before and after the sensitivity analysis. The rotor aspect ratio will not be included in the optimization but fixed to the upper bound used in the previous.

Another thing that can be observed from the graphs in Figure 4.6 is that the order of importance of the three principal factors being considered is translated in a respective drop in efficiency. An interesting observation is that, unlike the specific diameter and the stator exit hub-to-tip ratio — which in combination with the rotor aspect ratio reflect the proven curvature effects—, the rotor exit hub-to-tip ratio combined with the aspect ratio provides the highest efficiency at its minimum value. The same trend has been seen for the interaction between rotor inlet hub-to-tip ratio and aspect ratio. Nevertheless, the plot has not been included because it provides no longer relevant information. However, it will be presented in Appendix D for major information of interested readers, together with the plots of some of the other interaction effects that are not going to be considered within this section because they have shown to be less meaningful.

If, on the other hand, the interaction between the rotor inlet hub-to-tip ratio and the

three main factors is studied, the previous posed hypothesis cannot be accepted, as there is not a clear trend of decrease in efficiency while increasing the rotor inlet hub-to-tip ratio when combined with different factors, in particular when interacting with the rotor exit hub-to-tip ratio (r_{ht_6}) as seen in Figure 4.7 (b).

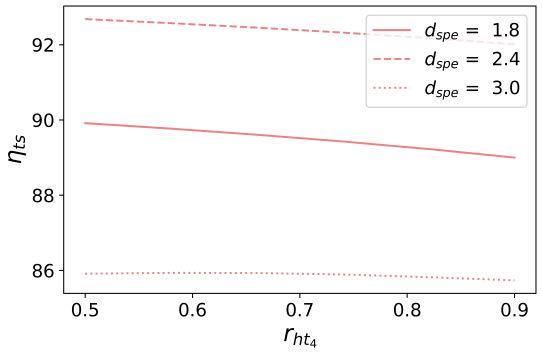

(a) Interaction effect between rotor inlet hub-to-tip ratio and specific diameter (r_{ht_4}&d_{spe}).

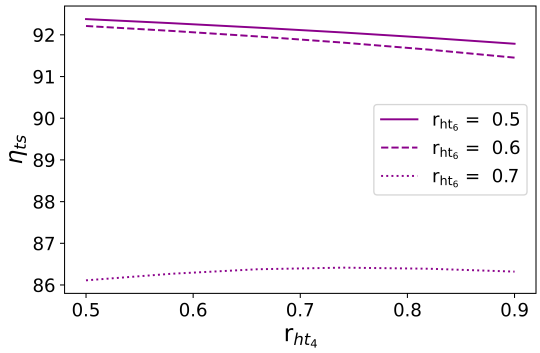

(b) Interaction effect between rotor inlet hub-to-tip ratio and rotor exit hub-to-tip ratio (r_{ht_4}&r_{ht_6}).

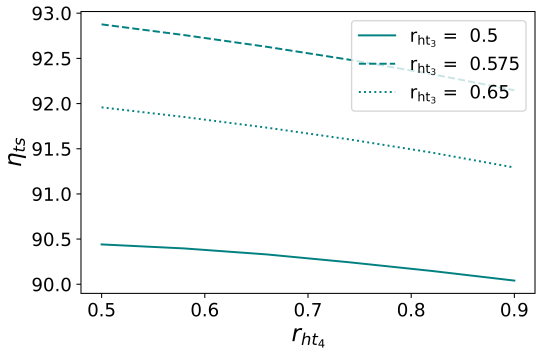

(c) Interaction effect between rotor inlet hub-to-tip ratio and stator exit hub-to-tip ratio (r_{ht_4}&r_{ht_3}).

Figure 4.7: Principal interaction effects of the rotor inlet hub-to-tip ratio (r_{ht_4})

By analyzing the interaction of the specific diameter with the rotor aspect ratio in Figure 4.6 (b) and with the rotor inlet hub-to-tip ratio in Figure 4.7 (a) it is noticeable that whereas the minimum specific diameter provides the lowest efficiency in the former, it provides a quite higher efficiency in the latter between the one provided by the medium and maximum levels of specific diameter. This reflects the complexity and interrelation of factors during the expansion process, which might suggest the need to carry out an exhaustive study of how each parameter affects each variable. However, this has not been done for a simple reason that will be discussed below. Furthermore, it would be unwise not to take into account the significance study carried out using confidence intervals, which indicates which are the most important factors and effects to be considered for the purpose of the analysis.

Finally, in view of Table 4.15 and the graphs obtained for the first analysis carried out for the selection of factors in Section 3.2.2, it is interesting to analyze the interaction

of the stator and rotor exit hub-to-tip ratio and stator trailing edge thickness to opening ratio. These effects are shown in Figure 4.8, together with the interaction between the rotor trailing edge thickness to opening ratio and stator exit hub-to-tip ratio.

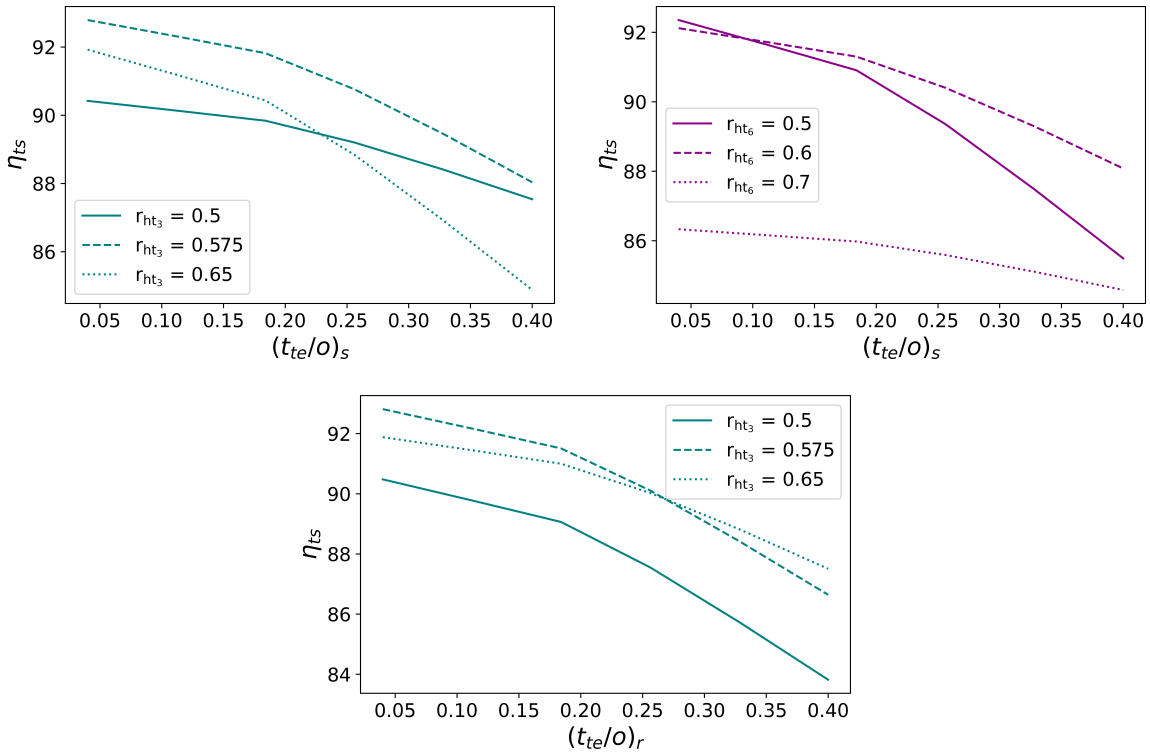

Figure 4.8: Interaction effects between stator TE thickness to opening ratio and stator exit hub-to-tip ratio ($(t_{te}/o)_s$&r_{ht_3}), stator TE thickness to opening ratio and rotor exit hub-to-tip ratio ($(t_{te}/o)_s$&r_{ht_6}) and rotor TE thickness to opening ratio and stator exit hub-to-tip ratio ($(te/o)_r$&r_{ht_3}) respectively.

The behaviour of the curves suggests that while an optimization of r_{ht_3} and r_{ht_6} is necessary to know which turbine design provides the best performance — since it is very complex to carry out a detailed analysis by studying the different interactions one by one —, both, stator and rotor trailing edge thickness to opening ratios can be set to their lower bound since this value will provide the best efficiency.

As has been said, the rest of the significant factors have been analyzed but no further graphs will be introduced as they do not provide new information and the aim is to avoid making the section longer than necessary. These figures can be found in the appendix mentioned above.

As with the rotor aspect ratio, it has been observed that the stator aspect ratio has the same tendency on the efficiency value, and therefore it would not be wrong to set it fixed in its upper boundary condition, knowing that this variable cannot be increased infinitely either, as although it limits secondary losses, it favours profile losses.

On the other hand, when analyzing the stator inlet hub-to-tip ratio, there are warnings of invalid values found, which suggest the student to take this factor into consideration,

even though the interaction effects are practically negligible. It can be seen in the graph presented in Section 3.2.2 that the efficiency is practically constant when this factor is varied, but falls sharply after a certain value.

As far as the stator inlet methal angle is concerned, only two interaction effects are significant, those with the exit hub-to-tip ratios of the stator and rotor. After analyzing them, it was found that there is little variation in efficiency above a certain value of this angle, although it is the other two factors that contribute to the significance of the interaction. However, θ_1 will be taken into account for the optimization.

A final comment regarding the factors that were not significant, and another factor that, although it had a significant main effect, did not have a significant interaction. Starting with the rotor inlet methal angle, which has a non-significant main effect, but has significant interaction effects with the rotor exit hub-to-tip ratio, stator exit hub-to-tip ratio and specific diameter. It has shown to have a small influence on the efficiency, but slightly different trends are followed depending on the factor it is interacting with. For this reason, despite its non-significance it will be considered for the optimization.

Finally, the two remaining factors are the stator and rotor blade solidities. While the first shows a significant main effect, the second does not. If they are further investigated, it can be seen that any of them present significant interaction effects. It was explained above, in the wide sensitivity analysis discussion, that this factor is not of critical importance in the turbine design, but it has to be taken into account since there is an optimum point for which profile losses are reduced and efficiency enhanced. Thereby, blade solidity has an important influence on incidence losses, which have to be cautiously considered at the stator inlet.

It is important to note that the graphs used to facilitate the analysis of the experimental results cover a much wider design space than the one studied in the local sensitivity analysis. In addition to facilitating the understanding of the possible reasons that have led to the results obtained, they have allowed to verify in some way that the experiment carried out is quite adequate.

Concerning the accuracy of the results, the verification was extended by means of the Python script created to check the tolerance that the model is using to provide them. The complete previous analysis was made after checking that indeed, the tolerance used by the model is much smaller than the tolerance set to accept the results, with an order of magnitude of 10^{-11}. Unlike the results provided in the wider design space SA, those presented above can be better relied upon, as there appears to be no uncertainty.

4.3.1 Limitations in the model for further experiments and independent analysis for the remaining factors

All the analysis carried out so far seems to suggest that the model used as a design tool makes sense. However, it is clear from the extensive analysis that the results are sensitive to the factors introduced and it is possible that the results would change if all the factors selected for the study had been introduced. As in the previous case, the 14-factor experiment is the last one that could be carried out due to limitations in the model.

After several attempts and combinations of factors, it has been found that the model fails when combining θ_3 and θ_6 with r_{ht_3} and r_{ht_6}. The reasons for this are unknown. Different warnings appear on the console as the experiment is running. They refer to invalid values found in the equations of state that result in an non-physical solution and therefore lead the experiment to failure.

In order to give some completeness to the analysis carried out in the previous subsection, it has been decided to examine the significance of the two remaining factors in smaller experiments. Before proceeding, however, the effect of the variation of these factors on efficiency was studied and can be seen in Figure 4.9.

From the figure it can be seen that both factors show some curvature, however, it should be remembered that angles greater than 80° in absolute value are not recommended for blade design. Thus, θ_3 has a more or less linear character, and θ_6 still has some curvature.

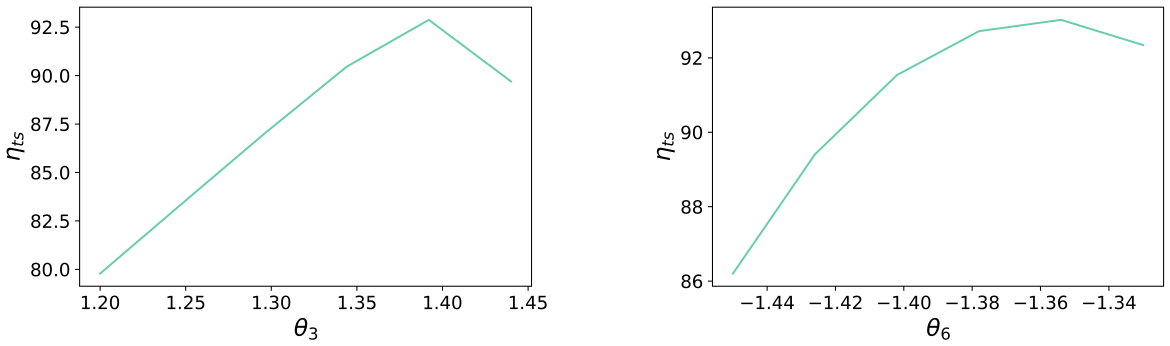

(a) Total to static efficiency vs. stator exit methal angle (θ_3)

(b) Total to static efficiency vs. rotor exit methal angle (θ_6)

Figure 4.9: Deeper analysis of the remaining factors

Having seen how the variation of each factor affects efficiency, the following experiments have been carried out, with the same boundary conditions as for the local sensitivity analysis (with 5% variation), in order to understand their significance:

- **Five factors: θ_3, θ_6, Ω_{spe}, d_{spe} and p_6**

  From this experiment it was seen that only θ_6 and p_6 had significant main effects, θ_3 a significant quadratic effect, and significant interactions between θ_3&θ_6, θ_3&p_6 and θ_6&p_6. The results for the efficiencies were provided with a tolerance of the order of 10^{-8}.

  This experiment was then extended to study individually θ_3 and θ_6 by adding the inlet methal angles.

- **Six factors: θ_1, θ_3, θ_4, Ω_{spe}, d_{spe} and p_6**

From this experiment it was seen that the fact of removing θ_6 and introducing the inlet methal angles made θ_3, d_{spe} and Ω_{spe} significant, while p_6 continued to be significant. As for the previous experiment, θ_3 presented a significant quadratic effect. As expected, significant interaction effects were seen between θ_3 and the other significant factors. The results for this experiment were also provided with a tolerance of the order of 10^{-8}.

- **Six factors: θ_1, θ_4, θ_6, Ω_{spe}, d_{spe} and p_6**

  When on the contrary θ_6 is independently analyzed, it can be seen that with a tolerance of 10^{-11}, θ_6, d_{spe}, Ω_{spe} and p_6 had significant main effects, θ_6 also a significant quadratic effect and significant interaction effects with the other relevant factors.

- **Seven factors: θ_1, θ_3, θ_4, θ_6, Ω_{spe}, d_{spe} and p_6**

  However, when θ_3 was added to the previous experiment in order to analyze all the angles together with the other 3 factors, the results were being provided with a tolerance of the order of 10^{-1} — not acceptable from the condition set to rely on the results—, and warnings of invalid values encountered appeared in the console.

  The factors that showed a significant main effect were θ_3, θ_6 and p_6. Significant interaction effects were seen between θ_3&θ_6, θ_3&p_6 and θ_6&p_6. Only θ_3 showed a significant quadratic effect.

Even though it is believed that both, θ_3 and θ_6 would have had a significant effect on the efficiency and the results from the last experiment are in accordance, they cannot be trusted. For this reason a last set of experiments was carried out. This set is characterized by varying all the design variables 5% of their value to set their lower and upper bounds, except for θ_3, that is only going to be varied 1% of its value. The set comprises the following experiments:

- **Five factors: θ_3, θ_6, Ω_{spe}, d_{spe} and p_6**

  By reducing the design space of θ_3, the results are now being provided with a tolerance of 10^{-11}. Regarding the significance of the effects it is found that now θ_3 also presents a significant main effect, as well as θ_6 and p_6 as seen from the experiment above. However, θ_3 does no longer show a significant quadratic effect, presenting it θ_6 instead. The interaction effects that prove to be significant are: θ_3&θ_6, and θ_6 combined with all the other factors.

- **Seven factors: θ_1, θ_3, θ_4, θ_6, Ω_{spe}, d_{spe} and p_6**

  The following experiment directly studied the same 7 factors that led to uncertain results in the previous set of experiments. By narrowing θ_3's design space it is seen that θ_3, θ_6, d_{spe}, Ω_{spe} and p_6 present a significant main effect. Only θ_6 shows to have a significant quadratic effect and both, θ_3 and θ_6 present significant interaction effects with d_{spe}, Ω_{spe}, p_6 and with each other. The results in this experiment are provided with a tolerance of 10^{-8}.

From this experiment it would be possible to draw with greater certainty the conclusions that could not be drawn from the experiment in the previous set. However, it would be interesting to see how the significance of the factors varies when the other factors are introduced. For this purpose, the following two 9-factor experiments have been carried out.

- **Nine factors:** BS_s, BS_r, AR_s, AR_r, θ_3, θ_6, Ω_{spe}, d_{spe} **and** p_6

  First, the blades' solidity and aspect ratios are being added to the 5-factors experiment. The results are given with a tolerance of 10^{-11}. It can be seen that AR_r, θ_3, θ_6, Ω_{spe}, d_{spe} and p_6 present significant main effects. As for the previous experiment, only θ_6 has a significant quadratic effect and both θ_3 and θ_6 present the same significant interaction effects as before.

- **Nine factors:** r_{ht_1}, r_{ht_3}, r_{ht_4}, r_{ht_6}, θ_3, θ_6, Ω_{spe}, d_{spe} **and** p_6

  It is when the inlet and exit hub-to-tip aspect ratios are combined with θ_3 and θ_6 that the model starts to fail, as it was said above.

  From this experiment it is seen that only θ_6 has a significant main and quadratic effect, and presents a significant interaction effect with r_{ht_3}, r_{ht_6}, p_6 and θ_3. The latter also presents some significant interaction effects. These results have no longer sense. While carrying out the experiments warnings of invalid encountered values were shown, and the tolerance that the model is using to provide the results is of 10^{-1}.

- **Ten factors:** AR_r, r_{ht_3}, r_{ht_6}, $(te/o)_s$, $(te/o)_r$, θ_3, θ_6, Ω_{spe}, d_{spe} **and** p_6

  Finally, the last experiment was carried out by analizing together the factors that were believed to be problematic. Surprisingly, the tolerance of the results is of the order of 10^{-10}, but non-physical values of efficiency were found among them. Having negative values of efficiency avoids relying on the provided results since they will be strongly influenced by these atypical values. The factors with significant main effects from this experiment are θ_3, θ_6, Ω_{spe} and d_{spe}.

The problem that leads the model to fail when combining all the factors in the same experiment has not been found. At first it was believed that the main reason for it was the wide design space, but the problem remains even with a really small one. The small design space has, however, proven to facilitate the model finding coherent and reliable solutions among the non-problematic factors. For this reason, the principal interaction effects obtained in almost all of the experiments presented so far within this particular analysis have been plotted in order to check the accuracy of the design. These are θ_3&θ_6, shown in Figure 4.10; θ_3&d_{spe}, shown in Figure 4.11 (a); θ_6&d_{spe}, shown in Figure 4.12 (a); θ_3&r_{ht_3}, in Figure 4.11 (b); θ_3&r_{ht_6}, in Figure 4.11 (c); θ_6&r_{ht_3}, in Figure 4.12 (b) and finally θ_6&r_{ht_6}, in Figure 4.12 (c).

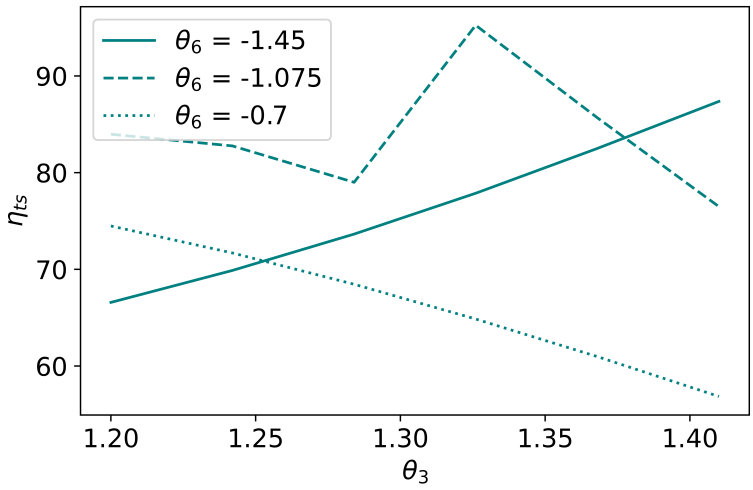

Figure 4.10: Interaction effect between stator and rotor exit methal angles (θ_3&θ_6).

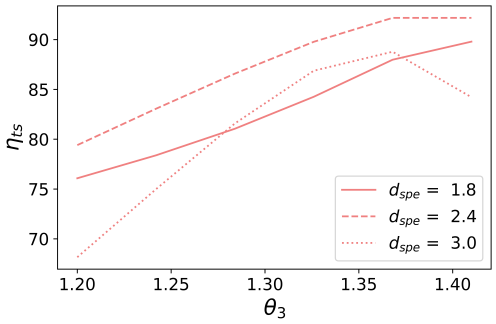

(a) Interaction effect between stator exit methal angle and specific diameter (θ_3&d_{spe}).

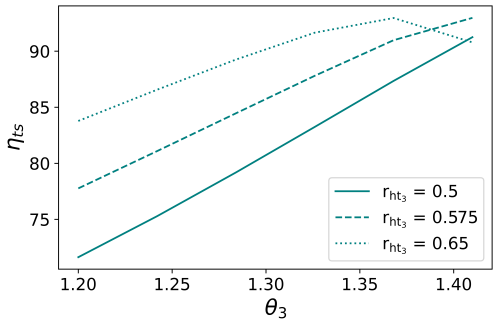

(b) Interaction effect between stator exit methal angle and stator exit hub-to-tip ratio (θ_3&r_{ht_3}).

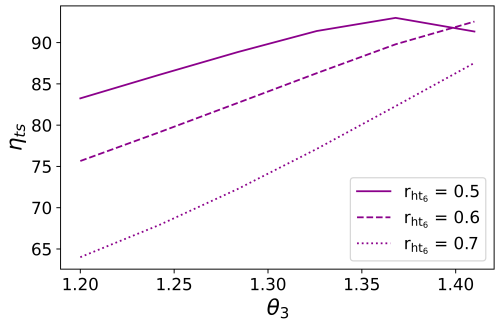

(c) Interaction effect between stator exit methal angle and rotor exit hub-to-tip ratio (θ_3&r_{ht_6}).

Figure 4.11: Principal interaction effects of the stator exit methal angle (θ_3)

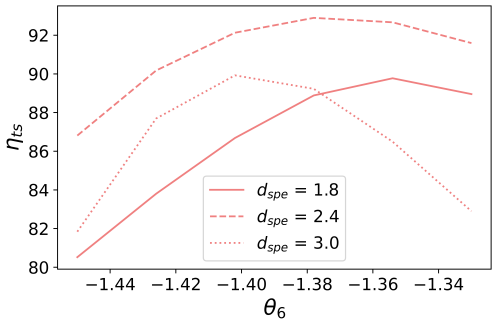

(a) Interaction effect between rotor exit methal angle and specific diameter (θ_6&d_{spe}).

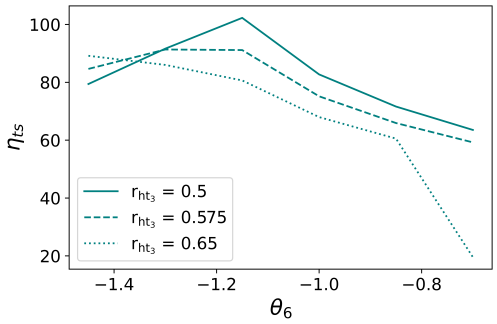

(b) Interaction effect between rotor exit methal angle and stator exit hub-to-tip ratio (θ_6&r_{ht_3}).

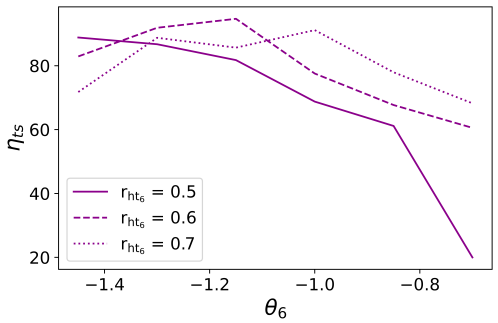

(c) Interaction effect between rotor exit methal angle and rotor exit hub-to-tip ratio (θ_6&r_{ht_6}).

Figure 4.12: Principal interaction effects of the rotor exit methal angle (θ_6)

As expected, both factors seem relevant to the response variable, thereby, they will be considered in the optimization.

4.3.2 Further comments

A final comment before turning to the last section of the results should be made on the validity of the technique used to obtain the coefficients on which the analysis is being performed, linear multiple regression. This model can be used to analyze the selected design of experiments technique, with caution, although it is not the ideal regression model to use.

It is necessary to remember that the design of experiments technique chosen to carry out the present study, face-centred central composite design, had a disadvantage compared to the multiple advantages for which it was chosen. It is a non-rotatable design, so the variance of the response variable, i.e. efficiency, is not constant at the same distance from the centre point. While this is not a critical problem for the present analysis since the regression model is being used to obtain the coefficients rather than to predict efficiency, the fact that it is non-rotatable means that there is minimal uncertainty in the assignment of the coefficients that must be taken into account when making decisions and drawing

conclusions.

After a careful literature review, it was found that there are more appropriate regression models to analyze the DOE technique used, namely Ridge regression. The reason why this technique could not be used is because it requires a cross validation to choose the value of the penalty factor that accounts for noise in the results — due to the fact that a non-rotatable design is being used—, and that better predicts output with the data being used to validate it.

On the other hand, the reason why the mean-line model proposed as design tool in the present work could not be validated is precisely the lack of database and technical means to carry out the validation.

This Ridge regression model has been implemented by establishing two different penalty coefficients, one of the order of unity and the other of the order of one tenth, with the penalty in the first case being stronger. Since it was not possible to carry out cross validation, the analysis carried out lacks any rigour and is therefore only briefly discussed here. The coefficients obtained with each of the two penalty factors have been compared with the coefficients of the local sensitivity analysis presented above, and it has been observed that the coefficients of the main and interaction effects are practically identical for the three cases studied, although they differ slightly for the quadratic effects. The quadratic coefficients provided by the Ridge regression are different from those of the local SA but are contained within the calculated 95% confidence interval. Thus, one can be fairly confident that all the discussion elaborated so far, while it may be subject to uncertainty, does not appear to be entirely incorrect. Nevertheless, it is recommended not to definitely discard any of the factors for turbine design. In the following, the results obtained from the optimization before and after the sensitivity analysis will be compared.

4.4 Comparison between the optimization results before and after the sensitivity analysis

This last section contains the results of the comparison between the optimization before and after the recently presented local sensitivity analysis. The following table (Table 4.16) summarizes the conditions under which the optimization post-SA has been performed.

Table 4.16: Conditions for optimization post-SA.

Factor	Resolution	Factor	Resolution
Ω_{spe}	Same bounds as before	$(t_{te}/o)_s$	Not included, fixed and set to lower bound
BS_s	Same bounds as before	$(t_{te}/o)_r$	Not included, fixed and set to lower bound
BS_r	Same bounds as before	d_{spe}	Same bounds as before
AR_s	Not included, fixed and set to upper bound	θ_1 [rad]	Same bounds as before
AR_r	Not included, fixed and set to upper bound	θ_3 [rad]	Same bounds as before
r_{ht_1}	Same bounds as before	θ_4 [rad]	Same bounds as before
r_{ht_3}	Same bounds as before	θ_6 [rad]	Same bounds as before
r_{ht_4}	Same bounds as before	$(le/s)_s$	Not included, fixed and set to upper bound
r_{ht_6}	Same bounds as before	$(le/s)_r$	Not included, fixed and set to upper bound
$(We)_s$ [rad]	Not included, fixed and set to upper bound	We_r [rad]	Not included, fixed and set to upper bound

These boundary conditions mentioned in the table above were presented in Section 3.1.4 in Methodology in Table 3.7, as well as the case study used (Table 3.8, Table 3.9 and Table 3.10). In order to see how the decisions made have an impact on efficiency, the above-mentioned bar-chart will be used for both the case study (shown in Figure 4.13) and the optimal turbine pre- and post- sensitivity analysis to see if there has been any considerable variation in losses. The optimal pre-SA turbine is shown in Table 4.18 and the associated losses in Figure 4.14 while the post-SA optimal turbine is given in Table 4.20 and the associated losses in Figure 4.15.

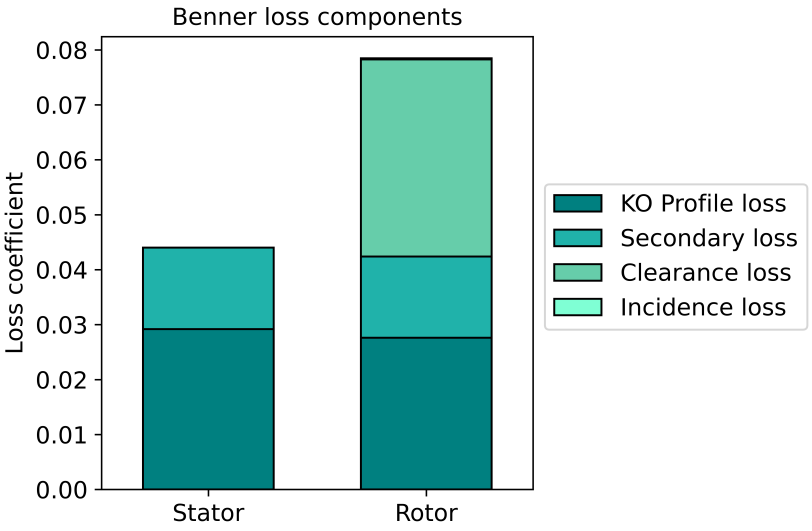

Figure 4.13: Loss breakdown for the case study with the Benner loss model

From Figure 4.13 it can be seen that losses in the rotor almost double the losses in the stator, which are divided into profile (and trailing edge) and secondary losses. The main difference between the losses in stator and rotor is due to the tip clearance component, which is quite big. However profile and secondary losses are slightly higher for the stator than for the rotor. On the other hand, no incidence losses are found in the stator, while an almost negligible incidence component can be found in the rotor. The value for each of these coefficients is gathered in Table 4.17.

Table 4.17: Loss components in case study with the Benner loss model.

Loss component	Stator	Rotor
$Y_{p,KO}$	0.0292	0.0276
Y_{sec}	0.0148	0.0147
Y_{cl}	0.0	0.0359
Y_{inc}	0.0	0.0002

The optimal turbine previous to the sensitivity analysis is shown below in Figure 4.18.

Table 4.18: Optimal turbine pre-SA: design variables and velocity triangles.

Factor	Lower Bound	Value	Upper Bound	Bounds reached
Ω_{spe}	0.100000	0.193115	10.0000	False
BS_s	0.900000	1.671415	3.500000	False
BS_r	0.900000	1.653265	3.500000	False
AR_s	1.000000	2.000000	2.000000	True
AR_r	1.000000	2.000000	2.000000	True
r_{ht_1}	0.500000	0.835881	0.900000	False
r_{ht_3}	0.500000	0.646324	0.900000	False
r_{ht_4}	0.500000	0.500000	0.900000	True
r_{ht6}	0.500000	0.500000	0.900000	True
$(t_{te}/o)_s$	0.050000	0.050000	0.400000	True
$(t_{te}/o)_r$	0.050000	0.050000	0.400000	True
d_{spe}	0.100000	10.0000	10.0000	True
θ_1 [°]	-15	-6.42	15	False
θ_3 [°]	40	80	80	True
θ_4 [°]	-15	0	15	False
θ_6 [°]	-80	-80	-40	True
$(le/s)_s$	0.030000	0.300000	0.300000	True
$(le/s)_r$	0.030000	0.300000	0.300000	True
We_s [°]	0	20	20	True
We_r [°]	0	20	20	True
v_1	0.010000	0.200000	0.200000	True
v_2	0.300000	0.721698	0.900000	False
v_3	0.300000	0.721698	0.900000	False
a_3 [°]	40	80	80	True
w_5	0.400000	0.679859	0.900000	False
w_6	0.400000	0.679859	0.900000	False
b_6 [°]	-80	-80	-40	True
p_2	0.400000	0.642807	0.900000	False
p_3	0.400000	0.642807	0.900000	False
p_5	0.300000	0.437845	0.800000	False

With a total of 95 iterations and after 71.4 seconds, the optimization was completed successfully. The results are given in the shaded column above. The last column indicates whether the bounds are being reached or not. This was also used to set the post-SA optimization together with the SA results.

In the same way as for the case study, the different loss components of the optimal turbine have been plotted in the figure below.

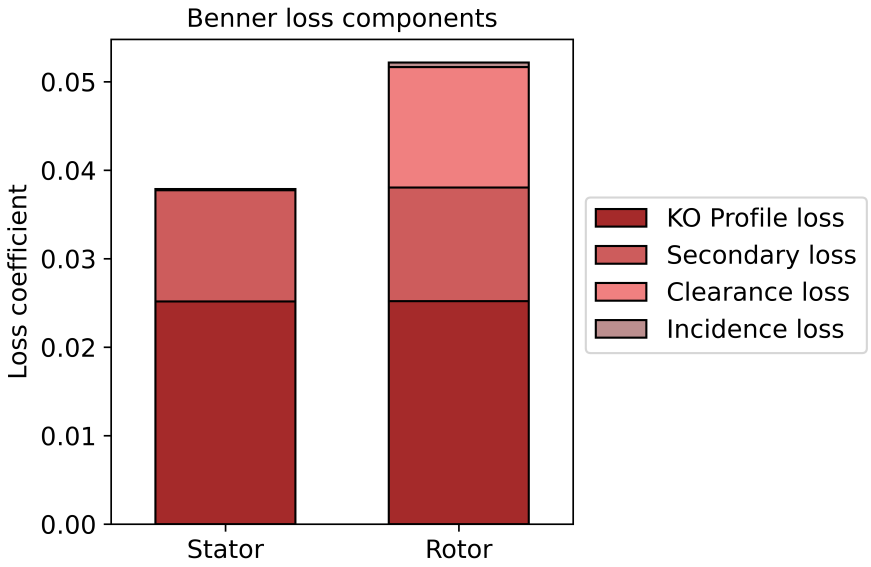

Figure 4.14: Loss breakdown for the optimal turbine with the Benner loss model before SA

From Figure 4.14 it can be seen that both total loss coefficients (stator and rotor) have decreased by optimizing the turbine efficiency, as expected. As before, both stator and rotor have practically the same profile and secondary loss components, with tip clearance losses (non-existent in the stator) making the difference. However, in this case, a negligible component of incidence losses can be seen in the stator, which is slightly higher than in the case study turbine, in the rotor. The values of the different components are presented in Table 4.19.

Table 4.19: Loss components in optimal pre-SA turbine with the Benner loss model.

Loss component	Stator	Rotor
$Y_{p,KO}$	0.0252	0.0252
Y_{sec}	0.0126	0.0129
Y_{cl}	0.0	0.0136
Y_{inc}	0.0001	0.0005

Finally, the optimal turbine after the sensitivity analysis has been presented in Table 4.20, shaded in grey as in the previous case. An interesting first comment is that despite the introduction of 8 fewer factors in the optimization, a total of 161 iterations and 95 seconds were required to complete it successfully.

Table 4.20: Optimal turbine post-SA: design variables and velocity triangles.

Factor	Lower Bound	Value	Upper Bound	Bounds reached
Ω_{spe}	0.100000	0.188243	10.0000	False
BS_s	0.900000	1.561704	3.500000	False
BS_r	0.900000	1.647759	3.500000	False
AR_s	—	2.0	—	Fixed
AR_r	—	2.0	—	Fixed
r_{ht_1}	0.500000	0.500000	0.900000	True
r_{ht_3}	0.500000	0.719080	0.900000	False
r_{ht_4}	0.500000	0.500000	0.900000	True
r_{ht_6}	0.500000	0.500000	0.900000	True
$(t_{te}/o)_s$	—	0.05	—	Fixed
$(t_{te}/o)_r$	—	0.05	—	Fixed
d_{spe}	0.100000	10.000000	10.0000	True
θ_1 [°]	-15	-4.12	15	False
θ_3 [°]	40	77.22	80	False
θ_4 [°]	-15	0.41	15	False
θ_6 [°]	-80	-80	-40	True
$(le/s)_s$	—	0.3	—	Fixed
$(le/s)_r$	—	0.3	—	Fixed
We_s [°]	—	20	—	Fixed
We_r [°]	—	20	—	Fixed
v_1	0.010000	0.050568	0.200000	False
v_2	0.300000	0.748699	0.900000	False
v_3	0.300000	0.748699	0.900000	False
a_3[°]	40	77.22	80	False
w_5	0.400000	0.661139	0.900000	False
w_6	0.400000	0.661139	0.900000	False
b_6 [°]	-80	-80	-40	True
p_2	0.400000	0.621687	0.900000	False
p_3	0.400000	0.621687	0.900000	False
p_5	0.300000	0.437845	0.800000	False

The coefficients of the different loss components have also been calculated for this optimal post-SA turbine, and presented in Table 4.21.

Table 4.21: Loss components in optimal post-SA turbine with the Benner loss model.

Loss component	Stator	Rotor
$Y_{p,KO}$	0.0236	0.0251
Y_{sec}	0.0142	0.0134
Y_{cl}	0.0	0.014
Y_{inc}	0.0001	0.0013

The same bar chart has also been created and presented below.

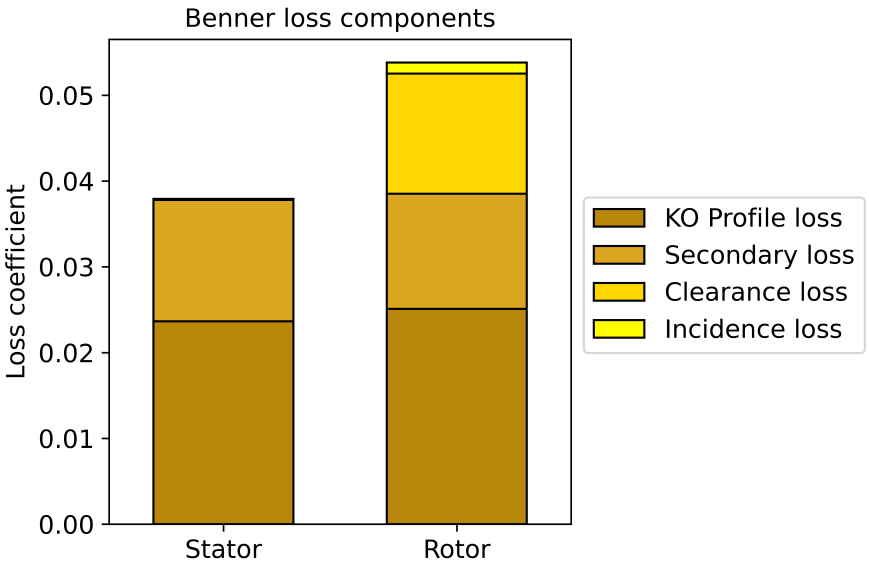

Figure 4.15: Loss breakdown for the optimal turbine with the Benner loss model after SA

From both Table 4.21 and Figure 4.15 it can be seen that as for the previous cases, stator and rotor profile and secondary loss coefficients are practically the same. While profile losses are smaller in the stator than in the rotor, secondary losses seem to be slightly higher in the former than in the latter. It can also be seen that the post-SA turbine has led to lower profile losses than in the pre-SA turbine, but higher secondary losses instead. Regarding tip clearance losses, these have also slightly increased compared to the previous turbine, as well as the incidence loss coefficient.

It can be seen that while the loss coefficient for the stator has remained the same from one turbine to the next, that of the rotor has increased slightly, so that the optimization carried out on the basis of the conclusions of the SA has not resulted in a better turbine, nor has it been executed more efficiently, as it has required more iterations and therefore more time than the previous one.

5 Conclusions

This section will present the conclusions derived from the thesis and results discussion as well as the next steps to be taken in a more in-depth study.

5.1 Conclusions from the sensitivity analyses

Some general conclusions can be drawn from the different carried out analyses:

1. The experiments results depend on the number and selection of the considered factors, as increasing the number of factors yields in a larger number of significant main and interaction effects, and these interactions are more or less important depending on the factors being introduced into the study, which in turn will affect the importance of the main effects.
2. The bounds selected to define the experiment design space do not only have a strong influence on the factor's significance and effect on the output, but also on the results being provided by the mean-line model for this output variable. Given that the technique employed for carrying out the experiments (CCF) by definition reaches these selected bounds, a good and robust model must be provided in order to handle them correctly. The smaller the design space the better the model provides results for the total to static efficiency and the more reliable the results obtained for the coefficients.
3. Despite the significance of the factors revealed by the experiments, none of them should be discarded when designing an axial turbine, since it was seen from the pre-sensitivity analysis optimization that except for those parameters that showed a clear trend, the others presented an optimal value within the bounds foreseen for the optimization.

In the following, the concrete findings for each of the analyses that have led to these general conclusions will be presented.

5.1.1 Conclusions from the wide SA

1. The bounds used for this wide sensitivity analysis require a robustness of the model that has not been achieved as the results for the efficiency are being provided — for some runs—, with an error larger than what has been established to be considered acceptable. For this reason, the results from this sensitivity analysis are not reliable as they are subject to uncertainty, meaning that non-physical values of the different thermodynamic variables may be the ones leading to these non-reliable efficiency results.

2. Exit stator and rotor hub-to-tip ratios (r_{ht_3} and r_{ht_6}) as well as rotor aspect ratio (AR_r) have proven to be significant — presenting the greatest main effects—, for all the performed experiments regardless of the factors being considered, while stator blade solidity (BS_S) and stator aspect ratio (AR_s) have resulted not significant.

3. Stator inlet hub-to-tip ratio (r_{ht_1}) has been found to be very sensitive to the factors considered in the experiment, as its main effect became significant when static pressure (p_6) was included, then became non-significant again when trailing edge thickness to opening ratios ($(t_{te}/o)_s$ and $(t_{te}/o)_r$) were added to the previous experiment, and finally became significant again when specific diameter (d_{spe}) and inlet methal angles (θ_1 and θ_4) were introduced.

4. Introducing both trailing edge thickness to opening ratios ($(t_{te}/o)_s$ and $(t_{te}/o)_r$) seems to first cause the model to find invalid values for thermodynamic variables during the experiment execution, leading to the non-reliability of the results mentioned in conclusion 1.

5. The experiment is not capturing the quadratic effects that had been noticed after the first non-rigorous factorial analysis for the factors selection, meaning that improvements have to be done in order to obtain better results.

6. Slightly reducing the design space has shown an effect on the results provided for the efficiency — resulting higher efficiencies for a narrower design space of the problematic variables—, but has shown no effect on the reliability of the results, since they are still being provided with a larger error than the one established. No big effect has been found on the factors significance by slightly reducing the design space, except for the variable mentioned in conclusion 2.

5.1.2 Conclusions from the local SA

1. The model seems to be robust enough to provide good and reliable results when the bounds are being reduced to examine the surroundings of the case study used for carrying out the experiments. This results are being provided with an error that is much smaller than the one set to accept them.

2. The experiment captures the significant quadratic and interaction effects that had been found in the non-rigorous first factorial analysis, meaning together with conclusion 1 that the mean-line model proposed and used as a design tool makes sense. This further demonstrates the ability of sensitivity analysis to facilitate understanding of how the model works.

3. Slight differences in the results obtained are expected since not all the factors could be analyzed in the same experiment due to limitations in the model, and those that could not be included (θ_3 and θ_6) have proven to be significant in an independent study conducted through two different set of experiments.

4. Stator exit hub-to-tip ratio (r_{ht_3}), specific diameter (d_{spe}) and static pressure (p_6) show to have the most important significant main effects. Despite the strong interaction and main effects seen for the rotor exit hub-to-tip ratio (r_{ht_6}), two other

factors seem to have a greater main effect. These are rotor aspect ratio (AR_r) and rotor inlet hub-to-tip ratio (r_{ht_4}).

5. Stator and rotor aspect ratios (AR_s and AR_r) have proven to always provide the best efficiency at their upper bound, regardless of the factor they are interacting with.

6. Stator and rotor trailing edge thickness to opening ratios ($(t_{te}/o)_s$ and $(t_{te}/o)_r$) have proven to always provide the best efficiency at their lower bound, regardless of the factor they are interacting with.

5.2 Conclusions from the comparison of optimizations

1. Reducing the design space of the optimization by fixing the parameters that had been found not to play an important role in the search for the optimal solution does not necessarily result in a more efficient optimization. The reason that more iterations and thus more time are needed to achieve this optimal solution may be the type of algorithm being used, gradient-based.

2. The fact of using this gradient-based optimization algorithm has also led to find a different optimal point even though the fixed parameters were given the same values that they had reached in the pre-sensitivity analysis optimization.

5.3 Conclusions from the mean-line model and validity of the techniques being used

1. The mean-line model provided as a preliminary design tool for one-stage axial turbines has shown to make sense even though it has not been validated, but presents some limitations which have disabled carrying out a complete experiment to understand how the design variables affect the output. This is linked to the lack of robustness for considering a wide design space, but the reason why it fails is unknown when a rather small design space is being studied. Limitations arose when the exit methal angles were studied together with the exit hub-to-tip ratios.

2. Regarding the different techniques being used in the thesis, addressing the sensitivity analysis by means of a design of experiments technique rather than by using the popular practice of the one-at-a-time analysis, is an appropriate method that meets the thesis requirements and provides the results in a considerably short time, as the face-centered central composite design — based on statistical theory—, estimates main, interaction and quadratic effects while the OAT is not able to detect interactions between factors. A similar conclusion is provided by Andrea Saltelli and Paola Annoni [55], who after presenting some examples and a case study demonstrating OAT inadequacy, propose both DOE techniques and regression models as a better alternative to carry out a sensitivity analysis.

3. Even though it is a common approach to estimate second order models, the regression model that has been used for analyzing the experimental results (multiple linear

regression) is not the most appropriate method for non-rotatable designs. However, it has been seen by means of a non-rigorous analysis that the results provided by the MLR seem to be acceptable, specially for the main and interaction effects. Nevertheless, this is a topic that could be explored further and will be discussed below in Section 5.5.

5.4 Evaluation of objectives

1. A deep and broad literature review was carried out on preliminary design of axial turbines, flow and losses in a turbine stage, off-design operation and loss model correlations. All the information that has been collected has been presented in Section 2 in such a way that the reader is being guided through the thesis, from the current energy trends to the DOE techniques that can be used in order to perform a statistical-based sensitivity analysis of the mean-line model used. A complete literature review on sensitivity analysis and these design of experiments techniques has also been carried out.

2. The loss model to be used for the present work — the Benner loss model—, selected after carrying out the aforementioned detailed literature review on loss correlations, had already been implemented in Pyhton by Lasse B. Andersson, already validated by the authors. Lack of cascade database in the open literature have disabled a study case reproduction.

3. For the same reason, as the principal limitation of the thesis work, the mean-line model validation could not be carried out due to the lack of information and tests in the open literature for ORC blades, as well as a delay in the availability of the department's test rig.

4. A set of sensitivity analyses has been carried out in Python by means of a Design of Experiments technique and regression model, in order to check if the mean-line model proposed as a tool for preliminary design of axial turbines provides reasonable results, to understand if the model makes sense and to try to improve the optimization mode after studying the effects of the different design variables over the response variable, the total to static efficiency. Not only the best sensitivity analysis has been presented, but also the ones that gave not reliable results and led to perform the former. However, these sensitivity analyses could not include all the selected factors due to limitations found in the model.

5. From the results of the local sensitivity analysis, a comparison between optimizations has been done in order to confirm a set of hypotheses posed for the purpose.

5.5 Further work

In the next, some future outlines derived from this Master's Thesis work are presented:

1. First, the validation of the model should be implemented as soon as the test rig is available and real experiments can be carried out, as the Benner loss model is not necessarily accurate for ORC blades since it is a cascade test-based model.

2. Another study line once a cascade database is available, could be employing the Ridge regression to analyze the results provided by the non-rotatable design obtained form implementing the Face-centered central composite design. A cross-validation must be done in order to account for the penalty factor appropriately, and with that, results should not be subject to any uncertainty.

3. Changing the DOE technique for another that does not present this drawback due to the rotatabilty could also be done, especially if more resources, e.g. computational, are available, in order to study all the factors selected for the analysis as a whole and to check whether the limitations found in the model with the chosen DOE technique really exist.

4. From the results presented in this Thesis, some of the factors that have been found to be significant can be selected and studied in depth, since due to the limited time available to carry out this work, it was only possible to see the overall impact, which was the objective.

Bibliography

[1] Meroni, Andrea La Seta, Angelo Andreasen, Jesper Pierobon, Leonardo Persico, Giacomo Haglind, Fredrik. (2016). Combined Turbine and Cycle Optimization for Organic Rankine Cycle Power Systems—Part A: Turbine Model. Energies. 9. 313. 10.3390/en9050313.

[2] ENERDATA. (2022). Global Energy & Climate Trends- Consolidated 2021 energy and climate statistics, and projections to 2030:36-37.

[3] bp (2022). bp Statistical Review of World Energy. 71st Edition, pp. 2,5,10.

[4] REN21- Renewables Now. (2022). Renewables 2022. Global Status Report.

[5] Sudharshan Reddy Paramati, U. S. (2022). The role of environmental technology for energy demand and energy efficiency: Evidence from OECD countries. Renewable and Sustainable Energy Reviews, 153, p. 111735.

[6] Hussam Jouhara, N. K. (2018). Waste heat recovery technologies and applications. Thermal Science and Engineering Progress, Volume 6, pp. 268-289.

[7] SINTEF. (n.d.). Energy efficiency in the industry. Research area.

[8] Agromayor, R. (2017). Turbomachinery design for Rankine cycles in waste heat recovery applications. NTNU- Norwegian University of Science and Technology, Trondheim, Norway.

[9] Colonna, P., Casati, E., Trapp, C., Mathijssen, T., Larjola, J., Turunen-Saaresti, T., Uusitalo, A., (2015). Organic Rankine Cycle Power Systems: From the Concept to Current Technology, Applications, and an Outlook to the Future. Journal of Engineering for Gas Turbines and Power 137 (10), 100801.

[10] Li, C., Wang, H., (2016). Power cycles for waste heat recovery from medium to high temperature flue gas sources from a view of thermodynamic optimization. Applied Energy 180, 707–721.

[11] Combined Heat and Power (CHP) Partnership - EPA. (2022, April). Waste heat to power systems.

[12] J.W. Lund. (2012). 7.05 - Direct Heat Utilization of Geothermal Energy. Comprehensive Renewable Energy, Elsevier. Pages 171-188.

[13] Zach, F., Erker, S. & Stoeglehner, G. (2019). Factors influencing the environmental and economic feasibility of district heating systems—a perspective from integrated spatial and energy planning. Energy, Sustainability and Society 9, 25. https://doi.org/10.1186/s13705-019-0202-7

[14] Heat Calc: Heat Recovery. Retrieved from https://heatcalc.com/heat-recovery

[15] Heat Calc: Electricity Generation from Heat. Retrieved from https://heatcalc.com/heat-to-powertechnologies

[16] Hussam Jouhara, N. K. (2018). Waste heat recovery technologies and applications. Thermal Science and Engineering Progress, Volume 6, pp. 268-289. Retrieved from https://www.sciencedirect.com/science/article/pii/S2451904918300015

[17] E. Macchi and M. Astolfi. (2016). Organic Rankine Cycle (ORC) Power Systems: Technologies and Applications. Woodhead Publising, 1st edition.

[18] Encabo Cáceres, Inés. (2018). Techno-economic and thermodynamic optimization of Rankine cycles. NTNU, Trondheim

[19] M.E Barbosa. (2018). Análisis del Ciclo de Rankine Orgánico Ideal mediante 8 Fluidos Orgánicos de Trabajo

[20] S. Quoilin. (2011). Sustainable Energy Conversion Through the Use of Organic Rankine Cycles for Waste Heat Recovery and Solar Applications. PhD thesis, University of Liege.

[21] Dixon, S.L. (2001) Fluid Mechanics and Thermodynamics of Turbomachinery. 5th Edition, Pergamon, UK.

[22] Gambini, M., Vellini, M. (2021). Preliminary Design of Axial Flow Turbines. In: Turbomachinery. Springer Tracts in Mechanical Engineering. Springer, Cham.

[23] Llera-Sastresa, E. &. (2020). Turbomáquinas Térmicas. Zaragoza.

[24] Moran, M.J. et al. (2015). Principles of Engineering Thermodynamics. Wiley. ISBN: 978-1-118-96088-2.

[25] Denton, JD. (1993). "Loss Mechanisms in Turbomachines." Proceedings of the ASME 1993 International Gas Turbine and Aeroengine Congress and Exposition. Volume 2: Combustion and Fuels; Oil and Gas Applications; Cycle Innovations; Heat Transfer; Electric Power; Industrial and Cogeneration; Ceramics; Structures and Dynamics; Controls, Diagnostics and Instrumentation; IGTI Scholar Award. Cincinnati, Ohio, USA. V002T14A001. ASME.

[26] N. Baines. (2019). Turbine Design and Analysis. Flow in a turbine blade passage, 38-57.

[27] N. Baines. (2019). Turbine Design and Analysis. Preliminary Design, 83-105.

[28] Lasse B. Anderson, R. A. (2022). Method for mean-line design and performance prediction of one-stage axial turbines. NTNU- Norwegian University of Science and Technology, Trondheim, Norway.

[29] Mr. Haftamu Menker Gebre Yohannes. (2019). Why is Mathematical Modelling so Important? Skyline University College.

[30] Agromayor, Roberto & Nord, Lars. (2019). Preliminary Design and Optimization of Axial Turbines Accounting for Diffuser Performance. International Journal of Turbomachinery, Propulsion and Power. 4. 32. 10.3390/ijtpp4030032.

[31] A Yu Tkachenko , Ya A Ostapyuk and E P Filinov. (2018). Mean-line Modeling of an Axial Turbine IOP Conf. Ser.: Mater. Sci. Eng. 302 012038

[32] Kowalewski, T. A. (2011). Validation problems in computational fluid mechanics. Computer Assisted Mechanics and Engineering Sciences, 18: 39-52.

[33] M.Cavazzuti. (2013). Optimization Methods: From Theory to Design. Springer-Verlag Berlin Heidelberg.

[34] WEI, N. (2000). Significance of Loss Models in Aerothermodynamic Simulation for Axial Turbines. Kungl Tekniska Högskolan, Stockholm.

[35] Stewart, W. L., Whitney, W. J., & Wong, R. Y. (1960). A Study of Boundary-Layer Characteristics of Turbomachine Blade Rows and Their Relation to Over-All Blade Loss. Journal of Fluids Engineering, 82(3), 588–592.

[36] M. W. Benner, S. A. Sjolander, and S. H. Moustapha. (2006a). An Empirical Prediction Method for Secondary Losses in Turbines—Part I: A New Loss Breakdown Scheme and Penetration Depth Correlation. Journal of turbomachinery, 128(2):273–280. ISSN 0889-504X. Place: NEW YORK Publisher: ASME.

[37] Phil Ligrani, Geoffrey Potts, Arshia Fatemi. (2017). Endwall aerodynamic losses from turbine components within gas turbine engines. Propulsion and Power Research, Volume 6, Issue 1, Pages 1-14, ISSN 2212-540X.

[38] Dahlquist, Adrian. (2008). Investigation of Losses Prediction Methods in 1D for Axial Gas Turbines.

[39] Jonas Person. (2015).1D Turbine Design Tool Validation and Loss Model Comparison: Performance Prediction of a 1-stage Turbine at Different Pressure Ratios. KTH School of Industrial Engineering and Management.

[40] Aungier, R. H. (2006). Turbine aerodynamics. American Society of Mechanical Engineers Press, New York.

[41] M. W Benner, S. A Sjolander, and S. H Moustapha. (1997). Influence of Leading-Edge Geometry on Profile Losses in Turbines at Off-Design Incidence: Experimental Results and an Improved Correlation. Journal of turbomachinery, 119(2):193–200. ISSN 0889-504X. Place: NEW YORK Publisher: ASME.

[42] Ainley, D. G., & Mathieson, G. C. R. (1951). A Method of Performance Estimation for Axial-Flow Turbines. Tech. rept. Aeronautical Research Council, London

[43] S. H Moustapha, S. C Kacker, and B Tremblay. (1990). An Improved Incidence Losses Prediction Method for Turbine Airfoils. Journal of turbomachinery, 112(2):267–276. ISSN 0889-504X. Place: NEW YORK Publisher: ASME.

[44] N. Baines. (2019). Turbine Design and Analysis. Turbine Blade Design, 155-198.

[45] N. Baines. (2019). Turbine Design and Analysis. Turbine Testing, 437-471.

[46] M. W. Benner, S. A. Sjolander, and S. H. Moustapha. (2006b). An Empirical Prediction Method For Secondary Losses In Turbines—Part II: A New Secondary Loss Correlation. Journal of turbomachinery, 128(2):281– 291. ISSN 0889-504X. Place: NEW YORK Publisher: ASME.

[47] Emanuele Borgonovo. (2018). Sensitivity Analysis: An Introduction for the Management Scientist. International Series in Operations Research & Management Science (ISOR, volume 251).

[48] Montgomery, Douglas C. (1984). Design and analysis of experiments. New York :Wiley.

[49] Bouzid Ait-Amir, Philippe Pougnet, Abdelkhalak El Hami. (2015). Meta-Model Development. Embedded Mechatronic Systems 2, pages 151-179. Elsevier.

[50] Kiyarash Rahbar, Saad Mahmoud, Raya K. Al-Dadah. (May 2016). Mean-line modeling and CFD analysis of a miniature radial turbine for distributed power generation systems, International Journal of Low-Carbon Technologies, Volume 11, Issue 2, Pages 157–168, https://doi.org/10.1093/ijlct/ctu028

[51] Virtanen, Pauli et al. (2020). "Author Correction: SciPy 1.0: fundamental algorithms for scientific computing in Python". eng. In: Nature methods 17.3. Backup Publisher: SciPy 1.0 Contributors Place: United States Publisher: Nature Publishing Group, pp. 352–352. ISSN: 1548-7091.

[52] M. Hillestad, T. Hertzberg. (2021) KP8105 Mathematical Modeling and Model Fitting. Department of Chemical Engineering, Norwegian Univ. of Science and Technology (NTNU), Trondheim

[53] A.Vinoth Kumar. (2016). Choice of Blade Profile, Pitch and Chord. Department of Aerospace Engineering, SRM University.

[54] Francesco Tosto; David Pasquale; Piero Colonna; Matteo Pini. (2021). The effect of working fluid and compressibility on the optimal solidity in ORC turbine cascades. Proceedings of the 6th International Seminar on ORC Power Systems. Technical University of Munich.

[55] Andrea Saltelli, Paola Annoni. (2010). How to avoid a perfunctory sensitivity analysis. Environmental Modelling & Software, Volume 25, Issue 12. Pages 1508-1517.

Appendix

A Results from the sensitivity analysis for a wide design space

This section presents the results obtained from the first 5 experiments carried out in the wide design space sensitivity analysis.

A.1 Results for the coefficients and confidence intervals of the main, interaction and quadratic effects in experiment 1

The results for the first experiment are shown in Table A.1, main, quadratic and interaction effects have been disaggregated in the tables below.

Table A.1: Results of Experiment 1 - Faced central composite design with 8 factors. Significant effects highlighted in pink.

Main effects							
$\mathbf{BS}_s$	$\mathbf{BS}_r$	$\mathbf{AR}_s$	$\mathbf{AR}_r$	$\mathbf{r}_{ht_1}$	$\mathbf{r}_{ht_3}$	$\mathbf{r}_{ht_4}$	$\mathbf{r}_{ht_6}$
$1.5572 \cdot 10^{-2}$	$-5.5494 \cdot 10^{-2}$	$1.7739 \cdot 10^{-2}$	2.0782	$-2.4339 \cdot 10^{-1}$	4.029	$-9.8352 \cdot 10^{-1}$	-4.8783
Interaction effects							
	$\mathbf{BS}_s\mathbf{BS}_r$	$\mathbf{BS}_s\mathbf{AR}_s$	$\mathbf{BS}_s\mathbf{AR}_r$	$\mathbf{BS}_s\mathbf{r}_{ht_1}$	$\mathbf{BS}_s\mathbf{r}_{ht_3}$	$\mathbf{BS}_s\mathbf{r}_{ht_4}$	$\mathbf{BS}_s\mathbf{r}_{ht_6}$
	$-1.4701 \cdot 10^{-4}$	$5.7325 \cdot 10^{-3}$	$1.0078 \cdot 10^{-3}$	$-6.9753 \cdot 10^{-3}$	$1.6527 \cdot 10^{-2}$	$-5.8038 \cdot 10^{-4}$	$-7.7214 \cdot 10^{-3}$
		$\mathbf{BS}_r\mathbf{AR}_s$	$\mathbf{BS}_r\mathbf{AR}_r$	$\mathbf{BS}_r\mathbf{r}_{ht1}$	$\mathbf{BS}_r\mathbf{r}_{ht3}$	$\mathbf{BS}_r\mathbf{r}_{ht4}$	$\mathbf{BS}_r\mathbf{r}_{ht6}$
		$-1.3961 \cdot 10^{-4}$	$1.7705 \cdot 10^{-2}$	$-6.2251 \cdot 10^{-4}$	$2.5072 \cdot 10^{-2}$	$1.6376 \cdot 10^{-2}$	$-3.3666 \cdot 10^{-2}$
			$\mathbf{AR}_s\mathbf{AR}_r$	$\mathbf{AR}_s\mathbf{r}_{ht_1}$	$\mathbf{AR}_s\mathbf{r}_{ht_3}$	$\mathbf{AR}_s\mathbf{r}_{ht_4}$	$\mathbf{AR}_s\mathbf{r}_{ht_6}$
			$-1.8561 \cdot 10^{-4}$	$-1.9402 \cdot 10^{-2}$	$3.1955 \cdot 10^{-2}$	$-1.1913 \cdot 10^{-4}$	$-1.1913 \cdot 10^{-3}$
				$\mathbf{AR}_r\mathbf{r}_{ht_1}$	$\mathbf{AR}_r\mathbf{r}_{ht_3}$	$\mathbf{AR}_r\mathbf{r}_{ht_4}$	$\mathbf{AR}_r\mathbf{r}_{ht_6}$
				$-1.3988 \cdot 10^{-2}$	-1.2963	$8.9130 \cdot 10^{-1}$	1.2389
					$\mathbf{r}_{ht_1}\mathbf{r}_{ht_3}$	$\mathbf{r}_{ht_1}\mathbf{r}_{ht_4}$	$\mathbf{r}_{ht_1}\mathbf{r}_{ht_6}$
					$2.6394 \cdot 10^{-1}$	$5.5092 \cdot 10^{-3}$	$2.5291 \cdot 10^{-1}$
						$\mathbf{r}_{ht_3}\mathbf{r}_{ht_4}$	$\mathbf{r}_{ht_3}\mathbf{r}_{ht_6}$
						$6.1446 \cdot 10^{-1}$	4.8770
							$\mathbf{r}_{ht_4}\mathbf{r}_{ht_6}$
							$-6.0017 \cdot 10^{-1}$
Quadratic effects							
$\mathbf{BS}_s^2$	$\mathbf{BS}_r^2$	$\mathbf{AR}_s^2$	$\mathbf{AR}_r^2$	$\mathbf{r}_{ht1}^2$	$\mathbf{r}_{ht3}^2$	$\mathbf{r}_{ht4}^2$	$\mathbf{r}_{ht6}^2$
$-4.3491 \cdot 10^{-1}$	$-5.5723 \cdot 10^{-1}$	$-3.7001 \cdot 10^{-1}$	$-7.4223 \cdot 10^{-1}$	$-3.6998 \cdot 10^{-1}$	-1.2091	$-4.1564 \cdot 10^{-1}$	-2.6621

Those effects that have resulted significant are highlighted in grey within Table A.2 and in pink in Table A.3 and A.4.

Table A.2: Confidence interval and relevance of the main effects in experiment 1. Significant effects highlighted in grey.

Main effect	IC lower bound	Coefficient	IC upper bound	Relevance
$\mathbf{BS}_s$	-0.2332	0.0156	0.2644	Not significant
$\mathbf{BS}_r$	-0.3043	-0.0555	0.1933	Not significant
$\mathbf{AR}_s$	-0.2311	0.0177	0.2665	Not significant
$\mathbf{AR}_r$	1.8295	2.0783	2.327	Significant
$\mathbf{r}_{ht_1}$	-0.4922	-0.2434	0.0054	Not significant
$\mathbf{r}_{ht_3}$	3.7803	4.0291	4.2779	Significant
$\mathbf{r}_{ht_4}$	-1.2323	-0.9835	-0.7347	Significant
$\mathbf{r}_{ht_6}$	-5.1272	-4.8784	-4.6296	Significant

Table A.3: Confidence interval and relevance of the quadratic effects in experiment 1. Significant effects highlighted in pink.

Quadratic effect	IC lower bound	Coefficient	IC upper bound	Relevance
$\mathbf{BS}_s^2$	-3.082	-0.4349	2.2121	Not significant
$\mathbf{BS}_r^2$	-3.2043	-0.5572	2.0898	Not significant
$\mathbf{AR}_s^2$	-3.0171	-0.37	2.277	Not significant
$\mathbf{AR}_r^2$	-3.3893	-0.7422	1.9048	Not significant
$\mathbf{r}_{ht1}^2$	-3.017	-0.37	2.2771	Not significant
$\mathbf{r}_{ht3}^2$	-3.8562	-1.2091	1.4379	Not significant
$\mathbf{r}_{ht4}^2$	-3.0627	-0.4156	2.2314	Not significant
$\mathbf{r}_{ht6}^2$	-5.3092	-2.6622	-0.0151	Significant

Table A.4: Confidence interval and relevance of the interaction effects in experiment 1. Significant effects highlighted in pink.

Parameter: BS_s				
Interaction effect	IC lower bound	Coefficient	IC upper bound	Relevance
$\mathbf{BS}_s\mathbf{BS}_r$	-0.2499	-0.0001	0.2496	Not significant
$\mathbf{BS}_s\mathbf{AR}_s$	-0.244	0.0057	0.2555	Not significant
$\mathbf{BS}_s\mathbf{AR}_r$	-0.2488	0.001	0.2508	Not significant
$\mathbf{BS}_s\mathbf{r}_{ht1}$	-0.2567	-0.007	0.2428	Not significant
$\mathbf{BS}_s\mathbf{r}_{ht3}$	-0.2332	0.0165	0.2663	Not significant
$\mathbf{BS}_s\mathbf{r}_{ht4}$	-0.2503	-0.0006	0.2492	Not significant
$\mathbf{BS}_s\mathbf{r}_{ht6}$	-0.2575	-0.0077	0.242	Not significant
Parameter: BS_r				
Interaction effect	IC lower bound	Coefficient	IC upper bound	Relevance
$\mathbf{BS}_r\mathbf{AR}_s$	-0.2499	-0.0001	0.2496	Not significant
$\mathbf{BS}_r\mathbf{AR}_r$	-0.2321	0.0177	0.2675	Not significant
$\mathbf{BS}_r\mathbf{r}_{ht1}$	-0.2491	0.0006	0.2504	Not significant
$\mathbf{BS}_r\mathbf{r}_{ht3}$	-0.2247	0.0251	0.2748	Not significant
$\mathbf{BS}_r\mathbf{r}_{ht4}$	-0.2334	0.0164	0.2661	Not significant

Interaction effect	IC lower bound	Coefficient	IC upper bound	Relevance
$\mathbf{BS}_r\mathbf{r}_{ht6}$	-0.2834	-0.0337	0.2161	Not significant
Parameter: AR_s				
Interaction effect	IC lower bound	Coefficient	IC upper bound	Relevance
$\mathbf{AR}_s\mathbf{AR}_r$	-0.25	-0.0002	0.2496	Not significant
$\mathbf{AR}_s\mathbf{r}_{ht1}$	-0.2692	-0.0194	0.2304	Not significant
$\mathbf{AR}_s\mathbf{r}_{ht3}$	-0.2178	0.032	0.2817	Not significant
$\mathbf{AR}_s\mathbf{r}_{ht4}$	-0.2499	-0.0001	0.2496	Not significant
$\mathbf{AR}_s\mathbf{r}_{ht6}$	-0.251	-0.0012	0.2486	Not significant
Parameter: AR_r				
Interaction effect	IC lower bound	Coefficient	IC upper bound	Relevance
$\mathbf{AR}_r\mathbf{r}_{ht1}$	-0.2638	-0.014	0.2358	Not significant
$\mathbf{AR}_r\mathbf{r}_{ht3}$	-1.5461	-1.2963	-1.0466	Significant
$\mathbf{AR}_r\mathbf{r}_{ht4}$	0.6415	0.8913	11.411	Significant
$\mathbf{AR}_r\mathbf{r}_{ht6}$	0.9892	1.2389	1.4887	Significant
Parameter: r_{ht1}				
Interaction effect	IC lower bound	Coefficient	IC upper bound	Relevance
$\mathbf{r}_{ht1}\mathbf{r}_{ht3}$	0.0142	0.2639	0.5137	Significant
$\mathbf{r}_{ht1}\mathbf{r}_{ht4}$	-0.2443	0.0055	0.2553	Not significant
$\mathbf{r}_{ht1}\mathbf{r}_{ht6}$	0.0031	0.2529	0.5027	Significant
Parameter: r_{ht3}				
Interaction effect	IC lower bound	Coefficient	IC upper bound	Relevance
$\mathbf{r}_{ht3}\mathbf{r}_{ht4}$	0.3647	0.6145	0.8642	Significant
$\mathbf{r}_{ht3}\mathbf{r}_{ht6}$	4.6273	4.877	5.1268	Significant
Parameter: r_{ht4}				
Interaction effect	IC lower bound	Coefficient	IC upper bound	Relevance
$\mathbf{r}_{ht4}\mathbf{r}_{ht6}$	-0.8499	-0.6002	-0.3504	Significant

A.2 Results for the coefficients and confidence intervals of the main, interaction and quadratic effects in experiment 2

The results of the second experiment are shown in Table A.5. Main, quadratic and interaction effects are shown in Tables A.6, A.7 and A.8 respectively.

Table A.5: Results of Experiment 2 - Faced central composite design with 9 factors. Significant effects highlighted in pink.

Main effects								
$\mathbf{BS}_s$	$\mathbf{BS}_r$	$\mathbf{AR}_s$	$\mathbf{AR}_r$	$\mathbf{r}_{ht1}$	$\mathbf{r}_{ht3}$	$\mathbf{r}_{ht4}$	$\mathbf{r}_{ht6}$	$\mathbf{p}_6$
$1.6280 \cdot 10^{-2}$	$-5.9760 \cdot 10^{-2}$	$1.7337 \cdot 10^{-2}$	2.0890	$-2.3637 \cdot 10^{-1}$	4.0655	$-9.9869 \cdot 10^{-1}$	-4.9295	$8.2969 \cdot 10^{-1}$
Interaction effects								
	$\mathbf{BS}_s\mathbf{BS}_r$	$\mathbf{BS}_s\mathbf{AR}_s$	$\mathbf{BS}_s\mathbf{AR}_r$	$\mathbf{BS}_s\mathbf{r}_{ht1}$	$\mathbf{BS}_s\mathbf{r}_{ht3}$	$\mathbf{BS}_s\mathbf{r}_{ht4}$	$\mathbf{BS}_s\mathbf{r}_{ht6}$	$\mathbf{BS}_s\mathbf{p}_6$
	$4.5619 \cdot 10^{-5}$	$6.0267 \cdot 10^{-3}$	$6.6486 \cdot 10^{-4}$	$-6.9525 \cdot 10^{-3}$	$1.6465 \cdot 10^{-2}$	$-2.4081 \cdot 10^{-4}$	$-7.6611 \cdot 10^{-3}$	$8.8243 \cdot 10^{-5}$
		$\mathbf{BS}_r\mathbf{AR}_s$	$\mathbf{BS}_r\mathbf{AR}_r$	$\mathbf{BS}_r\mathbf{r}_{ht1}$	$\mathbf{BS}_r\mathbf{r}_{ht3}$	$\mathbf{BS}_r\mathbf{r}_{ht4}$	$\mathbf{BS}_r\mathbf{r}_{ht6}$	$\mathbf{BS}_r\mathbf{p}_6$
		$7.0362 \cdot 10^{-5}$	$1.7803 \cdot 10^{-2}$	$1.7979 \cdot 10^{-5}$	$2.5805 \cdot 10^{-2}$	$1.6428 \cdot 10^{-2}$	$-3.6488 \cdot 10^{-2}$	$1.3814 \cdot 10^{-2}$
			$\mathbf{AR}_s\mathbf{AR}_r$	$\mathbf{AR}_s\mathbf{r}_{ht1}$	$\mathbf{AR}_s\mathbf{r}_{ht3}$	$\mathbf{AR}_s\mathbf{r}_{ht4}$	$\mathbf{AR}_s\mathbf{r}_{ht6}$	$\mathbf{AR}_s\mathbf{p}_6$
			$-3.7515 \cdot 10^{-4}$	$-1.8774 \cdot 10^{-2}$	$3.0597 \cdot 10^{-2}$	$7.1373 \cdot 10^{-5}$	$-1.8569 \cdot 10^{-4}$	$8.2647 \cdot 10^{-3}$
				$\mathbf{AR}_r\mathbf{r}_{ht1}$	$\mathbf{AR}_r\mathbf{r}_{ht3}$	$\mathbf{AR}_r\mathbf{r}_{ht4}$	$\mathbf{AR}_r\mathbf{r}_{ht6}$	$\mathbf{AR}_r\mathbf{p}_6$
				$-1.2068 \cdot 10^{-2}$	-1.3152	$9.0363 \cdot 10^{-1}$	1.2586	$3.2315 \cdot 10^{-2}$
					$\mathbf{r}_{ht1}\mathbf{r}_{ht3}$	$\mathbf{r}_{ht1}\mathbf{r}_{ht4}$	$\mathbf{r}_{ht1}\mathbf{r}_{ht6}$	$\mathbf{r}_{ht1}\mathbf{p}_6$
					$2.5629 \cdot 10^{-1}$	$5.3196 \cdot 10^{-3}$	$2.4517 \cdot 10^{-1}$	$-4.7081 \cdot 10^{-2}$
						$\mathbf{r}_{ht3}\mathbf{r}_{ht4}$	$\mathbf{r}_{ht3}\mathbf{r}_{ht6}$	$\mathbf{r}_{ht3}\mathbf{p}_6$
						$6.2750 \cdot 10^{-1}$	4.8245	$-7.5547 \cdot 10^{-1}$
							$\mathbf{r}_{ht4}\mathbf{r}_{ht6}$	$\mathbf{r}_{ht4}\mathbf{p}_6$
							$-6.1620 \cdot 10^{-1}$	$4.8475 \cdot 10^{-3}$
								$\mathbf{r}_{ht6}\mathbf{p}_6$
								1.3169
Quadratic effects								
$\mathbf{BS}_s^2$	$\mathbf{BS}_r^2$	$\mathbf{AR}_s^2$	$\mathbf{AR}_r^2$	$\mathbf{r}_{ht1}^2$	$\mathbf{r}_{ht3}^2$	$\mathbf{r}_{ht4}^2$	$\mathbf{r}_{ht6}^2$	$\mathbf{p}_6^2$
$-3.8393 \cdot 10^{-1}$	$-5.0983 \cdot 10^{-1}$	$-3.1987 \cdot 10^{-1}$	$-6.9068 \cdot 10^{-1}$	$-3.1984 \cdot 10^{-1}$	-1.1427	$-3.6557 \cdot 10^{-1}$	-2.5970	$-6.8524 \cdot 10^{-1}$

Table A.6: Confidence interval and relevance of the main effects in experiment 2. Significant effects highlighted in grey.

Main effect	IC lower bound	Coefficient	IC upper bound	Relevance
$\mathbf{BS}_s$	-0.1604	0.0163	0.193	Not significant
$\mathbf{BS}_r$	-0.2364	-0.0598	0.1169	Not significant
$\mathbf{AR}_s$	-0.1594	0.0173	0.194	Not significant
$\mathbf{AR}_r$	1.9123	2.089	2.2657	Significant
$\mathbf{r}_{ht1}$	-0.4131	-0.2364	-0.0597	Significant
$\mathbf{r}_{ht3}$	3.8889	4.0656	4.2423	Significant
$\mathbf{r}_{ht4}$	-1.1754	-0.9987	-0.822	Significant
$\mathbf{r}_{ht6}$	-5.1063	-4.9296	-4.7529	Significant
$\mathbf{p}_6$	0.653	0.8297	1.0064	Significant

Table A.7: Confidence interval and relevance of the quadratic effects in experiment 2.

Quadratic effect	IC lower bound	Coefficient	IC upper bound	Relevance
$\mathbf{BS}_s^2$	-3.057	-0.3839	2.2891	Not significant
$\mathbf{BS}_r^2$	-3.1829	-0.5098	2.1632	Not significant
$\mathbf{AR}_s^2$	-2.9929	-0.3199	2.3532	Not significant
$\mathbf{AR}_r^2$	-3.3638	-0.6907	1.9824	Not significant
$\mathbf{r}_{ht1}^2$	-2.9929	-0.3198	2.3532	Not significant
$\mathbf{r}_{ht3}^2$	-3.8158	-1.1427	1.5303	Not significant
$\mathbf{r}_{ht4}^2$	-3.0386	-0.3656	2.3075	Not significant
$\mathbf{r}_{ht6}^2$	-5.2701	-2.597	0.076	Not significant
$\mathbf{p}_6^2$	-3.3583	-0.6852	1.9878	Not significant

Table A.8: Confidence interval and relevance of the interaction effects in experiment 2. Significant effects highlighted in pink.

Parameter: BS_s				
Interaction effect	IC lower bound	Coefficient	IC upper bound	Relevance
$\mathbf{BS_sBS_r}$	-0.177	0.0	0.1771	Not significant
$\mathbf{BS_sAR_s}$	-0.171	0.006	0.1831	Not significant
$\mathbf{BS_sAR_r}$	-0.1764	0.0007	0.1777	Not significant
$\mathbf{BS_sr}_{ht1}$	-0.184	-0.007	0.1701	Not significant
$\mathbf{BS_sr}_{ht3}$	-0.1606	0.0165	0.1935	Not significant
$\mathbf{BS_sr}_{ht4}$	-0.1773	-0.0002	0.1768	Not significant
$\mathbf{BS_sr}_{ht6}$	-0.1847	-0.0077	0.1694	Not significant
$\mathbf{BS_sp}_6$	-0.1769	0.0001	0.1771	Not significant
Parameter: BS_r				
Interaction effect	IC lower bound	Coefficient	IC upper bound	Relevance
$\mathbf{BS_rAR_s}$	-0.177	0.0001	0.1771	Not significant
$\mathbf{BS_rAR_r}$	-0.1592	0.0178	0.1948	Not significant
$\mathbf{BS_rr}_{ht1}$	-0.177	0.0	0.1771	Not significant
$\mathbf{BS_rr}_{ht3}$	-0.1512	0.0258	0.2028	Not significant
$\mathbf{BS_rr}_{ht4}$	-0.1606	0.0164	0.1935	Not significant
$\mathbf{BS_rr}_{ht6}$	-0.2135	-0.0365	0.1405	Not significant
$\mathbf{BS_rp}_6$	-0.1632	0.0138	0.1908	Not significant
Parameter: AR_s				
Interaction effect	IC lower bound	Coefficient	IC upper bound	Relevance
$\mathbf{AR_sAR_r}$	-0.1774	-0.0004	0.1767	Not significant
$\mathbf{AR_sr}_{ht1}$	-0.1958	-0.0188	0.1583	Not significant
$\mathbf{AR_sr}_{ht3}$	-0.1464	0.0306	0.2076	Not significant
$\mathbf{AR_sr}_{ht4}$	-0.177	0.0001	0.1771	Not significant
$\mathbf{AR_sr}_{ht6}$	-0.1772	-0.0002	0.1768	Not significant
$\mathbf{AR_sp}_6$	-0.1688	0.0083	0.1853	Not significant
Parameter: AR_r				
Interaction effect	IC lower bound	Coefficient	IC upper bound	Relevance
$\mathbf{AR_rr}_{ht1}$	-0.1891	-0.0121	0.165	Not significant
$\mathbf{AR_rr}_{ht3}$	-1.4923	-1.3153	-1.1383	Significant
$\mathbf{AR_rr}_{ht4}$	0.7266	0.9036	1.0807	Significant
$\mathbf{AR_rr}_{ht6}$	1.0817	1.2587	1.4357	Significant
$\mathbf{AR_rp}_6$	-0.1447	0.0323	0.2093	Not significant
Parameter: r_{ht1}				
Interaction effect	IC lower bound	Coefficient	IC upper bound	Relevance
$\mathbf{r}_{ht1}\mathbf{r}_{ht3}$	0.0793	0.2563	0.4333	Significant
$\mathbf{r}_{ht1}\mathbf{r}_{ht4}$	-0.1717	0.0053	0.1824	Not significant
$\mathbf{r}_{ht1}\mathbf{r}_{ht6}$	0.0681	0.2452	0.4222	Significant
$\mathbf{r}_{ht1}\mathbf{p}_6$	-0.2241	-0.0471	0.13	Not significant
Parameter: r_{ht3}				
Interaction effect	IC lower bound	Coefficient	IC upper bound	Relevance
$\mathbf{r}_{ht3}\mathbf{r}_{ht4}$	0.4505	0.6275	0.8045	Significant
$\mathbf{r}_{ht3}\mathbf{r}_{ht6}$	4.6475	4.8246	5.0016	Significant
$\mathbf{r}_{ht3}\mathbf{p}_6$	-0.9325	-0.7555	-0.5784	Significant

Parameter: r_{ht4}				
Interaction effect	IC lower bound	Coefficient	IC upper bound	Relevance
$\mathbf{r}_{ht4}\mathbf{r}_{ht6}$	-0.7932	-0.6162	-0.4392	Significant
$\mathbf{r}_{ht4}\mathbf{p}_6$	-0.1722	0.0048	0.1819	Not significant
Parameter: r_{ht6}				
Interaction effect	IC lower bound	Coefficient	IC upper bound	Relevance
$\mathbf{r}_{ht6}\mathbf{p}_6$	1.1399	1.3169	1.4939	Significant

A.3 Results for the coefficients and confidence intervals of the main, interaction and quadratic effects in experiment 3

The results for the third experiments are shown in Table A.9. As for the previous experiments, main, quadratic and interaction effects have been disaggregated in Table A.10, A.11 and A.12 respectively.

Table A.9: Results of Experiment 3 - Faced central composite design with 11 factors.

Main effects										
$\mathbf{BS}_s$	$\mathbf{BS}_r$	$\mathbf{AR}_s$	$\mathbf{AR}_r$	$\mathbf{r}_{ht1}$	$\mathbf{r}_{ht3}$	$\mathbf{r}_{ht4}$	$\mathbf{r}_{ht6}$	$(\mathbf{t}_{te}/\mathbf{o})_s$	$(\mathbf{t}_{te}/\mathbf{o})_r$	$\mathbf{p}_6$
$-3.8725{\cdot}10^{-3}$	$-1.6350{\cdot}10^{-1}$	$9.0840{\cdot}10^{-3}$	2.1689	$-5.7529{\cdot}10^{-2}$	3.9723	-1.0473	-4.7438	-1.3139	-1.7387	$4.0689{\cdot}10^{-1}$
Interaction effects										
	$\mathbf{BS}_s\mathbf{BS}_r$	$\mathbf{BS}_s\mathbf{AR}_s$	$\mathbf{BS}_s\mathbf{AR}_r$	$\mathbf{BS}_s\mathbf{r}_{ht1}$	$\mathbf{BS}_s\mathbf{r}_{ht3}$	$\mathbf{BS}_s\mathbf{r}_{ht4}$	$\mathbf{BS}_s\mathbf{r}_{ht6}$	$\mathbf{BS}_s(\mathbf{t}_{te}/\mathbf{o})_s$	$\mathbf{BS}_s(\mathbf{t}_{te}/\mathbf{o})_r$	$\mathbf{BS}_s\mathbf{p}_6$
	$-1.5338{\cdot}10^{-4}$	$-3.1786{\cdot}10^{-2}$	$-1.8008{\cdot}10^{-4}$	$-5.5432{\cdot}10^{-3}$	$6.2370{\cdot}10^{-3}$	$2.2365{\cdot}10^{-4}$	$4.0951{\cdot}10^{-3}$	$-1.9604{\cdot}10^{-2}$	$-2.1664{\cdot}10^{-4}$	$-2.4325{\cdot}10^{-3}$
		$\mathbf{BS}_r\mathbf{AR}_s$	$\mathbf{BS}_r\mathbf{AR}_r$	$\mathbf{BS}_r\mathbf{r}_{ht1}$	$\mathbf{BS}_r\mathbf{r}_{ht3}$	$\mathbf{BS}_r\mathbf{r}_{ht4}$	$\mathbf{BS}_r\mathbf{r}_{ht6}$	$\mathbf{BS}_r(\mathbf{t}_{te}/\mathbf{o})_s$	$\mathbf{BS}_r(\mathbf{t}_{te}/\mathbf{o})_r$	$\mathbf{BS}_r\mathbf{p}_6$
		$9.1910{\cdot}10^{-5}$	$7.7901{\cdot}10^{-2}$	$4.1686{\cdot}10^{-2}$	$8.2942{\cdot}10^{-2}$	$-2.2358{\cdot}10^{-2}$	$-9.8841{\cdot}10^{-2}$	$-3.9289{\cdot}10^{-2}$	$-1.0157{\cdot}10^{-1}$	$-3.0354{\cdot}10^{-2}$
			$\mathbf{AR}_s\mathbf{AR}_r$	$\mathbf{AR}_s\mathbf{r}_{ht1}$	$\mathbf{AR}_s\mathbf{r}_{ht3}$	$\mathbf{AR}_s\mathbf{r}_{ht4}$	$\mathbf{AR}_s\mathbf{r}_{ht6}$	$\mathbf{AR}_s(\mathbf{t}_{te}/\mathbf{o})_s$	$\mathbf{AR}_s(\mathbf{t}_{te}/\mathbf{o})_r$	$\mathbf{AR}_s\mathbf{p}_6$
			$-2.913{\cdot}10^{-4}$	$-1.5341{\cdot}10^{-2}$	$2.4047{\cdot}10^{-2}$	$4.8235{\cdot}10^{-5}$	$2.3477{\cdot}10^{-3}$	$-9.3158{\cdot}10^{-3}$	$1.3155{\cdot}10^{-3}$	$5.0237{\cdot}10^{-3}$
				$\mathbf{AR}_r\mathbf{r}_{ht1}$	$\mathbf{AR}_r\mathbf{r}_{ht3}$	$\mathbf{AR}_r\mathbf{r}_{ht4}$	$\mathbf{AR}_r\mathbf{r}_{ht6}$	$\mathbf{AR}_r(\mathbf{t}_{te}/\mathbf{o})_s$	$\mathbf{AR}_r(\mathbf{t}_{te}/\mathbf{o})_r$	$\mathbf{AR}_r\mathbf{p}_6$
				$-1.3266{\cdot}10^{-1}$	-1.4643	$9.4217{\cdot}10^{-1}$	1.4084	$9.4777{\cdot}10^{-2}$	$1.1005{\cdot}10^{-1}$	$1.4843{\cdot}10^{-1}$
					$\mathbf{r}_{ht1}\mathbf{r}_{ht3}$	$\mathbf{r}_{ht1}\mathbf{r}_{ht4}$	$\mathbf{r}_{ht1}\mathbf{r}_{ht6}$	$\mathbf{r}_{ht1}(\mathbf{t}_{te}/\mathbf{o})_s$	$\mathbf{r}_{ht1}(\mathbf{t}_{te}/\mathbf{o})_r$	$\mathbf{r}_{ht1}\mathbf{p}_6$
					$7.4963{\cdot}10^{-2}$	$1.2817{\cdot}10^{-1}$	$3.1452{\cdot}10^{-1}$	$1.5750{\cdot}10^{-1}$	$1.4283{\cdot}10^{-1}$	$9.008{\cdot}10^{-2}$
						$\mathbf{r}_{ht3}\mathbf{r}_{ht4}$	$\mathbf{r}_{ht3}\mathbf{r}_{ht6}$	$\mathbf{r}_{ht3}(\mathbf{t}_{te}/\mathbf{o})_s$	$\mathbf{r}_{ht3}(\mathbf{t}_{te}/\mathbf{o})_r$	$\mathbf{r}_{ht3}\mathbf{p}_6$
						$7.1331{\cdot}10^{-1}$	5.0460	$-3.9726{\cdot}10^{-1}$	$4.3373{\cdot}10^{-1}$	$-6.5676{\cdot}10^{-1}$
							$\mathbf{r}_{ht4}\mathbf{r}_{ht6}$	$\mathbf{r}_{ht4}(\mathrm{t}_{te}/\mathrm{o})_s$	$\mathbf{r}_{ht4}(\mathbf{t}_{te}/\mathbf{o})_r$	$\mathbf{r}_{ht4}\mathbf{p}_6$
							$-6.9087{\cdot}10^{-1}$	$-1.1038{\cdot}10^{-1}$	$-6.5210{\cdot}10^{-2}$	$-1.2097{\cdot}10^{-1}$
								$\mathbf{r}_{ht6}(\mathbf{t}_{te}/\mathbf{o})_s$	$\mathbf{r}_{ht6}(\mathbf{t}_{te}/\mathbf{o})_r$	$\mathbf{r}_{ht6}\mathbf{p}_6$
								$5.4703{\cdot}10^{-1}$	$-4.9542{\cdot}10^{-1}$	1.1769
									$(\mathbf{t}_{te}/\mathbf{o})_s(\mathbf{t}_{te}/\mathbf{o})_r$	$(\mathbf{t}_{te}/\mathbf{o})_s\mathbf{p}_6$
									$-1.0105{\cdot}10^{-1}$	$-3.1463{\cdot}10^{-1}$
										$(\mathbf{t}_{te}/\mathbf{o})_r\mathbf{p}_6$
										$-2.2525{\cdot}10^{-1}$
Quadratic effects										
$\mathbf{BS}_s^2$	$\mathbf{BS}_r^2$	$\mathbf{AR}_s^2$	$\mathbf{AR}_r^2$	$\mathbf{r}_{ht1}^2$	$\mathbf{r}_{ht3}^2$	$\mathbf{r}_{ht4}^2$	$\mathbf{r}_{ht6}^2$	$(\mathbf{t}_{te}/\mathbf{o})_s^2$	$(\mathbf{t}_{te}/\mathbf{o})_r^2$	$\mathbf{p}_6^2$
$-3.2069{\cdot}10^{-1}$	$-4.1794{\cdot}10^{-1}$	$-2.6007{\cdot}10^{-1}$	$-6.0908{\cdot}10^{-1}$	$-2.5446{\cdot}10^{-1}$	-1.1097	$-3.0511{\cdot}10^{-1}$	-2.5415	$-7.2024{\cdot}10^{-1}$	$-9.4415{\cdot}10^{-1}$	$-6.1828{\cdot}10^{-1}$

Table A.10: Confidence interval and relevance of the main effects in experiment 3. Significant effects highlighted in grey.

Main effect	IC lower bound	Coefficient	IC upper bound	Relevance
$\mathbf{BS}_s$	-0.1381	-0.0039	0.1303	Not significant
$\mathbf{BS}_r$	-0.2977	-0.1635	-0.0293	Significant
$\mathbf{AR}_s$	-0.1251	0.0091	0.1433	Not significant
$\mathbf{AR}_r$	2.0348	2.169	2.3032	Significant
$\mathbf{r}_{ht1}$	-0.1917	-0.0575	0.0767	Not significant
$\mathbf{r}_{ht3}$	3.8381	3.9723	4.1065	Significant
$\mathbf{r}_{ht4}$	-1.1816	-1.0474	-0.9132	Significant
$\mathbf{r}_{ht6}$	-4.878	-4.7438	-4.6096	Significant
$(\mathbf{t}_{te}/\mathbf{o})_s$	-1.4482	-1.314	-1.1798	Significant
$(\mathbf{t}_{te}/\mathbf{o})_r$	-1.873	-1.7388	-1.6046	Significant
$\mathbf{p}_6$	0.2727	0.4069	0.5411	Significant

Table A.11: Confidence interval and relevance of the quadratic effects in experiment 3.

Quadratic effect	IC lower bound	Coefficient	IC upper bound	Relevance
$\mathbf{BS}_s^2$	-4.4192	-0.3207	3.7778	Not significant
$\mathbf{BS}_r^2$	-4.5164	-0.4179	3.6805	Not significant
$\mathbf{AR}_s^2$	-4.3585	-0.2601	3.8384	Not significant
$\mathbf{AR}_r^2$	-4.7076	-0.6091	3.4894	Not significant
$\mathbf{r}_{ht1}^2$	-4.3529	-0.2545	3.844	Not significant
$\mathbf{r}_{ht3}^2$	-5.2082	-1.1097	2.9887	Not significant
$\mathbf{r}_{ht4}^2$	-4.4036	-0.3051	3.7934	Not significant
$\mathbf{r}_{ht6}^2$	-6.64	-2.5415	1.5569	Not significant
$(\mathbf{t}_{te}/\mathbf{o})_s^2$	-4.8187	-0.7202	3.3782	Not significant
$(\mathbf{t}_{te}/\mathbf{o})_r^2$	-5.0426	-0.9442	3.1543	Not significant
$\mathbf{p}_6^2$	-4.7168	-0.6183	3.4802	Not significant

Table A.12: Confidence interval and relevance of the interaction effects in experiment 3. Significant effects highlighted in pink.

Parameter: BS_s				
Interaction effect	IC lower bound	Coefficient	IC upper bound	Relevance
$\mathbf{BS}_s\mathbf{BS}_r$	-0.1344	-0.0002	0.1341	Not significant
$\mathbf{BS}_s\mathbf{AR}_s$	-0.1661	-0.0318	0.1025	Not significant
$\mathbf{BS}_s\mathbf{AR}_r$	-0.1344	-0.0002	0.1341	Not significant
$\mathbf{BS}_s\mathbf{r}_{ht,1}$	-0.1398	-0.0055	0.1287	Not significant
$\mathbf{BS}_s\mathbf{r}_{ht,3}$	-0.128	0.0062	0.1405	Not significant
$\mathbf{BS}_s\mathbf{r}_{ht,4}$	-0.134	0.0002	0.1345	Not significant
$\mathbf{BS}_s\mathbf{r}_{ht,6}$	-0.1302	0.0041	0.1384	Not significant
$\mathbf{BS}_s(\mathbf{t}_{te}/\mathbf{o})_s$	-0.1539	-0.0196	0.1147	Not significant
$\mathbf{BS}_s(\mathbf{t}_{te}/\mathbf{o})_r$	-0.1345	-0.0002	0.134	Not significant

Interaction effect	IC lower bound	Coefficient	IC upper bound	Relevance
$\mathbf{BS}_s\mathbf{p}_6$	-0.1367	-0.0024	0.1318	Not significant
Parameter: BS_r				
Interaction effect	IC lower bound	Coefficient	IC upper bound	Relevance
$\mathbf{BS}_r\mathbf{AR}_s$	-0.1342	0.0001	0.1344	Not significant
$\mathbf{BS}_r\mathbf{AR}_r$	-0.0564	0.0779	0.2122	Not significant
$\mathbf{BS}_r\mathbf{r}_{ht,1}$	-0.0926	0.0417	0.176	Not significant
$\mathbf{BS}_r\mathbf{r}_{ht,3}$	-0.0513	0.0829	0.2172	Not significant
$\mathbf{BS}_r\mathbf{r}_{ht,4}$	-0.1566	-0.0224	0.1119	Not significant
$\mathbf{BS}_r\mathbf{r}_{ht,6}$	-0.2331	-0.0988	0.0354	Not significant
$\mathbf{BS}_r(\mathbf{t}_{te}/\mathbf{o})_s$	-0.1736	-0.0393	0.095	Not significant
$\mathbf{BS}_r(\mathbf{t}_{te}/\mathbf{o})_r$	-0.2358	-0.1016	0.0327	Not significant
$\mathbf{BS}_r\mathbf{p}_6$	-0.1646	-0.0304	0.1039	Not significant
Parameter: AR_s				
Interaction effect	IC lower bound	Coefficient	IC upper bound	Relevance
$\mathbf{AR}_s\mathbf{AR}_r$	-0.1346	-0.0003	0.134	Not significant
$\mathbf{AR}_s\mathbf{r}_{ht,1}$	-0.1496	-0.0153	0.1189	Not significant
$\mathbf{AR}_s\mathbf{r}_{ht,3}$	-0.1102	0.024	0.1583	Not significant
$\mathbf{AR}_s\mathbf{r}_{ht,4}$	-0.1342	0.0	0.1343	Not significant
$\mathbf{AR}_s\mathbf{r}_{ht,6}$	-0.1319	0.0023	0.1366	Not significant
$\mathbf{AR}_s(\mathbf{t}_{te}/\mathbf{o})_s$	-0.1436	-0.0093	0.1249	Not significant
$\mathbf{AR}_s(\mathbf{t}_{te}/\mathbf{o})_r$	-0.1329	0.0013	0.1356	Not significant
$\mathbf{AR}_s\mathbf{p}_6$	-0.1292	0.005	0.1393	Not significant
Parameter: AR_r				
Interaction effect	IC lower bound	Coefficient	IC upper bound	Relevance
$\mathbf{AR}_r\mathbf{r}_{ht,1}$	-0.2669	-0.1327	0.0016	Not significant
$\mathbf{AR}_r\mathbf{r}_{ht,3}$	-1.5986	-1.4644	-1.3301	Significant
$\mathbf{AR}_r\mathbf{r}_{ht,4}$	0.8079	0.9422	1.0764	Significant
$\mathbf{AR}_r\mathbf{r}_{ht,6}$	1.2742	1.4084	1.5427	Significant
$\mathbf{AR}_r(\mathbf{t}_{te}/\mathbf{o})_s$	-0.0395	0.0948	0.229	Not significant
$\mathbf{AR}_r(\mathbf{t}_{te}/\mathbf{o})_r$	-0.0242	0.1101	0.2443	Not significant
$\mathbf{AR}_r\mathbf{p}_6$	0.0142	0.1484	0.2827	Significant
Parameter: $\mathrm{r}_{ht,1}$				
Interaction effect	IC lower bound	Coefficient	IC upper bound	Relevance
$\mathbf{r}_{ht,1}\mathbf{r}_{ht,3}$	-0.0593	0.075	0.2092	Not significant
$\mathbf{r}_{ht,1}\mathbf{r}_{ht,4}$	-0.0061	0.1282	0.2624	Not significant
$\mathbf{r}_{ht,1}\mathbf{r}_{ht,6}$	0.1803	0.3145	0.4488	Significant
$\mathbf{r}_{ht,1}(\mathbf{t}_{te}/\mathbf{o})_s$	0.0232	0.1575	0.2918	Significant
$\mathbf{r}_{ht,1}(\mathbf{t}_{te}/\mathbf{o})_r$	0.0086	0.1428	0.2771	Significant
$\mathbf{r}_{ht,1}\mathbf{p}_6$	-0.0442	0.0901	0.2243	Not significant
Parameter: $\mathrm{r}_{ht,3}$				
Interaction effect	IC lower bound	Coefficient	IC upper bound	Relevance
$\mathbf{r}_{ht,3}\mathbf{r}_{ht,4}$	0.5791	0.7133	0.8476	Significant
$\mathbf{r}_{ht,3}\mathbf{r}_{ht,6}$	4.9118	5.046	5.1803	Significant
$\mathbf{r}_{ht,3}(\mathbf{t}_{te}/\mathbf{o})_s$	-0.5315	-0.3973	-0.263	Significant
$\mathbf{r}_{ht,3}(\mathbf{t}_{te}/\mathbf{o})_r$	0.2995	0.4337	0.568	Significant

Interaction effect	IC lower bound	Coefficient	IC upper bound	Relevance
$\mathbf{r}_{ht,3}\mathbf{p}_6$	-0.791	-0.6568	-0.5225	Significant
Parameter: $\mathrm{r}_{ht,4}$				
Interaction effect	IC lower bound	Coefficient	IC upper bound	Relevance
$\mathbf{r}_{ht,4}\mathbf{r}_{ht,6}$	-0.8251	-0.6909	-0.5566	Significant
$\mathbf{r}_{ht,4}(\mathrm{t}_{te}/\mathrm{o})_s$	-0.2447	-0.1104	0.0239	Not significant
$\mathbf{r}_{ht,4}(\mathbf{t}_{te}/\mathbf{o})_r$	-0.1995	-0.0652	0.0691	Not significant
$\mathbf{r}_{ht,4}\mathbf{p}_6$	-0.2552	-0.121	0.0133	Not significant
Parameter: $\mathrm{r}_{ht,6}$				
Interaction effect	IC lower bound	Coefficient	IC upper bound	Relevance
$\mathbf{r}_{ht,6}(\mathbf{t}_{te}/\mathbf{o})_s$	0.4128	0.547	0.6813	Significant
$\mathbf{r}_{ht,6}(\mathbf{t}_{te}/\mathbf{o})_r$	-0.6297	-0.4954	-0.3612	Significant
$\mathbf{r}_{ht,6}\mathbf{p}_6$	1.0427	1.1769	1.3112	Significant
Parameter: $(\mathrm{t}_{te}/\mathrm{o})_s$				
Interaction effect	IC lower bound	Coefficient	IC upper bound	Relevance
$(\mathbf{t}_{te}/\mathbf{o})_s(\mathbf{t}_{te}/\mathbf{o})_r$	-0.2353	-0.1011	0.0332	Not significant
$(\mathbf{t}_{te}/\mathbf{o})_s\mathbf{p}_6$	-0.4489	-0.3146	-0.1804	Significant
Parameter: $(\mathrm{t}_{te}/\mathrm{o})_r$				
Interaction effect	IC lower bound	Coefficient	IC upper bound	Relevance
$(\mathbf{t}_{te}/\mathbf{o})_r\mathbf{p}_6$	-0.3595	-0.2253	-0.091	Significant

A.4 Results for the coefficients and confidence intervals of the main, interaction and quadratic effects in experiment 4

The results from experiment 4, with 12 factors, are shown in Table A.13. Main, quadratic and interaction effects are respectively in Table A.14, A.15 and A.16.

Table A.13: Results of Experiment 4 - Faced central composite design with 12 factors. Significant effects highlighted in pink.

Main effects											
$\mathbf{BS}_s$	$\mathbf{BS}_r$	$\mathbf{AR}_s$	$\mathbf{AR}_r$	$\mathbf{r}_{ht1}$	$\mathbf{r}_{ht3}$	$\mathbf{r}_{ht4}$	$\mathbf{r}_{ht6}$	$(\mathbf{t}_{te}/\mathbf{o})_s$	$(\mathbf{t}_{te}/\mathbf{o})_r$	$\mathbf{d}_{spe}$	$\mathbf{p}_6$
$-3.2478\cdot10^{-2}$	$-1.9346\cdot10^{-1}$	$1.6921\cdot10^{-2}$	1.8158	$-1.6202\cdot10^{-1}$	3.5783	$-8.0996\cdot10^{-1}$	-4.4578	-1.2736	-1.7344	$-7.1845\cdot10^{-1}$	$5.5926\cdot10^{-1}$
Interaction effects											
	$\mathbf{BS}_s\mathbf{BS}_r$	$\mathbf{BS}_s\mathbf{AR}_s$	$\mathbf{BS}_s\mathbf{AR}_r$	$\mathbf{BS}_s\mathbf{r}_{ht1}$	$\mathbf{BS}_s\mathbf{r}_{ht3}$	$\mathbf{BS}_s\mathbf{r}_{ht4}$	$\mathbf{BS}_s\mathbf{r}_{ht6}$	$\mathbf{BS}_s(\mathbf{t}_{te}/\mathbf{o})_s$	$\mathbf{BS}_s(\mathbf{t}_{te}/\mathbf{o})_r$	$\mathbf{BS}_s\mathbf{d}_{spe}$	$\mathbf{BS}_s\mathbf{p}_6$
	$-8.0736\cdot10^{-3}$	$3.9053\cdot10^{-2}$	$1.2608\cdot10^{-2}$	$-1.3723\cdot10^{-2}$	$3.5157\cdot10^{-2}$	$-1.2547\cdot10^{-2}$	$-2.5147\cdot10^{-2}$	$-2.7459\cdot10^{-2}$	$-1.2468\cdot10^{-2}$	$-1.3030\cdot10^{-2}$	$-1.4685\cdot10^{-2}$
		$\mathbf{BS}_r\mathbf{AR}_s$	$\mathbf{BS}_r\mathbf{AR}_r$	$\mathbf{BS}_r\mathbf{r}_{ht1}$	$\mathbf{BS}_r\mathbf{r}_{ht3}$	$\mathbf{BS}_r\mathbf{r}_{ht4}$	$\mathbf{BS}_r\mathbf{r}_{ht6}$	$\mathbf{BS}_r(\mathbf{t}_{te}/\mathbf{o})_s$	$\mathbf{BS}_r(\mathbf{t}_{te}/\mathbf{o})_r$	$\mathbf{BS}_r\mathbf{d}_{spe}$	$\mathbf{BS}_r\mathbf{p}_6$
		$-1.2304\cdot10^{-2}$	$9.2731\cdot10^{-2}$	$-7.5387\cdot10^{-3}$	$1.0539\cdot10^{-1}$	$-4.0674\cdot10^{-2}$	$-1.2053\cdot10^{-1}$	$-4.3405\cdot10^{-2}$	$-1.1857\cdot10^{-1}$	$-5.2440\cdot10^{-2}$	$-4.0493\cdot10^{-2}$
			$\mathbf{AR}_s\mathbf{AR}_r$	$\mathbf{AR}_s\mathbf{r}_{ht1}$	$\mathbf{AR}_s\mathbf{r}_{ht3}$	$\mathbf{AR}_s\mathbf{r}_{ht4}$	$\mathbf{AR}_s\mathbf{r}_{ht6}$	$\mathbf{AR}_s(\mathbf{t}_{te}/\mathbf{o})_s$	$\mathbf{AR}_s(\mathbf{t}_{te}/\mathbf{o})_r$	$\mathbf{AR}_s\mathbf{d}_{spe}$	$\mathbf{AR}_s\mathbf{p}_6$
			$7.4255\cdot10^{-3}$	$1.3536\cdot10^{-2}$	$1.4596\cdot10^{-2}$	$-7.7482\cdot10^{-3}$	$1.0846\cdot10^{-2}$	$1.9556\cdot10^{-2}$	$-6.9240\cdot10^{-3}$	$-7.3291\cdot10^{-3}$	$-2.9237\cdot10^{-3}$
				$\mathbf{AR}_r\mathbf{r}_{ht1}$	$\mathbf{AR}_r\mathbf{r}_{ht3}$	$\mathbf{AR}_r\mathbf{r}_{ht4}$	$\mathbf{AR}_r\mathbf{r}_{ht6}$	$\mathbf{AR}_r(\mathbf{t}_{te}/\mathbf{o})_s$	$\mathbf{AR}_r(\mathbf{t}_{te}/\mathbf{o})_r$	$\mathbf{AR}_r\mathbf{d}_{spe}$	$\mathbf{AR}_r\mathbf{p}_6$
				$-3.7127\cdot10^{-2}$	-1.0767	$6.9213\cdot10^{-1}$	1.0228	$6.7814\cdot10^{-2}$	$1.5935\cdot10^{-1}$	$5.6471\cdot10^{-1}$	$1.6533\cdot10^{-1}$
					$\mathbf{r}_{ht1}\mathbf{r}_{ht3}$	$\mathbf{r}_{ht1}\mathbf{r}_{ht4}$	$\mathbf{r}_{ht1}\mathbf{r}_{ht6}$	$\mathbf{r}_{ht1}(\mathbf{t}_{te}/\mathbf{o})_s$	$\mathbf{r}_{ht1}(\mathbf{t}_{te}/\mathbf{o})_r$	$\mathbf{r}_{ht1}\mathbf{d}_{spe}$	$\mathbf{r}_{ht1}\mathbf{p}_6$
					$1.7895\cdot10^{-1}$	$3.2548\cdot10^{-2}$	$1.9491\cdot10^{-1}$	$2.3262\cdot10^{-2}$	$4.5468\cdot10^{-2}$	$1.5210\cdot10^{-2}$	$-4.9027\cdot10^{-3}$
						$\mathbf{r}_{ht3}\mathbf{r}_{ht4}$	$\mathbf{r}_{ht3}\mathbf{r}_{ht6}$	$\mathbf{r}_{ht3}(\mathbf{t}_{te}/\mathbf{o})_s$	$\mathbf{r}_{ht3}(\mathbf{t}_{te}/\mathbf{o})_r$	$\mathbf{r}_{ht3}\mathbf{d}_{spe}$	$\mathbf{r}_{ht3}\mathbf{p}_6$
						$4.4051\cdot10^{-1}$	4.3545	$-3.9478\cdot10^{-1}$	$4.5749\cdot10^{-1}$	$6.6199\cdot10^{-1}$	$-6.1850\cdot10^{-1}$
							$\mathbf{r}_{ht4}\mathbf{r}_{ht6}$	$\mathbf{r}_{ht4}(\mathrm{t}_{te}/\mathrm{o})_s$	$\mathbf{r}_{ht4}(\mathbf{t}_{te}/\mathbf{o})_r$	$\mathbf{r}_{ht4}\mathbf{d}_{spe}$	$\mathbf{r}_{ht4}\mathbf{p}_6$
							$-4.3456\cdot10^{-1}$	$-8.2241\cdot10^{-2}$	$-1.2510\cdot10^{-1}$	$-3.1827\cdot10^{-1}$	$-1.339\cdot10^{-1}$
								$\mathbf{r}_{ht6}(\mathbf{t}_{te}/\mathbf{o})_s$	$\mathbf{r}_{ht6}(\mathbf{t}_{te}/\mathbf{o})_r$	$\mathbf{r}_{ht6}\mathbf{d}_{spe}$	$\mathbf{r}_{ht6}\mathbf{p}_6$
								$5.4195\cdot10^{-1}$	$-5.1050\cdot10^{-1}$	$-4.8427\cdot10^{-1}$	1.1009
									$(\mathbf{t}_{te}/\mathbf{o})_s(\mathbf{t}_{te}/\mathbf{o})_r$	$(\mathbf{t}_{te}/\mathbf{o})_s\mathbf{d}_{spe}$	$(\mathbf{t}_{te}/\mathbf{o})_s\mathbf{p}_6$
									$-6.6676\cdot10^{-2}$	$-1.4047\cdot10^{-1}$	$-2.7769\cdot10^{-1}$
										$(\mathbf{t}_{te}/\mathbf{o})_r\mathbf{d}_{spe}$	$(\mathbf{t}_{te}/\mathbf{o})_r\mathbf{p}_6$
										$-1.5727\cdot10^{-1}$	$-2.2692\cdot10^{-1}$
											$\mathbf{d}_{spe}\mathbf{p}_6$
											$-3.7973\cdot10^{-1}$
Quadratic effects											
$\mathbf{BS}_s^2$	$\mathbf{BS}_r^2$	$\mathbf{AR}_s^2$	$\mathbf{AR}_r^2$	$\mathbf{r}_{ht1}^2$	$\mathbf{r}_{ht3}^2$	$\mathbf{r}_{ht4}^2$	$\mathbf{r}_{ht6}^2$	$(\mathbf{t}_{te}/\mathbf{o})_s^2$	$(\mathbf{t}_{te}/\mathbf{o})_r^2$	$\mathbf{d}_{spe}^2$	$\mathbf{p}_6^2$
$-2.6748\cdot10^{-1}$	$-3.6700\cdot10^{-1}$	$-2.0834\cdot10^{-1}$	$-5.7605\cdot10^{-1}$	$-2.0186\cdot10^{-1}$	$-9.1725\cdot10^{-1}$	$-2.5472\cdot10^{-1}$	-2.2472	$-6.5339\cdot10^{-1}$	$-8.8208\cdot10^{-1}$	$-2.9790\cdot10^{-1}$	$-5.4449\cdot10^{-1}$

Table A.14: Confidence interval and relevance of the main effects in experiment 4. Significant effects highlighted in grey.

Main effect	IC lower bound	Coefficient	IC upper bound	Relevance
$\mathbf{BS}_s$	-0.1316	-0.0325	0.0666	Not significant
$\mathbf{BS}_r$	-0.2926	-0.1935	-0.0944	Significant
$\mathbf{AR}_s$	-0.0822	0.0169	0.116	Not significant
$\mathbf{AR}_r$	1.7168	1.8159	1.915	Significant
$\mathbf{r}_{ht1}$	-0.2611	-0.162	-0.0629	Significant
$\mathbf{r}_{ht3}$	3.4793	3.5784	3.6775	Significant
$\mathbf{r}_{ht4}$	-0.9091	-0.81	-0.7109	Significant
$\mathbf{r}_{ht6}$	-4.5569	-4.4578	-4.3587	Significant
$(\mathbf{t}_{te}/\mathbf{o})_s$	-1.3728	-1.2737	-1.1746	Significant
$(\mathbf{t}_{te}/\mathbf{o})_r$	-1.8336	-1.7345	-1.6354	Significant
$\mathbf{d}_{spe}$	-0.8176	-0.7185	-0.6194	Significant
$\mathbf{p}_6$	0.4602	0.5593	0.6584	Significant

Table A.15: Confidence interval and relevance of the quadratic effects in experiment 4

Quadratic effect	IC lower bound	Coefficient	IC upper bound	Relevance
$\mathbf{BS}_s^2$	-4.5639	-0.2675	4.029	Not significant
$\mathbf{BS}_r^2$	-4.6635	-0.367	3.9295	Not significant
$\mathbf{AR}_s^2$	-4.5048	-0.2083	4.0881	Not significant
$\mathbf{AR}_r^2$	-4.8725	-0.5761	3.7204	Not significant
$\mathbf{r}_{ht1}^2$	-4.4983	-0.2019	4.0946	Not significant
$\mathbf{r}_{ht3}^2$	-5.2137	-0.9173	3.3792	Not significant
$\mathbf{r}_{ht4}^2$	-4.5512	-0.2547	4.0417	Not significant
$\mathbf{r}_{ht6}^2$	-6.5437	-2.2472	2.0493	Not significant
$(\mathbf{t}_{te}/\mathbf{o})_s^2$	-4.9499	-0.6534	3.6431	Not significant
$(\mathbf{t}_{te}/\mathbf{o})_r^2$	-5.1785	-0.8821	3.4144	Not significant
$\mathbf{d}_{spe}^2$	-4.5944	-0.2979	3.9986	Not significant
$\mathbf{p}_6^2$	-4.841	-0.5445	3.752	Not significant

Table A.16: Confidence interval and relevance of the interaction effects in experiment 4. Significant effects highlighted in pink.

Parameter: BS_s				
Interaction effect	IC lower bound	Coefficient	IC upper bound	Relevance
$\mathbf{BS}_s\mathbf{BS}_r$	-0.1072	-0.0081	0.0911	Not significant
$\mathbf{BS}_s\mathbf{AR}_s$	-0.0601	0.0391	0.1382	Not significant
$\mathbf{BS}_s\mathbf{AR}_r$	-0.0865	0.0126	0.1117	Not significant
$\mathbf{BS}_s\mathbf{r}_{ht1}$	-0.1128	-0.0137	0.0854	Not significant
$\mathbf{BS}_s\mathbf{r}_{ht3}$	-0.064	0.0352	0.1343	Not significant
$\mathbf{BS}_s\mathbf{r}_{ht4}$	-0.1117	-0.0125	0.0866	Not significant
$\mathbf{BS}_s\mathbf{r}_{ht6}$	-0.1243	-0.0251	0.074	Not significant

Interaction effect	IC lower bound	Coefficient	IC upper bound	Relevance
$\mathbf{BS}_s(\mathbf{t}_{te}/\mathbf{o})_s$	-0.1266	-0.0275	0.0717	Not significant
$\mathbf{BS}_s(\mathbf{t}_{te}/\mathbf{o})_r$	-0.1116	-0.0125	0.0867	Not significant
$\mathbf{BS}_s\mathbf{d}_{spe}$	-0.1122	-0.013	0.0861	Not significant
$\mathbf{BS}_s\mathbf{p}_6$	-0.1138	-0.0147	0.0844	Not significant
Parameter: BS_r				
Interaction effect	IC lower bound	Coefficient	IC upper bound	Relevance
$\mathbf{BS}_r\mathbf{AR}_s$	-0.1114	-0.0123	0.0868	Not significant
$\mathbf{BS}_r\mathbf{AR}_r$	-0.0064	0.0927	0.1919	Not significant
$\mathbf{BS}_r\mathbf{r}_{ht1}$	-0.1067	-0.0075	0.0916	Not significant
$\mathbf{BS}_r\mathbf{r}_{ht3}$	0.0063	0.1054	0.2045	Significant
$\mathbf{BS}_r\mathbf{r}_{ht4}$	-0.1398	-0.0407	0.0585	Not significant
$\mathbf{BS}_r\mathbf{r}_{ht6}$	-0.2197	-0.1205	-0.0214	Significant
$\mathbf{BS}_r(\mathbf{t}_{te}/\mathbf{o})_s$	-0.1425	-0.0434	0.0557	Not significant
$\mathbf{BS}_r(\mathbf{t}_{te}/\mathbf{o})_r$	-0.2177	-0.1186	-0.0195	Significant
$\mathbf{BS}_r\mathbf{d}_{spe}$	-0.1516	-0.0524	0.0467	Not significant
$\mathbf{BS}_r\mathbf{p}_6$	-0.1396	-0.0405	0.0586	Not significant
Parameter: AR_s				
Interaction effect	IC lower bound	Coefficient	IC upper bound	Relevance
$\mathbf{AR}_s\mathbf{AR}_r$	-0.0917	0.0074	0.1066	Not significant
$\mathbf{AR}_s\mathbf{r}_{ht1}$	-0.0856	0.0135	0.1127	Not significant
$\mathbf{AR}_s\mathbf{r}_{ht3}$	-0.0845	0.0146	0.1137	Not significant
$\mathbf{AR}_s\mathbf{r}_{ht4}$	-0.1069	-0.0077	0.0914	Not significant
$\mathbf{AR}_s\mathbf{r}_{ht6}$	-0.0883	0.0108	0.11	Not significant
$\mathbf{AR}_s(\mathbf{t}_{te}/\mathbf{o})_s$	-0.0796	0.0196	0.1187	Not significant
$\mathbf{AR}_s(\mathbf{t}_{te}/\mathbf{o})_r$	-0.106	-0.0069	0.0922	Not significant
$\mathbf{AR}_s\mathbf{d}_{spe}$	-0.1065	-0.0073	0.0918	Not significant
$\mathbf{AR}_s\mathbf{p}_6$	-0.102	-0.0029	0.0962	Not significant
Parameter: AR_r				
Interaction effect	IC lower bound	Coefficient	IC upper bound	Relevance
$\mathbf{AR}_r\mathbf{r}_{ht1}$	-0.1363	-0.0371	0.062	Not significant
$\mathbf{AR}_r\mathbf{r}_{ht3}$	-1.1759	-1.0768	-0.9776	Significant
$\mathbf{AR}_r\mathbf{r}_{ht4}$	0.593	0.6921	0.7913	Significant
$\mathbf{AR}_r\mathbf{r}_{ht6}$	0.9237	1.0229	1.122	Significant
$\mathbf{AR}_r(\mathbf{t}_{te}/\mathbf{o})_s$	-0.0313	0.0678	0.1669	Not significant
$\mathbf{AR}_r(\mathbf{t}_{te}/\mathbf{o})_r$	0.0602	0.1594	0.2585	Significant
$\mathbf{AR}_r\mathbf{d}_{spe}$	0.4656	0.5647	0.6638	Significant
$\mathbf{AR}_r\mathbf{p}_6$	0.0662	0.1653	0.2645	Significant
Parameter: r_{ht1}				
Interaction effect	IC lower bound	Coefficient	IC upper bound	Relevance
$\mathbf{r}_{ht1}\mathbf{r}_{ht3}$	0.0798	0.179	0.2781	Significant
$\mathbf{r}_{ht1}\mathbf{r}_{ht4}$	-0.0666	0.0325	0.1317	Not significant
$\mathbf{r}_{ht1}\mathbf{r}_{ht6}$	0.0958	0.1949	0.294	Significant
$\mathbf{r}_{ht1}(\mathbf{t}_{te}/\mathbf{o})_s$	-0.0759	0.0233	0.1224	Not significant
$\mathbf{r}_{ht1}(\mathbf{t}_{te}/\mathbf{o})_r$	-0.0537	0.0455	0.1446	Not significant
$\mathbf{r}_{ht1}\mathbf{d}_{spe}$	-0.0839	0.0152	0.1143	Not significant
$\mathbf{r}_{ht1}\mathbf{p}_6$	-0.104	-0.0049	0.0942	Not significant
Parameter: r_{ht3}				

Interaction effect	IC lower bound	Coefficient	IC upper bound	Relevance
$\mathbf{r}_{ht3}\mathbf{r}_{ht4}$	0.3414	0.4405	0.5396	Significant
$\mathbf{r}_{ht3}\mathbf{r}_{ht6}$	4.2555	4.3546	4.4537	Significant
$\mathbf{r}_{ht3}(\mathbf{t}_{te}/\mathbf{o})_s$	-0.4939	-0.3948	-0.2957	Significant
$\mathbf{r}_{ht3}(\mathbf{t}_{te}/\mathbf{o})_r$	0.3584	0.4575	0.5566	Significant
$\mathbf{r}_{ht3}\mathbf{d}_{spe}$	0.5629	0.662	0.7611	Significant
$\mathbf{r}_{ht3}\mathbf{p}_6$	-0.7176	-0.6185	-0.5194	Significant
Parameter: r_{ht4}				
Interaction effect	IC lower bound	Coefficient	IC upper bound	Relevance
$\mathbf{r}_{ht4}\mathbf{r}_{ht6}$	-0.5337	-0.4346	-0.3354	Significant
$\mathbf{r}_{ht4}(\mathrm{t}_{te}/\mathrm{o})_s$	-0.1814	-0.0822	0.0169	Not significant
$\mathbf{r}_{ht4}(\mathbf{t}_{te}/\mathbf{o})_r$	-0.2242	-0.1251	-0.026	Significant
$\mathbf{r}_{ht4}\mathbf{d}_{spe}$	-0.4174	-0.3183	-0.2191	Significant
$\mathbf{r}_{ht4}\mathbf{p}_6$	-0.233	-0.1339	-0.0348	Significant
Parameter: r_{ht6}				
Interaction effect	IC lower bound	Coefficient	IC upper bound	Relevance
$\mathbf{r}_{ht6}(\mathbf{t}_{te}/\mathbf{o})_s$	0.4428	0.542	0.6411	Significant
$\mathbf{r}_{ht6}(\mathbf{t}_{te}/\mathbf{o})_r$	-0.6096	-0.5105	-0.4114	Significant
$\mathbf{r}_{ht6}\mathbf{d}_{spe}$	-0.5834	-0.4843	-0.3851	Significant
$\mathbf{r}_{ht6}\mathbf{p}_6$	1.0018	1.1009	1.2	Significant
Parameter: $(\mathrm{t}_{te}/\mathrm{o})_s$				
Interaction effect	IC lower bound	Coefficient	IC upper bound	Relevance
$(\mathbf{t}_{te}/\mathbf{o})_s(\mathbf{t}_{te}/\mathbf{o})_r$	-0.1658	-0.0667	0.0324	Not significant
$(\mathbf{t}_{te}/\mathbf{o})_s\mathbf{d}_{spe}$	-0.2396	-0.1405	-0.0413	Significant
$(\mathbf{t}_{te}/\mathbf{o})_s\mathbf{p}_6$	-0.3768	-0.2777	-0.1786	Significant
Parameter: $(\mathrm{t}_{te}/\mathrm{o})_r$				
Interaction effect	IC lower bound	Coefficient	IC upper bound	Relevance
$(\mathbf{t}_{te}/\mathbf{o})_r\mathbf{d}_{spe}$	-0.2564	-0.1573	-0.0582	Significant
$(\mathbf{t}_{te}/\mathbf{o})_r\mathbf{p}_6$	-0.3261	-0.2269	-0.1278	Significant
Parameter: d_{spe}				
Interaction effect	IC lower bound	Coefficient	IC upper bound	Relevance
$\mathbf{d}_{spe}\mathbf{p}_6$	-0.4789	-0.3797	-0.2806	Significant

A.5 Results for the coefficients and confidence intervals of the main, interaction and quadratic effects in experiment 5

Results from the 13-factor experiment are shown in Table A.17. Main, quadratic and interaction effects are divided in Table A.18, Table A.19 and Table A.20.

Table A.17: Results of Experiment 5 - Faced central composite design with 13 factors.

Main effects												
$\mathbf{BS}_s$	$\mathbf{BS}_r$	$\mathbf{AR}_s$	$\mathbf{AR}_r$	$\mathbf{r}_{ht1}$	$\mathbf{r}_{ht3}$	$\mathbf{r}_{ht4}$	$\mathbf{r}_{ht6}$	$(\mathbf{t}_{te}/\mathbf{o})_s$	$(\mathbf{t}_{te}/\mathbf{o})_r$	$\mathbf{d}_{spe}$	θ_1	$\mathbf{p}_6$
$-2.8966 \cdot 10^{-2}$	$-1.9344 \cdot 10^{-1}$	$2.0018 \cdot 10^{-2}$	1.8162	$-1.6280 \cdot 10^{-1}$	3.5772	$-8.1011 \cdot 10^{-1}$	-4.4552	-1.2290	-1.7346	$-7.1888 \cdot 10^{-1}$	$-7.3178 \cdot 10^{-3}$	$5.5919 \cdot 10^{-1}$
Interaction effects												
	$\mathbf{BS}_s\mathbf{BS}_r$	$\mathbf{BS}_s\mathbf{AR}_s$	$\mathbf{BS}_s\mathbf{AR}_r$	$\mathbf{BS}_s\mathbf{r}_{ht1}$	$\mathbf{BS}_s\mathbf{r}_{ht3}$	$\mathbf{BS}_s\mathbf{r}_{ht4}$	$\mathbf{BS}_s\mathbf{r}_{ht6}$	$\mathbf{BS}_s(\mathbf{t}_{te}/\mathbf{o})_s$	$\mathbf{BS}_s(\mathbf{t}_{te}/\mathbf{o})_r$	$\mathbf{BS}_s\mathbf{d}_{spe}$	$\mathbf{BS}_s\theta_1$	$\mathbf{BS}_s\mathbf{p}_6$
	$-1.8568 \cdot 10^{-2}$	$1.1106 \cdot 10^{-2}$	$-3.8417 \cdot 10^{-2}$	$-2.5067 \cdot 10^{-2}$	$-1.0220 \cdot 10^{-2}$	$3.8681 \cdot 10^{-2}$	$2.0716 \cdot 10^{-2}$	$-1.6579 \cdot 10^{-2}$	$3.8507 \cdot 10^{-2}$	$3.8603 \cdot 10^{-2}$	$-4.6067 \cdot 10^{-2}$	$3.7140 \cdot 10^{-2}$
		$\mathbf{BS}_r\mathbf{AR}_s$	$\mathbf{BS}_r\mathbf{AR}_r$	$\mathbf{BS}_r\mathbf{r}_{ht1}$	$\mathbf{BS}_r\mathbf{r}_{ht3}$	$\mathbf{BS}_r\mathbf{r}_{ht4}$	$\mathbf{BS}_r\mathbf{r}_{ht6}$	$\mathbf{BS}_r(\mathbf{t}_{te}/\mathbf{o})_s$	$\mathbf{BS}_r(\mathbf{t}_{te}/\mathbf{o})_r$	$\mathbf{BS}_r\mathbf{d}_{spe}$	$\mathbf{BS}_r\theta_1$	$\mathbf{BS}_r\mathbf{p}_6$
		$-1.0169 \cdot 10^{-2}$	$9.2668 \cdot 10^{-2}$	$-2.8128 \cdot 10^{-2}$	$1.0533 \cdot 10^{-1}$	$-4.0607 \cdot 10^{-2}$	$-1.2047 \cdot 10^{-1}$	$-4.3660 \cdot 10^{-2}$	$-1.1858 \cdot 10^{-1}$	$-5.2376 \cdot 10^{-2}$	$1.2225 \cdot 10^{-2}$	$-4.0575 \cdot 10^{-2}$
			$\mathbf{AR}_s\mathbf{AR}_r$	$\mathbf{AR}_s\mathbf{r}_{ht1}$	$\mathbf{AR}_s\mathbf{r}_{ht3}$	$\mathbf{AR}_s\mathbf{r}_{ht4}$	$\mathbf{AR}_s\mathbf{r}_{ht6}$	$\mathbf{AR}_s(\mathbf{t}_{te}/\mathbf{o})_s$	$\mathbf{AR}_s(\mathbf{t}_{te}/\mathbf{o})_r$	$\mathbf{AR}_s\mathbf{d}_{spe}$	$\mathbf{AR}_s\theta_1$	$\mathbf{AR}_s\mathbf{p}_6$
			$-1.0847 \cdot 10^{-2}$	$-4.9136 \cdot 10^{-3}$	$1.3036 \cdot 10^{-2}$	$1.0540 \cdot 10^{-2}$	$1.2419 \cdot 10^{-2}$	$1.6216 \cdot 10^{-3}$	$1.1330 \cdot 10^{-2}$	$1.0996 \cdot 10^{-2}$	$1.0513 \cdot 10^{-2}$	$1.5501 \cdot 10^{-2}$
				$\mathbf{AR}_r\mathbf{r}_{ht1}$	$\mathbf{AR}_r\mathbf{r}_{ht3}$	$\mathbf{AR}_r\mathbf{r}_{ht4}$	$\mathbf{AR}_r\mathbf{r}_{ht6}$	$\mathbf{AR}_r(\mathbf{t}_{te}/\mathbf{o})_s$	$\mathbf{AR}_r(\mathbf{t}_{te}/\mathbf{o})_r$	$\mathbf{AR}_r\mathbf{d}_{spe}$	$\mathbf{AR}_r\theta_1$	$\mathbf{AR}_r\mathbf{p}_6$
				$-3.7219 \cdot 10^{-2}$	-1.0767	$6.9217 \cdot 10^{-1}$	1.0228	$6.8764 \cdot 10^{-2}$	$1.5935 \cdot 10^{-1}$	$5.6473 \cdot 10^{-1}$	$-7.4769 \cdot 10^{-3}$	$1.6511 \cdot 10^{-1}$
					$\mathbf{r}_{ht1}\mathbf{r}_{ht3}$	$\mathbf{r}_{ht1}\mathbf{r}_{ht4}$	$\mathbf{r}_{ht1}\mathbf{r}_{ht6}$	$\mathbf{r}_{ht1}(\mathbf{t}_{te}/\mathbf{o})_s$	$\mathbf{r}_{ht1}(\mathbf{t}_{te}/\mathbf{o})_r$	$\mathbf{r}_{ht1}\mathbf{d}_{spe}$	$\mathbf{r}_{ht1}\theta_1$	$\mathbf{r}_{ht1}\mathbf{p}_6$
					$1.7933 \cdot 10^{-1}$	$3.2639 \cdot 10^{-2}$	$1.9565 \cdot 10^{-1}$	$4.2583 \cdot 10^{-2}$	$4.5557 \cdot 10^{-2}$	$1.5296 \cdot 10^{-2}$	$-1.1655 \cdot 10^{-2}$	$-4.9540 \cdot 10^{-3}$
						$\mathbf{r}_{ht3}\mathbf{r}_{ht4}$	$\mathbf{r}_{ht3}\mathbf{r}_{ht6}$	$\mathbf{r}_{ht3}(\mathbf{t}_{te}/\mathbf{o})_s$	$\mathbf{r}_{ht3}(\mathbf{t}_{te}/\mathbf{o})_r$	$\mathbf{r}_{ht3}\mathbf{d}_{spe}$	$\mathbf{r}_{ht3}\theta_1$	$\mathbf{r}_{ht3}\mathbf{p}_6$
						$4.4052 \cdot 10^{-1}$	4.3578	$-3.7542 \cdot 10^{-1}$	$4.5746 \cdot 10^{-1}$	$6.6191 \cdot 10^{-1}$	$1.6760 \cdot 10^{-2}$	$-6.1917 \cdot 10^{-1}$
							$\mathbf{r}_{ht4}\mathbf{r}_{ht6}$	$\mathbf{r}_{ht4}(\mathrm{t}_{te}/\mathrm{o})_s$	$\mathbf{r}_{ht4}(\mathbf{t}_{te}/\mathbf{o})_r$	$\mathbf{r}_{ht4}\mathbf{d}_{spe}$	$\mathbf{r}_{ht4}\theta_1$	$\mathbf{r}_{ht4}\mathbf{p}_6$
							$-4.3456 \cdot 10^{-1}$	$-8.2664 \cdot 10^{-2}$	$-1.2512 \cdot 10^{-1}$	$-3.1826 \cdot 10^{-1}$	$7.7606 \cdot 10^{-3}$	$-1.3373 \cdot 10^{-1}$
								$\mathbf{r}_{ht6}(\mathbf{t}_{te}/\mathbf{o})_s$	$\mathbf{r}_{ht6}(\mathbf{t}_{te}/\mathbf{o})_r$	$\mathbf{r}_{ht6}\mathbf{d}_{spe}$	$\mathbf{r}_{ht6}\theta_1$	$\mathbf{r}_{ht6}\mathbf{p}_6$
								$5.1694 \cdot 10^{-1}$	$-5.1051 \cdot 10^{-1}$	$-4.8413 \cdot 10^{-1}$	$-1.1300 \cdot 10^{-2}$	1.1020
									$(\mathbf{t}_{te}/\mathbf{o})_s(\mathbf{t}_{te}/\mathbf{o})_r$	$(\mathbf{t}_{te}/\mathbf{o})_s\mathbf{d}_{spe}$	$(\mathbf{t}_{te}/\mathbf{o})_s\theta_1$	$(\mathbf{t}_{te}/\mathbf{o})_s\mathbf{p}_6$
									$-6.7575 \cdot 10^{-2}$	$-1.3867 \cdot 10^{-1}$	$-9.8514 \cdot 10^{-2}$	$-2.7046 \cdot 10^{-1}$
										$(\mathbf{t}_{te}/\mathbf{o})_r\mathbf{d}_{spe}$	$(\mathbf{t}_{te}/\mathbf{o})_r\theta_1$	$(\mathbf{t}_{te}/\mathbf{o})_r\mathbf{p}_6$
										$-1.5732 \cdot 10^{-1}$	$7.4928 \cdot 10^{-3}$	$-2.2685 \cdot 10^{-1}$
											$\mathbf{d}_{spe}\theta_1$	$\mathbf{d}_{spe}\mathbf{p}_6$
											$7.4431 \cdot 10^{-3}$	$-3.7959 \cdot 10^{-1}$
												$\theta_1\mathbf{p}_6$
												$4.1365 \cdot 10^{-3}$
Quadratic effects												
$\mathbf{BS}_s^2$	$\mathbf{BS}_r^2$	$\mathbf{AR}_s^2$	$\mathbf{AR}_r^2$	$\mathbf{r}_{ht1}^2$	$\mathbf{r}_{ht3}^2$	$\mathbf{r}_{ht4}^2$	$\mathbf{r}_{ht6}^2$	$(\mathbf{t}_{te}/\mathbf{o})_s^2$	$(\mathbf{t}_{te}/\mathbf{o})_r^2$	$\mathbf{d}_{spe}^2$	θ_1^2	$\mathbf{p}_6^2$
$-2.4750 \cdot 10^{-1}$	$-3.5042 \cdot 10^{-1}$	$-1.9212 \cdot 10^{-1}$	$-5.5943 \cdot 10^{-1}$	$-1.8804 \cdot 10^{-1}$	$-8.9826 \cdot 10^{-1}$	$-2.3803 \cdot 10^{-1}$	-2.2285	$-6.3353 \cdot 10^{-1}$	$-8.6557 \cdot 10^{-1}$	$-2.8119 \cdot 10^{-1}$	$-2.0495 \cdot 10^{-1}$	$-5.2765 \cdot 10^{-1}$

Table A.18: Confidence interval for the main effects in experiment 5. Significant effects highlighted in grey.

Main effect	IC lower bound	Coefficient	IC upper bound	Relevance
$\mathbf{BS}_s$	-0.0408	0.029	0.0988	Not significant
$\mathbf{BS}_r$	-0.2632	-0.1934	-0.1237	Significant
$\mathbf{AR}_s$	-0.0498	0.02	0.0898	Not significant
$\mathbf{AR}_r$	1.7465	1.8162	1.886	Significant
$\mathbf{r}_{ht1}$	-0.2326	-0.1628	-0.093	Significant
$\mathbf{r}_{ht3}$	3.5074	3.5772	3.647	Significant
$\mathbf{r}_{ht4}$	-0.8799	-0.8101	-0.7403	Significant
$\mathbf{r}_{ht6}$	-4.525	-4.4552	-4.3854	Significant
$(\mathbf{t}_{te}/\mathbf{o})_s$	-1.2989	-1.2291	-1.1593	Significant
$(\mathbf{t}_{te}/\mathbf{o})_r$	-1.8044	-1.7346	-1.6648	Significant
$\mathbf{d}_{spe}$	-0.7887	-0.7189	-0.6491	Significant
θ_1	-0.0771	-0.0073	0.0625	Not significant
$\mathbf{p}_6$	0.4894	0.5592	0.629	Significant

Table A.19: Confidence interval and relevance of the quadratic effects in experiment 5

Quadratic effect	IC lower bound	Coefficient	IC upper bound	Relevance
$\mathbf{BS}_s^2$	-4.541	-0.2475	4.046	Not significant
$\mathbf{BS}_r^2$	-4.644	-0.3504	3.9431	Not significant
$\mathbf{AR}_s^2$	-4.4857	-0.1921	4.1014	Not significant
$\mathbf{AR}_r^2$	-4.853	-0.5594	3.7341	Not significant
$\mathbf{r}_{ht1}^2$	-4.4816	-0.188	4.1055	Not significant
$\mathbf{r}_{ht3}^2$	-5.1918	-0.8983	3.3953	Not significant
$\mathbf{r}_{ht4}^2$	-4.5316	-0.238	4.0555	Not significant
$\mathbf{r}_{ht6}^2$	-6.5221	-2.2286	2.065	Not significant
$(\mathbf{t}_{te}/\mathbf{o})_s^2$	-4.9271	-0.6335	3.66	Not significant
$(\mathbf{t}_{te}/\mathbf{o})_r^2$	-5.1591	-0.8656	3.428	Not significant
$\mathbf{d}_{spe}^2$	-4.5747	-0.2812	4.0123	Not significant
θ_1^2	-4.4985	-0.205	4.0886	Not significant
$\mathbf{p}_6^2$	-4.8212	-0.5277	3.7659	Not significant

Table A.20: Confidence interval and relevance of the interaction effects in experiment 5. Significant effects highlighted in pink.

Parameter: BS_s				
Interaction effect	IC lower bound	Coefficient	IC upper bound	Relevance
$\mathbf{BS}_s\mathbf{BS}_r$	-0.0884	-0.0186	0.0512	Not significant
$\mathbf{BS}_s\mathbf{AR}_s$	-0.0587	0.0111	0.0809	Not significant
$\mathbf{BS}_s\mathbf{AR}_r$	-0.1082	-0.0384	0.0314	Not significant
$\mathbf{BS}_s\mathbf{r}_{ht1}$	-0.0949	-0.0251	0.0447	Not significant
$\mathbf{BS}_s\mathbf{r}_{ht3}$	-0.08	-0.0102	0.0596	Not significant

Interaction effect	IC lower bound	Coefficient	IC upper bound	Relevance
$\mathbf{BS}_s\mathbf{r}_{ht4}$	-0.0311	0.0387	0.1085	Not significant
$\mathbf{BS}_s\mathbf{r}_{ht6}$	-0.0491	0.0207	0.0905	Not significant
$\mathbf{BS}_s(\mathbf{t}_{te}/\mathbf{o})_s$	-0.0864	-0.0166	0.0532	Not significant
$\mathbf{BS}_s(\mathbf{t}_{te}/\mathbf{o})_r$	-0.0313	0.0385	0.1083	Not significant
$\mathbf{BS}_s\mathbf{d}_{spe}$	-0.0312	0.0386	0.1084	Not significant
$\mathbf{BS}_s\theta_1$	-0.1159	-0.0461	0.0237	Not significant
$\mathbf{BS}_s\mathbf{p}_6$	-0.0327	0.0371	0.1069	Not significant
Parameter: BS_r				
Interaction effect	IC lower bound	Coefficient	IC upper bound	Relevance
$\mathbf{BS}_r\mathbf{AR}_s$	-0.08	-0.0102	0.0596	Not significant
$\mathbf{BS}_r\mathbf{AR}_r$	0.0229	0.0927	0.1625	Significant
$\mathbf{BS}_r\mathbf{r}_{ht1}$	-0.0979	-0.0281	0.0417	Not significant
$\mathbf{BS}_r\mathbf{r}_{ht3}$	0.0355	0.1053	0.1751	Significant
$\mathbf{BS}_r\mathbf{r}_{ht4}$	-0.1104	-0.0406	0.0292	Not significant
$\mathbf{BS}_r\mathbf{r}_{ht6}$	-0.1903	-0.1205	-0.0507	Significant
$\mathbf{BS}_r(\mathbf{t}_{te}/\mathbf{o})_s$	-0.1135	-0.0437	0.0261	Not significant
$\mathbf{BS}_r(\mathbf{t}_{te}/\mathbf{o})_r$	-0.1884	-0.1186	-0.0488	Significant
$\mathbf{BS}_r\mathbf{d}_{spe}$	-0.1222	-0.0524	0.0174	Not significant
$\mathbf{BS}_r\theta_1$	-0.0576	0.0122	0.082	Not significant
$\mathbf{BS}_r\mathbf{p}_6$	-0.1104	-0.0406	0.0292	Not significant
Parameter: AR_s				
Interaction effect	IC lower bound	Coefficient	IC upper bound	Relevance
$\mathbf{AR}_s\mathbf{AR}_r$	-0.0807	-0.0108	0.059	Not significant
$\mathbf{AR}_s\mathbf{r}_{ht1}$	-0.0747	-0.0049	0.0649	Not significant
$\mathbf{AR}_s\mathbf{r}_{ht3}$	-0.0568	0.013	0.0828	Not significant
$\mathbf{AR}_s\mathbf{r}_{ht4}$	-0.0593	0.0105	0.0803	Not significant
$\mathbf{AR}_s\mathbf{r}_{ht6}$	-0.0574	0.0124	0.0822	Not significant
$\mathbf{AR}_s(\mathbf{t}_{te}/\mathbf{o})_s$	-0.0682	0.0016	0.0714	Not significant
$\mathbf{AR}_s(\mathbf{t}_{te}/\mathbf{o})_r$	-0.0585	0.0113	0.0811	Not significant
$\mathbf{AR}_s\mathbf{d}_{spe}$	-0.0588	0.011	0.0808	Not significant
$\mathbf{AR}_s\theta_1$	-0.0593	0.0105	0.0803	Not significant
$\mathbf{AR}_s\mathbf{p}_6$	-0.0543	0.0155	0.0853	Not significant
Parameter: AR_r				
Interaction effect	IC lower bound	Coefficient	IC upper bound	Relevance
$\mathbf{AR}_r\mathbf{r}_{ht1}$	-0.107	-0.0372	0.0326	Not significant
$\mathbf{AR}_r\mathbf{r}_{ht3}$	-1.1466	-1.0768	-1.007	Significant
$\mathbf{AR}_r\mathbf{r}_{ht4}$	0.6224	0.6922	0.762	Significant
$\mathbf{AR}_r\mathbf{r}_{ht6}$	0.9531	1.0229	1.0927	Significant
$\mathbf{AR}_r(\mathbf{t}_{te}/\mathbf{o})_s$	-0.001	0.0688	0.1386	Not significant
$\mathbf{AR}_r(\mathbf{t}_{te}/\mathbf{o})_r$	0.0896	0.1594	0.2292	Significant
$\mathbf{AR}_r\mathbf{d}_{spe}$	0.4949	0.5647	0.6345	Significant
$\mathbf{AR}_r\theta_1$	-0.0773	-0.0075	0.0623	Not significant
$\mathbf{AR}_r\mathbf{p}_6$	0.0953	0.1651	0.2349	Significant
Parameter: r_{ht1}				
Interaction effect	IC lower bound	Coefficient	IC upper bound	Relevance
$\mathbf{r}_{ht1}\mathbf{r}_{ht3}$	0.1095	0.1793	0.2491	Significant
$\mathbf{r}_{ht1}\mathbf{r}_{ht4}$	-0.0372	0.0326	0.1024	Not significant

Interaction effect	IC lower bound	Coefficient	IC upper bound	Relevance
$\mathbf{r}_{ht1}\mathbf{r}_{ht6}$	0.1258	0.1957	0.2655	Significant
$\mathbf{r}_{ht1}(\mathbf{t}_{te}/\mathbf{o})_s$	-0.0272	0.0426	0.1124	Not significant
$\mathbf{r}_{ht1}(\mathbf{t}_{te}/\mathbf{o})_r$	-0.0242	0.0456	0.1154	Not significant
$\mathbf{r}_{ht1}\mathbf{d}_{spe}$	-0.0545	0.0153	0.0851	Not significant
$\mathbf{r}_{ht1}\theta_1$	-0.0815	-0.0117	0.0582	Not significant
$\mathbf{r}_{ht1}\mathbf{p}_6$	-0.0748	-0.005	0.0649	Not significant
Parameter: r_{ht3}				
Interaction effect	IC lower bound	Coefficient	IC upper bound	Relevance
$\mathbf{r}_{ht3}\mathbf{r}_{ht4}$	0.3707	0.4405	0.5103	Significant
$\mathbf{r}_{ht3}\mathbf{r}_{ht6}$	4.288	4.3578	4.4276	Significant
$\mathbf{r}_{ht3}(\mathbf{t}_{te}/\mathbf{o})_s$	-0.4452	-0.3754	-0.3056	Significant
$\mathbf{r}_{ht3}(\mathbf{t}_{te}/\mathbf{o})_r$	0.3877	0.4575	0.5273	Significant
$\mathbf{r}_{ht3}\mathbf{d}_{spe}$	0.5921	0.6619	0.7317	Significant
$\mathbf{r}_{ht3}\theta_1$	-0.053	0.0168	0.0866	Not significant
$\mathbf{r}_{ht3}\mathbf{p}_6$	-0.689	-0.6192	-0.5494	Significant
Parameter: r_{ht4}				
Interaction effect	IC lower bound	Coefficient	IC upper bound	Relevance
$\mathbf{r}_{ht4}\mathbf{r}_{ht6}$	-0.5044	-0.4346	-0.3648	Significant
$\mathbf{r}_{ht4}(\mathrm{t}_{te}/\mathrm{o})_s$	-0.1525	-0.0827	-0.0129	Significant
$\mathbf{r}_{ht4}(\mathbf{t}_{te}/\mathbf{o})_r$	-0.1949	-0.1251	-0.0553	Significant
$\mathbf{r}_{ht4}\mathbf{d}_{spe}$	-0.3881	-0.3183	-0.2485	Significant
$\mathbf{r}_{ht4}\theta_1$	-0.062	0.0078	0.0776	Not significant
$\mathbf{r}_{ht4}\mathbf{p}_6$	-0.2035	-0.1337	-0.0639	Significant
Parameter: r_{ht6}				
Interaction effect	IC lower bound	Coefficient	IC upper bound	Relevance
$\mathbf{r}_{ht6}(\mathbf{t}_{te}/\mathbf{o})_s$	0.4471	0.5169	0.5867	Significant
$\mathbf{r}_{ht6}(\mathbf{t}_{te}/\mathbf{o})_r$	-0.5803	-0.5105	-0.4407	Significant
$\mathbf{r}_{ht6}\mathbf{d}_{spe}$	-0.5539	-0.4841	-0.4143	Significant
$\mathbf{r}_{ht6}\theta_1$	-0.0811	-0.0113	0.0585	Not significant
$\mathbf{r}_{ht6}\mathbf{p}_6$	1.0322	1.102	1.1718	Significant
Parameter: $(\mathrm{t}_{te}/\mathrm{o})_s$				
Interaction effect	IC lower bound	Coefficient	IC upper bound	Relevance
$(\mathbf{t}_{te}/\mathbf{o})_s(\mathbf{t}_{te}/\mathbf{o})_r$	-0.1374	-0.0676	0.0022	Not significant
$(\mathbf{t}_{te}/\mathbf{o})_s\mathbf{d}_{spe}$	-0.2085	-0.1387	-0.0689	Significant
$(\mathbf{t}_{te}/\mathbf{o})_s\theta_1$	-0.1683	-0.0985	-0.0287	Significant
$(\mathbf{t}_{te}/\mathbf{o})_s\mathbf{p}_6$	-0.3403	-0.2705	-0.2007	Significant
Parameter: $(\mathrm{t}_{te}/\mathrm{o})_r$				
Interaction effect	IC lower bound	Coefficient	IC upper bound	Relevance
$(\mathbf{t}_{te}/\mathbf{o})_r\mathbf{d}_{spe}$	-0.2271	-0.1573	-0.0875	Significant
$(\mathbf{t}_{te}/\mathbf{o})_r\theta_1$	-0.0623	0.0075	0.0773	Not significant
$(\mathbf{te}/\mathbf{o})_r\mathbf{p}_6$	-0.2967	-0.2269	-0.157	Significant
Parameter: d_{spe}				
Interaction effect	IC lower bound	Coefficient	IC upper bound	Relevance
$\mathbf{d}_{spe}\theta_1$	-0.0624	0.0074	0.0772	Not significant
$\mathbf{d}_{spe}\mathbf{p}_6$	-0.4494	-0.3796	-0.3098	Significant
Parameter: θ_1				

Interaction effect	IC lower bound	Coefficient	IC upper bound	Relevance
Interaction effect	IC lower bound	Coefficient	IC upper bound	Relevance
$\theta_1\mathbf{p}_6$	-0.0657	0.0041	0.0739	Not significant

A.6 Results for the confidence intervals of the interaction and quadratic effects in experiment 6

The quadratic effects from experiment 6 are gathered in Table A.21, and the interaction effects in Table A.22.

Table A.21: Confidence interval and relevance of the quadratic effects in experiment 6

Quadratic effect	IC lower bound	Coefficient	IC upper bound	Relevance
$\mathbf{BS}_s^2$	-4.9945	-0.2384	4.5176	Not significant
$\mathbf{BS}_r^2$	-5.1168	-0.3607	4.3953	Not significant
$\mathbf{AR}_s^2$	-4.9393	-0.1832	4.5728	Not significant
$\mathbf{AR}_r^2$	-5.3057	-0.5496	4.2064	Not significant
$\mathbf{r}_{ht1}^2$	-4.935	-0.179	4.5771	Not significant
$\mathbf{r}_{ht3}^2$	-5.6412	-0.8852	3.8709	Not significant
$\mathbf{r}_{ht4}^2$	-4.9852	-0.2292	4.5269	Not significant
$\mathbf{r}_{ht6}^2$	-6.9545	-2.1985	2.5576	Not significant
$(\mathbf{t}_{te}/\mathbf{o})_s^2$	-5.3793	-0.6232	4.1328	Not significant
$(\mathbf{t}_{te}/\mathbf{o})_r^2$	-5.599	-0.8429	3.9131	Not significant
$\mathbf{d}_{spe}^2$	-5.0281	-0.2721	4.484	Not significant
θ_1^2	-4.9521	-0.196	4.56	Not significant
θ_4^2	-4.9922	-0.2361	4.5199	Not significant
$\mathbf{p}_6^2$	-5.282	-0.526	4.2301	Not significant

Table A.22: Confidence interval and relevance of the interaction effects in experiment 6. Significant effects highlighted in pink.

Parameter: BS_s				
Interaction effect	IC lower bound	Coefficient	IC upper bound	Relevance
$\mathbf{BS}_s\mathbf{BS}_r$	-0.0572	-0.0027	0.0518	Not significant
$\mathbf{BS}_s\mathbf{AR}_s$	-0.0417	0.0129	0.0674	Not significant
$\mathbf{BS}_s\mathbf{AR}_r$	-0.0709	-0.0164	0.0381	Not significant
$\mathbf{BS}_s\mathbf{r}_{ht1}$	-0.0752	-0.0207	0.0338	Not significant
$\mathbf{BS}_s\mathbf{r}_{ht3}$	-0.0506	0.004	0.0585	Not significant
$\mathbf{BS}_s\mathbf{r}_{ht4}$	-0.0378	0.0167	0.0712	Not significant
$\mathbf{BS}_s\mathbf{r}_{ht6}$	-0.0481	0.0064	0.061	Not significant
$\mathbf{BS}_s(\mathbf{t}_{te}/\mathbf{o})_s$	-0.08	-0.0255	0.029	Not significant
$\mathbf{BS}_s(\mathbf{t}_{te}/\mathbf{o})_r$	-0.0381	0.0164	0.071	Not significant
$\mathbf{BS}_s\mathbf{d}_{spe}$	-0.038	0.0165	0.071	Not significant
$\mathbf{BS}_s\theta_1$	-0.0983	-0.0438	0.0108	Not significant
$\mathbf{BS}_s\theta_4$	-0.063	-0.0084	0.0461	Not significant
$\mathbf{BS}_s\mathbf{p}_6$	-0.0396	0.0149	0.0694	Not significant

Interaction effect	IC lower bound	Coefficient	IC upper bound	Relevance
Parameter: BS_r				
Interaction effect	IC lower bound	Coefficient	IC upper bound	Relevance
$\mathbf{BS}_r\mathbf{AR}_s$	-0.057	-0.0025	0.052	Not significant
$\mathbf{BS}_r\mathbf{AR}_r$	0.0189	0.0734	0.1279	Significant
$\mathbf{BS}_r\mathbf{r}_{ht1}$	-0.0598	-0.0052	0.0493	Not significant
$\mathbf{BS}_r\mathbf{r}_{ht3}$	0.0422	0.0967	0.1512	Significant
$\mathbf{BS}_r\mathbf{r}_{ht4}$	-0.0741	-0.0196	0.035	Not significant
$\mathbf{BS}_r\mathbf{r}_{ht6}$	-0.1624	-0.1079	-0.0533	Significant
$\mathbf{BS}_r(\mathbf{t}_{te}/\mathbf{o})_s$	-0.0693	-0.0148	0.0398	Not significant
$\mathbf{BS}_r(\mathbf{t}_{te}/\mathbf{o})_r$	-0.1477	-0.0932	-0.0387	Significant
$\mathbf{BS}_r\mathbf{d}_{spe}$	-0.0876	-0.033	0.0215	Not significant
$\mathbf{BS}_r\theta_1$	-0.0459	0.0086	0.0631	Not significant
$\mathbf{BS}_r\theta_4$	0.0034	0.0579	0.1125	Significant
$\mathbf{BS}_r\mathbf{p}_6$	-0.0778	-0.0233	0.0312	Not significant
Parameter: AR_s				
Interaction effect	IC lower bound	Coefficient	IC upper bound	Relevance
$\mathbf{AR}_s\mathbf{AR}_r$	-0.0537	0.0008	0.0553	Not significant
$\mathbf{AR}_s\mathbf{r}_{ht1}$	-0.0527	0.0018	0.0563	Not significant
$\mathbf{AR}_s\mathbf{r}_{ht3}$	-0.0382	0.0163	0.0708	Not significant
$\mathbf{AR}_s\mathbf{r}_{ht4}$	-0.0557	-0.0012	0.0533	Not significant
$\mathbf{AR}_s\mathbf{r}_{ht6}$	-0.0457	0.0089	0.0634	Not significant
$\mathbf{AR}_s(\mathbf{t}_{te}/\mathbf{o})_s$	-0.0515	0.003	0.0575	Not significant
$\mathbf{AR}_s(\mathbf{t}_{te}/\mathbf{o})_r$	-0.0549	-0.0004	0.0541	Not significant
$\mathbf{AR}_s\mathbf{d}_{spe}$	-0.0551	-0.0006	0.0539	Not significant
$\mathbf{AR}_s\theta_1$	-0.0619	-0.0074	0.0472	Not significant
$\mathbf{AR}_s\theta_4$	-0.0613	-0.0068	0.0477	Not significant
$\mathbf{AR}_s\mathbf{p}_6$	-0.0505	0.004	0.0585	Not significant
Parameter: AR_r				
Interaction effect	IC lower bound	Coefficient	IC upper bound	Relevance
$\mathbf{AR}_r\mathbf{r}_{ht1}$	-0.0928	-0.0383	0.0162	Not significant
$\mathbf{AR}_r\mathbf{r}_{ht3}$	-1.1582	-1.1037	-1.0491	Significant
$\mathbf{AR}_r\mathbf{r}_{ht4}$	0.6866	0.7411	0.7957	Significant
$\mathbf{AR}_r\mathbf{r}_{ht6}$	0.9917	1.0462	1.1007	Significant
$\mathbf{AR}_r(\mathbf{t}_{te}/\mathbf{o})_s$	-0.001	0.0535	0.108	Not significant
$\mathbf{AR}_r(\mathbf{t}_{te}/\mathbf{o})_r$	0.1667	0.2212	0.2757	Significant
$\mathbf{AR}_r\mathbf{d}_{spe}$	0.5545	0.609	0.6635	Significant
$\mathbf{AR}_r\theta_1$	-0.0696	-0.0151	0.0394	Not significant
$\mathbf{AR}_r\theta_4$	0.0098	0.0643	0.1188	Significant
$\mathbf{AR}_r\mathbf{p}_6$	0.1688	0.2234	0.2779	Significant
Parameter: r_{ht1}				
Interaction effect	IC lower bound	Coefficient	IC upper bound	Relevance
$\mathbf{r}_{ht1}\mathbf{r}_{ht3}$	0.1294	0.1839	0.2385	Significant
$\mathbf{r}_{ht1}\mathbf{r}_{ht4}$	-0.0205	0.034	0.0885	Not significant
$\mathbf{r}_{ht1}\mathbf{r}_{ht6}$	0.1321	0.1867	0.2412	Significant
$\mathbf{r}_{ht1}(\mathbf{t}_{te}/\mathbf{o})_s$	-0.0346	0.02	0.0745	Not significant
$\mathbf{r}_{ht1}(\mathbf{t}_{te}/\mathbf{o})_r$	-0.0081	0.0464	0.1009	Not significant
$\mathbf{r}_{ht1}\mathbf{d}_{spe}$	-0.0377	0.0169	0.0714	Not significant

Interaction effect	IC lower bound	Coefficient	IC upper bound	Relevance
$\mathbf{r}_{ht1}\theta_1$	-0.081	-0.0265	0.028	Not significant
$\mathbf{r}_{ht1}\theta_4$	-0.0479	0.0067	0.0612	Not significant
$\mathbf{r}_{ht1}\mathbf{p}_6$	-0.0582	-0.0037	0.0508	Not significant
Parameter: r_{ht3}				
Interaction effect	IC lower bound	Coefficient	IC upper bound	Relevance
$\mathbf{r}_{ht3}\mathbf{r}_{ht4}$	0.4187	0.4733	0.5278	Significant
$\mathbf{r}_{ht3}\mathbf{r}_{ht6}$	4.3178	4.3723	4.4268	Significant
$\mathbf{r}_{ht3}(\mathbf{t}_{te}/\mathbf{o})_s$	-0.4284	-0.3739	-0.3194	Significant
$\mathbf{r}_{ht3}(\mathbf{t}_{te}/\mathbf{o})_r$	0.4241	0.4787	0.5332	Significant
$\mathbf{r}_{ht3}\mathbf{d}_{spe}$	0.605	0.6595	0.714	Significant
$\mathbf{r}_{ht3}\theta_1$	-0.045	0.0095	0.064	Not significant
$\mathbf{r}_{ht3}\theta_4$	0.1105	0.165	0.2195	Significant
$\mathbf{r}_{ht3}\mathbf{p}_6$	-0.6638	-0.6093	-0.5547	Significant
Parameter: r_{ht4}				
Interaction effect	IC lower bound	Coefficient	IC upper bound	Relevance
$\mathbf{r}_{ht4}\mathbf{r}_{ht6}$	-0.5223	-0.4677	-0.4132	Significant
$\mathbf{r}_{ht4}(\mathrm{t}_{te}/\mathrm{o})_s$	-0.1218	-0.0673	-0.0128	Significant
$\mathbf{r}_{ht4}(\mathbf{t}_{te}/\mathbf{o})_r$	-0.2359	-0.1814	-0.1268	Significant
$\mathbf{r}_{ht4}\mathbf{d}_{spe}$	-0.4164	-0.3619	-0.3074	Significant
$\mathbf{r}_{ht4}\theta_1$	-0.0391	0.0155	0.07	Not significant
$\mathbf{r}_{ht4}\theta_4$	-0.1325	-0.078	-0.0235	Significant
$\mathbf{r}_{ht4}\mathbf{p}_6$	-0.2425	-0.188	-0.1334	Significant
Parameter: r_{ht6}				
Interaction effect	IC lower bound	Coefficient	IC upper bound	Relevance
$\mathbf{r}_{ht6}(\mathbf{t}_{te}/\mathbf{o})_s$	0.4623	0.5168	0.5713	Significant
$\mathbf{r}_{ht6}(\mathbf{t}_{te}/\mathbf{o})_r$	-0.582	-0.5275	-0.473	Significant
$\mathbf{r}_{ht6}\mathbf{d}_{spe}$	-0.5384	-0.4838	-0.4293	Significant
$\mathbf{r}_{ht6}\theta_1$	-0.0586	-0.004	0.0505	Not significant
$\mathbf{r}_{ht6}\theta_4$	-0.2618	-0.2073	-0.1527	Significant
$\mathbf{r}_{ht6}\mathbf{p}_6$	1.0514	1.1059	1.1604	Significant
Parameter: $(\mathrm{t}_{te}/\mathrm{o})_s$				
Interaction effect	IC lower bound	Coefficient	IC upper bound	Relevance
$(\mathbf{t}_{te}/\mathbf{o})_s(\mathbf{t}_{te}/\mathbf{o})_r$	-0.1073	-0.0528	0.0017	Not significant
$(\mathbf{t}_{te}/\mathbf{o})_s\mathbf{d}_{spe}$	-0.1753	-0.1208	-0.0663	Significant
$(\mathbf{t}_{te}/\mathbf{o})_s\theta_1$	-0.1609	-0.1064	-0.0519	Significant
$(\mathbf{t}_{te}/\mathbf{o})_s\theta_4$	-0.0399	0.0146	0.0691	Not significant
$(\mathbf{t}_{te}/\mathbf{o})_s\mathbf{p}_6$	-0.31	-0.2555	-0.201	Significant
Parameter: $(\mathrm{t}_{te}/\mathrm{o})_r$				
Interaction effect	IC lower bound	Coefficient	IC upper bound	Relevance
$(\mathbf{t}_{te}/\mathbf{o})_r\mathbf{d}_{spe}$	-0.2638	-0.2093	-0.1548	Significant
$(\mathbf{t}_{te}/\mathbf{o})_r\theta_1$	-0.0394	0.0151	0.0696	Not significant
$(\mathbf{t}_{te}/\mathbf{o})_r\theta_4$	-0.0968	-0.0422	0.0123	Not significant
$(\mathbf{t}_{te}/\mathbf{o})_r\mathbf{p}_6$	-0.337	-0.2825	-0.228	Significant
Parameter: d_{spe}				
Interaction effect	IC lower bound	Coefficient	IC upper bound	Relevance
$\mathbf{d}_{spe}\theta_1$	-0.0395	0.015	0.0695	Not significant
$\mathbf{d}_{spe}\theta_4$	-0.1525	-0.098	-0.0435	Significant

Interaction effect	IC lower bound	Coefficient	IC upper bound	Relevance
$\mathbf{d}_{spe}\mathbf{p}_6$	-0.4853	-0.4308	-0.3763	Significant
Parameter: θ_1				
Interaction effect	IC lower bound	Coefficient	IC upper bound	Relevance
$\theta_1\theta_4$	-0.0331	0.0214	0.0759	Not significant
$\theta_1\mathbf{p}_6$	-0.0429	0.0116	0.0661	Not significant
Parameter: θ_4				
Interaction effect	IC lower bound	Coefficient	IC upper bound	Relevance
$\theta_4\mathbf{p}_6$	-0.1283	-0.0738	-0.0193	Significant

B Results from the sensitivity analysis for a narrower design space

This section presents the results from the two experiments carried out by narrowing the design space of the wide sensitivity analysis for both trailing edge thickness to opening ratios.

B.1 Results for the confidence intervals of the main, interaction and quadratic effects in the 11-factor experiment

The results for the main effects of the first 11-factor experiment are shown in Table B.23, the quadratic effects in Table B.24 and the interaction effects in Table B.25.

Table B.23: Confidence interval for the main effects in a narrower 11-factor sensitivity analysis. Significant effects highlighted in grey.

Main effect	IC lower bound	Coefficient	IC upper bound	Relevance
$\mathbf{BS}_s$	-0.0724	0.0056	0.0836	Not significant
$\mathbf{BS}_r$	-0.1868	-0.1088	-0.0308	Significant
$\mathbf{AR}_s$	-0.0647	0.0133	0.0913	Not significant
$\mathbf{AR}_r$	1.9109	1.9889	2.0669	Significant
$\mathbf{r}_{ht1}$	-0.2824	-0.2044	-0.1264	Significant
$\mathbf{r}_{ht3}$	3.8277	3.9057	3.9837	Significant
$\mathbf{r}_{ht4}$	-0.9578	-0.8798	-0.8018	Significant
$\mathbf{r}_{ht6}$	-4.8086	-4.7306	-4.6526	Significant
$(\mathbf{t}_{te}/\mathbf{o})_s$	-0.8237	-0.7457	-0.6677	Significant
$(\mathbf{t}_{te}/\mathbf{o})_r$	-1.3731	-1.2951	-1.2171	Significant
$\mathbf{p}_6$	0.584	0.662	0.74	Significant

Table B.24: Confidence interval for the quadratic effects in the 11-factor narrower sensitivity analysis

Quadratic effect	IC lower bound	Coefficient	IC upper bound	Relevance
$\mathbf{BS}_s^2$	-2.6899	-0.3077	2.0745	Not significant
$\mathbf{BS}_r^2$	-2.7962	-0.414	1.9682	Not significant
$\mathbf{AR}_s^2$	-2.628	-0.2458	2.1364	Not significant
$\mathbf{AR}_r^2$	-2.9841	-0.6019	1.7802	Not significant
$\mathbf{r}_{ht1}^2$	-2.6243	-0.2421	2.1401	Not significant
$\mathbf{r}_{ht3}^2$	-3.4616	-1.0794	1.3027	Not significant
$\mathbf{r}_{ht4}^2$	-2.6731	-0.2909	2.0912	Not significant
$(\mathbf{t}_{te}/\mathbf{o})_s^2$	-2.7885	-0.4063	1.9759	Not significant
$(\mathbf{t}_{te}/\mathbf{o})_r^2$	-2.9605	-0.5783	1.8038	Not significant
$\mathbf{p}_6^2$	-2.9882	-0.606	1.7761	Not significant

Table B.25: Confidence interval for the interaction effects in the 11-factor narrower sensitivity analysis. Significant effects highlighted in pink.

Parameter: BS_s				
Interaction effect	IC lower bound	Coefficient	IC upper bound	Relevance
$\mathbf{BS}_s\mathbf{BS}_r$	-0.078	0.0001	0.0781	Not significant
$\mathbf{BS}_s\mathbf{AR}_s$	-0.0699	0.0082	0.0862	Not significant
$\mathbf{BS}_s\mathbf{AR}_r$	-0.0776	0.0004	0.0785	Not significant
$\mathbf{BS}_s\mathbf{r}_{ht1}$	-0.084	-0.006	0.072	Not significant
$\mathbf{BS}_s\mathbf{r}_{ht3}$	-0.0668	0.0112	0.0893	Not significant
$\mathbf{BS}_s\mathbf{r}_{ht4}$	-0.0783	-0.0002	0.0778	Not significant
$\mathbf{BS}_s\mathbf{r}_{ht6}$	-0.0798	-0.0017	0.0763	Not significant
$\mathbf{BS}_s(\mathbf{t}_{te}/\mathbf{o})_s$	-0.0906	-0.0126	0.0655	Not significant
$\mathbf{BS}_s(\mathbf{t}_{te}/\mathbf{o})_r$	-0.0782	-0.0002	0.0779	Not significant
$\mathbf{BS}_s\mathbf{p}_6$	-0.0793	-0.0013	0.0767	Not significant
Parameter: BS_r				
Interaction effect	IC lower bound	Coefficient	IC upper bound	Relevance
$\mathbf{BS}_r\mathbf{AR}_s$	-0.078	0.0	0.078	Not significant
$\mathbf{BS}_r\mathbf{AR}_r$	-0.0383	0.0397	0.1178	Not significant
$\mathbf{BS}_r\mathbf{r}_{ht1}$	-0.0774	0.0006	0.0787	Not significant
$\mathbf{BS}_r\mathbf{r}_{ht3}$	-0.0325	0.0455	0.1236	Not significant
$\mathbf{BS}_r\mathbf{r}_{ht4}$	-0.0709	0.0071	0.0852	Not significant
$\mathbf{BS}_r\mathbf{r}_{ht6}$	-0.1375	-0.0595	0.0186	Not significant
$\mathbf{BS}_r(\mathbf{t}_{te}/\mathbf{o})_s$	-0.0753	0.0027	0.0808	Not significant
$\mathbf{BS}_r(\mathbf{t}_{te}/\mathbf{o})_r$	-0.114	-0.036	0.0421	Not significant
$\mathbf{BS}_r\mathbf{p}_6$	-0.0657	0.0123	0.0903	Not significant
Parameter: AR_s				
Interaction effect	IC lower bound	Coefficient	IC upper bound	Relevance
$\mathbf{AR}_s\mathbf{AR}_r$	-0.0783	-0.0003	0.0778	Not significant
$\mathbf{AR}_s\mathbf{r}_{ht1}$	-0.0951	-0.0171	0.0609	Not significant
$\mathbf{AR}_s\mathbf{r}_{ht3}$	-0.0507	0.0273	0.1054	Not significant
$\mathbf{AR}_s\mathbf{r}_{ht4}$	-0.078	0.0	0.0781	Not significant

Interaction effect	IC lower bound	Coefficient	IC upper bound	Relevance
$\mathbf{AR}_s\mathbf{r}_{ht6}$	-0.0772	0.0008	0.0788	Not significant
$\mathbf{AR}_s(\mathbf{t}_{te}/\mathbf{o})_s$	-0.0837	-0.0056	0.0724	Not significant
$\mathbf{AR}_s(\mathbf{t}_{te}/\mathbf{o})_r$	-0.0771	0.0009	0.0789	Not significant
$\mathbf{AR}_s\mathbf{p}_6$	-0.0715	0.0065	0.0845	Not significant
Parameter: AR_r				
Interaction effect	IC lower bound	Coefficient	IC upper bound	Relevance
$\mathbf{AR}_r\mathbf{r}_{ht1}$	-0.0878	-0.0097	0.0683	Not significant
$\mathbf{AR}_r\mathbf{r}_{ht3}$	-1.3315	-1.2534	-1.1754	Significant
$\mathbf{AR}_r\mathbf{r}_{ht4}$	0.7001	0.7781	0.8562	Significant
$\mathbf{AR}_r\mathbf{r}_{ht6}$	1.1185	1.1965	1.2746	Significant
$\mathbf{AR}_r(\mathbf{t}_{te}/\mathbf{o})_s$	-0.0982	-0.0201	0.0579	Not significant
$\mathbf{AR}_r(\mathbf{t}_{te}/\mathbf{o})_r$	-0.0172	0.0609	0.1389	Not significant
$\mathbf{AR}_r\mathbf{p}_6$	-0.0467	0.0313	0.1093	Not significant
Parameter: $\mathrm{r}_{ht,1}$				
Interaction effect	IC lower bound	Coefficient	IC upper bound	Relevance
$\mathbf{r}_{ht1}\mathbf{r}_{ht3}$	0.1448	0.2229	0.3009	Significant
$\mathbf{r}_{ht1}\mathbf{r}_{ht4}$	-0.0737	0.0043	0.0824	Not significant
$\mathbf{r}_{ht1}\mathbf{r}_{ht6}$	0.1346	0.2127	0.2907	Significant
$\mathbf{r}_{ht1}(\mathbf{t}_{te}/\mathbf{o})_s$	-0.0538	0.0243	0.1023	Not significant
$\mathbf{r}_{ht1}(\mathbf{t}_{te}/\mathbf{o})_r$	-0.0627	0.0153	0.0934	Not significant
$\mathbf{r}_{ht1}\mathbf{p}_6$	-0.1178	-0.0397	0.0383	Not significant
Parameter: $\mathrm{r}_{ht,3}$				
Interaction effect	IC lower bound	Coefficient	IC upper bound	Relevance
$\mathbf{r}_{ht3}\mathbf{r}_{ht4}$	0.4512	0.5293	0.6073	Significant
$\mathbf{r}_{ht3}\mathbf{r}_{ht6}$	4.7099	4.788	4.866	Significant
$\mathbf{r}_{ht3}(\mathbf{t}_{te}/\mathbf{o})_s$	-0.4149	-0.3369	-0.2589	Significant
$\mathbf{r}_{ht3}(\mathbf{t}_{te}/\mathbf{o})_r$	0.2243	0.3023	0.3804	Significant
$\mathbf{r}_{ht3}\mathbf{p}_6$	-0.8427	-0.7647	-0.6866	Significant
Parameter: $\mathrm{r}_{ht,4}$				
Interaction effect	IC lower bound	Coefficient	IC upper bound	Relevance
$\mathbf{r}_{ht4}\mathbf{r}_{ht6}$	-0.5887	-0.5107	-0.4326	Significant
$\mathbf{r}_{ht4}(\mathrm{t}_{te}/\mathrm{o})_s$	-0.0671	0.011	0.089	Not significant
$\mathbf{r}_{ht4}(\mathbf{t}_{te}/\mathbf{o})_r$	-0.1097	-0.0317	0.0464	Not significant
$\mathbf{r}_{ht4}\mathbf{p}_6$	-0.0777	0.0003	0.0784	Not significant
Parameter: $\mathrm{r}_{ht,6}$				
Interaction effect	IC lower bound	Coefficient	IC upper bound	Relevance
$\mathbf{r}_{ht6}(\mathbf{t}_{te}/\mathbf{o})_s$	0.3474	0.4254	0.5035	Significant
$\mathbf{r}_{ht6}(\mathbf{t}_{te}/\mathbf{o})_r$	-0.4262	-0.3482	-0.2701	Significant
$\mathbf{r}_{ht6}\mathbf{p}_6$	1.221	1.2991	1.3771	Significant
Parameter: $(\mathrm{t}_{te}/\mathrm{o})_s$				
Interaction effect	IC lower bound	Coefficient	IC upper bound	Relevance
$(\mathbf{t}_{te}/\mathbf{o})_s(\mathbf{t}_{te}/\mathbf{o})_r$	-0.0697	0.0083	0.0864	Not significant
$(\mathbf{t}_{te}/\mathbf{o})_s\mathbf{p}_6$	-0.1994	-0.1213	-0.0433	Significant
Parameter: $(\mathrm{t}_{te}/\mathrm{o})_r$				
Interaction effect	IC lower bound	Coefficient	IC upper bound	Relevance
$(\mathbf{t}_{te}/\mathbf{o})_r\mathbf{p}_6$	-0.1529	-0.0749	0.0031	Not significant

B.2 Results for the confidence intervals of the main, interaction and quadratic effects in 13-factor experiment

The results for the main effects of the 13-factor experiment in the narrower SA are presented in Table B.26, the quadratic effects in Table B.27 and the interaction effects in Table B.28.

Table B.26: Confidence interval for the main effects in a narrower 13-factor sensitivity analysis. Significant effects highlighted in grey.

Main effect	IC lower bound	Coefficient	IC upper bound	Relevance
$\mathbf{BS}_s$	-0.024	0.016	0.056	Not significant
$\mathbf{BS}_r$	-0.1148	-0.0748	-0.0348	Significant
$\mathbf{AR}_s$	-0.0259	0.0141	0.0541	Not significant
$\mathbf{AR}_r$	1.9694	2.0093	2.0493	Significant
$\mathbf{r}_{ht1}$	-0.242	-0.202	-0.162	Significant
$\mathbf{r}_{ht3}$	4.0	4.04	4.0799	Significant
$\mathbf{r}_{ht4}$	-0.9567	-0.9168	-0.8768	Significant
$\mathbf{r}_{ht6}$	-4.9437	-4.9037	-4.8637	Significant
$(\mathbf{t}_{te}/\mathbf{o})_s$	-0.7622	-0.7222	-0.6822	Significant
$(\mathbf{t}_{te}/\mathbf{o})_r$	-1.2787	-1.2387	-1.1987	Significant
θ_1	-0.0009	0.0391	0.0791	Not significant
θ_4	-0.2777	-0.2377	-0.1977	Significant
$\mathbf{p}_6$	0.6158	0.6558	0.6958	Significant

Table B.27: Confidence interval for the quadratic effects in the 13-factor narrower sensitivity analysis. Significant effects highlighted in pink.

Quadratic effect	IC lower bound	Coefficient	IC upper bound	Relevance
$\mathbf{BS}_s^2$	-2.7278	-0.2682	2.1915	Not significant
$\mathbf{BS}_r^2$	-2.857	-0.3974	2.0622	Not significant
$\mathbf{AR}_s^2$	-2.67	-0.2104	2.2492	Not significant
$\mathbf{AR}_r^2$	-3.0247	-0.5651	1.8945	Not significant
$\mathbf{r}_{ht1}^2$	-2.6687	-0.2091	2.2505	Not significant
$\mathbf{r}_{ht3}^2$	-3.5027	-1.0431	1.4165	Not significant
$\mathbf{r}_{ht4}^2$	-2.7149	-0.2552	2.2044	Not significant
$\mathbf{r}_{ht6}^2$	-4.9377	-2.4781	-0.0185	Significant
$(\mathbf{t}_{te}/\mathbf{o})_s^2$	-2.8284	-0.3688	2.0908	Not significant
$(\mathbf{t}_{te}/\mathbf{o})_r^2$	-2.9953	-0.5357	1.9239	Not significant
θ_1^2	-2.6899	-0.2303	2.2293	Not significant
θ_4^2	-2.7248	-0.2652	2.1944	Not significant
$\mathbf{p}_6^2$	-3.0375	-0.5779	1.8818	Not significant

Table B.28: Confidence interval for the interaction effects in the 13-factor narrower sensitivity analysis. Significant effects highlighted in pink.

Parameter: BS_s				
Interaction effect	IC lower bound	Coefficient	IC upper bound	Relevance
$\mathbf{BS}_s\mathbf{BS}_r$	-0.0401	-0.0001	0.0399	Not significant
$\mathbf{BS}_s\mathbf{AR}_s$	-0.0307	0.0093	0.0493	Not significant
$\mathbf{BS}_s\mathbf{AR}_r$	-0.0391	0.0009	0.0409	Not significant
$\mathbf{BS}_s\mathbf{r}_{ht1}$	-0.0474	-0.0074	0.0326	Not significant
$\mathbf{BS}_s\mathbf{r}_{ht3}$	-0.0222	0.0178	0.0578	Not significant
$\mathbf{BS}_s\mathbf{r}_{ht4}$	-0.0404	-0.0004	0.0396	Not significant
$\mathbf{BS}_s\mathbf{r}_{ht6}$	-0.0477	-0.0078	0.0322	Not significant
$\mathbf{BS}_s(\mathbf{t}_{te}/\mathbf{o})_s$	-0.0522	-0.0122	0.0278	Not significant
$\mathbf{BS}_s(\mathbf{t}_{te}/\mathbf{o})_r$	-0.0405	-0.0005	0.0395	Not significant
$\mathbf{BS}_s\theta_1$	-0.0672	-0.0272	0.0128	Not significant
$\mathbf{BS}_s\theta_4$	-0.0397	0.0003	0.0403	Not significant
$\mathbf{BS}_s\mathbf{p}_6$	-0.041	-0.001	0.039	Not significant
Parameter: BS_r				
Interaction effect	IC lower bound	Coefficient	IC upper bound	Relevance
$\mathbf{BS}_r\mathbf{AR}_s$	-0.04	-0.0001	0.0399	Not significant
$\mathbf{BS}_r\mathbf{AR}_r$	-0.0027	0.0373	0.0773	Not significant
$\mathbf{BS}_r\mathbf{r}_{ht1}$	-0.0397	0.0002	0.0402	Not significant
$\mathbf{BS}_r\mathbf{r}_{ht3}$	-0.0042	0.0358	0.0757	Not significant
$\mathbf{BS}_r\mathbf{r}_{ht4}$	-0.0277	0.0123	0.0523	Not significant
$\mathbf{BS}_r\mathbf{r}_{ht6}$	-0.0855	-0.0455	-0.0055	Significant
$\mathbf{BS}_r(\mathbf{t}_{te}/\mathbf{o})_s$	-0.0383	0.0017	0.0417	Not significant
$\mathbf{BS}_r(\mathbf{t}_{te}/\mathbf{o})_r$	-0.0789	-0.0389	0.0011	Not significant
$\mathbf{BS}_r\theta_1$	-0.0401	-0.0001	0.0399	Not significant
$\mathbf{BS}_r\theta_4$	-0.0034	0.0366	0.0766	Not significant
$\mathbf{BS}_r\mathbf{p}_6$	-0.0318	0.0082	0.0481	Not significant
Parameter: AR_s				
Interaction effect	IC lower bound	Coefficient	IC upper bound	Relevance
$\mathbf{AR}_s\mathbf{AR}_r$	-0.0404	-0.0004	0.0395	Not significant
$\mathbf{AR}_s\mathbf{r}_{ht1}$	-0.0569	-0.0169	0.0231	Not significant
$\mathbf{AR}_s\mathbf{r}_{ht3}$	-0.0126	0.0274	0.0674	Not significant
$\mathbf{AR}_s\mathbf{r}_{ht4}$	-0.0398	0.0002	0.0402	Not significant
$\mathbf{AR}_s\mathbf{r}_{ht6}$	-0.0396	0.0004	0.0404	Not significant
$\mathbf{AR}_s(\mathbf{t}_{te}/\mathbf{o})_s$	-0.0455	-0.0055	0.0345	Not significant
$\mathbf{AR}_s(\mathbf{t}_{te}/\mathbf{o})_r$	-0.0391	0.0009	0.0409	Not significant
$\mathbf{AR}_s\theta_1$	-0.0387	0.0013	0.0413	Not significant
$\mathbf{AR}_s\theta_4$	-0.0402	-0.0002	0.0398	Not significant
$\mathbf{AR}_s\mathbf{p}_6$	-0.0332	0.0068	0.0467	Not significant
Parameter: AR_r				
Interaction effect	IC lower bound	Coefficient	IC upper bound	Relevance
$\mathbf{AR}_r\mathbf{r}_{ht1}$	-0.0494	-0.0094	0.0306	Not significant
$\mathbf{AR}_r\mathbf{r}_{ht3}$	-1.3167	-1.2768	-1.2368	Significant
$\mathbf{AR}_r\mathbf{r}_{ht4}$	0.7575	0.7975	0.8375	Significant
$\mathbf{AR}_r\mathbf{r}_{ht6}$	1.1762	1.2162	1.2562	Significant

Interaction effect	IC lower bound	Coefficient	IC upper bound	Relevance
$\mathbf{AR}_r(\mathbf{t}_{te}/\mathbf{o})_s$	-0.0577	-0.0178	0.0222	Not significant
$\mathbf{AR}_r(\mathbf{t}_{te}/\mathbf{o})_r$	-0.0124	0.0276	0.0676	Not significant
$\mathbf{AR}_r\theta_1$	-0.0384	0.0016	0.0416	Not significant
$\mathbf{AR}_r\theta_4$	-0.0179	0.022	0.062	Not significant
$\mathbf{AR}_r\mathbf{p}_6$	-0.0065	0.0334	0.0734	Not significant
Parameter: r_{ht1}				
Interaction effect	IC lower bound	Coefficient	IC upper bound	Relevance
$\mathbf{r}_{ht1}\mathbf{r}_{ht3}$	0.1798	0.2198	0.2598	Significant
$\mathbf{r}_{ht1}\mathbf{r}_{ht4}$	-0.0356	0.0044	0.0444	Not significant
$\mathbf{r}_{ht1}\mathbf{r}_{ht6}$	0.17	0.21	0.2499	Significant
$\mathbf{r}_{ht1}(\mathbf{t}_{te}/\mathbf{o})_s$	-0.0171	0.0229	0.0629	Not significant
$\mathbf{r}_{ht1}(\mathbf{t}_{te}/\mathbf{o})_r$	-0.0254	0.0145	0.0545	Not significant
$\mathbf{r}_{ht1}\theta_1$	-0.0446	-0.0046	0.0354	Not significant
$\mathbf{r}_{ht1}\theta_4$	-0.037	0.003	0.043	Not significant
$\mathbf{r}_{ht1}\mathbf{p}_6$	-0.0801	-0.0402	-0.0002	Significant
Parameter: r_{ht3}				
Interaction effect	IC lower bound	Coefficient	IC upper bound	Relevance
$\mathbf{r}_{ht3}\mathbf{r}_{ht4}$	0.5186	0.5586	0.5986	Significant
$\mathbf{r}_{ht3}\mathbf{r}_{ht6}$	4.7531	4.7931	4.8331	Significant
$\mathbf{r}_{ht3}(\mathbf{t}_{te}/\mathbf{o})_s$	-0.367	-0.327	-0.287	Significant
$\mathbf{r}_{ht3}(\mathbf{t}_{te}/\mathbf{o})_r$	0.2169	0.2569	0.2969	Significant
$\mathbf{r}_{ht3}\theta_1$	-0.0143	0.0256	0.0656	Not significant
$\mathbf{r}_{ht3}\theta_4$	0.1161	0.156	0.196	Significant
$\mathbf{r}_{ht3}\mathbf{p}_6$	-0.826	-0.786	-0.746	Significant
Parameter: r_{ht4}				
Interaction effect	IC lower bound	Coefficient	IC upper bound	Relevance
$\mathbf{r}_{ht4}\mathbf{r}_{ht6}$	-0.5807	-0.5407	-0.5007	Significant
$\mathbf{r}_{ht4}(\mathrm{t}_{te}/\mathrm{o})_s$	-0.031	0.009	0.049	Not significant
$\mathbf{r}_{ht4}(\mathbf{t}_{te}/\mathbf{o})_r$	-0.034	0.0059	0.0459	Not significant
$\mathbf{r}_{ht4}\theta_1$	-0.0408	-0.0008	0.0392	Not significant
$\mathbf{r}_{ht4}\theta_4$	-0.0794	-0.0394	0.0006	Not significant
$\mathbf{r}_{ht4}\mathbf{p}_6$	-0.0374	0.0026	0.0426	Not significant
Parameter: r_{ht6}				
Interaction effect	IC lower bound	Coefficient	IC upper bound	Relevance
$\mathbf{r}_{ht6}(\mathbf{t}_{te}/\mathbf{o})_s$	0.3737	0.4137	0.4537	Significant
$\mathbf{r}_{ht6}(\mathbf{t}_{te}/\mathbf{o})_r$	-0.3394	-0.2994	-0.2594	Significant
$\mathbf{r}_{ht6}\theta_1$	-0.0651	-0.0251	0.0149	Not significant
$\mathbf{r}_{ht6}\theta_4$	-0.2419	-0.202	-0.162	Significant
$\mathbf{r}_{ht6}\mathbf{p}_6$	1.2967	1.3367	1.3767	Significant
Parameter: $(\mathrm{t}_{te}/\mathrm{o})_s$				
Interaction effect	IC lower bound	Coefficient	IC upper bound	Relevance
$(\mathbf{t}_{te}/\mathbf{o})_s(\mathbf{t}_{te}/\mathbf{o})_r$	-0.0306	0.0094	0.0494	Not significant
$(\mathbf{t}_{te}/\mathbf{o})_s\theta_1$	-0.0811	-0.0411	-0.0012	Significant
$(\mathbf{t}_{te}/\mathbf{o})_s\theta_4$	-0.0428	-0.0028	0.0372	Not significant
$(\mathbf{t}_{te}/\mathbf{o})_s\mathbf{p}_6$	-0.1565	-0.1165	-0.0765	Significant
Parameter: $(\mathrm{t}_{te}/\mathrm{o})_r$				
$(\mathbf{t}_{te}/\mathbf{o})_r\theta_1$	-0.041	-0.001	0.039	Not significant

Interaction effect	IC lower bound	Coefficient	IC upper bound	Relevance
$(\mathbf{t}_{te}/\mathbf{o})_r\theta_4$	0.02	0.06	0.1	Significant
$(\mathbf{t}_{te}/\mathbf{o})_r\mathbf{p}_6$	-0.1166	-0.0766	-0.0366	Significant
Parameter: θ_1				
Interaction effect	IC lower bound	Coefficient	IC upper bound	Relevance
$\theta_1\theta_4$	-0.0394	0.0006	0.0406	Not significant
$\theta_1\mathbf{p}_6$	-0.0389	0.0011	0.0411	Not significant
Parameter: θ_4				
Interaction effect	IC lower bound	Coefficient	IC upper bound	Relevance
$\theta_4\mathbf{p}_6$	-0.0439	-0.0039	0.0361	Not significant

C Results from the local sensitivity analysis

Finally, the results for the local sensitivity analysis will be presented. First the 9-factor experiment will be shown, followed by the 11-factor experiment. To finish, the quadratic and interaction effects of the 14-factor experiment will be introduced.

C.1 Results for the confidence intervals of the main, interaction and quadratic effects for 9 factors

Table C.29: Confidence interval for the main effects in the 9-factor local sensitivity analysis. Significant effects highlighted in pink.

Main effect	IC lower bound	Coefficient	IC upper bound	Relevance
$\mathbf{BS}_s$	-0.0005	0.0024	0.0054	Not significant
$\mathbf{BS}_r$	-0.0026	0.0004	0.0033	Not significant
$\mathbf{AR}_s$	0.004	0.0069	0.0099	Significant
$\mathbf{AR}_r$	0.0725	0.0755	0.0785	Significant
$\mathbf{r}_{ht1}$	-0.0071	-0.0042	-0.0012	Significant
$\mathbf{r}_{ht3}$	-0.0463	-0.0434	-0.0404	Significant
$\mathbf{r}_{ht4}$	-0.0484	-0.0455	-0.0425	Significant
$\mathbf{r}_{ht6}$	-0.0056	-0.0026	0.0004	Not significant
$\mathbf{p}_6$	-0.1511	-0.1481	-0.1451	Significant

Table C.30: Confidence interval for the quadratic effects in the 9-factor local sensitivity analysis. Significant effects highlighted in pink.

Quadratic effect	IC lower bound	Coefficient	IC upper bound	Relevance
$\mathbf{BS}_s^2$	-0.04	0.0049	0.0498	Not significant
$\mathbf{BS}_r^2$	-0.0403	0.0046	0.0495	Not significant
$\mathbf{AR}_s^2$	-0.0388	0.0061	0.051	Not significant
$\mathbf{AR}_r^2$	-0.0367	0.0082	0.0531	Not significant
$\mathbf{r}_{ht1}^2$	-0.0383	0.0066	0.0515	Not significant
$\mathbf{r}_{ht3}^2$	-0.4152	-0.3703	-0.3254	Significant
$\mathbf{r}_{ht4}^2$	-0.0393	0.0056	0.0505	Not significant
$\mathbf{r}_{ht6}^2$	-0.3096	-0.2647	-0.2198	Significant
$\mathbf{p}_6^2$	-0.1687	-0.1238	-0.0789	Significant

Table C.31: Confidence interval for the interaction effects in the 9-factor local sensitivity analysis. Significant effects highlighted in pink.

Parameter: BS_s				
Interaction effect	IC lower bound	Coefficient	IC upper bound	Relevance
$\mathbf{BS}_s\mathbf{BS}_r$	-0.003	-0.0	0.003	Not significant
$\mathbf{BS}_s\mathbf{AR}_s$	-0.0029	0.0001	0.003	Not significant
$\mathbf{BS}_s\mathbf{AR}_r$	-0.003	0.0	0.003	Not significant
$\mathbf{BS}_s\mathbf{r}_{ht1}$	-0.003	0.0	0.003	Not significant
$\mathbf{BS}_s\mathbf{r}_{ht3}$	-0.0025	0.0005	0.0034	Not significant
$\mathbf{BS}_s\mathbf{r}_{ht4}$	-0.003	-0.0	0.003	Not significant
$\mathbf{BS}_s\mathbf{r}_{ht6}$	-0.0033	-0.0004	0.0026	Not significant
$\mathbf{BS}_s\mathbf{p}_6$	-0.0028	0.0002	0.0032	Not significant
Parameter: BS_r				
Interaction effect	IC lower bound	Coefficient	IC upper bound	Relevance
$\mathbf{BS}_r\mathbf{AR}_s$	-0.003	-0.0	0.003	Not significant
$\mathbf{BS}_r\mathbf{AR}_r$	-0.0029	0.0001	0.003	Not significant
$\mathbf{BS}_r\mathbf{r}_{ht1}$	-0.003	0.0	0.003	Not significant
$\mathbf{BS}_r\mathbf{r}_{ht3}$	-0.0031	-0.0001	0.0028	Not significant
$\mathbf{BS}_r\mathbf{r}_{ht4}$	-0.003	0.0	0.003	Not significant
$\mathbf{BS}_r\mathbf{r}_{ht6}$	-0.0028	0.0002	0.0031	Not significant
$\mathbf{BS}_r\mathbf{p}_6$	-0.0029	0.0001	0.003	Not significant
Parameter: AR_s				
Interaction effect	IC lower bound	Coefficient	IC upper bound	Relevance
$\mathbf{AR}_s\mathbf{AR}_r$	-0.003	0.0	0.003	Not significant
$\mathbf{AR}_s\mathbf{r}_{ht1}$	-0.003	-0.0001	0.0029	Not significant
$\mathbf{AR}_s\mathbf{r}_{ht3}$	-0.0018	0.0012	0.0041	Not significant
$\mathbf{AR}_s\mathbf{r}_{ht4}$	-0.003	-0.0	0.003	Not significant
$\mathbf{AR}_s\mathbf{r}_{ht6}$	-0.004	-0.001	0.002	Not significant
$\mathbf{AR}_s\mathbf{p}_6$	-0.0023	0.0007	0.0036	Not significant
Parameter: AR_r				
Interaction effect	IC lower bound	Coefficient	IC upper bound	Relevance
$\mathbf{AR}_r\mathbf{r}_{ht1}$	-0.003	-0.0	0.003	Not significant

Interaction effect	IC lower bound	Coefficient	IC upper bound	Relevance
$\mathbf{AR}_r\mathbf{r}_{ht3}$	-0.0062	-0.0032	-0.0003	Significant
$\mathbf{AR}_r\mathbf{r}_{ht4}$	-0.0011	0.0019	0.0048	Not significant
$\mathbf{AR}_r\mathbf{r}_{ht6}$	0.0016	0.0046	0.0075	Significant
$\mathbf{AR}_r\mathbf{p}_6$	-0.0033	-0.0003	0.0027	Not significant
Parameter: r_{ht1}				
Interaction effect	IC lower bound	Coefficient	IC upper bound	Relevance
$\mathbf{r}_{ht1}\mathbf{r}_{ht3}$	-0.0043	-0.0013	0.0017	Not significant
$\mathbf{r}_{ht1}\mathbf{r}_{ht4}$	-0.003	0.0	0.003	Not significant
$\mathbf{r}_{ht1}\mathbf{r}_{ht6}$	-0.0023	0.0006	0.0036	Not significant
$\mathbf{r}_{ht1}\mathbf{p}_6$	-0.0033	-0.0003	0.0026	Not significant
Parameter: r_{ht3}				
Interaction effect	IC lower bound	Coefficient	IC upper bound	Relevance
$\mathbf{r}_{ht3}\mathbf{r}_{ht4}$	-0.0037	-0.0007	0.0023	Not significant
$\mathbf{r}_{ht3}\mathbf{r}_{ht6}$	0.5815	0.5845	0.5875	Significant
$\mathbf{r}_{ht3}\mathbf{p}_6$	-0.3237	-0.3208	-0.3178	Significant
Parameter: r_{ht4}				
Interaction effect	IC lower bound	Coefficient	IC upper bound	Relevance
$\mathbf{r}_{ht4}\mathbf{r}_{ht6}$	-0.0057	-0.0027	0.0002	Not significant
$\mathbf{r}_{ht4}\mathbf{p}_6$	-0.0025	0.0005	0.0034	Not significant
Parameter: r_{ht6}				
Interaction effect	IC lower bound	Coefficient	IC upper bound	Relevance
$\mathbf{r}_{ht6}\mathbf{p}_6$	0.2628	0.2658	0.2687	Significant

C.2 Results for the confidence intervals of the main, interaction and quadratic effects for 11 factors

Table C.32: Confidence interval for the main effects in the 11-factor local sensitivity analysis. Significant effects highlighted in pink.

Main effect	IC lower bound	Coefficient	IC upper bound	Relevance
$\mathbf{BS}_s$	0.001	0.0024	0.0039	Significant
$\mathbf{BS}_r$	-0.0011	0.0004	0.0018	Not significant
$\mathbf{AR}_s$	0.0055	0.0069	0.0083	Significant
$\mathbf{AR}_r$	0.074	0.0755	0.0769	Significant
$\mathbf{r}_{ht1}$	-0.0056	-0.0042	-0.0027	Significant
$\mathbf{r}_{ht3}$	-0.0451	-0.0436	-0.0422	Significant
$\mathbf{r}_{ht4}$	-0.0469	-0.0455	-0.044	Significant
$\mathbf{r}_{ht6}$	-0.0036	-0.0022	-0.0008	Significant
$(\mathbf{t}_{te}/\mathbf{o})_s$	-0.0207	-0.0193	-0.0178	Significant
$(\mathbf{t}_{te}/\mathbf{o})_r$	-0.0211	-0.0197	-0.0182	Significant
$\mathbf{p}_6$	-0.1498	-0.1484	-0.1469	Significant

Table C.33: Confidence interval for the quadratic effects in the 11-factor local sensitivity analysis. Significant effects highlighted in pink.

Quadratic effect	IC lower bound	Coefficient	IC upper bound	Relevance
$\mathbf{BS}_s^2$	-0.0402	0.0036	0.0474	Not significant
$\mathbf{BS}_r^2$	-0.0405	0.0033	0.0471	Not significant
$\mathbf{AR}_s^2$	-0.039	0.0048	0.0486	Not significant
$\mathbf{AR}_r^2$	-0.0369	0.0069	0.0507	Not significant
$\mathbf{r}_{ht1}^2$	-0.0385	0.0053	0.0491	Not significant
$\mathbf{r}_{ht3}^2$	-0.4153	-0.3714	-0.3276	Significant
$\mathbf{r}_{ht4}^2$	-0.0395	0.0043	0.0481	Not significant
$\mathbf{r}_{ht6}^2$	-0.3097	-0.2659	-0.2221	Significant
$(\mathbf{t}_{te}/\mathbf{o})_s^2$	-0.0386	0.0052	0.049	Not significant
$(\mathbf{t}_{te}/\mathbf{o})_r^2$	-0.0386	0.0052	0.049	Not significant
$\mathbf{p}_6^2$	-0.1689	-0.1251	-0.0813	Significant

Table C.34: Confidence interval for the interaction effects in the 11-factor local sensitivity analysis. Significant effects highlighted in pink.

Parameter: BS_s				
Interaction effect	IC lower bound	Coefficient	IC upper bound	Relevance
$\mathbf{BS}_s\mathbf{BS}_r$	-0.0014	-0.0	0.0014	Not significant
$\mathbf{BS}_s\mathbf{AR}_s$	-0.0014	0.0001	0.0015	Not significant
$\mathbf{BS}_s\mathbf{AR}_r$	-0.0014	0.0	0.0014	Not significant
$\mathbf{BS}_s\mathbf{r}_{ht1}$	-0.0014	0.0	0.0015	Not significant
$\mathbf{BS}_s\mathbf{r}_{ht3}$	-0.001	0.0005	0.0019	Not significant
$\mathbf{BS}_s\mathbf{r}_{ht4}$	-0.0014	-0.0	0.0014	Not significant
$\mathbf{BS}_s\mathbf{r}_{ht6}$	-0.0018	-0.0004	0.0011	Not significant
$\mathbf{BS}_s(\mathbf{t}_{te}/\mathbf{o})_s$	-0.0015	-0.0	0.0014	Not significant
$\mathbf{BS}_s(\mathbf{t}_{te}/\mathbf{o})_r$	-0.0014	-0.0	0.0014	Not significant
$\mathbf{BS}_s\mathbf{p}_6$	-0.0012	0.0002	0.0017	Not significant
Parameter: BS_r				
Interaction effect	IC lower bound	Coefficient	IC upper bound	Relevance
$\mathbf{BS}_r\mathbf{AR}_s$	-0.0014	-0.0	0.0014	Not significant
$\mathbf{BS}_r\mathbf{AR}_r$	-0.0014	0.0001	0.0015	Not significant
$\mathbf{BS}_r\mathbf{r}_{ht1}$	-0.0014	0.0	0.0014	Not significant
$\mathbf{BS}_r\mathbf{r}_{ht3}$	-0.0016	-0.0001	0.0013	Not significant
$\mathbf{BS}_r\mathbf{r}_{ht4}$	-0.0014	0.0	0.0014	Not significant
$\mathbf{BS}_r\mathbf{r}_{ht6}$	-0.0013	0.0002	0.0016	Not significant
$\mathbf{BS}_r(\mathbf{t}_{te}/\mathbf{o})_s$	-0.0014	0.0	0.0014	Not significant
$\mathbf{BS}_r(\mathbf{t}_{te}/\mathbf{o})_r$	-0.0015	-0.0	0.0014	Not significant
$\mathbf{BS}_r\mathbf{p}_6$	-0.0014	0.0001	0.0015	Not significant
Parameter: AR_s				
Interaction effect	IC lower bound	Coefficient	IC upper bound	Relevance
$\mathbf{AR}_s\mathbf{AR}_r$	-0.0014	0.0	0.0014	Not significant
$\mathbf{AR}_s\mathbf{r}_{ht1}$	-0.0015	-0.0001	0.0014	Not significant
$\mathbf{AR}_s\mathbf{r}_{ht3}$	-0.0003	0.0012	0.0026	Not significant

Interaction effect	IC lower bound	Coefficient	IC upper bound	Relevance
$\mathbf{AR}_s\mathbf{r}_{ht4}$	-0.0014	-0.0	0.0014	Not significant
$\mathbf{AR}_s\mathbf{r}_{ht6}$	-0.0025	-0.001	0.0004	Not significant
$\mathbf{AR}_s(\mathbf{t}_{te}/\mathbf{o})_s$	-0.0015	-0.0	0.0014	Not significant
$\mathbf{AR}_s(\mathbf{t}_{te}/\mathbf{o})_r$	-0.0014	-0.0	0.0014	Not significant
$\mathbf{AR}_s\mathbf{p}_6$	-0.0008	0.0007	0.0021	Not significant
Parameter: AR_r				
Interaction effect	IC lower bound	Coefficient	IC upper bound	Relevance
$\mathbf{AR}_r\mathbf{r}_{ht1}$	-0.0014	-0.0	0.0014	Not significant
$\mathbf{AR}_r\mathbf{r}_{ht3}$	-0.0047	-0.0032	-0.0018	Significant
$\mathbf{AR}_r\mathbf{r}_{ht4}$	0.0004	0.0019	0.0033	Significant
$\mathbf{AR}_r\mathbf{r}_{ht6}$	0.0031	0.0046	0.006	Significant
$\mathbf{AR}_r(\mathbf{t}_{te}/\mathbf{o})_s$	-0.0015	-0.0	0.0014	Not significant
$\mathbf{AR}_r(\mathbf{t}_{te}/\mathbf{o})_r$	-0.0015	-0.0001	0.0014	Not significant
$\mathbf{AR}_r\mathbf{p}_6$	-0.0017	-0.0003	0.0011	Not significant
Parameter: $\mathrm{r}_{ht,1}$				
Interaction effect	IC lower bound	Coefficient	IC upper bound	Relevance
$\mathbf{r}_{ht1}\mathbf{r}_{ht3}$	-0.0028	-0.0013	0.0001	Not significant
$\mathbf{r}_{ht1}\mathbf{r}_{ht4}$	-0.0014	0.0	0.0014	Not significant
$\mathbf{r}_{ht1}\mathbf{r}_{ht6}$	-0.0008	0.0006	0.0021	Not significant
$\mathbf{r}_{ht1}(\mathbf{t}_{te}/\mathbf{o})_s$	-0.0014	-0.0	0.0014	Not significant
$\mathbf{r}_{ht1}(\mathbf{t}_{te}/\mathbf{o})_r$	-0.0014	0.0	0.0014	Not significant
$\mathbf{r}_{ht1}\mathbf{p}_6$	-0.0018	-0.0003	0.0011	Not significant
Parameter: $\mathrm{r}_{ht,3}$				
Interaction effect	IC lower bound	Coefficient	IC upper bound	Relevance
$\mathbf{r}_{ht3}\mathbf{r}_{ht4}$	-0.0022	-0.0007	0.0007	Not significant
$\mathbf{r}_{ht3}\mathbf{r}_{ht6}$	0.5829	0.5844	0.5858	Significant
$\mathbf{r}_{ht3}(\mathbf{t}_{te}/\mathbf{o})_s$	-0.0048	-0.0034	-0.002	Significant
$\mathbf{r}_{ht3}(\mathbf{t}_{te}/\mathbf{o})_r$	0.001	0.0025	0.0039	Significant
$\mathbf{r}_{ht3}\mathbf{p}_6$	-0.3222	-0.3208	-0.3193	Significant
Parameter: $\mathrm{r}_{ht,4}$				
Interaction effect	IC lower bound	Coefficient	IC upper bound	Relevance
$\mathbf{r}_{ht4}\mathbf{r}_{ht6}$	-0.0042	-0.0027	-0.0013	Significant
$\mathbf{r}_{ht4}(\mathrm{t}_{te}/\mathrm{o})_s$	-0.0014	0.0	0.0015	Not significant
$\mathbf{r}_{ht4}(\mathbf{t}_{te}/\mathbf{o})_r$	-0.0014	0.0	0.0015	Not significant
$\mathbf{r}_{ht4}\mathbf{p}_6$	-0.001	0.0005	0.0019	Not significant
Parameter: $\mathrm{r}_{ht,6}$				
Interaction effect	IC lower bound	Coefficient	IC upper bound	Relevance
$\mathbf{r}_{ht6}(\mathbf{t}_{te}/\mathbf{o})_s$	0.0014	0.0028	0.0043	Significant
$\mathbf{r}_{ht6}(\mathbf{t}_{te}/\mathbf{o})_r$	-0.0034	-0.002	-0.0005	Significant
$\mathbf{r}_{ht6}\mathbf{p}_6$	0.2643	0.2658	0.2672	Significant
Parameter: $(\mathrm{t}_{te}/\mathrm{o})_s$				
Interaction effect	IC lower bound	Coefficient	IC upper bound	Relevance
$(\mathbf{t}_{te}/\mathbf{o})_s(\mathbf{t}_{te}/\mathbf{o})_r$	-0.0014	0.0	0.0014	Not significant
$(\mathbf{t}_{te}/\mathbf{o})_s\mathbf{p}_6$	-0.0032	-0.0018	-0.0004	Significant
Parameter: $(\mathrm{t}_{te}/\mathrm{o})_r$				
Interaction effect	IC lower bound	Coefficient	IC upper bound	Relevance

Interaction effect	IC lower bound	Coefficient	IC upper bound	Relevance
$(\mathbf{t}_{te}/\mathbf{o})_r\mathbf{p}_6$	-0.0015	-0.0001	0.0014	Not significant

C.3 Results for the confidence intervals of the interaction and quadratic effects for 14 factors

Table C.35: Confidence interval for the quadratic effects in the 14-factor local sensitivity analysis. Significant effects highlighted in pink.

Quadratic effect	IC lower bound	Coefficient	IC upper bound	Relevance
$\mathbf{BS}_s^2$	-0.0795	0.0024	0.0844	Not significant
$\mathbf{BS}_r^2$	-0.0799	0.0021	0.0841	Not significant
$\mathbf{AR}_s^2$	-0.0783	0.0036	0.0856	Not significant
$\mathbf{AR}_r^2$	-0.0762	0.0057	0.0877	Not significant
$\mathbf{r}_{ht1}^2$	-0.0778	0.0041	0.0861	Not significant
$\mathbf{r}_{ht3}^2$	-0.4556	-0.3737	-0.2917	Significant
$\mathbf{r}_{ht4}^2$	-0.0788	0.0031	0.0851	Not significant
$\mathbf{r}_{ht6}^2$	-0.3499	-0.2679	-0.186	Significant
$(\mathbf{t}_{te}/\mathbf{o})_s^2$	-0.078	0.004	0.0859	Not significant
$(\mathbf{t}_{te}/\mathbf{o})_r^2$	-0.078	0.004	0.0859	Not significant
$\mathbf{d}_{spe}^2$	-0.2622	-0.1803	-0.0983	Significant
θ_1^2	-0.0735	0.0085	0.0904	Not significant
θ_4^2	-0.0778	0.0042	0.0862	Not significant
$\mathbf{p}_6^2$	-0.2082	-0.1263	-0.0443	Significant

Table C.36: Confidence interval for the interaction effects in the 14-factor local sensitivity analysis. Significant effects highlighted in pink.

Parameter: BS_s				
Interaction effect	IC lower bound	Coefficient	IC upper bound	Relevance
$\mathbf{BS}_s\mathbf{BS}_r$	-0.0009	-0.0	0.0009	Not significant
$\mathbf{BS}_s\mathbf{AR}_s$	-0.0009	0.0001	0.001	Not significant
$\mathbf{BS}_s\mathbf{AR}_r$	-0.0009	0.0	0.0009	Not significant
$\mathbf{BS}_s\mathbf{r}_{ht1}$	-0.0009	0.0	0.001	Not significant
$\mathbf{BS}_s\mathbf{r}_{ht3}$	-0.0005	0.0004	0.0014	Not significant
$\mathbf{BS}_s\mathbf{r}_{ht4}$	-0.0009	-0.0	0.0009	Not significant
$\mathbf{BS}_s\mathbf{r}_{ht6}$	-0.0013	-0.0003	0.0006	Not significant
$\mathbf{BS}_s(\mathbf{t}_{te}/\mathbf{o})_s$	-0.001	-0.0	0.0009	Not significant
$\mathbf{BS}_s(\mathbf{t}_{te}/\mathbf{o})_r$	-0.0009	-0.0	0.0009	Not significant
$\mathbf{BS}_s\mathbf{d}_{spe}$	-0.0008	0.0001	0.001	Not significant
$\mathbf{BS}_s\theta_1$	-0.001	-0.0001	0.0009	Not significant
$\mathbf{BS}_s\theta_4$	-0.0009	0.0	0.0009	Not significant
$\mathbf{BS}_s\mathbf{p}_6$	-0.0007	0.0002	0.0012	Not significant
Parameter: BS_r				
Interaction effect	IC lower bound	Coefficient	IC upper bound	Relevance

Interaction effect	IC lower bound	Coefficient	IC upper bound	Relevance
$\mathbf{BS}_r\mathbf{AR}_s$	-0.0009	-0.0	0.0009	Not significant
$\mathbf{BS}_r\mathbf{AR}_r$	-0.0009	0.0001	0.001	Not significant
$\mathbf{BS}_r\mathbf{r}_{ht1}$	-0.0009	0.0	0.0009	Not significant
$\mathbf{BS}_r\mathbf{r}_{ht3}$	-0.0012	-0.0002	0.0007	Not significant
$\mathbf{BS}_r\mathbf{r}_{ht4}$	-0.0009	0.0	0.001	Not significant
$\mathbf{BS}_r\mathbf{r}_{ht6}$	-0.0007	0.0002	0.0012	Not significant
$\mathbf{BS}_r(\mathbf{t}_{te}/\mathbf{o})_s$	-0.0009	0.0	0.0009	Not significant
$\mathbf{BS}_r(\mathbf{t}_{te}/\mathbf{o})_r$	-0.001	-0.0	0.0009	Not significant
$\mathbf{BS}_r\mathbf{d}_{spe}$	-0.0008	0.0002	0.0011	Not significant
$\mathbf{BS}_r\theta_1$	-0.0009	0.0	0.0009	Not significant
$\mathbf{BS}_r\theta_4$	-0.0006	0.0003	0.0013	Not significant
$\mathbf{BS}_r\mathbf{p}_6$	-0.0008	0.0001	0.001	Not significant
Parameter: AR_s				
Interaction effect	IC lower bound	Coefficient	IC upper bound	Relevance
$\mathbf{AR}_s\mathbf{AR}_r$	-0.0009	0.0	0.001	Not significant
$\mathbf{AR}_s\mathbf{r}_{ht1}$	-0.001	-0.0001	0.0009	Not significant
$\mathbf{AR}_s\mathbf{r}_{ht3}$	0.0002	0.0012	0.0021	Significant
$\mathbf{AR}_s\mathbf{r}_{ht4}$	-0.0009	-0.0	0.0009	Not significant
$\mathbf{AR}_s\mathbf{r}_{ht6}$	-0.002	-0.001	-0.0001	Significant
$\mathbf{AR}_s(\mathbf{t}_{te}/\mathbf{o})_s$	-0.001	-0.0	0.0009	Not significant
$\mathbf{AR}_s(\mathbf{t}_{te}/\mathbf{o})_r$	-0.0009	-0.0	0.0009	Not significant
$\mathbf{AR}_s\mathbf{d}_{spe}$	-0.0005	0.0004	0.0014	Not significant
$\mathbf{AR}_s\theta_1$	-0.001	-0.0001	0.0009	Not significant
$\mathbf{AR}_s\theta_4$	-0.0009	0.0	0.0009	Not significant
$\mathbf{AR}_s\mathbf{p}_6$	-0.0003	0.0007	0.0016	Not significant
Parameter: AR_r				
Interaction effect	IC lower bound	Coefficient	IC upper bound	Relevance
$\mathbf{AR}_r\mathbf{r}_{ht1}$	-0.0009	-0.0	0.0009	Not significant
$\mathbf{AR}_r\mathbf{r}_{ht3}$	-0.0043	-0.0034	-0.0025	Significant
$\mathbf{AR}_r\mathbf{r}_{ht4}$	0.0009	0.0018	0.0028	Significant
$\mathbf{AR}_r\mathbf{r}_{ht6}$	0.0039	0.0049	0.0058	Significant
$\mathbf{AR}_r(\mathbf{t}_{te}/\mathbf{o})_s$	-0.001	-0.0	0.0009	Not significant
$\mathbf{AR}_r(\mathbf{t}_{te}/\mathbf{o})_r$	-0.001	-0.0001	0.0009	Not significant
$\mathbf{AR}_r\mathbf{d}_{spe}$	-0.0048	-0.0038	-0.0029	Significant
$\mathbf{AR}_r\theta_1$	-0.001	-0.0	0.0009	Not significant
$\mathbf{AR}_r\theta_4$	-0.0009	0.0	0.001	Not significant
$\mathbf{AR}_r\mathbf{p}_6$	-0.0013	-0.0004	0.0006	Not significant
Parameter: r_{ht1}				
Interaction effect	IC lower bound	Coefficient	IC upper bound	Relevance
$\mathbf{r}_{ht1}\mathbf{r}_{ht3}$	-0.0022	-0.0013	-0.0004	Significant
$\mathbf{r}_{ht1}\mathbf{r}_{ht4}$	-0.0009	0.0	0.0009	Not significant
$\mathbf{r}_{ht1}\mathbf{r}_{ht6}$	-0.0003	0.0006	0.0016	Not significant
$\mathbf{r}_{ht1}(\mathbf{t}_{te}/\mathbf{o})_s$	-0.0009	-0.0	0.0009	Not significant
$\mathbf{r}_{ht1}(\mathbf{t}_{te}/\mathbf{o})_r$	-0.0009	0.0	0.0009	Not significant
$\mathbf{r}_{ht1}\mathbf{d}_{spe}$	-0.0011	-0.0002	0.0008	Not significant
$\mathbf{r}_{ht1}\theta_1$	-0.001	-0.0	0.0009	Not significant
$\mathbf{r}_{ht1}\theta_4$	-0.0009	-0.0	0.0009	Not significant

Interaction effect	IC lower bound	Coefficient	IC upper bound	Relevance
$\mathbf{r}_{ht1}\mathbf{p}_6$	-0.0013	-0.0003	0.0006	Not significant
Parameter: r_{ht3}				
Interaction effect	IC lower bound	Coefficient	IC upper bound	Relevance
$\mathbf{r}_{ht3}\mathbf{r}_{ht4}$	-0.0019	-0.0009	-0.0	Significant
$\mathbf{r}_{ht3}\mathbf{r}_{ht6}$	0.5888	0.5897	0.5907	Significant
$\mathbf{r}_{ht3}(\mathbf{t}_{te}/\mathbf{o})_s$	-0.0043	-0.0034	-0.0024	Significant
$\mathbf{r}_{ht3}(\mathbf{t}_{te}/\mathbf{o})_r$	0.0015	0.0025	0.0034	Significant
$\mathbf{r}_{ht3}\mathbf{d}_{spe}$	-0.248	-0.247	-0.2461	Significant
$\mathbf{r}_{ht3}\theta_1$	-0.0022	-0.0012	-0.0003	Significant
$\mathbf{r}_{ht3}\theta_4$	0.0085	0.0094	0.0104	Significant
$\mathbf{r}_{ht3}\mathbf{p}_6$	-0.3193	-0.3184	-0.3175	Significant
Parameter: r_{ht4}				
Interaction effect	IC lower bound	Coefficient	IC upper bound	Relevance
$\mathbf{r}_{ht4}\mathbf{r}_{ht6}$	-0.0035	-0.0026	-0.0016	Significant
$\mathbf{r}_{ht4}(\mathrm{t}_{te}/\mathrm{o})_s$	-0.0009	0.0	0.001	Not significant
$\mathbf{r}_{ht4}(\mathbf{t}_{te}/\mathbf{o})_r$	-0.0009	0.0	0.001	Not significant
$\mathbf{r}_{ht4}\mathbf{d}_{spe}$	0.0035	0.0045	0.0054	Significant
$\mathbf{r}_{ht4}\theta_1$	-0.0009	0.0	0.0009	Not significant
$\mathbf{r}_{ht4}\theta_4$	-0.0011	-0.0001	0.0008	Not significant
$\mathbf{r}_{ht4}\mathbf{p}_6$	-0.0004	0.0005	0.0015	Not significant
Parameter: r_{ht6}				
Interaction effect	IC lower bound	Coefficient	IC upper bound	Relevance
$\mathbf{r}_{ht6}(\mathbf{t}_{te}/\mathbf{o})_s$	0.0019	0.0028	0.0038	Significant
$\mathbf{r}_{ht6}(\mathbf{t}_{te}/\mathbf{o})_r$	-0.003	-0.002	-0.0011	Significant
$\mathbf{r}_{ht6}\mathbf{d}_{spe}$	0.2121	0.213	0.2139	Significant
$\mathbf{r}_{ht6}\theta_1$	0.0	0.001	0.0019	Significant
$\mathbf{r}_{ht6}\theta_4$	-0.0097	-0.0088	-0.0078	Significant
$\mathbf{r}_{ht6}\mathbf{p}_6$	0.2619	0.2628	0.2638	Significant
Parameter: $(\mathrm{t}_{te}/\mathrm{o})_s$				
Interaction effect	IC lower bound	Coefficient	IC upper bound	Relevance
$(\mathbf{t}_{te}/\mathbf{o})_s(\mathbf{t}_{te}/\mathbf{o})_r$	-0.0009	0.0	0.0009	Not significant
$(\mathbf{t}_{te}/\mathbf{o})_s\mathbf{d}_{spe}$	-0.002	-0.001	-0.0001	Significant
$(\mathbf{t}_{te}/\mathbf{o})_s\theta_1$	-0.0009	0.0	0.0009	Not significant
$(\mathbf{t}_{te}/\mathbf{o})_s\theta_4$	-0.0009	-0.0	0.0009	Not significant
$(\mathbf{t}_{te}/\mathbf{o})_s\mathbf{p}_6$	-0.0027	-0.0018	-0.0008	Significant
Parameter: $(\mathrm{t}_{te}/\mathrm{o})_r$				
Interaction effect	IC lower bound	Coefficient	IC upper bound	Relevance
$(\mathbf{t}_{te}/\mathbf{o})_r\mathbf{d}_{spe}$	-0.0015	-0.0006	0.0004	Not significant
$(\mathbf{t}_{te}/\mathbf{o})_r\theta_1$	-0.0009	0.0	0.0009	Not significant
$(\mathbf{t}_{te}/\mathbf{o})_r\theta_4$	-0.0009	0.0	0.001	Not significant
$(\mathbf{t}_{te}/\mathbf{o})_r\mathbf{p}_6$	-0.001	-0.0001	0.0009	Not significant
Parameter: d_{spe}				
Interaction effect	IC lower bound	Coefficient	IC upper bound	Relevance
$\mathbf{d}_{spe}\theta_1$	-0.0012	-0.0003	0.0006	Not significant
$\mathbf{d}_{spe}\theta_4$	-0.0084	-0.0075	-0.0065	Significant

Interaction effect	IC lower bound	Coefficient	IC upper bound	Relevance
$\mathbf{d}_{spe}\mathbf{p}_6$	-0.2814	-0.2804	-0.2795	Significant
Parameter: θ_1				
Interaction effect	IC lower bound	Coefficient	IC upper bound	Relevance
$\theta_1\theta_4$	-0.0009	-0.0	0.0009	Not significant
$\theta_1\mathbf{p}_6$	-0.0015	-0.0006	0.0004	Not significant
Parameter: θ_4				
Interaction effect	IC lower bound	Coefficient	IC upper bound	Relevance
$\theta_4\mathbf{p}_6$	-0.0031	-0.0021	-0.0012	Significant

D 2-way interaction effects from the 14-factor local sensitivity analysis

D.1 Significant interaction effects

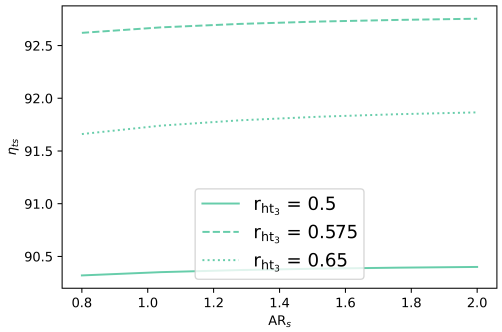

(a) Interaction between stator aspect ratio and stator exit hub-to-tip ratio.

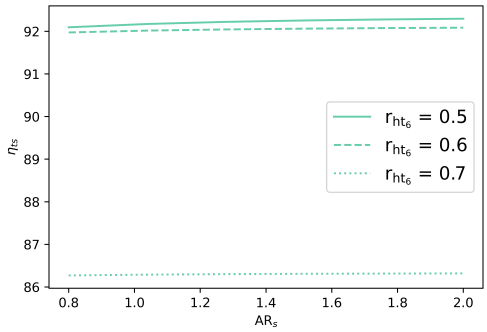

(b) Interaction between stator aspect ratio and rotor exit hub-to-tip ratio.

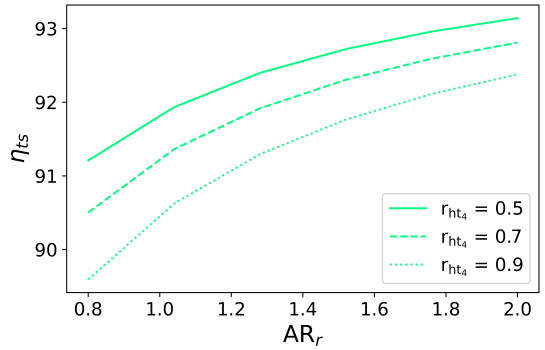

(c) Interaction between rotor aspect ratio and rotor inlet hub-to-tip ratio.

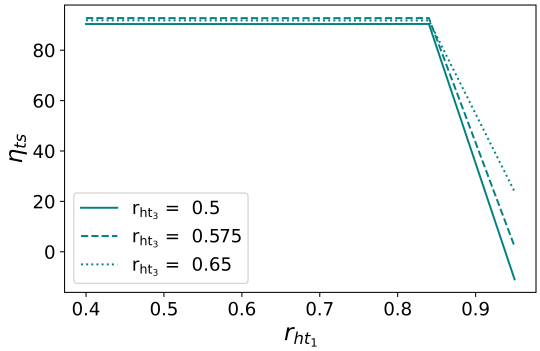

(d) Interaction between stator inlet hub-to-tip ratio and stator exit hub-to-tip ratio.

Figure D.1: Screening of the remaining significant interaction effects.

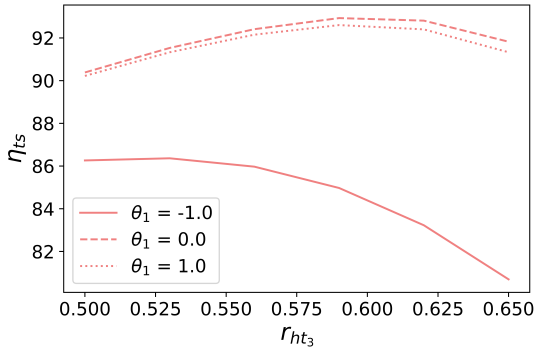

(e) Interaction between stator exit hub-to-tip ratio and stator inlet methal angle.

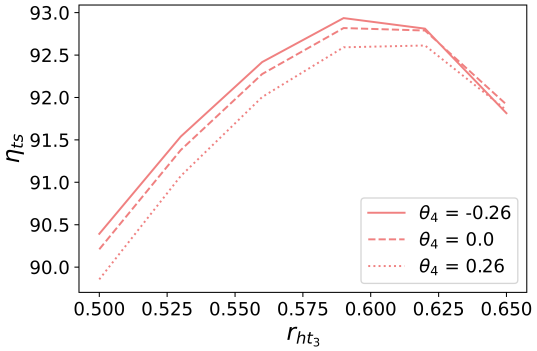

(f) Interaction between stator exit hub-to-tip ratio and rotor inlet methal angle.

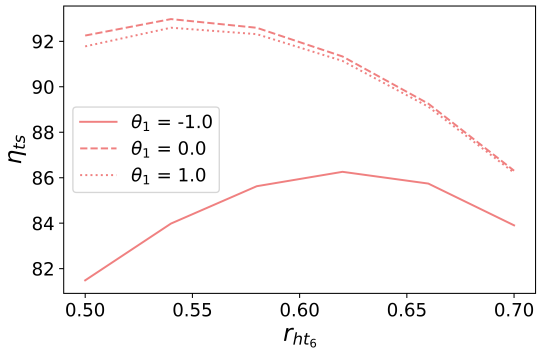

(g) Interaction between rotor exit hub-to-tip ratio and stator inlet methal angle.

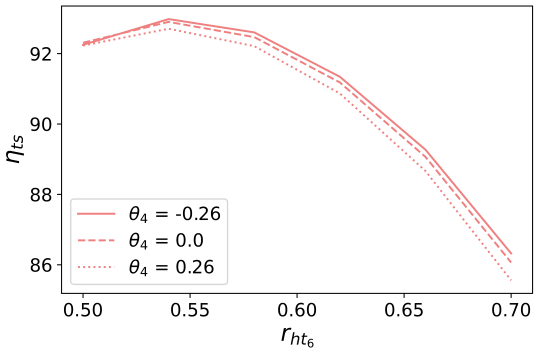

(h) Interaction between rotor exit hub-to-tip ratio and rotor inlet methal angle.

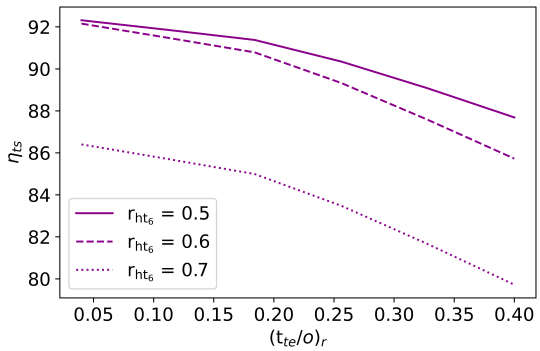

(i) Interaction between rotor TE thickness to opening ratio and rotor exit hub-to-tip ratio.

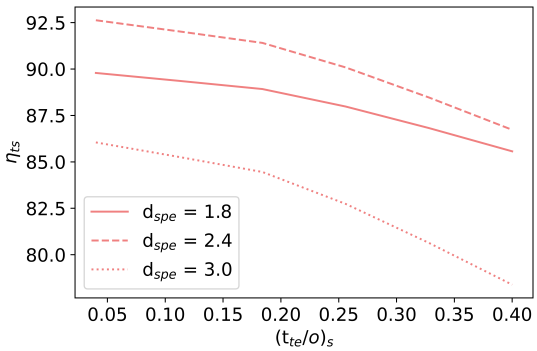

(j) Interaction between stator TE thickness to opening ratio and specific diameter.

Figure D.1: Screening of the remaining significant interaction effects (cont).

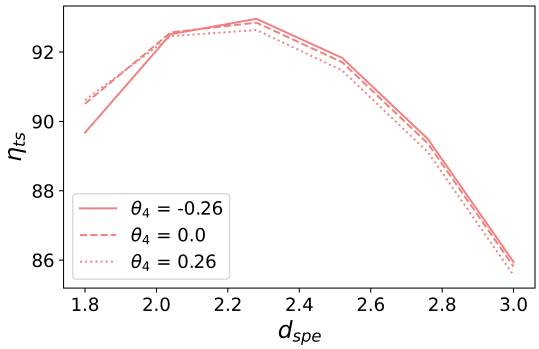

(k) Interaction between specific diameter and rotor inlet methal angle.

Figure D.1: Screening of the remaining significant interaction effects (cont).

D.2 Not significant interaction effects of stator blade solidity BS_s

Since the not significant interaction effects that have not been included in the thesis report are not relevant, in order not to extend more the document, only the stator blade solidity interaction effects are going to be shown.

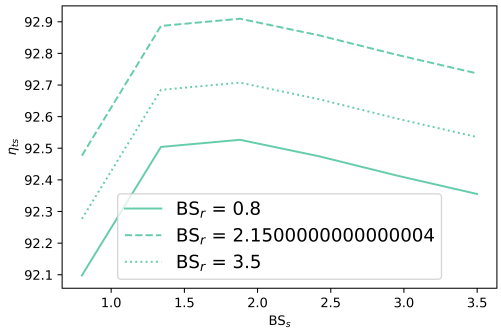

(l) Interaction between stator blade solidity and rotor blade solidity.

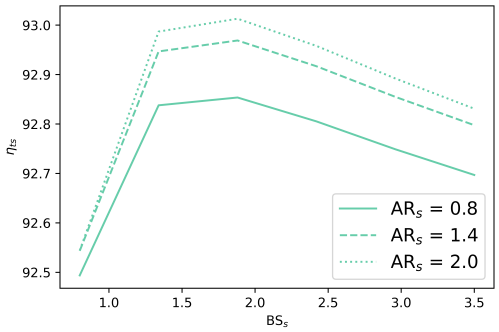

(m) Interaction between stator blade solidity and stator aspect ratio.

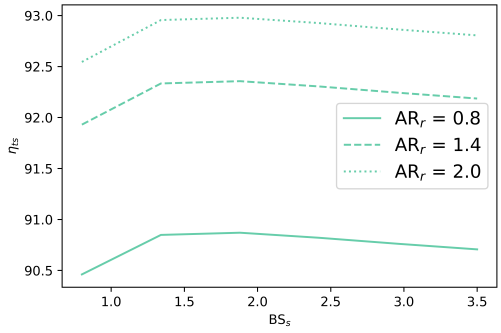

(n) Interaction between stator blade solidity and rotor aspect ratio.

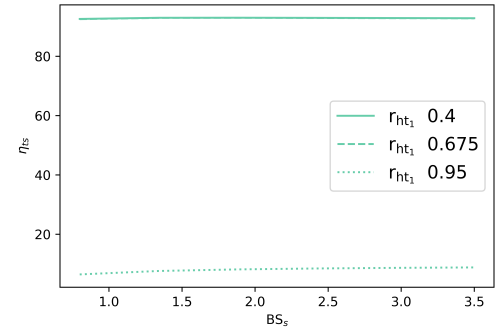

(o) Interaction between stator blade solidity and stator inlet hub-to-tip ratio.

Figure D.2: Screening of the stator blade solidity interaction effects.

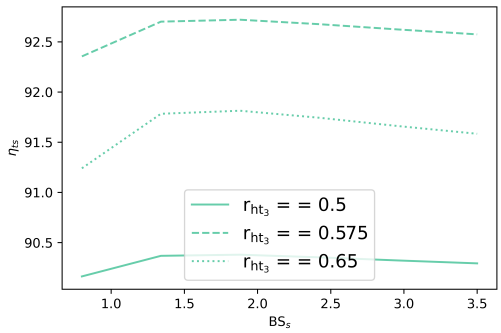

(p) Interaction between stator blade solidity and stator exit hub-to-tip ratio.

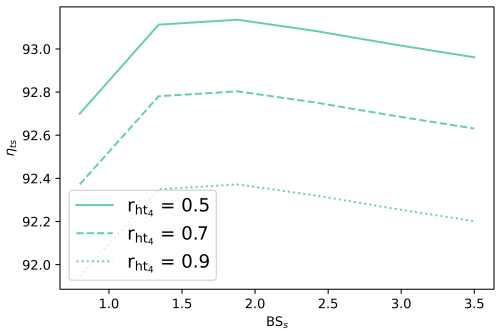

(q) Interaction between stator blade solidity and rotor inlet hub-to-tip ratio.

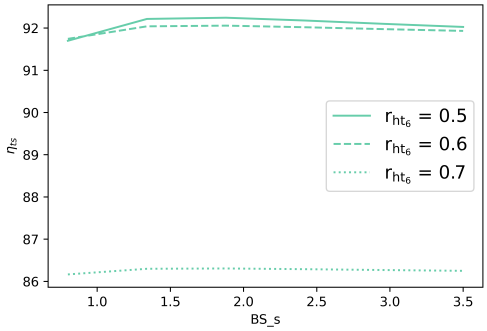

(r) Interaction between stator blade solidity and rotor exit hub-to-tip ratio.

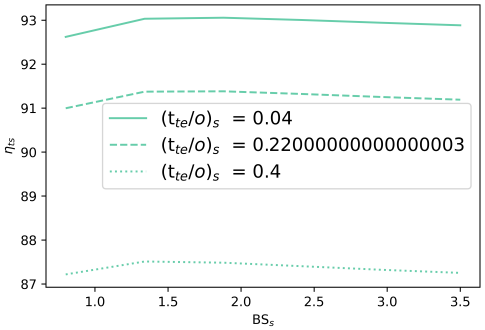

(s) Interaction between stator blade solidity and stator TE thickness to opening ratio.

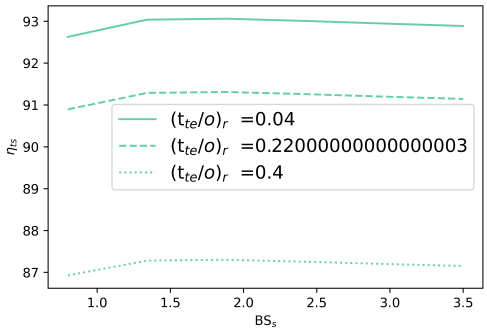

(t) Interaction between stator blade solidity and rotor TE thickness to opening ratio.

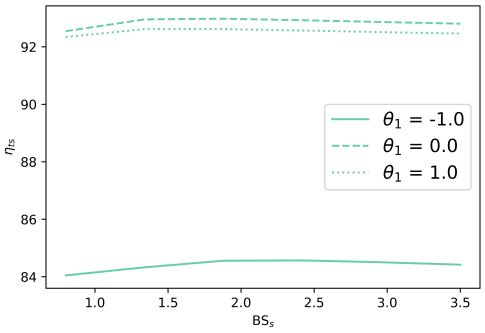

(u) Interaction between stator blade solidity and stator inlet methal angle.

Figure D.2: Screening of the stator blade solidity interaction effects (cont).

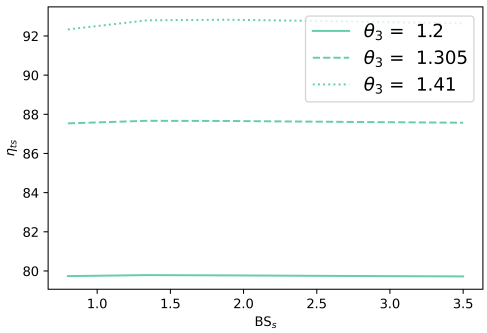

(v) Interaction between stator blade solidity and stator exit methal angle.

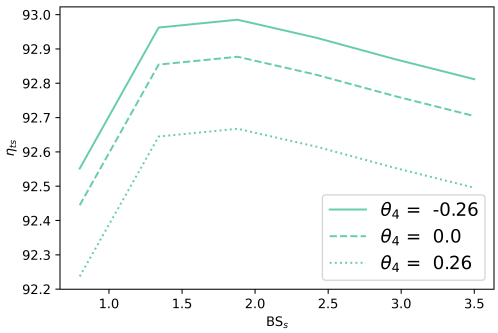

(w) Interaction between stator blade solidity and rotor inlet methal angle.

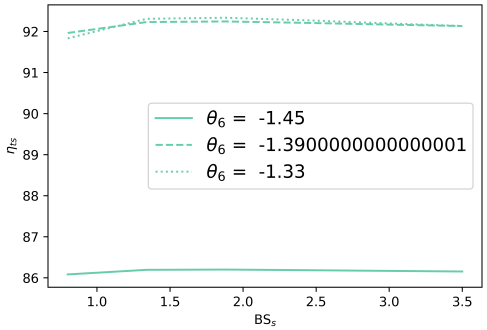

(x) Interaction between stator blade solidity and rotor exit methal angle.

Figure D.2: Screening of the stator blade solidity interaction effects (cont).

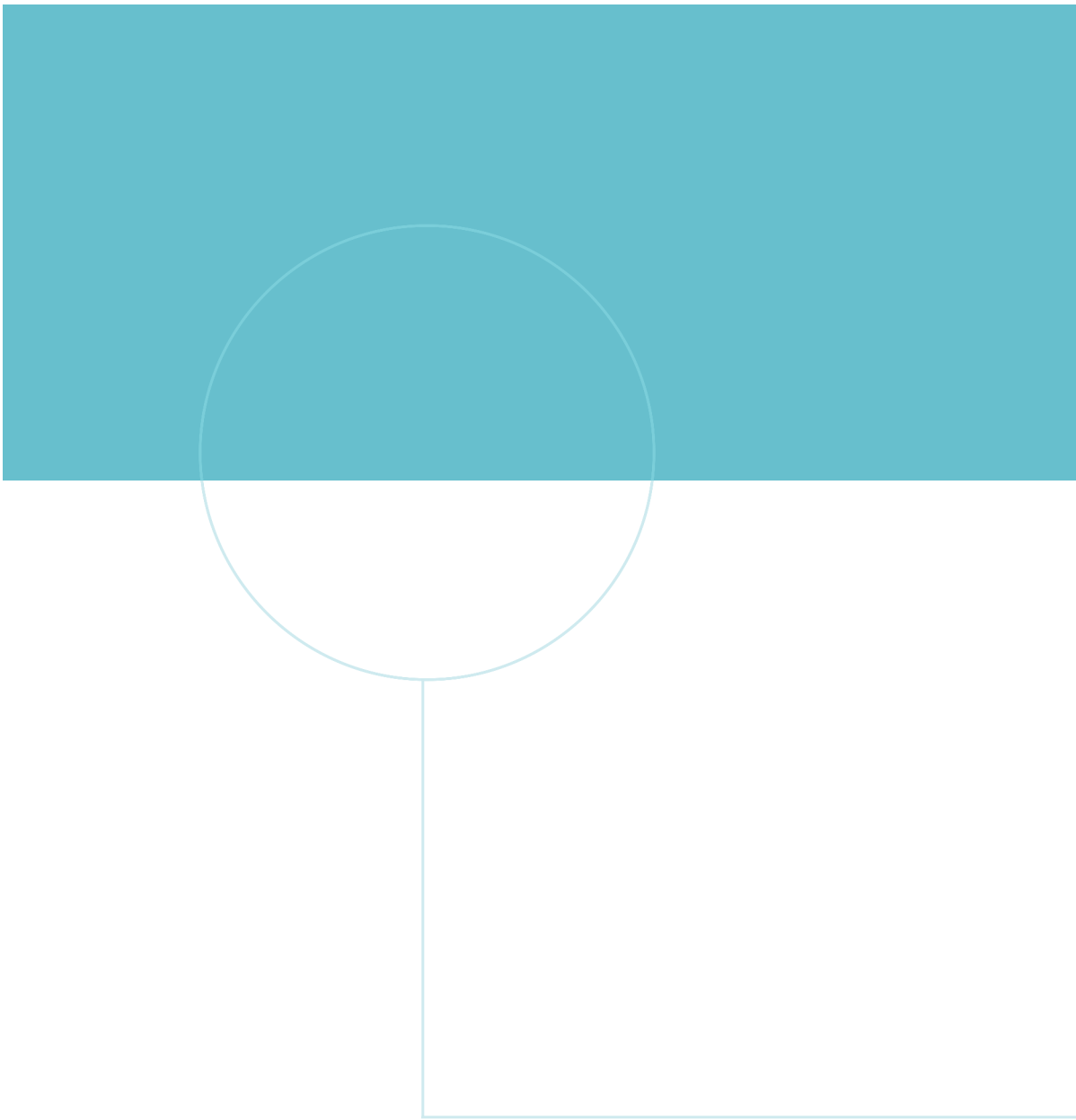

NTNU

Norwegian University of
Science and Technology